Radiation Exposure and Mission Strategies for Interplanetary Manned Mission

Radiation Hazard and Space Weather Warning System

WP 5000

Final Version: 14 December 2004

Compiled by

Claire Foullon[1], Andrew Holmes-Siedle[2], Norma Bock Crosby[1], Daniel Heynderickx[1]

[1] Belgian Institute for Space Aeronomy
Ringlaan-3-Avenue Circulaire
1180 Brussels, Belgium

[2] REM OXFORD Ltd.
64A Acre End St.
Eynsham, Oxford OX29 4PD, England

INTRODUCTION

Radiation protection is a prime issue for space station operations, for extended missions to planets in our solar system (e.g. Mars), or for a return visit to the Moon. The radiation environment encountered by solar system missions mainly consists of the following components:

1. Trapped radiation in the Earth's Van Allen Belts and in the magnetosphere of Jupiter
2. Galactic Cosmic Ray (GCR) background radiation
3. Solar Energetic Particle Events – Solar Proton Events (SPEs)

Along with the continuous GCR background, SPEs constitute the main hazard for interplanetary missions. Up to now, prediction of SPE events is not possible. Future interplanetary manned missions will need to consider solar activity (e.g. solar flares, coronal mass ejections, …) very carefully due to the obvious detrimental effects of radiation on humans. Very high doses during the transit phase of a mission can result in radiation sickness or even death. This is equally true for extended visits to surfaces of other planets (for example to Mars) and moons lacking a strong magnetic field capable of deflecting solar particles. The risk of developing cancer several years after a mission is somewhat more difficult to quantify, but must also be considered in mission planning.

Adequate radiation protection measures must be conceived for any lengthy interplanetary endeavours. There are two ways to go about this and both approaches (1. Engineering, 2. Space Weather Forecasting) complement each other:

1. Engineering Approach

- The design of radiation shielding for a spacecraft is much more difficult given the inherent limitations associated with the construction of an interplanetary space vehicle.

Storm shelters will be necessary both on the transit spacecraft and on the planet surface. The latter can be provided to a certain extent by:

- Atmospheric shielding (altitude variations): in this respect, radiation climate maps of the surface of Mars illustrate the level of detail that is now available for analysing risks from galactic cosmic rays (Saganti et al., 2004; Cucinotta et al., 2002). Variations of the order of 50% are predicted due to changes in the atmosphere (see Figure A).
- Geological features of the visited body, such as lunar lava tubes on the Moon (see e.g., De Angelis et al., 2002).

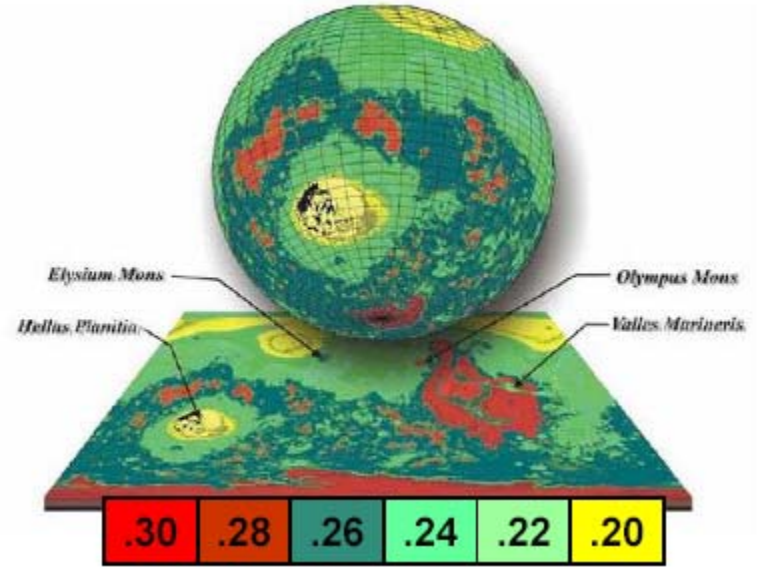

Figure A. Annual skin dose equivalent (Sv/yr) for astronauts on the surface of Mars near solar minimum. The variation in the dose with respect to altitude is shown. Higher altitudes (such as Olympus Mons offer less shielding from the CO2 atmosphere than lower altitudes (such as Hellas Planatia). The effective total dose has a range between 20 and 30 cSv/yr as a function of altitude for a static atmospheric model. (In Saganti et al., 2004 and Zeitlin et al., 2003).

2. Space Weather Monitoring and Forecasting Approach

To protect against SPEs one must also understand their origin, in this way providing guidelines for space weather forecasting purposes.

The ESA project "Radiation Exposure and Mission Strategies for Interplanetary Manned Missions" (REMSIM) is lead by Alenia Spazio in Italy and is divided into various work-packages regarding the subject. Work-package 5000 (WP5000) studies "Radiation Hazard and Space Weather Warning Systems" and is lead by the Belgian Institute for Space Aeronomy (BIRA). REM Oxford Ltd. of England is sub-contracted to BIRA to perform the studies regarding "Radiation Sensors" and "Recommendations for Warning Systems". WP5000 is divided into two parts: Part I. "Interplanetary Space Weather Review" and Part II. "Interplanetary Space Weather Requirement Analysis", each Part containing three chapters:

PART I. Interplanetary Space Weather Review
1. Solar Precursors (BIRA)
2. Existing Monitoring and Warning Systems (BIRA)
3. Radiation Monitors (REM)

PART II. Interplanetary Space Weather Requirement Analysis
4. Feasibility to Use and Integrate Existing Systems (BIRA)
5. Integration of Models and Data Systems (BIRA)
6. Recommendations for Warning Systems (REM)

Chapter 1 of WP5000 reviews the precursors of solar and interplanetary phenomena at work in interplanetary space weather using input from WP1100 (preliminary definition of the radiation environment). Thereafter a presentation of existing monitoring and warning systems is given in Chapter 2. This includes available remote sensing and *in-situ* databases, and models that are used at present. Chapter 3 introduces radiation monitor technologies that are available and explains how they are converted to space-radiation monitors by selection of structure and circuitry. In Chapter 4 the feasibility to use and integrate the existing systems, that were presented in Part I of this WP, is assessed taking the radiation dose thresholds (output of WP1200) into consideration. Various integrations of models and data systems from future planned missions are also considered and they are discussed in Chapter 5. The final Chapter gives recommendations for warning systems.

Drs. Claire Foullon and Norma Bock Crosby of BIRA wrote Chapters 1, 2, 4, 5 and Dr. Andrew Holmes-Siedle of REM wrote Chapters 3 and 6. Dr. Daniel Heynderickx is Work-Package Manager.

TABLE OF CONTENTS

Part I
Interplanetary Space Weather Review

Part II
Interplanetary Space Weather Requirement Analysis

1. SOLAR PRECURSORS

Solar protons have energies ranging from around 1 keV to greater than 500 MeV. In this document only solar protons with energies above 1 MeV are considered. They are produced in what are called solar energetic particle events (SEPEs) or solar particle/proton events (SPEs) and are the main hazard for interplanetary missions.

The mechanism for proton acceleration and the cause of SPEs is widely debated in the literature (see Gosling, 1993; and e.g., the review paper by Reames, 1999b). SPEs tend either to be associated with activity in the most complex and flare-rich sunspot groups or with massive, fast coronal mass ejections (CMEs). A contributing factor to the possibility of an energetic proton event is the physical location of the active region on the solar surface relative to the observer and the characteristics of energy release in an accompanying solar flare. This chapter begins with the characterization of SPEs. Thereafter the various signatures and structures that precede and accompany SPEs, as well as the signatures the SPEs leave behind, are presented and discussed.

1.1 Introduction

1.1.1 SPE Types

During the last two decades it has been widely accepted that there are two kinds of SPE events (gradual and impulsive) based on solar X-ray observations, each with distinct signatures and broad characteristics (Cane et al., 1986; Miller et al., 1995; Reames, 1995, 1997a, b):

- The "gradual" events have duration of several days, they are proton rich and they have, on average, the same element composition and ionisation states as those in the low-density ambient plasma of the high solar corona or solar wind. They are associated with gradual X-ray flares, type II and type IV radio emission and are produced by the shock associated with fast CMEs (Kahler, 1994; Cane, 1997; Reames, 1997a). Such events are observed over a broad range of heliolongitudes, in some case over 180 degrees.

- The "impulsive" short-duration (hours) events are only observed from magnetically well-connected locations on the Sun: they are generally limited to within a 30 degree longitude band about the footprint of the nominal field line connected to the active region. They are electron-rich and they have a strong association with impulsive H-alpha and X-ray flares, and type III radio bursts. The high ion charge state indicates that their origin is in plasma heated by solar flares.

The characteristics of these two types of SPEs (impulsive and gradual events) are listed in Table 1.

Properties	Impulsive Events	Gradual Events
Particles	Electron-rich	Proton-rich
$^3He/^4He$	~1	~0.0005
Fe/O	~1	~0.1
H/He	~10	~100
Q_{Fe}	~20	~11
Duration	Hours	Days
Longitude Cone	<30 deg	~180 deg
Radio Type	III,V (II)	II, IV
Coronograph	-	CME (96%)
Solar wind	-	IP Shock
Flares/year	~1000	~10

Table 1. Properties of impulsive and gradual events based on X-ray signature (Reames, 1995)

However, as mentioned above, the above classification is based on the X-ray characteristics of the associated flare activity and recent observations challenge this strict separation of all SPE events into these two types. For example, there are large gradual events with abundances more like those of impulsive events. It also seems that abundance variations are organized by the heliolongitude of the parent solar activity (flare or CME).

Recently, Smart and Shea (2003) suggested an alternative classification of events based on other distinctions (interplanetary (IP) shock dominated and near-Sun injection):

- The "IP events" are those associated with solar activity near the central meridian of the Sun (presumably the result of a very fast CME) and the resulting powerful fast interplanetary shock, directed toward the observer, that continues to accelerate particles at the shock front that propagates along the pre-existing interplanetary magnetic field lines toward the observer. These types of events may further be subdivided into two sub-classes:

  1. Regular shock events
  2. Converging shock events.

- The "near-Sun injection events" are those that are the result of solar activity on the western hemisphere of the Sun near the "favourable propagation position" for field lines connecting to an observer. This class covers both the "impulsive" flare associated events and the western heliolongitude fast CME associated events.

The characterization of this classification is found in Table 2.

	Type of SPE	
	Near-Sun injection	IP shock dominated
Solar origins	Western (front and far side) hemisphere: "impulsive" flares and fast CMEs.	Fast CMEs from - Western (front and far side): rapid rise and decline - Halo (front sided): well-connected, flat profile - Eastern: poorly connected until shock passes
Time of arrival at 1 AU after the event onset at the Sun	~8-80 mn	~12 hours - 2 days or more
Peak intensities	~5 orders of magnitude	~2 orders of magnitude
Duration	Limited (hours)	Several days
Radiation hazard	Low	High
Forecasting goals	Warning (probability) levels	Flux profile predictions

Table 2. Space weather characteristics for the two types of SPEs based on the classification of Smart and Shea (2003).

1.1.2 Overview of Solar Flares and CMEs

1.1.2.1 Solar Flares

Solar flares are enormous explosions in the solar atmosphere, involving sudden bursts of particle acceleration, plasma heating, and bulk mass motion. They are generally believed to result from the sudden release of magnetic energy stored in the magnetic fields that thread the solar corona in active regions around sunspots. The magnetic energy is released through a process called magnetic reconnection, in which oppositely directed magnetic field lines "break" and connect to each other and part of their energy is transferred to the solar plasma.

In general, a solar flare produces copious radiation across the full electromagnetic spectrum from the longest wavelength radio waves to the highest energy gamma rays. Solar flares were first detected from their visible or optical emissions. These so-called "white light" flares are rarely reported since they are difficult to detect against the intense and constant optical emission from the photosphere. High-energy radiation at the shorter X-ray and gamma-ray wavelengths carries direct information about the energetically dominant products of the energy release that is not available from emissions at any other wavelength.

Particles from solar flares have unusual abundances of elements and isotopes produced by wave-particle interaction and they are highly ionised by the hot flare plasma where they originate. Most of the accelerated particles are confined to magnetic loops in

the flare region and they eventually plunge at the solar atmosphere at the footpoint of the loops to produce X-rays, gamma-rays and heat, which contributes to the brilliant flash phase of the flare. The X-rays result from the interactions of the high-energy electrons energized during the flare, and the gamma rays result primarily from nuclear interactions of the high-energy protons and other heavier ions.

During a large solar flare, the X-ray and gamma-ray flux is observed to increase by many orders of magnitude over pre-flare levels. The time profile at several different energies for a large flare on 6 March 1989 is shown in Figure 1. The following different stages can be recognized from this plot:

1. The pre-flare or precursor stage from about 13:50 to 13:56 UT in which the soft X-ray emission gradually increases but little if any hard X rays or gamma rays are detected above the instrumental background level. In this stage, the release of magnetic energy is triggered.

2. This is followed by the so-called impulsive phase in which the hard X-ray and gamma-ray emission rises impulsively, often with many short but intense spikes of emission, each lasting a few seconds to tens of seconds. The soft X-ray flux rises more rapidly during this phase with its time profile roughly matching the time integral of the hard X-ray profile in many cases. In this stage, protons and electrons are accelerated to energies exceeding 1 MeV and radio waves are emitted.

3. After about 14:06 UT the gradual phase begins, and the hard X-ray and gamma-ray fluxes start to decay away more or less exponentially with a time constant of minutes. The soft X-ray flux continues to rise to a later peak and then it too falls exponentially but with a significantly longer time constant, sometimes as long as several hours.

In the particular flare shown above, a second phase of hard X-ray and gamma-ray emission occurs after about 14:10 UT in which the fluxes vary more gradually than during the impulsive phase. This later, more gradual phase of high-energy emissions is not detected in most flares. Note that the soft X-ray flux continues to fall smoothly during this phase.

This has become known as the 6 March 1989 X15 solar flare event. A huge solar proton event occurred on 8 March at 17:35 UT (reaching maximum on 13 March at 06:45 UT <http://www.sel.noaa.gov/ftpdir/indices/SPE.txt>.

The arrival of a shock on 8 March 1989, was presumably associated with the X-ray flare on 6 March, and the associated small increase in the geomagnetic indice Dst. This increase in Dst is probably a sudden storm commencement / sudden impulse (SSC/SI) due to compression of the magnetopause and the concomitant increase in the magnetic field of the magnetopause current layer detectable on Earth's surface. This famous 6 March 1989 flare was related to the disruption of the power grids in Canada.

At this time no systematic coronagraph onboard spacecraft observations were being conducted. Not until the launch of the Solar and Heliospheric Observatory (SOHO) on 2 December 1995 has it been possible to track CMEs around-the-clock.

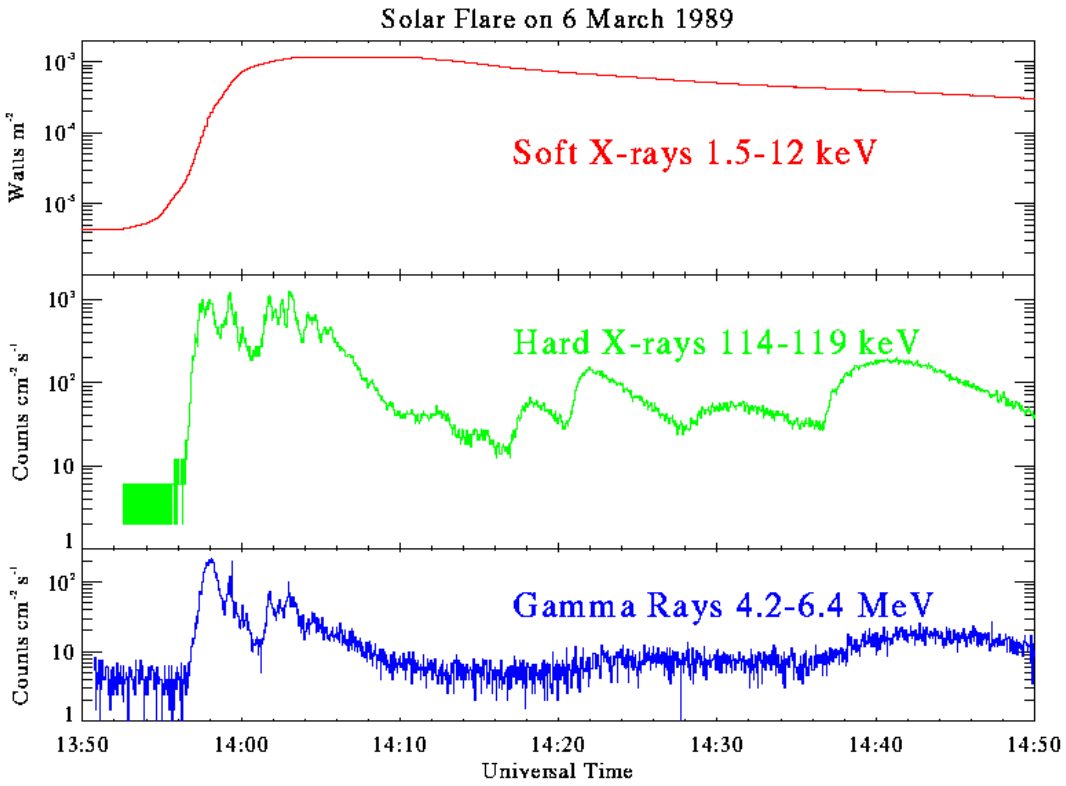

Figure 1. Example of a solar flare observed in three wavelengths on 6 March 1989. <http://hesperia.gsfc.nasa.gov/hessi/flares.htm>.

On 6 November 1997 the Sun produced a X9 solar flare at 11:55 UT. Figure 2 shows the total soft X-ray flux observations that were made of it by the GOES X-ray monitors at two energies in the thermal range. This massive X-ray event was rapidly followed by energetic particles starting at 13:05 UT on 6 November (maximum on 7 November at 02:55 UT) (Figure 3) and became known as one of the "Solar Energetic Proton Events of 3-9 November 1997". The event was large and energetic enough to be measurable also on ground level.and a number of neutron monitors registered the solar event (e.g. IZMIRAN group at <ftp://helios.izmiran.troitsk.ru/anonymous>). Around the time of the Solar flare a halo CME was detected at 12:10:41 UT.

1.1.2.2 Coronal Mass Ejections (CMEs)

CMEs are huge bubbles of gas threaded with magnetic field lines that are ejected from the Sun over the course of several hours. They are seen as bright features moving outwards through the solar corona at speeds from 10 to 2000 km/s (Hundhausen, 1999).

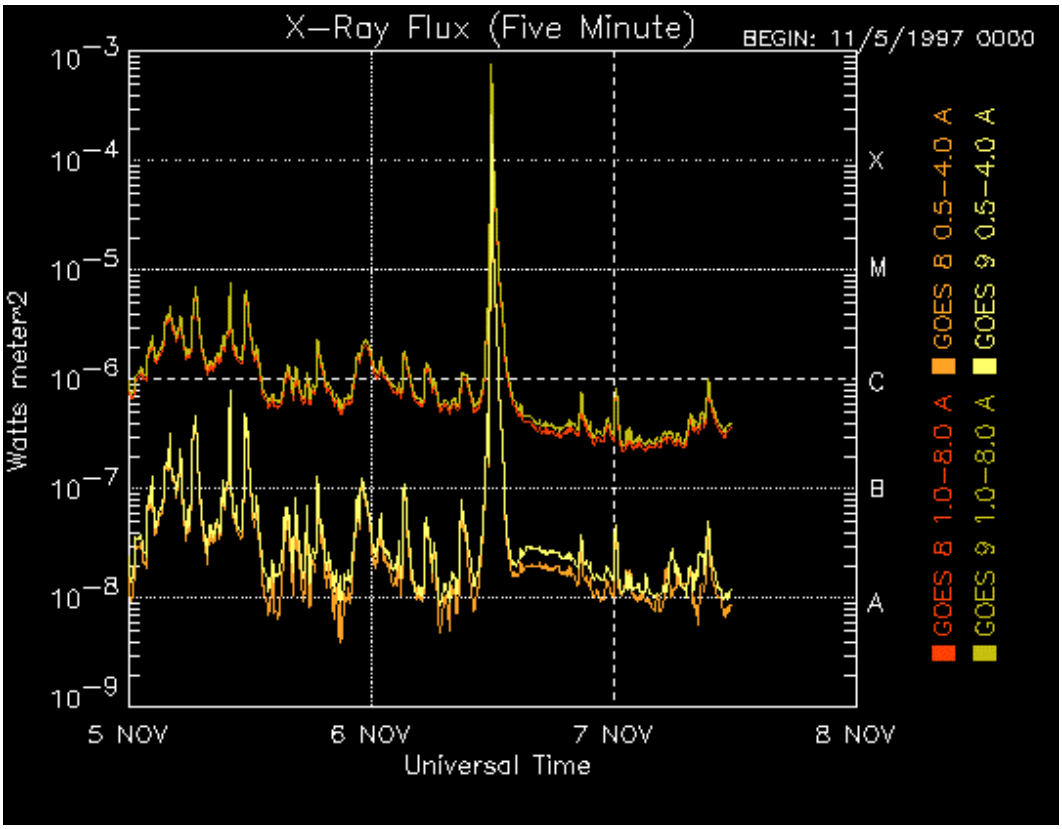

Figure 2. On 6 Nov. 1997 the Sun produced a X9 solar flare at 11:55 UT. Courtesy of NOAA/SEC.

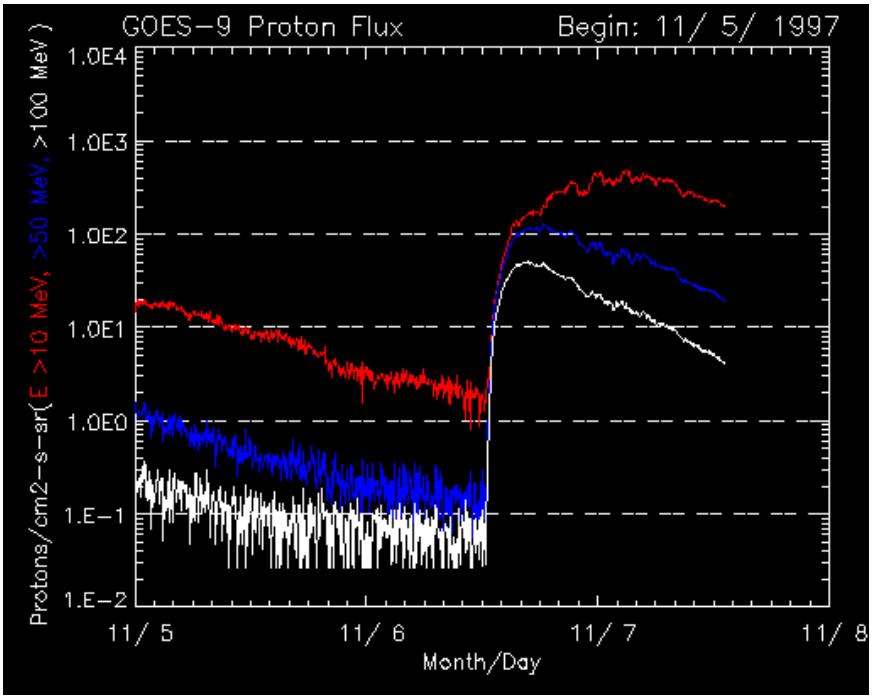

Figure 3. A SPE started on 6 Nov. 1997 at 13:05 UT. Courtesy of NOAA/SEC.

Although the Sun's corona has been observed during total eclipses of the Sun for thousands of years, the existence of coronal mass ejections was not known until the space age. The earliest evidence of these dynamical events came from observations made with a coronagraph on the 7th Orbiting Solar Observatory (OSO 7) from 1971 to 1973. A coronagraph produces an artificial eclipse of the Sun by placing an "occulting disk" over the image of the Sun. During a natural eclipse of the Sun the corona is only visible for a few minutes at most, too short a period of time to notice any changes in coronal features. With ground based coronagraphs only the innermost corona is visible above the brightness of the sky. From space the corona is visible out to large distances from the Sun and can be viewed continuously.

The energy of a CME is mostly kinetic, that is due to its motion. The total energy released by a CME is comparable to the energy released during a large flare, i.e. from 10^{31}-10^{32} ergs. Ejection masses are typically in the range from 10^{15}-10^{16} g (e.g., Vilmer, 1999).

CMEs disrupt the flow of the solar wind and produce disturbances that strike the Earth with, sometimes, catastrophic results. The Large Angle and Spectrometric Coronagraph (LASCO) on the SOHO spacecraft has observed a large number of CMEs. The event of 7 April 1997 is shown in Figure 4. It produced a "halo event" in which the entire Sun appeared to be surrounded by the CME. Halo events are produced by CMEs that are directed toward the Earth. As they loom larger and larger they appear to envelope the Sun itself.

CMEs are often associated with solar flares and prominence eruptions but they can also occur in the absence of either of these processes. The frequency of CMEs varies with the sunspot cycle. At solar minimum we observe about one CME a week, i.e. 0.2 events per day (Gosling, 1997). Near solar maximum we observe an average of 2 to 3 CMEs per day.

1.1.2.3 Summary

Fast CMEs and solar flares are the first links in the chain of causes that connects eruptions on the Sun to SPEs at 1 AU and beyond. To understand the solar origins of SPEs, therefore, we must understand how CMEs and solar flares are initiated. Because of their limited intensities and duration, impulsive flare events do not constitute a significant radiation hazard. Most of the impulsive SPEs reach Earth nearly as rapidly as any electromagnetic signatures (~8 to 80 minutes), leaving insufficient time to make appropriate changes during for example extra-vehicular activity (EVA) which is defined as when work is being done by an astronaut away from the Earth outside of his or her spacecraft.

As a result, solar flare monitoring with present and upcoming spacecraft will provide only short-term warning, at best, of oncoming energetic particles from such events. On the contrary, gradual flare events are usually associated with those CMEs that drive large particle events, where peak intensities occur at the time of shock passage. On 4 August 1972, the highest fluxes of >30 MeV protons observed to date peaked 14.2 hours after the event occurred on the Sun. Therefore, in the rest of this chapter, CMEs alone and in connection with gradual flares will be considered.

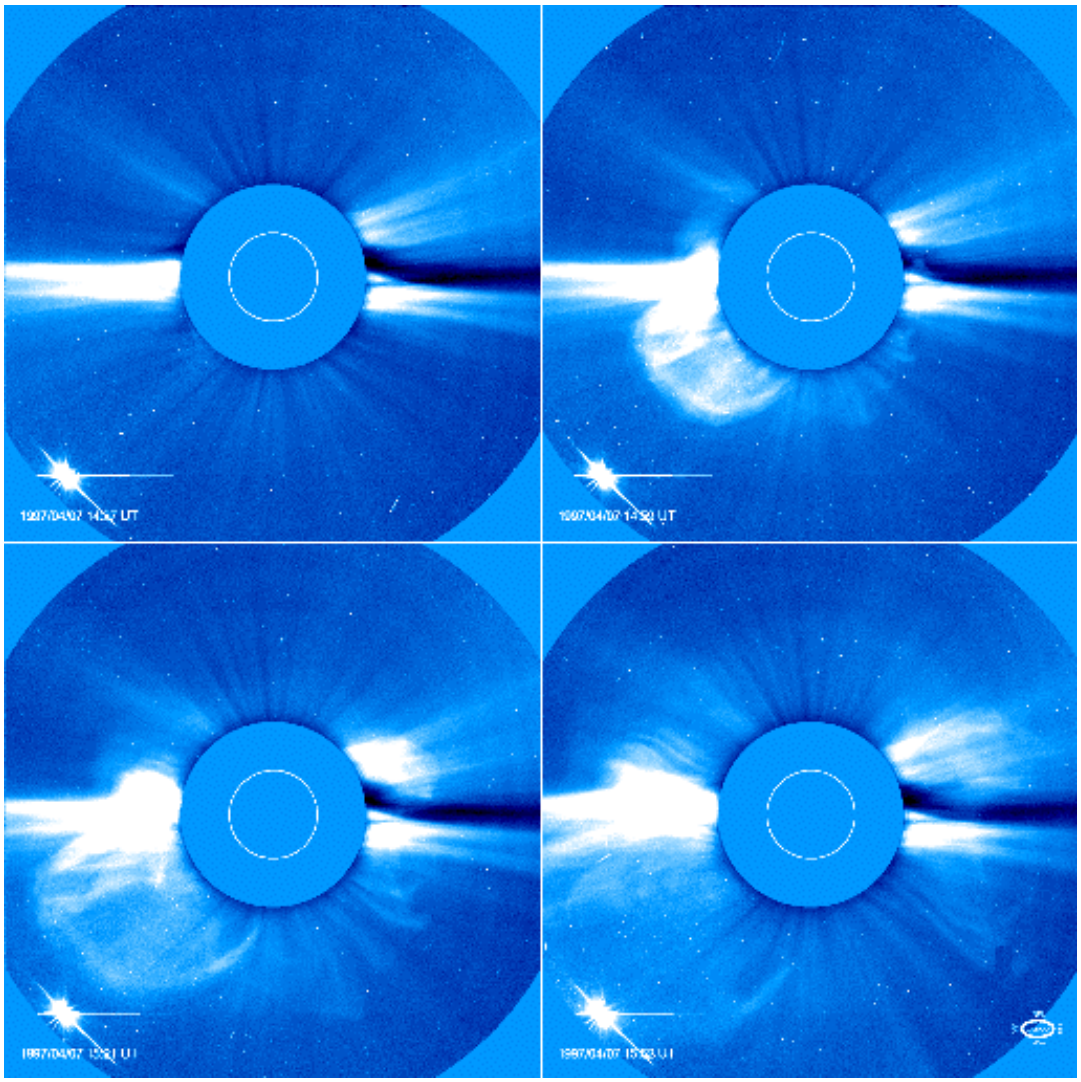

Figure 4. The 7 April 1997 CME event as seen by the LASCO C2 coronagraph onboard the SOHO spacecraft
<http://sohowww.nascom.nasa.gov/gallery/current/19970407/>

1.2 CME Initiation and Associations

Fast CMEs and some slow CMEs drive interplanetary shocks (Sheeley et al., 1995), which in turn accelerate particles (see e.g., Tylka, 2001). Thus, one needs to understand CME initiation, which is still poorly understood. For this purpose, one needs to have complete information on the structure and dynamics of the pre-eruption, source regions on the Sun. Here an overview is given (for more details see the review paper by Gopalswamy, 2003).

1.2.1 Source Regions

The Sun's magnetic field is the most likely source of the substantial energy needed to launch and maintain a CME. CMEs can originate from two possible regions of large-scale closed magnetic field regions:

1. Active regions and filament/prominence regions, which often form complexes.
2. Large-scale closed field lines interconnecting active regions (e.g. transequatorial active regions).

Most CMEs come from the streamer belt (location of active regions) or from the boundary between the polar coronal holes and adjacent active regions (location of the polar crown filaments).

It is important to note that CMEs are not caused or driven by solar flares; in some cases the causal relationship appears to be reversed, but in many cases the relationship appears more complex.

1.2.2 Pre-Eruption Structures

Continuous monitoring of the Sun is necessary when searching for CME pre-eruption structures. At present there exist three structures (1. Helmet-Streamer, 2. Sigmoidal, and 3. Flux Rope) that are used for this task and they all can be observed in X-rays. Examples of these structures are illustrated in the various plots in Figure 5. The data originates from the Soft X-ray Telescope (SXT) on the Yohkoh solar research spacecraft Japan during 3 October 3 1991 to 25 January 1992. Descriptions of these structures are listed below:

1. The "helmet-streamer structure", known for a long time from eclipse pictures, is a large-scale closed field region (example seen in Figure 5A). The closed field part of the streamer deforms to become the frontal structure of the CME, followed by the coronal cavity and the prominence core (Hundhausen, 1999). Thus the "three-part structure of CMEs" can be readily observed in the pre-eruption phase.

2. Sheared magnetic structures, inferred from photospheric magnetograms, have been thought of as indicative of imminent eruption (Ambastha et al., 1993). The coronal manifestation of the photospheric shear is the characteristic "sigmoidal structure" in X-ray images (Figure 5G), observed as a S- or reverse S-shaped feature (Rust and Kumar, 1996). This structure was found statistically to be a reliable precursor of eruptions (Canfield et al., 1999; Glover et al., 2000). This precursor, together with the size of an active region, should allow forecasters to predict the location of an eruption (the location of the sigmoid). However, forecasters would not know precisely when, within a period of a few days, the flare or CME would occur. Combining vector magnetograms with the Yohkoh soft X-ray images, Falconer (2001) has identified two characteristics of active regions that may be useful in discriminating productive active regions: the length of the strong field, strong shear main neutral line and the global net current in the active region. Above certain values of these parameters, production of CMEs is likely.

3. Many CMEs in the interplanetary medium (called ICMEs) have been found to have a "flux rope structure" as they develop (e.g. Low and Smith, 1993; Chen, 1996) and/or as they leave the Sun (Gosling, 1990). Whether flux ropes are pre-eruption structures or are formed during eruption is still a subject of debate (Gosling, 1990; Low and Hundhausen, 1995). Central to this debate is the formation and eruption of prominences: some authors consider the prominence eruption as the cause of CMEs (Fillipov, 1996; Wu et al., 2000), contrary to arguments that prominence cores are not energetically favorable to cause CMEs (Hundhausen, 1999). Those ICMEs with clear field rotations coincident with low temperature and strong magnetic field are called "magnetic clouds", see Figure 6 (Burlaga et al., 1981). It is not clear which part of the CME becomes the cloud (see e.g., Bothmer and Schwenn, 1994). In spite of opposite interpretations, either the filament chirality or the larger-scale coronal arcade skew pattern (Figure 5B) can be used as a predictive tool for cloud chirality and axis polarity, while the hemisphere of origin predicts chirality in a statistical sense (McAllister et al., 2001).

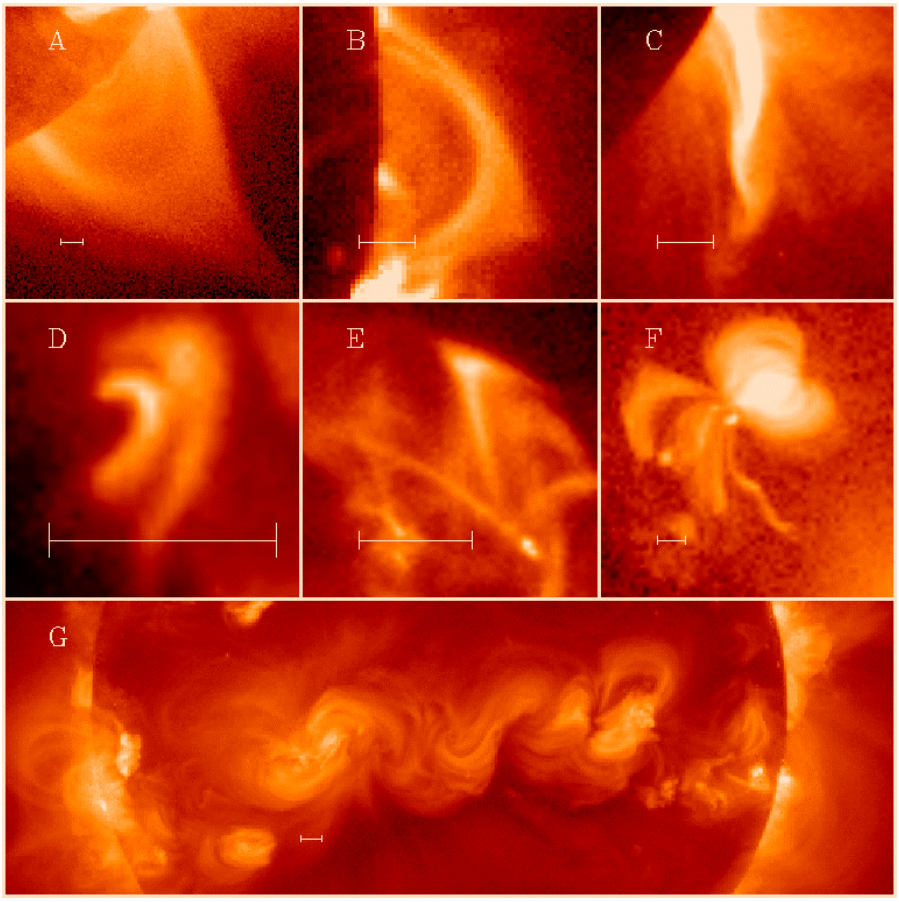

Figure 5. Examples of a variety of solar coronal features seen in soft x-rays: A) a large "helmet type structure"; B) an arcade of X-ray loops seen end-on; C) a dynamic eruptive phenomenon that grew at a velocity of about 30km/sec; D) one of many small symmetric flaring loops seen by SXT; E) two cusped loops, with heating in the northern loop; F) a tightly beamed x-ray jet moving toward the southwest at 200 km/sec; and G) the sinuous magnetic connection between some active regions of the Sun. Courtesy of SXT/Yohkoh.

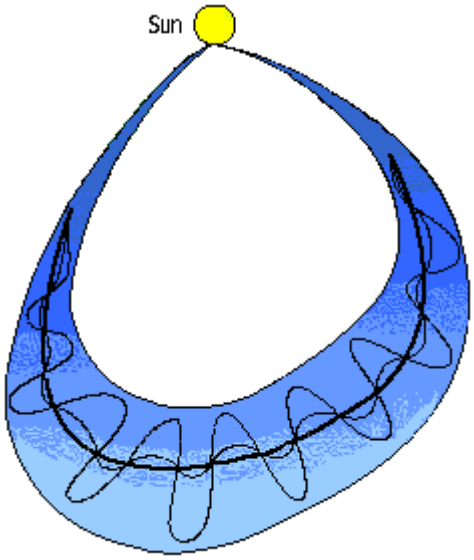

Figure 6. A magnetic cloud contains clear field rotations coincident with low temperature and strong magnetic field (Burlaga et al., 1981).

1.2.3 Pre-Eruption Signatures and Theories of CME Initiation

1.2.3.1 Pre-Eruption Signatures

Both thermal and non-thermal signatures of energy release have been reported on various occasions in connection with the onset of CMEs:

- Thermal signatures are in the form of small-scale X-ray or EUV brightening in the eruptive region.
- Non-thermal signatures are in the form of radio bursts of type III, produced by energetic electrons escaping along open field lines. Jackson et al. (1978) found that, statistically, the number of type III radio bursts peaked an hour before CMEs, suggesting that small-scale energy release in the form of energetic electrons preceded the CME eruption. Gopalswamy et al. (1987) reported on precursor type III bursts located above the region of eruption.

The evidence for small-scale energy release is consistent with the flux emergence reported by Feynman and Martin (1995) and the simulation studies of Chen and Shibata (2000) and points to the possibility of reconnection in the vicinity of filaments in the pre-eruption phase.

1.2.3.2 CME Initiation Theories

Existing theories of CME initiation generally can be categorized according to the underlying driver (Dryer, 1982; chapters by Low; Mikic and Linker; Chen; Wu and Guo in Crooker et al., eds, 1997; Sturrock, 1989; Antiochos, 1998) and they are as follows:

- Gas-pressure-driven models, including buoyancy and flare-driven mechanisms.
- Ideal magnetohydrodynamic (MHD) models based on the emergence of subphotospheric flux ropes into the corona and their subsequent loss of equilibrium (for example, through prominence draining, which removes "ballast" holding down the flux rope).
- Resistive MHD models, which invoke either the formation and detachment of a flux rope through reconnection underneath (the so-called tether-cutting process) or the removal through coronal reconnection of magnetic flux above a stressed configuration, which then is free to erupt (the so-called breakout model).

Most CME initiation models have only been studied analytically or through two-dimensional simulations.

1.2.4 Associations and Signatures

Solar flares and prominences (filaments) are two phenomena that are generally associated with CMEs and in some cases CMEs can be expected when these phenomena are observed. The characteristics of the CMEs differ with the associated phenomenon:

- Flares, in particular long duration flares (visible as events in H-alpha light and X-rays). Those CMEs move generally fast. In such cases the composition of energetic particles associated with the CME-driven shock wave may reflect the large heating or ionization of the local impulsive acceleration in the solar corona.
- Quiescent prominence (filament) eruptions. Those CMEs are generally slower. Prominences are clouds of cold and dense plasma, typically found at the boundary between the polar coronal holes and adjacent active regions.

But so far, CMEs are observed rather than predicted. However, before seeing them on white-light coronagraphs (such as with the LASCO coronograph onboard SOHO) and determining their speed in the plane of the sky, one can suspect that a CME has formed, especially after a long duration flare or a "disparition brusque" of a quiescent prominence.

1.2.4.1 Inner Coronal Signatures of CMEs

Inner coronal imagers measuring in X-ray, microwave and EUV can detect most of the early signatures of CMEs:

- Coronal dimming. Sometimes, a prolonged (~1 hr) weak dimming in EUV and X-rays occurs in the pre-eruption phase, followed by a deep dimming corresponding to

the CME eruption-phase (Gopalswamy et al., 1999a; Gopalswamy and Kaiser, 2002). Coronal dimming represents depletion of coronal material due to a CME (see e.g., Hudson and Webb, 1997; Hudson et al., 1998). Therefore, pre-eruption dimming may correspond to small-scale opening of magnetic field lines in the eruption region. Coronal dimming is best observed in the EIT FeXII 195Å images, and displays considerable variations from event to event.

- Ejected plasmoid. It is most likely the heated prominence core of the CME. Depending upon its temperature, the eruptive prominence can be seen in absorption and in emission lines (Gopalswamy et al., 1999b).
- Arcade formation. It is a post-eruption signature (e.g., McAllister et al., 1996) often used to identify the location and extent of an eruption.
- EUV wave transients (EIT waves). They represent the early phase of CMEs (Thompson et al., 1999).
- Global enhancement.

1.2.4.2 Radio Signatures of CMEs

In the radio spectrum, type II and Type IV bursts are closely related to CMEs. They are usually observed below 400 MHz. Kilometric type II radio emissions from 30 kHz to a few MHz are produced in the interplanetary medium (Pick et al., 2001). Type II bursts are produced by electrons confined to shock fronts, while type IV bursts are produced by electrons trapped in moving coronal structures. It is not clear whether the shock is driven by the CME or the CME presents favorable conditions for shock propagation (Cane, 1984; Gopalspamy et al., 1998; Cliver et al., 1999).

- Radio type II bursts. Type II radio bursts are attributed to plasma waves excited by shocks and converted into radio waves at the local plasma frequency and/or its harmonics. On spectrograph data, the type II emission is observed to drift toward lower frequencies. This frequency drift results from the decrease of the plasma density as the shock propagates further from the Sun. Recent results based on the combination of radio and coronagraphic images show that weak bursts drifting in frequency as type II bursts are associated with the leading edge of the CMEs (Maia et al., 2000). This result shows that early phase of shock development (so called interplanetary shock) can be detected in the corona.

  Thus, radio frequency emissions associated with type II bursts give information on the outward propagation speed of the ejected plasma, in particular, providing important clues as to the origin and speed of shocks both close to the Sun and in interplanetary space. However, type II bursts that are first detected in the low corona are primarily associated with 'impulsive' flares, whereas interplanetary type II emissions are poorly understood. Some type II emissions have been detected during slow CMEs, which in theory should not be able to drive shocks. Gopalswamy et al. (2000) showed however that most type II bursts in the Decameter-Hectometric (DH) domain are associated with faster and wider CMEs. While the relation between metric

and DH type II bursts is controversial (Reiner et al., 2001), there is no doubt that the DH type II bursts are indicative of CMEs leaving the outer corona and provide an essential tool to detect faster and wider CMEs, which are potentially more effective for accelerating particles (Reiner and Kaiser, 1999; Gopalswamy et al., 2000).

- Radio type IV bursts. The moving type IV bursts come in three varieties: advancing fronts, expanding arches and isolated plasmoids (see the review by Stewart, 1985). The isolated sources originate from heated prominence material, also detected in X-rays and EUV. The advancing fronts and expanding arches must be structures associated with the CME itself. These substructures are "visible" only because of the nonthermal particles trapped in them. They were found to move roughly with the speed of the associated white-light CME (Gopalswamy and Kundu, 1989) or to correspond to the frontal structures of CMEs (Maia et al., 2000).

- Radio type III-l bursts. It has been found that there are groups of type III radio bursts that start after, or extend beyond, the impulsive phase of flares that occur at the times of the fast, large, coronal mass ejections (CMEs) accompanying >20 MeV, >24 hour duration, solar proton events. These type III-like bursts are usually intense and relatively long lasting at radio frequencies generated in the interplanetary medium and have been called type III-l. The low frequency drift rates of the type III-l bursts determine the proton data distribution, i.e. the slower the drift rate the slower the proton increase and, in general, the lower the early intensities. For the most intense proton events the fast drift of the radio burst indicates good magnetic connection to the longitude of the flare (see e.g., Cane et al., 1981).

1.2.4.3 Difficulties in Tracking SPEs

One of the difficulties with solar particle observations is that they are made far from the Sun (usually at 1 AU). Extrapolating such in situ observations back to their origin on the Sun is very difficult and involves many uncertainties. On the other hand, solar radio emissions, which are observed as type II and type III bursts, as well as observed in the decimeter/microwave radio range, are believed to be signatures of the acceleration of solar electrons. Since these radio emissions are observed remotely, they can facilitate tracing the signatures of solar energetic particles back to their solar origin, as well as providing information on the location of the acceleration regions in the corona. By the usage of Compton telescopes in space, solar gamma rays and solar neutrons are also used as a signature to support analysis of solar proton events.

However, comparisons of these remote radio observations with in situ particle observations have suggested that the acceleration and/or transport of solar energetic particles may be more complex than previously expected. For example, recent analyses suggest that solar proton and electron events originating in the corona may be the result of different acceleration times, different acceleration locations, and different acceleration mechanisms, even when associated with the same solar event (Reiner, 2003, see Table 3 for details).

Particle species	Electromagnetic signature (wavelength)	In situ signature	Accelerating source
Low-energy electrons	Simple type III bursts (~300 MHz - ~20 kHz)	Prompt (delayed) scatter-free electrons (≤20 keV)	Flare/ reconnection
?	Complex type III-like bursts (~3 GHz - ~20 kHz)	?	Flare/ reconnection?
Near relativistic electrons	Decimeter/microwave radio (≥1 GHz) Hard X-ray	Delayed (prompt) scatter-free electrons (≥20 keV)	CME ?
Energetic protons	?	Impulsive/Gradual SEP events (≥10 MeV)	CME ?
Relativistic protons	?	Ground level events (GLEs ≥1 GeV)	CME ?
Above rows from Reiner (2003)			
Solar gamma-rays and Solar neutrons		Compton telescopes in space	

Table 3. Electromagnetic and in-situ signatures of solar accelerated particle events.

1.3 Heliospheric Environment

The heliosphere can be thought of a vast magnetic bubble containing the solar system, the solar wind, and the entire solar magnetic field. At the outermost boundary of the heliosphere, called the heliopause, the solar wind meets the interstellar medium, a plasma that permeates our Milky Way galaxy. Although electrically neutral atoms from interstellar space can penetrate this bubble, virtually all of the material in the heliosphere emanates from the Sun itself.

Characteristics of the heliosphere are caused by inhomogeneities in the heliospheric environment, changes in the interplanetary magnetic field and the creation of corotating interaction regions (CIRs). It is important to characterize the heliosphere so that one can better understand how phenomena traversing this environment are affected.

1.3.1 Influence of Interplanetary Inhomogeneities

Shock waves will travel through an inhomogeneous interplanetary medium caused by two main variations: variations in velocity and variations in the density of the ambient medium. These two major sources cause an uncertainty in estimating the arrival time of the shock wave. The theory of propagation of strong shock waves through inhomogeneous media relates errors of estimate of shock arrival time to the inhomogeneities. It shows that increases in the velocity along the Sun-Earth line lead to decreases in transit time and increases in the density lead to increases in transit time. Much of the variance of observed transit times results from the influence of interplanetary inhomogeneities (Heinemann, 2002).

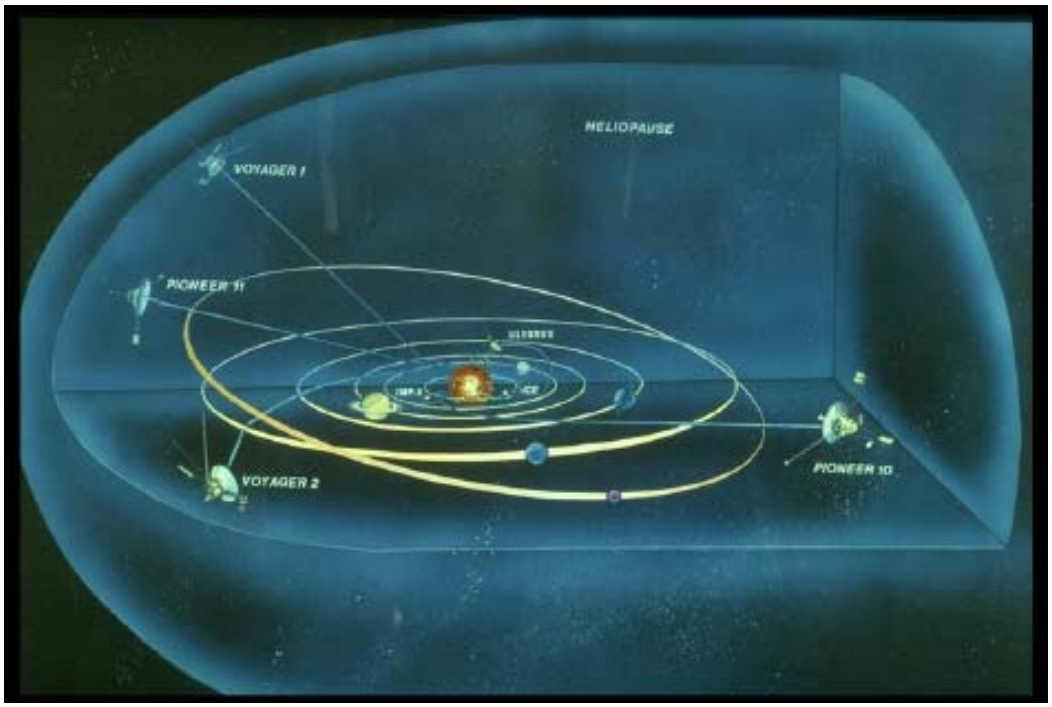

Figure 7. Schematic representation of the heliosphere.
Drawing courtesy of Tom Krimigis, Space Science Institute.

As the eruption traverses the heliosphere, the magnetic topology of the CME and the associated shock that is typically present for a "fast" CME continue to evolve owing to variations in the surrounding plasma and magnetic field characteristics, compression and draping of the interplanetary field around the propagating disturbance, and interactions with preceding (slower) or following (faster) solar storms (transient) and solar wind structures (corotating flows).

Since CMEs propagate long distances before reaching an observer, they are considerably evolved and hence it is difficult to relate in-situ observations, represented in Figure 8, to the CME substructures observed near the Sun. The sheath is the solar wind compressed behind the shock front. When the ejecta contains ordered magnetic field, it is known as a magnetic cloud. On rare occasions, one observes cool dense material towards the end of the ejecta, called the pressure plug, that resemble the prominence resting at the bottom of the coronal cavity in the pre-eruption phase of CMEs. Table 4 shows the correspondence between CME and ICME substructures (Gopalswamy, 2003).

CME near the Sun substructures	**CME in the solar wind (ICME) substructures**
Coronal shock	IP Shock
Frontal Structure	Sheath
Cavity/Void	Magnetic Cloud/Ejecta
Prominence Core	Pressure Plug

Table 4. Correspondence between CME and ICME substructures (Gopalswamy, 2003).

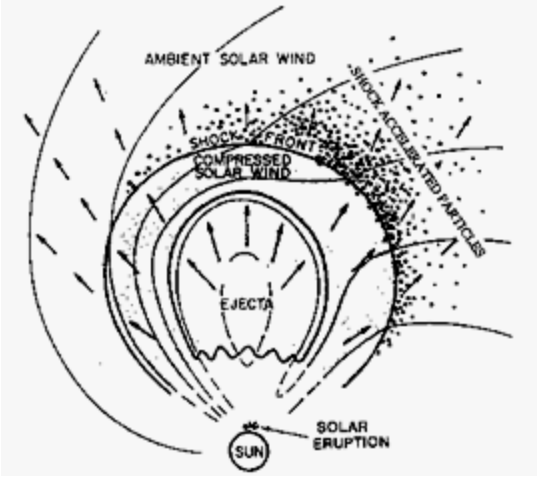

Figure 8. Schematic representation of a CME in the solar wind.
<http://cse.ssl.berkeley.edu/impact/science.html>

1.3.2 The Interplanetary Magnetic Field (IMF)

The interplanetary magnetic field (IMF) is a part of the Sun's magnetic field that is carried into interplanetary space by the solar wind. It is found that during the years around each solar sunspot minimum, the heliospheric magnetic field is generally organised into two hemispheres separated by a thin "current sheet" across which the field reverses direction. Rotating with the Sun the current sheet has folds like the skirt of a whirling ballerina. In each hemisphere the field is a classical Parker archimedean spiral, with the sense of the field being outward in one hemisphere and inward in the other. The drawing illustrated in Figure 9 demonstrates the three-dimensional structure of the current sheet as it would evolve in a constant solar wind flow resulting in the usual two-sector pattern. In practice, a four-sector per solar rotation pattern (and sometimes even higher) is quite usual implying that the 3-D shape of the HCS is even more complex than shown on this picture.

Observations indicate that the waviness, or inclination, of the current sheet is a minimum at sunspot minimum and increases as a function of time away from sunspot minimum. At sunspot minimum the sense changes sign in each hemisphere, and its structure is not simple and probably not well described in terms of a simple current sheet. The over-all magnetic field direction therefore alternates with each 11-year sunspot cycle. The region of interplanetary magnetic field reversal is shaped like a wavy disk, which rotates with the Sun once in 25 days. This current sheet separates the solar wind that originates in the northern solar hemisphere from that originating in the southern hemisphere.

This spiral field results from the solar rotation and the solar wind that brings the magnetic field out in the radial direction. It is easy to understand how the longitude of the field lines connecting the Sun and the Earth changes with the solar wind speed, as shown in Figure 10. For fast solar wind, the well-connected longitudes move eastward from ~W60, corresponding to ~400 km/s, and the length of the spiral between the Sun and the Earth gets shorter.

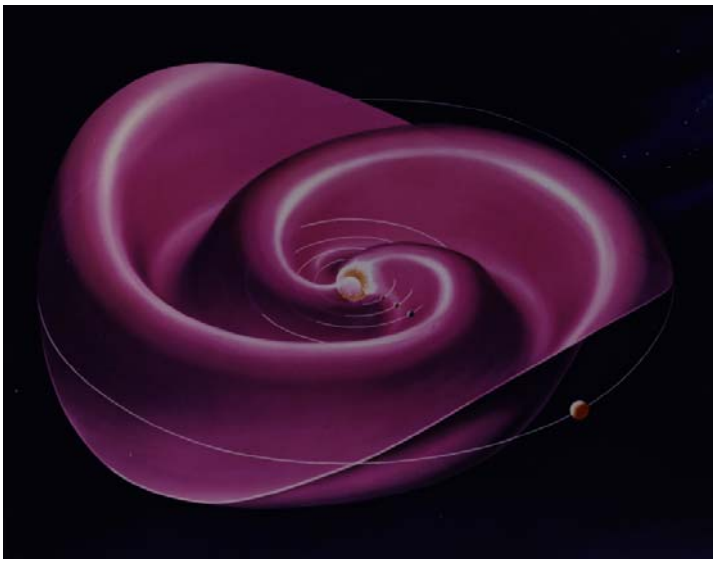

Figure 9. Artist's rendition of the heliospheric current sheet (HCS) for a slightly inclined circular neutral line on a solar source surface. From <http://lepmfi.gsfc.nasa.gov/mfi/hcs/hcs_shape.html>.

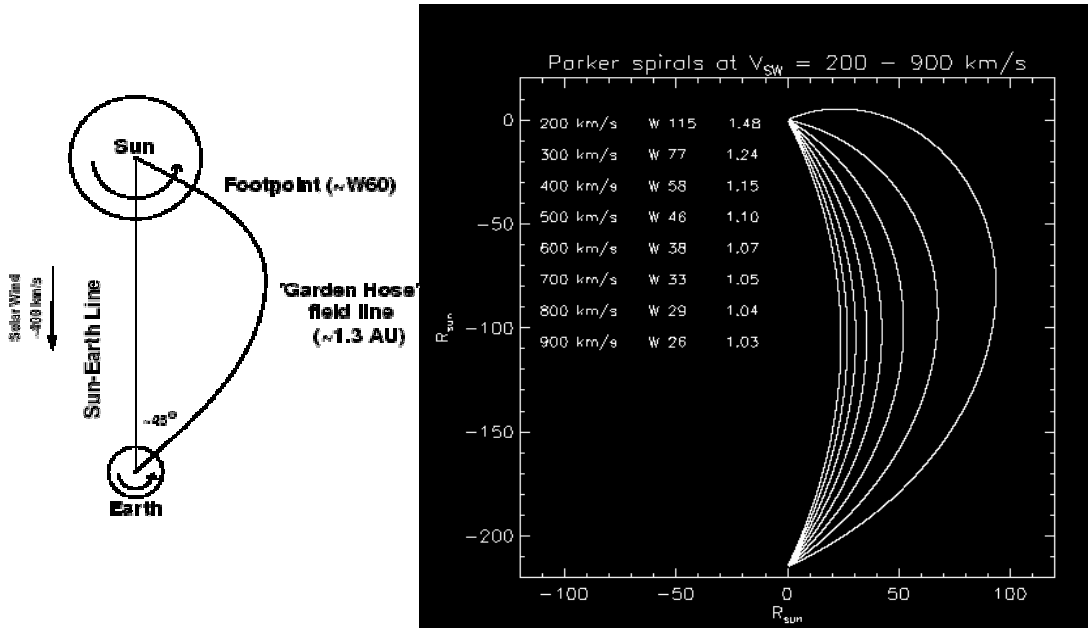

Figure 10. Left panel: Schematic representation of the "garden hose" field line connecting the Sun and the Earth. (from Duldig et al., 1993). Right panel: From N. Nitta, 2002 in <http://isass1.solar.isas.ac.jp/sxt_co/021004.html>.

1.3.3 Co-Rotating Interacting Regions (CIRs)

It has been well demonstrated by the Ulysses spacecraft that there exist two regimes of the solar wind (high speed and slow speed). Solar wind observations collected by the Ulysses spacecraft during two separate polar orbits of the Sun, six years apart, at nearly opposite times in the solar cycle are shown in Figure 11. Near solar minimum (left) activity is focused at low altitudes, high-speed solar wind prevails, and magnetic fields are dipolar. Near solar maximum (right), the solar winds are slower and more chaotic, with fluctuating magnetic fields.

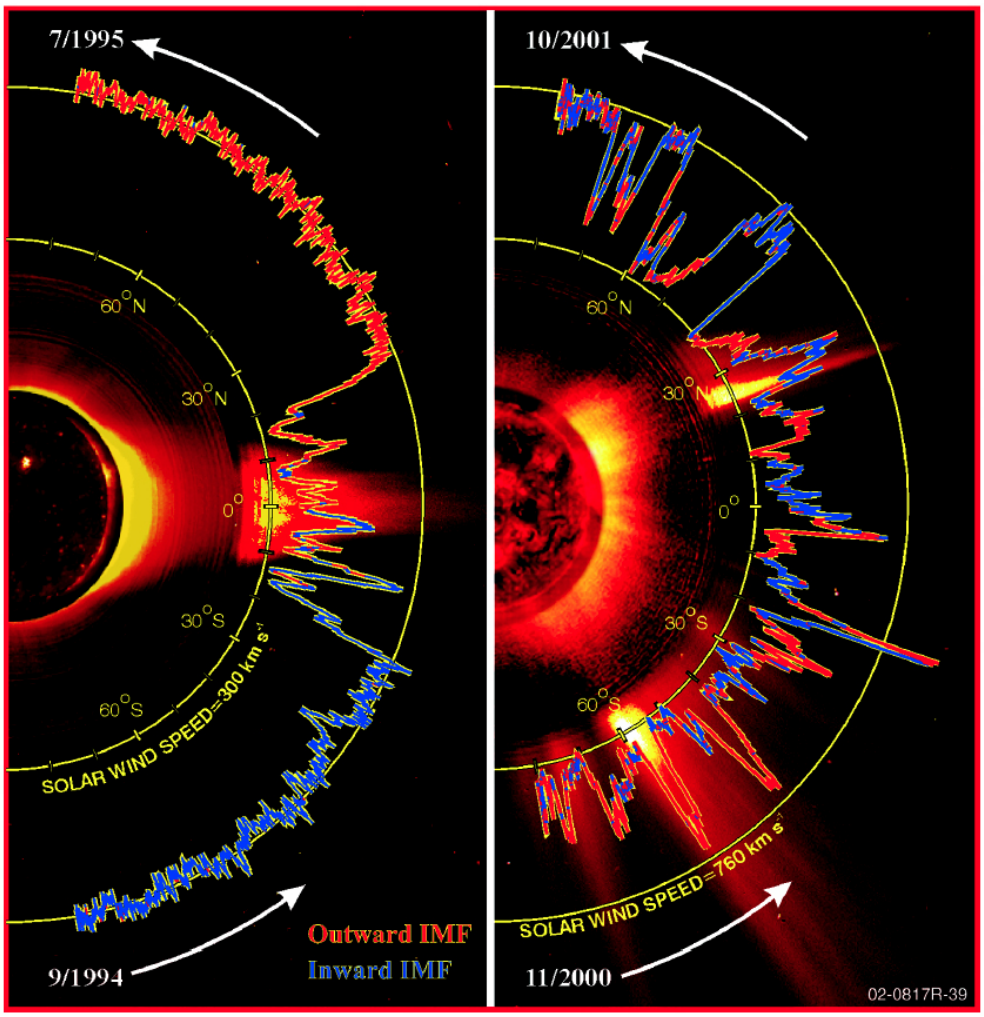

Figure 11. Ulysses solar wind observations during two separate polar orbits of the Sun. Courtesy of Southwest Research Institute and the Ulysses/SWOOPS team.

Corotating streams (high speed solar wind) originate in coronal holes at the Sun. Coronal holes are associated with "open" magnetic field lines and are often found at the Sun's poles, but may also be found at lower latitudes. As the Sun rotates these various streams rotate as well (co-rotation) and produce a pattern in the solar wind much like that

of a rotating lawn sprinkler. Low speed winds come from the regions above helmet streamers. The interaction of high speed (~800 km/s) and low speed (~300 km/s) winds lead to 3-D CIRs in the heliosphere. Interaction regions are regions at transient and corotating flows in the solar wind where the magnetic field strength and pressure are high. Maps of the coronal holes on the Sun are used to predict the arrival time at 1 AU of corotating streams driving CIRs.

If a slow moving stream is followed by a fast moving stream the faster moving material will catch-up to the slower material and plow into it. This interaction produces shock waves that can accelerate particles to very high speeds. A "forward" shock continues in the direction of the overtaking fast wind, while a so-called "reverse" shock propagates in the opposite direction (see Figure 12). A large amount of energy is concentrated in the compressed region close to the shock and charged particles passing through a shock can acquire part of this energy. At low solar latitudes, within the domain occupied by the wavy current sheet, the interaction of fast and slow solar wind is a common occurrence.

The acceleration of charged particles by CIRs leads to a permanent generation of high energy particles in the heliosphere, even in times when the Sun is quiet (solar minimum), as there are more high speed winds during this phase of the solar cycle.

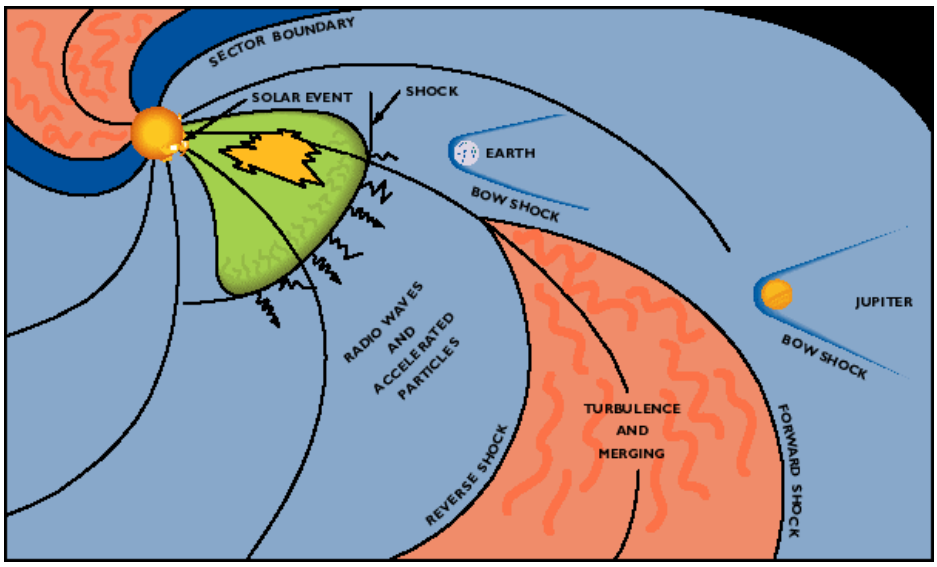

Figure 12. The solar wind. Source: <http://lep694.gsfc.nasa.gov/lepedu/solar.gif>.

1.4 CME-Driven Shocks and Particle Acceleration

In order to provide accurate models of SPEs, we need to identify both in situ and remote signatures of the physical processes that lead to particle acceleration and ultimately to relate them to the observed spatial and intensity particle flux profiles. Here an overview of these signatures in the solar wind is given, as well as an understanding of the resulting proton flux profiles.

1.4.1 Signatures in the Solar Wind

1.4.1.1 Commonly used In-Situ Signatures

Identification of CME signatures in the solar wind is complicated and is often not unique from other signatures (see, e.g., Neugebauer, 1997 and references therein). Commonly used signatures are:

- Counterstreaming superthermal electrons and protons;
- Helium abundance enhancement (up to 30%);
- Anomalously low electron and proton temperatures;
- Magnetic cloud signatures: strong magnetic fields, smooth rotation of magnetic fields, low plasma beta, low magnetic field variance;
- Flux reduction of low energy cosmic rays;
- Unusual ionization states and elemental abundances (Fe16+, He+, Etc…).

Not all signatures are seen for all events and different signatures do not always coincide temporally and spatially.

1.4.1.2 Remote Radio Signatures

What has been firmly established is the association between interplanetary type II radio bursts and CME-driven shocks. Cane et al. (1987) clearly demonstrated that all interplanetary shocks that generate interplanetary type II radio bursts were associated with CMEs and that CMEs associated with interplanetary type II events were the most massive and energetic, with shock transit speeds in excess of 500 km/s. The chain of physics that lies between a CME and the observed type II radio burst is very complex. It includes the CME-shock interaction, electron energization at the shock (which depends on shock geometry), electrostatic wave generation, electromagnetic mode conversion, and scattering. Interplanetary radio emission is generated upstream of the CME-driven shock (Reiner et al., 1997; Reiner and Kaiser, 1999).

Figure 13 displays an example of interplanetary type II bursts where the radio intensity in the dynamic spectrum has been plotted versus 1/f where f is the frequency for the period of 24-26 August 1997. As the shock approaches Earth, these Type II bursts drift down in frequency because the electron density of the interplanetary medium to which the solar bursts are 'tied' is also constantly decreasing. As the interplanetary electron density n_e varies as R^{-2}, R being the radial distance from the Sun, and the emission frequency goes as $\sqrt{n_e}$, it follows that 1/f versus time will vary as R. Assuming a shock is travelling with a constant velocity v, type II radio emissions will be expected to be organized as a straight line since R=v(t-t0), t0 being the lift-off time. This representation facilitates tracking of the CME from the Sun to Earth and beyond. The shock speed can be determined from the slope of the line, provided that the electron density at 1 AU is known.

Dynamic radio spectra of type III bursts also allows one to determinate the propagation velocity of energetic electron beams (in the order of 100000 km/s) and

consequently the estimation of the arrival time at near Earth orbit for shock waves and electrons (Mann et al., 1999). An example of a type III burst is also seen in Figure 13.

Table 5 summarizes the radio signatures that may be observed in connection with physical processes (e.g. solar flare, shock, CME) that occur.

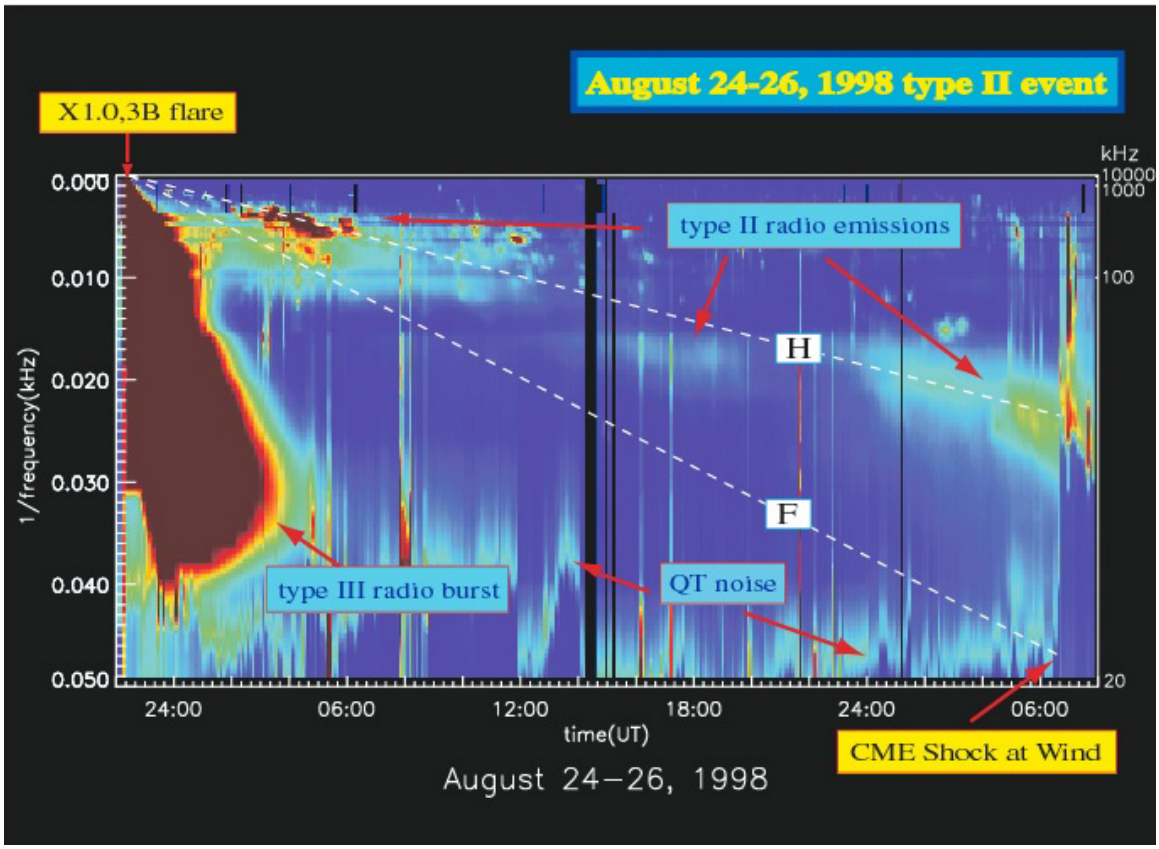

Figure 13. Wind/WAVES radio spectrogram as a function of inverse frequency along the ordinate and time. The slowly frequency-drifting emission of a type II burst starts shortly after the onset time of an X1.0, 3B solar flare on 24 August 1998. The observed weak type II radio emissions lie along straight lines, labeled F (fundamental) and H (harmonic), that originate from the CME solar lift-off time of ~23:10 UT on August 24. These radio emissions are generated up stream of the CME-driven shock at the fundamental and harmonic of the plasma frequency (Reiner et al., 1998). These emissions continued right up until the arrival of the CME shock at the Wind spacecraft at 06:40 UT on 26 August 1998.

Physical process	Flare/CME pre-eruption	Coronal shock dynamics (CME, Flare)	IP shock dynamics (CME)	Shock arrival at Earth (1 AU)
Radio signatures	Complex type III	Coronal type II	IP type II	Quasi-thermal noise

Table 5. Relations between physical processes and radio signatures.

1.4.2 Spatial and Intensity Particle Profiles

Particle fluxes turn into "Solar Particle Events" when a defined threshold is reached. SPEs depend both on the location of the observer (spatial profile) and the intensity of the particles (intensity profile). In the following an introduction to these two ways of observing the particles is given.

1.4.2.1 Spatial Profiles

The events of greatest interest are the large "gradual" events where an expanding CME drives a shock wave that can easily cross magnetic field lines and accelerate particles as the shock forms in the solar corona and continues as the shock moves out into the interplanetary medium. As the shock expands, it crosses many IMF lines, accelerating particles as it goes, out of the solar wind and/or from remnant particles of previous SPEs (Desai et al., 2001). These energetic particles propagate along the IMF lines flowing outward from the shock. Within tens of minutes of shock formation, particles are streaming outward over an extremely broad front.

Maximum acceleration occurs near the nose of the shock, ahead of the CME, and the intensity falls off around the flanks of the shock. As the structure propagates outward, the successive magnetic field lines that connect an observer with the shock sweeps counterclockwise across the shock's surface, averaging over diverse shock conditions.

When these particles arrive at the spacecraft, particle intensity increases are detected which constitute the SPEs. The details of the proton flux profiles during these gradual SPEs are consistent with the presence of a traveling CME-driven shock which continuously injects energetic particles as it propagates away from the Sun. Figure 14 shows the proton flux profiles as a function of longitude for several recent events observed by the ACE and IMP-8 spacecraft. The concept of "cobpoint" (Connecting-with-the-OBserver Point), defined by Heras et al. (1995) as the point of the shock front, which magnetically connects to the observer, is very useful to describe the different types of SPE flux profiles.

Solar events from the western hemisphere have rapid rises to maxima because, initially, the cobpoint is close to the nose of the shock near the Sun. These rapid rises are followed by gradual decreasing intensities because the cobpoint is at the eastern flank of the shock just where and when the shock is weaker. The observation of the shock at 1 AU in these western events depends on the width and strength of the shock.

Near central meridian the cobpoint is initially located on the western flank of the shock and progressively moves toward the nose of the shock. Low-energy proton fluxes usually peak at the arrival of the shock, being part of what are known as energetic storm particle (ESP) events.

For events originating from eastern longitudes, connection with the shock is established just a few hours before the arrival of the shock and the cobpoint moves from the weak western flank to the central parts of the shock; connection with the shock nose is only established when the shock is beyond the spacecraft and, usually, it is at this time when the peak particle flux is observed. The evolution of the low-energy ion flow anisotropy profiles throughout the SPEs reflects also the cobpoint motion along the shock front (Domingo et al., 1989).

For additional examples see Cane et al. (1988), Heras et al. (1995) or Kahler (2001).

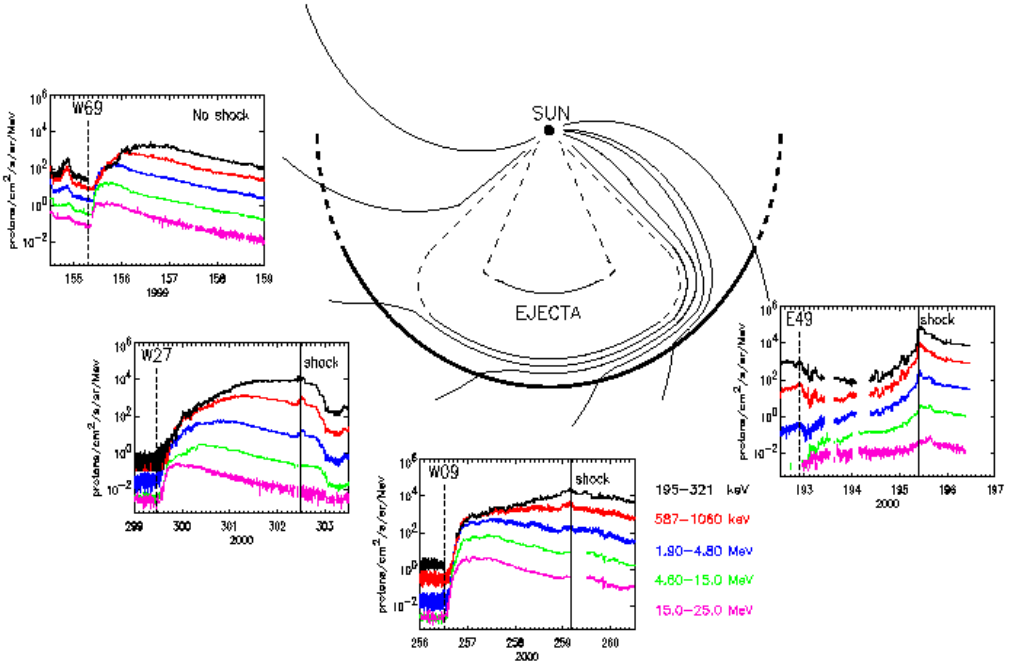

Figure 14. Illustration of the way in which typical energetic particle fluxes in large gradual events depend on the longitude of the observer. The observer of a western event (left panel) is well connected to the nose of the shock early on and sees a rapid rise and decline. An observer near central meridian is well connected until the shock passes, thus seeing a flat profile. The observer of an eastern event is poorly connected until the local shock has passed.
(Figure 15 of Cane et al. 1988)

1.4.2.2 Intensity Profiles

Particle "intensity profile" of SPEs take different forms depending on (Heras et al., 1988; Heras et al., 1995; Cane et al., 1988; Lario et al., 1998; Kahler et al., 1999):

- The heliolongitude of the source region with respect to the observer location.
- The strength of the shock and its efficiency at accelerating particles.
- The presence of a seed particle population to be further accelerated.
- The evolution of the shock (its speed, size, shape and efficiency in particle acceleration).
- The conditions for the propagation of shock-accelerated particles.
- The energy considered.

The current picture of intensity profiles can be summarized as follows:

- The SPE intensity is correlated with both the angular width and the speed of a CME (Kahler et al., 1984; 1987). However, some fast, well-positioned CMEs are not associated with SPEs, and some CMEs of modest speeds are associated with intense SPEs. In addition, the speeds, angular extents, and locations of the shocks relative to the CMEs are poorly known and currently measured only in situ at 1 AU or inferred at fixed points in space using radio scintillation observations.
- The peak particle intensities are better correlated with shock speed than with the measured CME speed (Reames et al., 1997). To reliably accelerate particles above 10MeV, the shock speed must exceed 750 km/s (Kahler, et al. 1987; Reames et al. 1997), thus it is only the largest and fastest ~1% of CMEs that produce SPEs. In the largest of these, shock speeds reach ~2500 km/s and particle intensities can increase as the 4^{th} or the 5^{th} power of the shock speed (Reames, 1999a, b).
- The precise location of the different particle populations and their relative importance depends on the speed and width of the CME and shock.
- There is a "streaming limit" to the maximum proton flux that can be accelerated by the interplanetary shock. The concept of streaming limit is that at some critical proton density, the self-generated waves by the protons gyrating around the magnetic field will scatter the particles out of the shock acceleration region thereby limiting the maximum flux (Ng and Reames, 1994; Reames and Ng, 1998). The streaming limit seems to apply to flux values exceeding 100 $(cm^2\ s\ sr\ MeV)^{-1}$. This steaming limit also generates a spectral hardening as the proton energy decreases.

2. EXISTING MONITORING AND WARNING SYSTEMS

2.1 Introduction

Relevant parameters for space flight beyond the Earth's magnetosphere include the structure of the spacecraft, the materials used to construct the vehicle, EVA start time and duration, the interplanetary proton and heavy ion flux and the position in the solar cycle.

For space flight beyond the Earth's magnetosphere, both crew and spacecraft equipment face a significant hazard from the natural ionizing environment. The primary radiation sources of this environment are energetic protons and heavy ions during SPEs, with energies up to a few 100 MeV, and Galactic Cosmic Rays (GCR), which consist of protons and heavy ions with energies in the GeV range. For some transportation scenarios the Earth's proton belts may also be a factor. Here only SPEs are considered.

The 10 MeV-threshold, for which particles penetrate a space suit, is also the energy that forecasters at the Space Environment Center (SEC) at the National Oceanic and Atmospheric Administration (NOAA) in Boulder, Colorado, USA <http://www.sec.noaa.gov/> monitor to watch for the onset of an SPE. SEC's proton event threshold is 10 protons/(cm^2.s.sr) at ≥10 MeV. The particles in an SPE can come either from a solar flare or from the shock wave driven by a CME. The shock-accelerated SPE particles travel toward and away from the Sun along the IMF threading the solar wind, but a significant fraction are trapped near the propagating shock by wave-particle interactions (Reames, 1997a). Thus, once the shock reaches Earth, the energetic proton flux can increase suddenly by as much as two orders of magnitude, making this shock spike the most dangerous portion of the solar particle event itself. The majority of SPE events are associated with CME-driven shocks, which take a day or two to reach us.

The existing warning centres that focus on SPEs are presented below. This is followed by an introduction to the various databases and models that are used for forecasting (warning) purposes.

2.2 Existing Warning Centres

The mission of the International Space Environment Service (ISES) is to encourage and facilitate near-real-time international monitoring and prediction of the space environment by the: 1. rapid exchange of space environment information; 2. standardization of the methodology for space environment observations and data reduction; 3. uniform publication of observations and statistics; and 4. application of standardized space environment products and services to assist users reduce the impact of space weather on activities of human interest.

Three basic functions accomplish the task of the ISES. First, the International URSIgram Service provides standardized rapid free exchange of space weather information and forecasts thru its Regional Warning Centres (RWC). Second, ISES prepares the International Geophysical Calendar (IGC) each year. This calendar gives a list of 'World Days' during which scientists are encouraged to carry out their

experiments. And third, the monthly Spacewarn Bulletins summarize the status of satellites in Earth orbit and in the interplanetary medium.

At present, there are eleven Regional Warning Centres scattered around the globe. These centres are located in China (Beijing), USA (Boulder), Russia (Moscow), India (New Delhi), Canada (Ottawa), Czech Republic (Prague), Japan (Tokyo), Australia (Sydney), Sweden (Lund), Belgium (Brussels) and Poland (Warsaw). The European Space Agency (Noordwijk) is the 12th centre, providing a venue for data and product exchange for activities in Europe. A data exchange schedule operates with each centre providing and relaying data to the other centres. The centre in Boulder plays a special role as "World Warning Agency", acting as a hub for data exchange and forecasts. For more information on the ISES and the RWCs see <http://ises-spaceweather.org/>.

For manned flight operations, specifically on the International Space Station (ISS), the USA and Russia rely on the same source of forecast and assessment, namely the Space Environment Center (SEC). SEC's Space Weather Operations Center (SWO) is the national and world warning center for disturbances that can affect people and equipment working in the space environment. Jointly operated by NOAA and the U.S. Air Force, SWO continuously monitors, analyzes, and forecasts the environment between the Sun and Earth. The Forecast Center receives solar and geophysical data in real time from a large number of ground-based observatories and satellite sensors around the world. SWO forecasters use these data to predict solar and geomagnetic activity and issue worldwide alerts of extreme events.

The Space and Radiation Analysis Group (SRAG) at Johnson Space Center (USA) is responsible for ensuring that the radiation exposure received by astronauts is within established safety limits. The radiation consoles in the Mission Control Center are staffed four hours daily during nominal space weather conditions, and continuously during extra-vehicular activities (EVA's) and significant space weather activity. SRAG works very closely with the SEC, which provides round the clock support, alerts and warnings about space weather conditions by telephone and pager and by displaying real time operational space weather data via the Internet.

When space weather reports indicate that conditions for significant change are present (even though an increase may not occur), the radiation consoles are manned for longer periods, and the team ensures that radiation monitoring hardware is fully functional. They may also recommend restricting or rescheduling of EVAs. When there is a confirmed increase in radiation exposure levels, SRAG monitoring operations in Mission Control increase to 24 hours per day. During such times, SRAG team members may recommend active seeking of shielded areas inside the spacecraft, and either the cancellation or revised scheduling of EVAs. In order to support mission planning, the Space Radiation Analysis Group maintains an extensive set of tools for estimating the exposure received by the crews of manned missions in Low Earth Orbit (LEO).

Figure 15 attempts to show the effectiveness of SRAG recommendations during ISS missions to reduce EVA exposures. The bars labelled "pre-EVA" were predictions/forecasts provided to the Flight Director the day prior to the actual EVA, using the planned EVA start/stop times. These predictions/forecasts attempted to include the effects of enhancements to the outer electron belt. Included in these forecasts/predictions were recommendations on how to reduce the anticipated EVA

exposures by adjusting the planned start/stop times. The bars labelled "as flown" were computed immediately following the EVA using the actual EVA start/stop times, trajectory segment, and status of the outer electron belt.

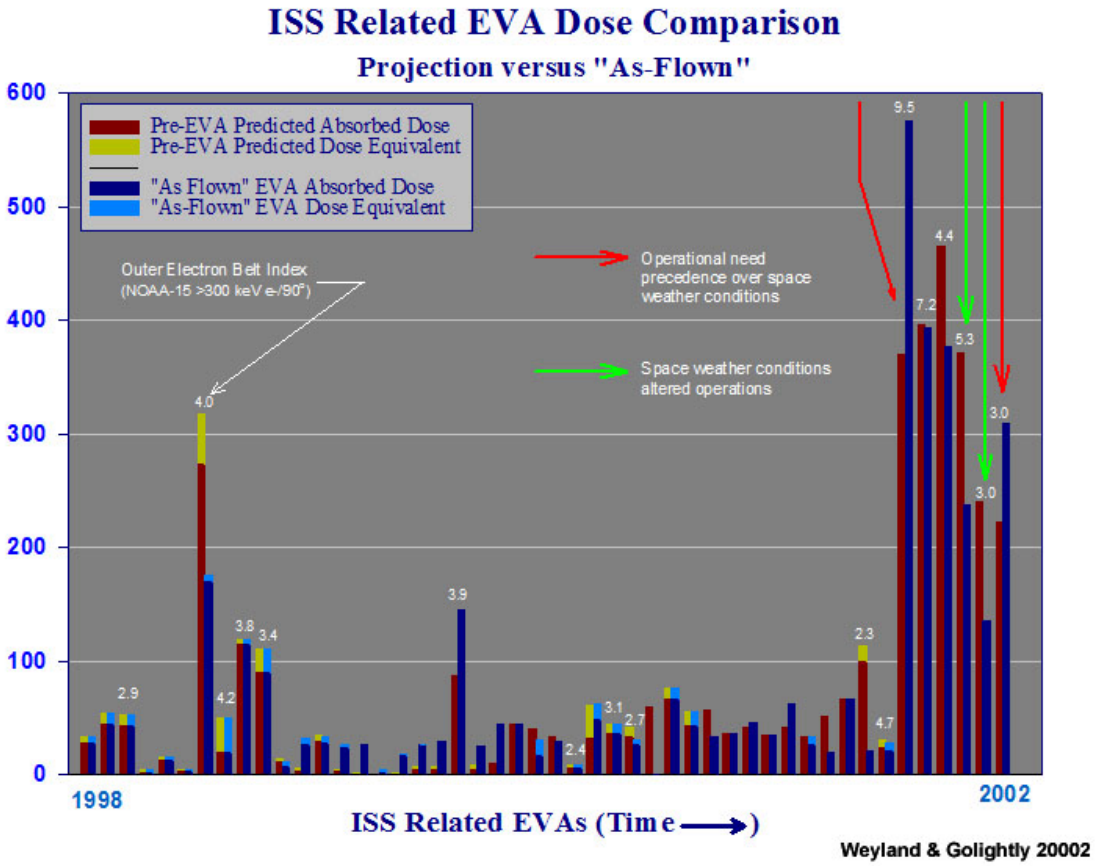

Figure 15. Chart of additional skin exposure (mrad/mrem). Courtesy of Golightly and Weyland (2002).

2.3 Spacecraft and Data Sources Relevant to Interplanetary Mission

Since SPE events present one of the most severe hazards in the space environment it is important to be able to predict when and how important an event may be on the basis of routine observation of the Sun and the upstream solar wind.

2.3.1 Continuous Monitoring of the Sun

Spacecraft in geostationary and Lagrange-1 (L1) orbits monitor the Sun and its corona in multiple wavelengths and so can diagnose solar flare potency and warn of oncoming CMEs with considerable skill. The upstream Lagrangian point (L1) is the position where the Sun's gravity and Earth's gravity balance to form, curiously enough, a virtual planet around which satellites can orbit in a plane perpendicular to a line connecting the Sun and

Earth. This orbital plane is about a half-hour to an hour of solar-wind travel time upwind from Earth, depending on solar wind speed.

Although active regions on the Sun that produce SPE events can be observed for a long period (up to months in some cases), until recently the ability to predict when an actual region might erupt into a large flare has been poor. Although a propensity to a flare may be noted, each flare onset is essentially a surprise.

2.3.1.1 Solar Flare Forecasting

Continuous monitoring of the Sun is essential for solar flare forecasting. Especially monitoring the solar global X-ray flux of the solar corona is a useful tool (see Figure 16). This figure originates from the NOAA/SEC "Today's Space Weather" web page <http://www.sec.noaa.gov/today.html> and illustrates the continuous global X-ray flux measured by monitors on geosynchronous satellites (GOES) as a function of time. GOES flares are classified in such a way that if the peak flux exceeds 1 x 10^{-6} Wm^{-2} (but less than 10^{-5}) then a C-class flare event has occurred. An event with a peak flux 10 times larger than this is a M-class flare, and 10 times larger still is denoted as an X-class event. Roughly speaking, there are about 20,000 C-class events in the period of a solar cycle, 2000 M-class events and 200 X-class events. This system of quantitatively classifying solar flare output, initiated in 1969, was defined on the basis of radio propagation effects on High Frequency (HF 3-30 MHz) broadcasts (Joselyn, 2001).

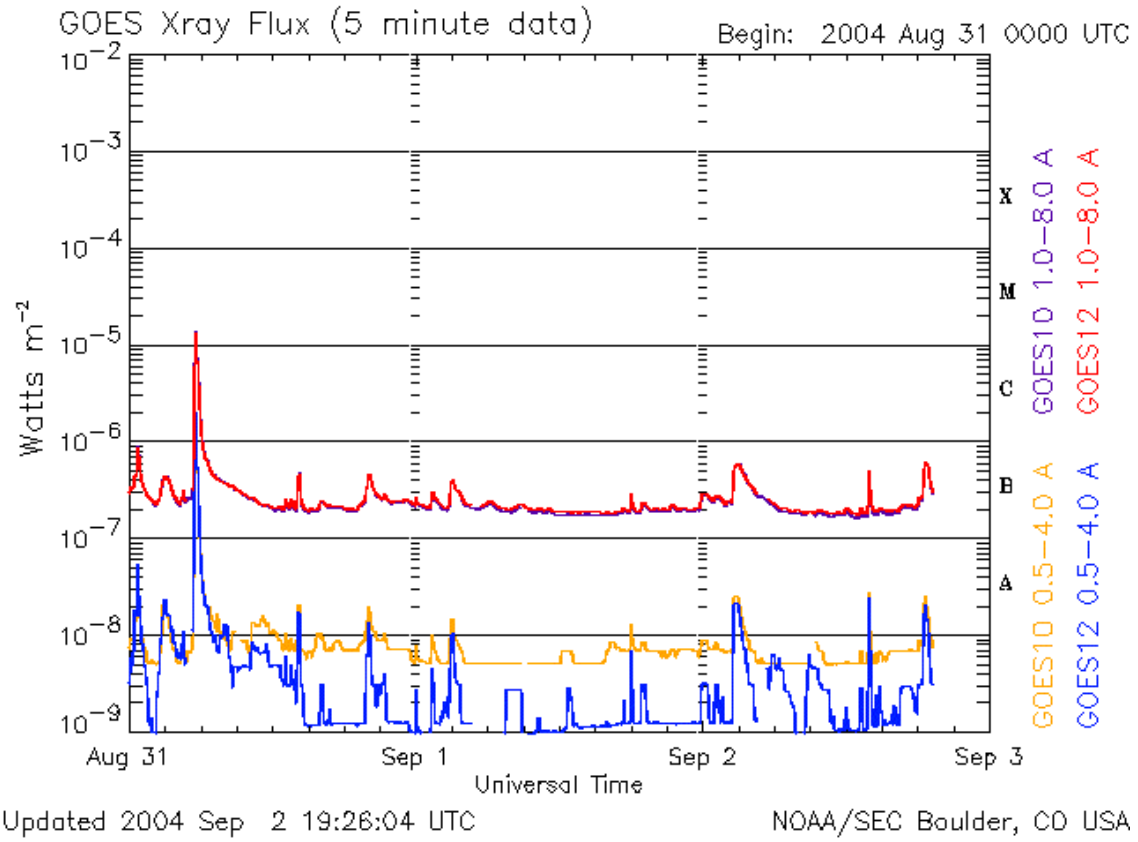

Figure 16. The total X-ray flux time profiles provided by the GOES spacecraft.

SEC delivers probability forecasts for the occurrence of one or more C-, M-, or X-class flares from on-disk active regions. Thresholds for alerts include X-ray events exceeding M5 (5×10^{-5} Watts m^{-2}) and X1 (1×10^{-4} Wm^{-2}) levels as measured in the 0.1-0.8 nm wavelength band. M and X-class events are forecast by analysing solar active region (sunspot group) characteristics. The larger and more complex a region, the more likely it is to produce the bigger events. Persistence is a factor in the forecasts: if a region is producing M or X-class activity, it is expected that it will persist in that behaviour.

The Flare Prediction System at Big Bear Solar Observatory (BBSO) gives alternative predictions based on the number of flares produced by regions classified using the McIntosh classification scheme (McIntosh, 1990) during cycle 22.

- Active region monitor at BBSO <http://beauty.nascom.nasa.gov/arm/latest/>.
- BBSO Flare Prediction System <http://beauty.nascom.nasa.gov/arm/latest/forecast.html>

A similar system is used at the Solar Influences Data analysis Center (SIDC), the RWC in Belgium.

- SIDC <http://sidc.oma.be>

Solar Events Lists edited by SEC show GOES 12 and GOES 10 X-ray events (see details at <http://www.sec.noaa.gov/GOES.html>). In addition, they include GOES Solar X-ray Imager (SXI) flare reports, which provide valuable flare location and other information, especially when no optical observations are available. For near-real-time SXI images and a description of the GOES SXI instrument see <http://sec.noaa.gov/sxi/>.

In addition the Reuven Ramaty High Energy Solar Spectroscopic Imager (RHESSI) also provide flare reports <http://hesperia.gsfc.nasa.gov/rhessidatacenter/>.

Like solar X-rays, energetic protons at geosynchronous orbit are also measured onboard the GOES spacecraft and a 3-day plot, updated at 15-minute intervals, is available at SEC's "Today's Space Weather" web page <http://www.sec.noaa.gov/today.html>.

2.3.1.2 CME Velocity Forecasting

Possible indicators of CME speed that can be used in forecasting are:

1. The flux emergence in underlying active regions: the field strength changes at the base of newly opening field lines, reflecting only the average strength of the photospheric fields, is somewhat subjective at this stage.
2. The "fs" value of the newly opened fields, where "fs" indicates the flux tube divergence between the photosphere and source surface considered by Wang and Sheeley (1990) to determine solar wind velocity.
3. Observable coronal hole changes.

The first two possibilities more generally reflect the idea that CMEs are produced when coronal fields open in response to photospheric field changes, whether or not a noticeable coronal hole change occurs. CMEs are presumed to be associated with solar magnetic field changes visible on the solar "surface" or photosphere (Luhmann et al., 1998). Even though they involve the opening of new regions on the Sun, the opening regions can be at the edges of helmet streamer belts and barely change adjacent coronal hole areas or shapes. On the other hand, the newly opening region can in principle alter a coronal hole in an important and observable way. More information can be found at: <http://sprg.ssl.berkeley.edu/mf_evol>.

2.3.2 Far Side Imaging Services

Continuous monitoring of the Sun, using SOHO-type instruments could provide early warning for many if not the majority of SPE events aimed towards Earth. Of particular interest for a manned mission to Mars are the far side imaging services provided by SOHO's Solar Wind Anisotropies (SWAN) instrument and the Michelson-Doppler Imager (MDI)/SOHO. These tools may be used to monitor the magnetic activity of the far side of the Sun, but their reliability for delivering a backsided space weather forecast is difficult to assess at this time.

The SWAN instrument is designed to observe solar Lyman alpha photons (121.6 nm) backscattered by the neutral hydrogen atoms present in the interplanetary medium. The background images show the distribution pattern of the backscattered Lyman alpha photons as observed from SOHO. This image, obtained in approximately 24 hours, is then processed to reveal spatial variations of the solar illuminating flux. These spatial variations are correlated to the actual activity on the solar disk. Because SWAN observes backscattered photons, it is actually possible to 'see' those which originate from the farside of the Sun. SWAN performs three 'full-sky' observations per week. Images of the solar flux spatial distribution are displayed on-line 2 to 4 days after the observation. See <http://sohowww.nascom.nasa.gov/data/summary/swan/> for more information.

The farside MDI images are maps of wave speed variations with locations of faster wave speed shown darker. These darker regions indicate locations where there is an accumulation of magnetic field on the far surface. The farside images can only be computed out to 45 degrees from the farside disk centre as (un)seen from Earth. A full 24-hours of MDI surface velocity data is used to compute each image. A new whole-Sun map is computed for each 12 hours. For more information see Lindsey and Braun (2000) and <http://soi.stanford.edu/data/farside/index.html>.

2.3.3 Coronagraphs and EUV Imaging

For the monitoring of CMEs, coronagraphs are important to have onboard satellites. The Solar & Heliospheric Observatory (SOHO) project, supported by ESA and NASA (see <http://sohowww.nascom.nasa.gov/>) carries the Large Angle and Spectrometric Coronagraph (LASCO) experiments. LASCO observes a number of halo CMEs directed at or away from Earth, which appear as expanding annuli or disks of enhanced density roughly centred on the Sun.

Because coronagraphs are constrained to observe limb events best, however, their data alone do not distinguish those CMEs aimed toward Earth from those originating from the far side of the Sun. The source region can be derived best from concurrent extreme ultraviolet observations of the lower corona using, for example, the Extreme Ultraviolet Imaging Telescope (EIT), also onboard SOHO, which is sensitive to the high-temperature plasmas and transient dimmings that are characteristics of eruptive events.

2.3.4 Radio Frequency Emissions

Metric Type II radio bursts that are signatures of coronal shock waves are usually associated with solar flares. Accordingly, the United States Air Force (USAF) established a worldwide network of sweep frequency recorders from which, given a coronal density model, estimates of the shock speed in the corona can be made. This network, called the Radio Solar Telescope Network (RSTN), uses a bandwidth from 25 MHz to 85 MHz. It is complemented in this real-time capability by a radio telescope operated from 25 MHz (the ionospheric cutoff) to 1800 MHz by the Ionospheric Prediction Service in Culgoora, Australia. The USAF/RSTN system is currently being upgraded in frequency to a bandwidth from 25 MHz to 180 MHz by the Solar Radio Spectrometer (SRS) system at Palehua, Hawaii; San Vito, Italy; Sagamore Hill, Massachusetts (site to be or moved to Holloman AFB, New Mexico); and Learmonth, Australia.

A list of radio bursts compiled and updated every 30 mn by SEC is available at <http://www.sel.noaa.gov/ftpdir/lists/radio/radio_bursts.txt>.

Instruments on Earth cannot detect interplanetary type II bursts because the ionosphere blocks the waves. Only an observatory in space can detect them. Figure 17 clearly illustrates the importance of tracking the radio disturbances in the interplanetary medium and particularly when the radio instrument is equipped with antennas having the direction finding capability. Radio direction-finding measurements on one spacecraft, such as Wind or Ulysses, give the radio source direction and angular size as a function of frequency (Manning and Fainberg, 1980). If one assumes an emission mode, fundamental or harmonic, and a density model (Saito et al, 1977 or $n_e \sim 1/R^2$), this measurement gives the heliospheric position of the radio source as a function of time. This method is used successfully with Wind/WAVES data, in conjunction with the SOHO/LASCO coronagraph images of halo CMEs, to predict the encounter times of CMEs with Earth. This method, however, overlooks the radiation pattern of the burst, which again depends on the mode (e.g. Steinberg and Caroubalos, 1970).

The WAVES investigation on the WIND spacecraft provides comprehensive coverage of radio and plasma wave phenomena in the frequency range from a fraction of a Hertz up to about 14 MHz for the electric field and 3 kHz for the magnetic field. For more information see <http://www-lep.gsfc.nasa.gov/waves/waves.html>.

The same example, however, shows also the limitation of this method. Indeed, interplanetary type II emissions are composed of discrete, narrow frequency bandwidth features, dispersed in time and thus the type II identification may be rather delicate to establish before having obtained the full history of the event, i.e. before the disturbance has reached the Lagrange point. Methods for automatic detection and identification are currently being developed (Hoang, private communication).

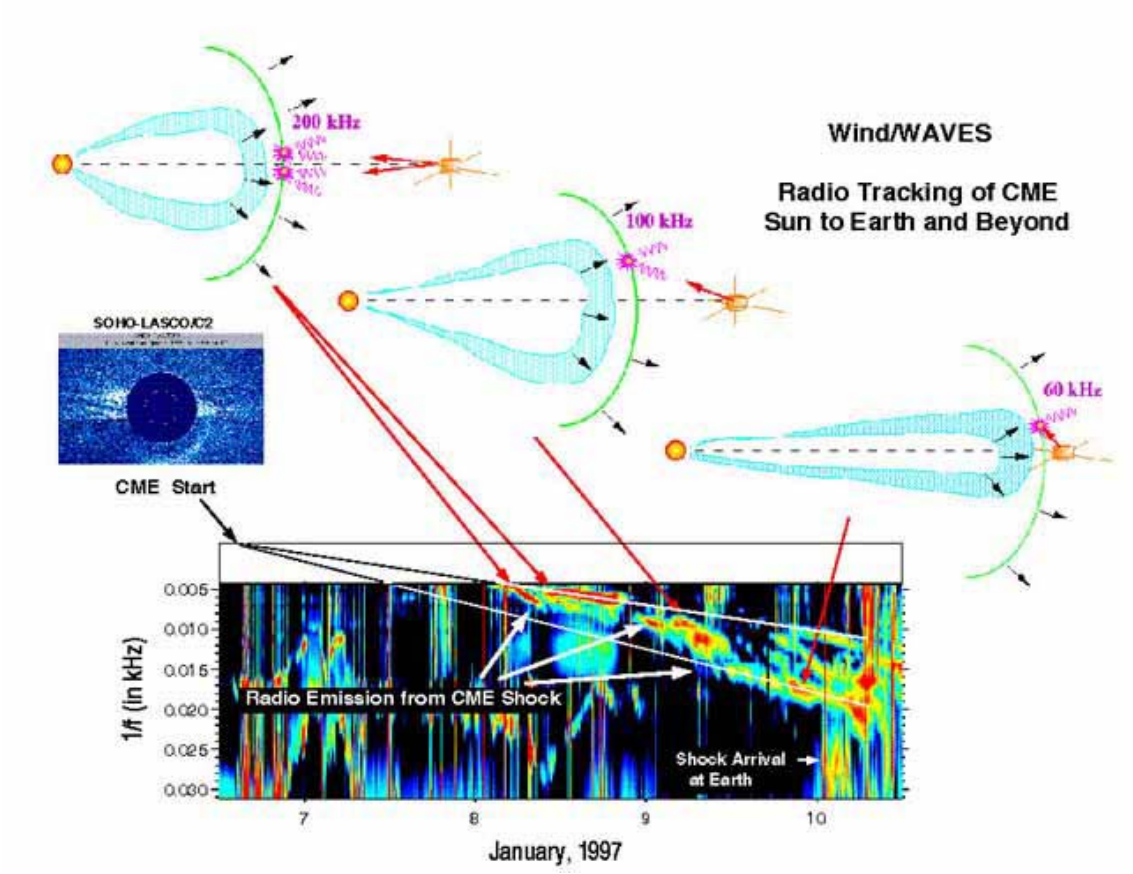

Figure 17. Wind/WAVES radio spectrogram of the CME/magnetic cloud event of 6-10 January 1997. After it was launched from the Sun in the direction of Earth, the CME of January 6 was quickly lost from view because it became too diffuse to be seen by the LASCO telescope. Thus for its long journey of 1AU to Earth, the CME would have been completely out of sight except for the remote sensing capability of the WAVES instrument on the WIND spacecraft. The cartoons above the spectrogram illustrate the derived location of the shock at three times during its traverse from the Sun to Earth.
From <http://www-istp.gsfc.nasa.gov/istp/cloud_jan97/waves_cme.html> , courtesy of M. Kaiser.

2.3.5 Early Warning from the L1 Point

In situ data from satellites along the Sun-Earth line at L1 are in a position to issue warnings that an interplanetary CME is in a direct line with Earth. Certain conditions indicating the passage of a shock or interplanetary CME structure may be observed, for example, high alpha to proton (a/p) density ratios (>10%) or higher than nominal ionisation states (e.g., O^{+7}/O^{+6} ratios) in the solar wind, kinetic temperatures and their anisotropies for solar wind ions and electrons, electron bi-directional heat flux, and large deltas in the magnitudes of the interplanetary magnetic field (IMF), solar wind velocity (V) or density (n).

Monitoring the solar wind speed, the IMF and the proton levels at the Earth's L1 point provides an input to models of the interplanetary space. A strategically placed fleet of spacecraft, described below, is currently providing space weather information on the radiation environment at 1 AU.

2.3.5.1 Solar Heliospheric Observatory (SOHO) Spacecraft

The ESA/NASA SOHO spacecraft was launched on 2 Dec. 1995 and is still operational <http://sohowww.nascom.nasa.gov/>. SOHO consists of many instruments for monitoing the Sun, especially those that detect particles:

1. The Charge, Element, Isotope Analysis System (CELIAS) experiment is comprised of five sensors (CTOF, MTOF, PM, STOF/HSTOF, SEM). The Mass Time-of-Flight spectrometer (MTOF) is made up of the 1.) MTOF/Main**:** the primary unit, providing solar wind elemental and isotopic abundance measurements 2.) MTOF/Proton Monitor: an auxiliary unit designed to measure the solar wind proton parameters, including speed and direction. For more information see <http://umtof.umd.edu/pm/instrument.html> and <http://umtof.umd.edu/pm>.

2. The Energetic and Relativistic Nuclei and Electron experiment (ERNE) investigates the solar atmosphere by detecting charged particles produced in various solar energy release processes and is undertaking the first systematic survey of solar energetic particle isotopic abundance <http://www.srl.utu.fi/projects/erne/main_english.html>.

2.3.5.2 Advanced Composition Explorer (ACE) Spacecraft

By continuously measuring the solar wind and the IMF, ACE and the solar wind monitor CELIAS/SOHO detect a CME's bow shock a half hour or more before it reaches Earth and after that the CME itself. Moreover, the Solar Isotope Spectrometer (SIS) onboard ACE continuously monitors the full, unshielded intensity of the SPEs. ACE web-sites of interest are located at:

1. ACE Near Real-Time Data: <http://sec.noaa.gov/ace/ACErtsw_home.html>.
2. SIS/ACE: <http://www.srl.caltech.edu/ACE/CRIS_SIS/sis.html>.

2.3.5.3 WIND and the Triana Mission

WIND Spacecraft: Solar-wind measurements from the spin-stabilized WIND spacecraft can only be made when the Faraday Cup points towards the Sun. As a result, measurements are not continuous. WIND near real-time data is made available at <http://pwg.gsfc.nasa.gov/windnrt/>.

Triana Mission: The future Triana mission is a 3-axis stabilized spacecraft permitting near-continuous measurements at several times per second. The ion and electron instruments (Faraday Cup) and magnetometer making up the Plasma-Mag instrument are all improvements over their counterparts presently flying in a highly successful manner

on the WIND spacecraft. The software system to be used to reduce and interpret the data from this package is derived directly from the system in use for WIND. For more details see the Plasma-Mag/Triana web-page:
<http://triana.gsfc.nasa.gov/instruments/plasmag.htm>.

At the moment Triana is in a storage container and will reside in GSFC's large clean room until a viable flight opportunity has been identified.

2.3.5.4 Genesis Mission

Genesis is a solar-wind sample return mission that was launched August 8, 2001. It is spending 2+ years collecting solar wind on large-area ultra pure substrates while in a halo orbit around the Earth-Sun L1 point <http://genesismission.jpl.nasa.gov/>. These samples are to be returned to Earth in September 2004 for high-precision isotopic and elemental analysis. A key aspect of the mission is to collect separate samples of different types of solar wind-interstream, coronal hole, and coronal mass ejection.

To distinguish these types in real time the spacecraft is equipped with a Genesis Electron Monitor (GEM) and a Genesis Ion Monitor (GIM). These *in situ* spectrometers have dual roles of (1) providing raw data to a science algorithm in the spacecraft C&DH unit to command the collection arrays, and (2) providing a solar-wind plasma data set available to the Space Physics community. The website <http://genesis.lanl.gov/> provides the GIM and GEM data set.

Both the GEM and GIM have been in continuous operation since shortly after launch and continue to return high-quality data on the solar wind flow near 1 AU. The plan is to continue solar wind data acquisition until approximately thirty days before the Genesis samples are returned to Earth and then, if funding is approved, the Monitors will again resume solar wind measurements, this time for a new space physics mission called Exodus.

2.4 Long Term Phenomena Variability

Space weather also includes the ability to forecast the solar cycle and the phenomena dependent upon the long-term variation in solar activity. A reliable prediction of the activity expected during future solar cycles would greatly aid in selection of the optimum time for the launch of a manned mission to interplanetary space.

2.4.1 Solar Cycle Variations

The solar cycle has nominally an eleven year duration, but can vary by a few years. Solar flares, CMEs and associated solar emissions are most prevalent during a seven-year period around solar maximum. The regularly occurring co-rotating structures are prevalent during the declining years of the cycle.

Using solar proton data from the past four solar cycles, Shea and Smart (2002) found that there is a surprising consistency in the total number of proton events over each cycle. In comparing the distribution of solar proton events during the rising portion of cycles 19-23, they find a similarity between the 20^{th} and the 23^{rd} solar cycles. During

solar cycle 20, only 17% of the proton events for the entire cycle had occurred during the first three years of the cycle and 28% had occurred during the first four years. If cycles 20 and 23 are similar, they would expect the majority of solar proton events to occur during years 5-8 of the 23rd cycle (i.e. from 2001-2004). Figure 18 shows this tendency for the years (1955-1995).

2.4.2 Long-Term Prediction of Solar Proton Fluences

Essentially three solar proton event models are available to the spacecraft engineer for predicting long-term solar proton fluences: 1 the King model, 2. the JPL model, and 3. the Emission of Solar Protons (ESP) total fluence and worst case event models. These models are reviewed and made available for use on the SPENVIS website and are described here: <http://www.spenvis.oma.be/spenvis/help/models/sep.html>.

1. The King model (King, 1974), was for a long time the standard model used to predict mission integrated solar proton fluences. It has been coded and made available to the community by NSSDC (Stassinopoulos, 1975). The King solar proton model was constructed using data obtained exclusively during the active years of solar cycle 20 (1966-1972). There are 25 individual events used in this database, including the great proton event of August 1972, which accounted for about 70% of the total >10 MeV fluence for the complete solar cycle. Additional information on the SOLPRO Model 1975 is available at <http://nssdc.gsfc.nasa.gov/space/model/sun/solpro.html>.

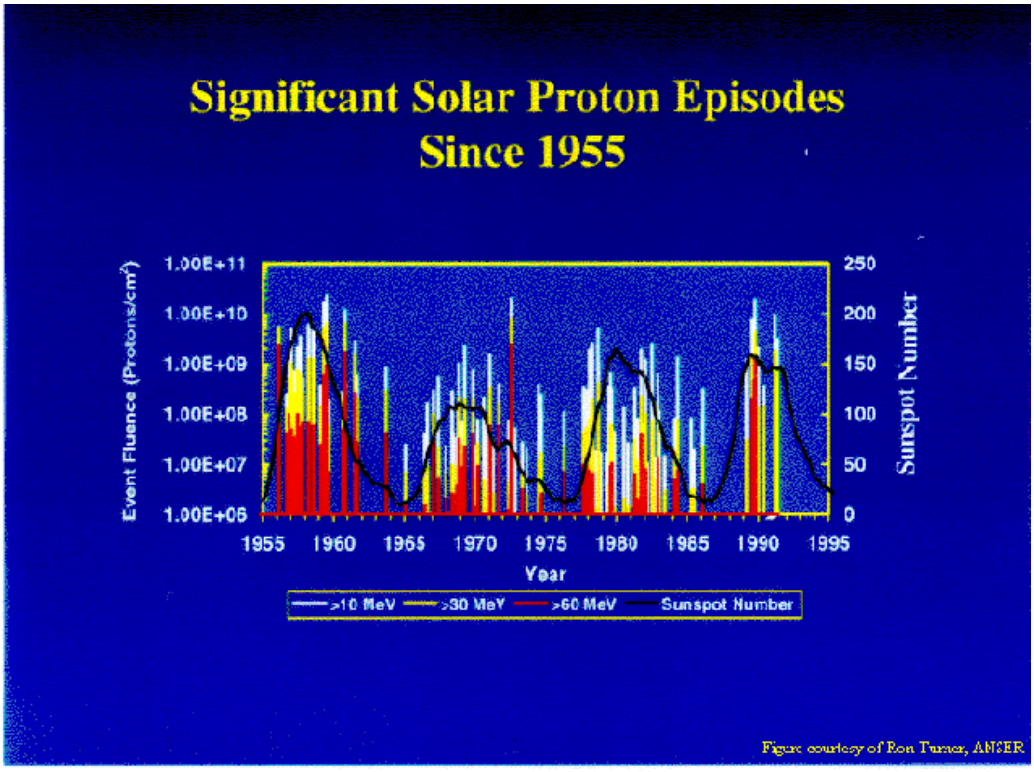

Figure 18. Solar proton episodes (at different energies) as a function of sunspot number. Image courtesy of Ron Turner of ANSER and Robert C. Reedy of Los Alamos National Lab.

2. The JPL model has been recommended for use for mission planning (Shea et al., 1988). Additional information on the JPL Proton Model 1989 is available at: <http://nssdc.gsfc.nasa.gov/space/model/sun/jpl.html>. The newer version is the JPL-91 model (Feynman et al., 1993). The data set used includes observations obtained since 1956 (covering solar cycles 19 up to the middle of cycle 22) and consists of a nearly continuous record of daily average fluxes above the energy thresholds of 1, 4, 10, 30, and 60 MeV. The proton events considered in the JPL models are defined as the total fluence occurring over series of days during which the proton fluence exceeded a selected threshold. The thresholds for the JPL-91 model (in cm^{-2} s^{-1} sr^{-1}) are 10, 5, 1, 1, and 1 for the five energy thresholds.

3. The King and JPL models are very useful for predicting event fluences for long-term degradation but do have limitations due to the incomplete nature of the data sets upon which they were based. The Emission of Solar Protons (ESP) total fluence and worst case event models (Xapsos et al., 1999, 2000) provides the underlying or initial distribution of solar proton event fluences. Solar proton event data from the last three complete solar cycles (20-22) were processed to obtain the event fluences. Additional information is available at:
<http://www.spenvis.oma.be/spenvis/help/background/flare/flare.html>.

2.5 Solar Flare Protons: Forecast and Models

2.5.1 Flare Models

The solar magnetic field plays a fundamental role in the production of flares and is the essence of several areas of flare modelling. Because the coronal magnetic field cannot be observed directly, as yet, the only method for determining the field there is to observe it at the photosphere and use numerical modelling to extrapolate it into the corona. This method has had considerable success in matching observations from present magnetographs and the Yohkoh satellite. Because much higher quality data is expected in the next few years, magnetic extrapolation models must be extended to much higher numerical resolution.

The fundamental process by which magnetic free energy in the corona is released is believed to be magnetic reconnection. Rigorous models for 3D reconnection, including consideration of the processes that determine the distribution and magnitude of resistivity, are the most important challenge to understanding flare physics, and to obtaining a physics-based model for flare prediction.

Models relating to the processes that produce flare-generated transient UV, EUV, and X-ray bursts are potentially valuable for flare effect prediction because they can tell us something about the energetics of the flare and in particular about the potential for producing flare-generated solar energetic particles. Similarly models of the processes that accelerate particles in flares and determine whether and where they are released from the flare site are useful in building forecasting schemes for this particular component of the SPE population.

2.5.2 Short-Term Prediction of Solar Proton Events

A product tested at SEC is the forecast of the probability of energetic protons (MeV energies) from solar flares. This algorithm uses the ratio of the fluxes in the two X-Ray bands measured by GOES to estimate the likelihood of prompt arrival of energetic protons (Garcia et al, 1999).

SEC uses a computer program known as PROTONS (Kunches, 1991). The inputs to this program are as follows (ISU, 1998):

- Flare X-ray data: the X-ray flux from a flare integrated over time can act as a quantitative measure of the energy output leading to an estimate of the flux of particles accelerated in the event.
- Location of the flare site from observations of the solar disk in H-alpha. This can then be related to the foot of the best-connected field line to the Earth (given an estimate of the topology of the interplanetary medium).
- Radio data, both of type II (associated with accelerating shocks) and type IV (associated with high energy electrons, from flares, trapped in the coronal magnetic field). These data are not direct indicators of proton events but are often associated with them and so may be used to give a probabilistic weighting to any predictions.
- The bulk velocity of the solar wind can be used to estimate the time of arrival of the proton event.

The output of this model is then a percentage probability of a particle event occurring and an estimate of the peak flux of the event.

2.6 Solar Protons from Interplanetary Shock Dominated Events: Forecasts and Modeling

2.6.1 Modeling SPE Acceleration and Transport

The simulation of particle events requires knowledge of how particles and shocks propagate through the interplanetary medium, and how shocks accelerate and inject particles into interplanetary space.

For the moment, no theoretical and/or numerical model treats SPE acceleration and transport near its full complexity. The modelling of particle fluxes and fluences associated with SPE events has to consider:

- The changes in shock characteristics as it travels through the interplanetary medium.
- The different points of the shock where the observer is connected to.
- The conditions under which shocks accelerate and inject particles into interplanetary space.
- The conditions under which particles propagate.

There have been several attempts to model these events. Each model presents its own simplifying assumptions in order to tackle the series of complex phenomena occurring during the development of SPE events. There exist several models for describing the propagation of particles. Two main approximations have been used to describe the particle transport: the cosmic ray diffusion equation (Jokipii, 1966) and the focusing-diffusion transport equation (Roelof, 1969; Ruffolo, 1995). A summary of the state-of-the-art and historical development of the modelling of SPE events associated with CME-driven shocks can be found in this page by D. Lario:
<http://www.am.ub.es/~blai/enginmodel/SEP_History.html>.

To describe the shock propagation, approximations range from considering a simple semicircle centred at the Sun propagating radially at constant velocity, to fully developed magnetohydrodynamic (MHD) models. There are few fully developed MHD models to describe the evolution of interplanetary shocks. This is a problem since the injection of shock-accelerated particles is assumed to occur from the instantaneous position of the front of the shock as it propagates. Different models are in different stages of maturity. Some are empirical, some are "physics-based"; most are hybrid. We review the following models that predict solar wind speeds or interplanetary shock arrivals:

- CME models (empirical).
- Solar magnetogram-based models (semi-empirical).
- Metric type II-based models (physics-based).

They will be discussed in the next three sub-sections.

2.6.2 CME Models (Empirical)

A number of empirical models based on CME observations are being developed to predict ICME arrivals and/or effects at Earth. Because the frequency of occurrence of CMEs is much higher of that of IP shocks, a sub-set of CMEs, the halo or partial halo CMEs are used by these models. All the models require the CME speeds and some also require the location of the sources, obtained from image data. The speed values are obtained in near real time from SOHO/LASCO data analysed by SEC/SWO forecasters.
See <http://lasco-www.nrl.navy.mil/cgi-bin/halocme_parse> for event list.

2.6.2.1 Schwenn Model

This model uses the fastest plane-of-the-sky CME speed as well as the speed measured in the perpendicular direction, and requires that the CME also be observed in the LASCO C3 detector. Details about this model are described in Schwenn et al. (2000).

2.6.2.2 Gopal Model

This model uses the fastest plane-of-the-sky CME speed, requires information on the source location, and uses a threshold speed. This model was derived to predict arrival of ICMEs (magnetic clouds) and is described in Gopalswamy et al. (2001).

2.6.2.3 Smithtro Model

The model is based on halo CMEs only. As input it requires the fastest plane-of-the-sky CME speed and information on the source location. If the source location is east of E45, then little or no response is expected at 1 AU. This model is described in Smith et al. (2003).

Although the (plane-of-the-sky) speed of a CME can be estimated out to ~30 R_S from coronagraph images, the speed at these distances is often significantly greater than the CME transit speed through the interplanetary medium and can therefore lead to predicted encounter times that may be in error by a day or more.

2.6.3 Solar Magnetogram-Based Models (Semi-Empirical)

Photospheric daily updated WSO, MWO, and NSO synoptic maps from Wilcox (WSO), Mount Wilson (MWO), and National/Kitt Peak (NSO) Solar Observatories are used for models at NOAA-SEC to make predictions of solar wind stream structures based on the Wang/Sheeley approach, and at the University of California at Berkeley (UCB) to track newly opening coronal magnetic fields.

Wilcox Solar Observatory (WSO) <http://quake.stanford.edu/~wso/wso.html> full disk magnetograms (e.g., Hoeksema and Scherrer, WDCA Report UAG-94)
Kitt Peak National Solar Observatory (NSO) <http://nsokp.nso.edu/> magnetograms
Mt. Wilson Observatory (MWO) <http://www.astro.ucla.edu/~obs/intro.html>

2.6.3.1 Wang-Sheeley Model

The Wang and Sheeley scheme involves a semi-empirical approach (Wang and Sheeley, 1990) and does not include transients. High speed/low speed solar wind stream interactions are treated using simplified parameterisations. Similarly, the opening coronal fields monitor at UCB uses potential field source surface models that cannot describe transients or their interplanetary evolution.

They consider the flux tube divergence between the photosphere and source surface to determine solar wind velocity. 72 5^o x 5^o cells lie along the ecliptic line of each synoptic map, therefore the solar wind speed/IMF polarity can be predicted with a time resolution of about 1/3 day (i.e., 27.2753/72 = 0.38 days). Typically, 3-day and 4-day advanced predictions provide the best overall agreement with the observations, because the mean propagation time from the source surface to Earth is about 3 to 4 days.

More information about the Wang-Sheeley Model can be found at:
<http://solar.sec.noaa.gov/ws>.

2.6.3.2 Opening Coronal Field Model

The scheme applied is based on the presumption that CMEs are associated with solar magnetic field changes visible on the solar "surface" or photosphere (Luhmann et al., 1998). The coronal PFSS (Potential Field Source Surface Model) is used to see coronal magnetic field changes between two consecutive photospheric magnetic field observations. The coronal field lines are traced from a fixed grid on the photosphere at two times and compared. Only those fields that were closed at an earlier time and open at the later time (newly opening field lines) are selected and plotted.

Field line tracings from a 1 deg. x 1 deg. grid of starting points on the photosphere to a spherical source surface at 2.5 Rs are used to determine which regions on the Sun change from magnetically closed to open between consecutive magnetograms. The starting points in the newly open regions are then used to trace the subset of field lines showing the locations for possible eruptions. CMEs, if associated with photospheric field changes, typically erupt in minutes to hours. While it would be best to use the highest time resolution data available to construct the models, (e.g. the SOHO MDI data with 96 min. resolution), it is also possible to use the daily magnetograms from WSO or KPNO to provide a running "update" as they are processed. The current version automatically uses the most recent daily update model together with the previous model (regardless of the time elapsed between). See <http://sprg.ssl.berkeley.edu/mf_evol> for details.

2.6.4 Metric Type II-Based Models (Physics-Based)

Modeling the propagation of fast CMEs and their associated shocks through the heliosphere, even with one- and two-dimensional MHD codes, has reached the point of demonstrating measurable skill in predicting shock speeds and arrival times at Earth (Dryer, 1994). Recent improvements to these models include the incorporation of three dimensions, the ambient solar wind structure, and the heliospheric current and plasma sheets (Odstrcil and Pizzo, 1999a, b).

These models are run in near real time (NRT) (predictions are made and sent out before the arrival of the IP shock) whenever a metric type-II report is received, together with estimates of the shock velocity, and with observations of a simultaneous GOES Soft-X-ray flare and an optical or image identification which gives the source location. These mailings are called the 'fearless forecasts'. The models used are:

2.6.4.1 Shock Time of Arrival (STOA) Model

The "STOA" model is based on similarity theory of blast waves, modified by the piston-driving concept, that emanate from point explosions. The initial explosion (flare) drives a shock. The shock is assumed to be initially driven at a constant speed, V_s, for a specified length of time (using GOES X-ray duration as discussed by Smith et al., 1994) and then allowed to decelerate as a blast wave ($V_s \sim R^{-1/2}$ where R is the heliocentric radius) as it expands outward. The magnitude of the total energy conversion process determines the solid angle of quasi-spherical shock propagation and how far it would propagate as it "rides over" a uniform background solar wind. It is assumed that the fastest part of the shock is nearly coincident with the heliocentric radius vector from the centre of the Sun

through the flare site. The flanks of the shock would first decay via viscous and ohmic dissipation to an MHD (magnetohydrodynamic) wave. The shock speed directly above the flare is calculated from the Type II radio frequency drift rate (together with an assumed coronal density model) via the plasma frequency, which is proportional to the square root of the local electron density. Based on the empirical studies of Lepping and Chao, (1976), STOA uses a cosine function to account for longitudinal dependence of the shock geometry in the ecliptic plane. The shock speed is assumed to decrease from the maximum in the direction of the flare via this cosine function, to give a non-spherical shape in longitude. This spatially dependent shock speed is taken to be constant during the piston driven phase. During the blast wave phase, the longitudinal cosine shape is maintained. STOA allows for a radially variable background solar wind, which is uniform in heliolongitude. No structures such as stream-stream interactions are considered.

This model is described in Dryer and Smart (1984) and information about the model can be found on the web-site <http://www.expi.net/expinet/stoa-ispm.html>.

2.6.4.2 Interplanetary Shock Propagation (ISPM) Model

The "ISPM" is based on a 2.5 D MHD parametric study of numerically simulated shocks (Smith and Dryer, 1990). This study showed that the net energy input into the solar wind is the organizing parameter. If the net energy ejected into the solar wind by a solar source and its longitude are known, then the transit time and strength of the shock to 1AU may be computed from algebraic equations given in that paper. That study also showed that, for drivers longer than ~2hrs, the properties of the leading shock remain unchanged. Therefore, drivers with durations longer than 2 hours are truncated to 2 hours in the ISPM. Smith and Dryer (1995) give the details of this model and the functions in energy-longitude space. Since the energies of solar ejecta are not available from observations, they describe how the net input energy is estimated from proxy input data. The ISPM uses the same observational data as the STOA model.

This model is described in Smith et al (2000) and more information is located at the web site: <http://www.expi.net/expinet/stoa-ispm.html>.

2.6.4.3 Hakamada-Akasofu-Fry (HAFv2) Model

The "HAF" solar wind code is under continued development by the Geophysical Institute, University of Alaska, Fairbanks, and EXPI. The HAF model is a "modified kinematic" model. "Kinematic" in that the model kinetically projects the flow of the solar wind from inhomogeneous sources near the sun out into interplanetary space. "Modified" in that the model adjusts the flow for stream-stream interactions as faster streams overtake slower ones. Whereas the MHD solutions integrate the equations of motion to obtain velocity, the kinematic model begins with the equations integrated twice to yield the fluid-parcel positions; velocity then comes from dx/dt.

The HAF model has two components: 1. ambient and 2. event-driven.

1. Ambient Wind

The ambient, or background, solar wind is established by the model's initial conditions on the inner boundary. The outflow of plasma is radial from a rotating, inhomogeneous source surface at 2.5 solar radii from the centre of the sun. The IMF lines have their foot-points anchored to the source surface, and are dragged along with the plasma flow. The rotation of the Sun and the frozen-field condition results in a garden-hose pattern (the so-called "Parker model") when the IMF lines are displayed in the ecliptic plane. Alternating slower and faster streams are emitted from the Sun along fixed radials as the rotating source region sweeps past. If the speed differential is great enough, co-rotating interaction regions and even shock interfaces may form.

2. Event-Driven Wind

During events, the propagation of disturbances is taken care of in the following way: Energy is input at the inner boundary. The event-driven component is represented by time-dependent boundary conditions. Solar observations provide the start time and evolution of the energy source, its location and size. Disturbance energy is characterized by enhanced solar wind speeds on the source surface. The compression of solar wind streams at the stream-stream interaction region may lead to the development of shocks.

It is important to note that the HAF model inputs are handled in a standardized and consistent way. The internal parameters have been calibrated by comparisons with MHD simulations (e.g., Sun et al., 1985). The event-period conditions are based upon empirical algorithms and parameters derived from observational studies.

Only this model displays the evolution of the IP disturbance in the ecliptic plane as a function of time, and takes into account the varying background solar wind through which the IP disturbances travel, and also the interactions that the IP shock may undergo during their transit to 1 AU.

The original HAF model is described in Hakamada and Akasofu (1982) and Fry et al (2003) and on-line information can be found at:
<http://www.expi.net/expinet/kinematic.html>.

2.6.5 An Engineering Model for SPEs

An engineering model is being developed at the Departament d'Astronomica i Meteorologia (DAM), University of Barcelona, to predict the level of low energy particles at a particular location in interplanetary space, when a CME has been detected. The proposed scenario to account for SPE events involves the presence of a fast CME able to drive shocks. Presently the code has been used to derive the injection rate and its evolution for different events, and to test its reliability. First applications to synthesise flux profiles have been presented in Lario et al. (1998) and Aran et al. (2001).

More information to be found at:
<http://www.am.ub.es/%7Eblai/enginmodel/SEP_Abstract.html>.

Simulations of shock propagation and related particle storms, courtesy of D. Lario, B. Sanahuja, A. Aran, Z. Smith, T. Detmann and M. Dryer, can be found on this page: <http://canopy.lmsal.com/schryver/Public/homepage/movies/Lario_CME.html>.
These simulations result from combining the energetic particle model from Lario et al. (1998) and the 2 1/2D-MHD modelling of shock propagation from Wu et al. (1983).

The long-term objective of the DAM Solar-Terrestrial Physics and Space Weather Group is to develop an engineering code for characterising solar energetic particle population at user-specified locations in space from outside the solar corona up to the orbit of Mars. The model will estimate time-dependent particle fluxes and fluences as a function of the energy over the range 50 keV to 100 MeV, with a familiar user interface for running the engineering tool.

The inputs will be those that are now available in real time from SEC/NOAA. Those include:

- CME and/or flare location;
- Time of the optical/H-alpha detection;
- Onset of GOES X-ray flux;
- Solar wind velocity, from L1 spacecraft if available (default: 400 km/s); and
- Spacecraft location, at L1, earth, or any point relative to fixed Sun-Earth axis.

The outputs will be in a form that is readily available to the mission designer or operational user. For example, as a graphical time series that includes the solar event of interest and will be continuously updated in real time, or as a table of values for different scenarios. The plots will display the following information:

- Expected flux (particles/cm²-s-sr-MeV), which will be continuously compared on the same plot, in designated energy channels;
- Expected duration of the event, which will be continuously updated;
- Expected flux, which will continuously be compared on the same plot with actual observations, if available in real time; plots would also be configured for post-event comparisons;
- Integrated fluences in the designated energy channels.

Algorithms for solar proton event parameters predictions are done at the Institute of Geophysics and Astronomy, Hvana, Cuba:

<www.estec.esa.nl/wmwww/wma/spweather/workshops/proceedings_w1/POSTER3/pozo3.pdf>
<www.estec.esa.nl/wmwww/wma/ spweather/workshops/spw_w5/abs/pozo_1.pdf>

2.6.6 The Community Coordinated Modeling Center

The Community Coordinated Modeling Center (CCMC) was established to aid in the development of models for specifying and forecasting conditions in the space environment <http://ccmc.gsfc.nasa.gov/>. The CCMS concept was initiated in 1998 as a result of efforts by US government agencies to enhance space weather research, develop space weather models; and provide a means for more effective transitioning of research models to operations. The CCMC Space Weather Models are listed at the above-mentioned web-site under "Space Weather Models" and includes Solar Models and Heliospheric Models.

2.6.6.1 Solar Models

- MAS Model – This is a MHD Model of the Solar Corona. Predicts the structure of the solar corona (magnetic field, density, and flow velocity) based on numerical solution of MHD equations.
- Potential Field Source Surface (PFS) Models – These models provide an approximate description of the solar coronal magnetic field based on observed photospheric fields (magnetograms).

2.6.6.2 Heliospheric Models

- Heliospheric Tomography Model – The model makes use of interplanetary scintillation (IPS) to tomographically reconstract the global structure of the solar wind.
- Exopheric Solar Wind Model - This code is an exospheric model of the solar wind with only protons and electrons (we defer the inclusion of heavy ions to upcoming versions of the code), with a non-monotonic total potential for the protons and with a Lorentzian (kappa) velocity distribution function (VDF) for the electrons. This code is developed for the coronal holes.

2.6.7 The Center for Integrated Space Weather Modeling

The Center for Integrated Space Weather Modeling (CISM), is a National Science Foundation (NSF) Science and Technology Center (STC). CISM formally began operations in August 2002 and consists of research groups at eight universities and several government and private non-profit research organizations and commercial firms. The Center's mandate is to construct a comprehensive physics-based numerical simulation model that describes the space environment from the sun to the Earth. For more information see <http://www.bu.edu/cism/>.

3. RADIATION MONITORS

3.1 Introduction

In Work Package 5000 of the REMSIM programme, one objective is to develop a system concept for giving warning to astronauts of space radiation hazards in Deep Space. We discuss here some options for technical approaches, which are in accord with the radiation risk policies which REMSIM has adopted. The topic of instrumentation is being studied by REM Oxford Ltd, England, under the leadership of BIRA, Brussels, who have responsibility for the wider topic of Space Weather, especially the key topic of predicting solar flares from a systematic network of detectors. REM has studied the existing instrumentation of space stations, shuttles and biosatellites, consisting of arrays of on-board sensors inside and outside a pressure vessel, if any. At this stage, no hardware is to be designed so, in this Chapter, we give factual descriptions of the sensor technology available and how they are built into space-radiation monitors by selection of structure and circuitry. In Chapter 6 we will continue the theme with "Recommendations for Warning Systems".

The job of the monitors is to give all concerned a true feeling for the "chronic GCR condition" and timely warning of the solar proton event. In Sections 6.2.2.1 and 6.6.6, we use a homely comparison to bring this task alive. We are talking about the use of a Geiger counter to give reassurance on Earth :

" … one click per second on Earth; a hundred clicks per second in Deep Space, except in a large flare, when the click rate would be "off-scale" … ".

This has been adopted as the motto of the project in the REMSIM summary report by Alenia (REMSIM 2004a). In our review, we describe the technologies of the bulky Geiger and its much smaller solid-state successors.

3.2 Principles of Sensor Technology

3.2.1 General

In this section, we make brief general remarks about sensors and their technology, paying most attention to the special considerations of a manned deep-space mission. General information on sensor types will be found in a variety of books, mainly in related fields of medicine and physics. These include Williams and Thwaites (1993), Knoll (1986), Delaney (1986), McKeever, Moscovitch and Townsend (1995), Furetta (2002), and Holmes-Siedle and Adams (2002). The chapter on dosimetry in the last-named book deals mainly with the measurements required for radiation-testing of components, where particle tracking and spectrometry is not central to the task. There are no well-known books on space-borne detector technology but many journal and conference papers on space-based detector projects - see for instance the proceedings of the annual Workshop on Radiation Monitoring on the International SpaceStation (WRMISS 2003) - are referred to in later discussion.

By examining Table 6, we can appreciate the type of "rugged dose monitors" which is necessary to survive a seriously hazardous spaceflight in deep space. We will be attempting to compare these "principles of dosimetry" with reference to the dose levels to be measured, the needed power, weight and size and other advantages and disadvantages of each principle. Once a number of these detector candidates have been chosen for its special suitability, there should be adequate time for technology development in the Aurora programme (Section 3.6). The context in which this would be done is discussed at the end of Chapter 6 on warning systems.

In the following text we will present a number of the detector types listed in the below Table and discuss the technical background to their design and use. It should be noted that the design of radiation monitors tends to originate in two separate needs:

1. to track and count individual particles or photons
2. to measure the energy absorbed in a material (especially tissue) during exposure to particles and photons.

Principle	Quantity Measured	Dose or dose rate?	Advantages	Disadvantages
Geiger counter	counts	rate	v. sensitive Simple circuits	HV req'd
Proportional Chamber	rad(tissue)/sec	rate	special TE. medium	No particle information
Ionization Chamber	rad(air)/sec	rate	std. medium	HV Electrometer circuit
Scintillation Counter	flux & energy	rate	precision resolution	HV Small signal/MCA
Semiconductor Diode	current or count rate	rate	small size array/telescopes	As for scintillator
Thermo-luminescent Dosimeters (TLD)	rad [tissue or bone]	D	small size	Destructive read. Not remote
Film	rad (gelatin)	D	precision	As for TLD
Glass & Plastic	Rad (medium)	D	Small size	Optics required. As for film, TLD
Track-Etch		D	precision	As for TLD
Solutions & Gels	rad (H_2O)	D	precision	Optics req'd. As for film, TLD
Space Charge (RADFET)	rad (Si/SiO_2)	D	ultra-small integrate with IC	Sensitivity lower than above mtds.
Biosensors	Rad (tissue)	D	ultra-small integrate with human technology	Infant technology

Table 6. Comparison of rugged dose monitors.

An early example of category (1.) is the Geiger counter a very different approach from an early dosimeter, category (2.), a solution of a chemical in water. The two needs can sometimes be merged, such as in the tissue-equivalent proportional counter, described in Section 3.2.6.

3.2.2 Solid-State Sensors

The designs of solid-state detectors presented here are discussed mainly as to how they respond to high-energy particles and photons, usually in the energy range above 1 MeV. Later in the Section there is also a suggestion to use EUV or soft X-ray variation as a warning of eruptive events. For these relatively low energies, many conventional photosensitive devices would also come into use such as the Charge-Coupled Device [already used in soft X-ray astronomy] (Holmes-Siedle, Watts and Holland 1995) or photodiode arrays. The one proposed for EUV is a new approach, based on oxide trapping. In Section 6 we go further and attempt to show how solid-state detectors can assist the special task of protecting crews from deep-space radiation.

3.2.3 Solid Diode Point Sensor

Any p-n junction will produce a surge of current if a particle deposits energy within the depletion region. Silicon is widely used but materials of higher atomic weight (e.g. HgI) can be used for special cases. Silicon diodes are used in the reverse-biased mode when a large collection region is desired. For high dose rates, a photovoltaic mode is more convenient. Medium-sized diodes are used in a very efficient range of personnel pocket dosimeters and unmanned spacecraft monitors. The current from the background dose in the environment is logged by means of an operational amplifier and the data stored in digital semiconductor memory. Enhanced forms of this commercial design will probably be produced for individual crew protection as the monitors of entry dose accumulated various for parts of the body. The data can be extrapolated to organ dose, especially if instrumented phantoms are used to assist the extrapolation (see Section 3.6.9). The pros and cons of this device are traded off here against a competing device, the Metal-Oxide-Semiconductor Field-Effect Transistor (MOSFET) dosimeter. In general, the diode working with matched circuitry produces a more sensitive system.

3.2.4 Solid-state Arrays and Telescopes

Many forms of arrayed diode have been designed for high-energy physics, including the microstrip array and the CCD particle-tracker (see e.g. Holmes-Siedle and Adams 2002). These are designed to sense gigavolt protons, muons and other nuclear fragments. On the ISS, a double plane of silicon diodes, the Charged Particle Directional Spectrometer (CPDS) is giving data including type, energy and direction of the megavolt and gigavolt particles likely to affect the blood-forming organs in the crew.

3.2.5 The MOSFET or RADFET

The Radiation-Sensing Field-Effect Transistor (RADFET) is a microminiature type of integrating radiation dosimeter. The sensor has a microscopically small sensitive volume, about 10^{-7} cubic millimetre. This enabling technology makes it possible to design the smallest conceivable radiation sensing system but also limits total-dose sensitivity. The individual sensor units are made by the mounting of very small MOSFET chips; the sensitive volume covers only a small fraction of the chip area. The sensing principle derives from the field produced when space-charge is trapped semipermanently in the oxide region of the field-Effect Transistor (FET). An electrical measurement then gives a relative value of cumulative dose in rad or Gy(Si). The dose resolution of the MOSFET slightly less than 1 rad [1 cGy] is not as good as for chambers, film badges and TLDs, which achieve "millirad resolution", as needed for terrestrial personnel-protection. For a bibliography of MOSFET dosimetry, see Holmes-Siedle and Adams (2002).

3.2.6 TLDs

The phenomenon of thermoluminescence is described in Holmes-Siedle and Adams [2002] and many books and papers see (e.g. McKeever et al. 1995, Furetta et al 2002). Thermoluminescent Dosimeters (TLD), because they are minute in size (volume about 1 cubic millimetre), passive in action and are made of material which is roughly tissue-equivalent are used very widely in radiobiology, medicine and radiation protection on Earth and in space. In the thermoluminescence or "glow" process, the small "TLD chip" of pressed powder is subjected to a temperature ramp between 50 and 400 degC. The "reader" is a PMT coupled to a heater and a computer. The drawback arises from the small amount of light emitted. Despite these drawbacks, the TLD has been one of the main tools for monitoring crew dose in early manned orbital flight. Those TLD chips were returned to earth and read out there. In long deep-space missions, reading out on Earth is not an option. It is possible that one or more TLD readers, designed for lightness, will fly on the spacecraft.

3.2.7 Scintillator with Photodiode

A scintillator is any material which gives off a useful pulse of light when an ionizing particle passes through. This phenomenon is what gives light flashes in the eyeball in space. Crystals, liquids and polymers have been adapted as scintillation counters (see e.g. Delaney 1995, Knoll 1986). The classical photomultiplier [see below] can be replaced as a light-sensor by a photodiode. The much lower light-sensitivity means that lower levels of particle discrimination are possible but the miniaturization possible with diodes makes the system attractive for some applications.

3.2.8 Nuclear Track-etch Detectors

The nuclear track-etch detector makes use of the well-known effect in organics that radiation damage often increases the solubility or reactivity of the material. A particle with high Linear Energy Transfer (LET) leaves a track of damage, which can then be

"developed" with a reactive solution, revealing an etched track. Since the sample can be much thicker than photographic film and has a more linear response to dose, the method is a useful complement to film in particle tracking and can be better used in estimating tissue doses.

From 1995 to the present, Heinrich and co-workers [Heinrich 1997] report the doses and particle types found in stacks of TLDs and CR-39 plastic sheets from the flights of EUROMIR 95, MIR97 and STS missions.

The nuclear-track-etch technique is more versatile than film in tracking certain particles. It is also give more information than film about the likely tissue-absorbed dose deriving from the space environment.

3.2.9 Chambers

Chambers which detect radiation are typically metal cylinders or spheres which have been evacuated and sometimes re-filled with a suitable special gas. Very often, the chamber has a central, rod-shaped electrode which has a high positive voltage on it while the outer vessel is grounded. The fields across the chamber may be as high as 2 megavolts/cm. The principle is that charged particles are generated by the impinging radiation, either in the wall of the chamber or in the gas. The chamber wall may be thinned at some point to admit heavily-absorbed particles or photons, or heavily shielded to modify or collimate the radiation. The usual signal presented is due to the current of electrons formed in the medium and collected on the central electrode, although some chambers [such as the spark chamber] may use optical effects. The above description covers a huge variety of structures and physicists are ingenious in designing special collimation and signal treatment. We discuss relevant aspects of a few of the more rugged, miniature forms applicable to space physics and dosimetry. The first chamber of the satellite age was the Geiger counter flown by James Van Allen on the Explorer I satellite, which discovered the inner trapped radiation belt. The basic physics and the required signal analysis methods for chambers are given in Knoll 1986 and in encyclopedias such as Encyclopedia of Astronomy and Astrophysics

3.2.9.1 The Geiger Counter

This is a gas-filled tube carrying a very high electric field (over 1E6 V/cm) near the central electrode. The generation of one or more electrons leads to an avalanche discharge. The intensity of the avalanche bears no relation to the original number of electrons produced. The resulting electrical pulse therefore yields no information about particle type. The chamber has an unfortunate "dead time" so that it can be overwhelmed by unexpectedly high particle fluxes, although sometimes correction factors will rectify error of this sort. Particles can be "counted" but the energy deposited cannot be analyzed by a Multi-Channel sorter of pulse heights (MCA) as for many other methods [see below] and safety warnings may be invalidated when fast count rates cause the system to become completely "dead".

3.2.9.2 The Proportional Chamber

This is a gas-filled tube carrying a medium electric field (over 1E3 V/cm). The generation of one or more electrons leads to an avalanche multiplication event - picked up as an electrical pulse. This pulse height IS proportional to the original number of electrons so that, unlike the Geiger counter, particle energy CAN be analyzed by a Multi-Channel Analyzer (MCA), a sorter of pulse heights. An energy spectrum for particles can thus be obtained. In the Tissue-Equivalent Proportional chamber, propane substitutes for air and other design features give the simulation of ionization in human cells (see later section about the TEPC on ISS).

3.2.9.3 Ionization Chambers

The most common ionization chamber is an air-filled tube carrying an electric field well below the avalanche point [less than 1E3 V/cm]. In this case, the quantity of energy deposited CAN be analyzed but it is in the form of a DC current and not in the form of pulses. An energy spectrum for particles is not obtained but the dose[air] is accurately obtained if fields and pressures are carefully controlled. Lacking multiplication, the current per electron released is, of course smaller than for the chambers with high fields. For dose rates in the range expected in deep space, very sensitive electrometers are required to handle the signals produced. In such a case both noise and reliability may make the method impractical for protection use. Semiconductor diodes and MOSFETs, operated as described here, can be described as the solid-state analogue of the gas ionization chamber. Some designs of ionisation chambers contain a dielectric liquid rather than a gas. This allows the ionization process to occur in a smaller volume - a useful performance parameter in a spaceborne application.

3.2.9.4 Other Chambers

In high-energy physics, special chambers containing wet air, liquid hydrogen and spark gaps are used as imaging particle trackers.

3.2.10 Advanced Solid Counters

3.2.10.1 Scintillator with PMT

A scintillator is any material which gives off a useful pulse of light when an ionizing particle passes through. This is what gives light flashes in the eyeball in space. Crystals, liquids and polymers have been adapted as scintillation counters. The classical form has a photomultiplier as light-pulse detector, which allows low-noise multi-channel pulse-height analysis of the light pulse and particle discrimination using light-pulse length and coincidence. The result is very accurate well-resolved energy spectra and dose information as an extra. This is the ultimate scientific radiation monitor but is usually too complex to suit warning system requirements.

3.2.10.2 Unconventional Scintillator Approach

Unconventional approaches for the assessment of the cosmic ray environment include the scintillator as a "real-time track detector". A different use of the technology combines a "bundle" of scintillators with a CCD, a segmented scintillator, an intensified CCD and a small cathode-ray tube (Bambaugh 2000). The machine could possibly be the size of a mobile phone. Dr. R. Ruchti, the inventor of the method (personal communication), says:

"The visual image of the tracks is a powerful display method of what is the source of high-energy events. For example heavily ionizing particles (multiply-charged) will look vastly different (and brighter) than minimum ionizing particles (such as protons). A photosensor could be attached to trigger on the amount of light at a given time. This could be used for alarm purposes and would be relatively easy to implement. We used a variation on this technique to trigger devices like this one when we were using fiber-plate imagers to study charm particles (in GeV colliders)."

A human might gain quite useful information on ambient high-energy particle fluxes by a visual display similar to the Ruchti device. Awareness of the frequency, type and direction of the particle tracks in the scintillator may make it possible to move/alter work practices and rest positions intuitively to minimize exposure. This technology might be thought of as a descendant of the Wilson Cloud Chamber and the bubble and spark chambers which heralded in the major nuclear discoveries of the 20th Century by revealing the information available in the tracks of a particle shower when visualised under a magnetic field.

3.2.10.3 Yeast Suspension

An ESA programme has developed a biological dosimeter containing immobilised "yeast biosensor cells". When exposed to UV or gamma radiation, or chemicals which mimic such exposure, the yeast cells became fluorescent indicating the increase of DNA repair in response to damage. A badge reader was developed, by Woelfl of Jena University, to illuminate and then record the fluorescence from the badges. A separate controlled experiment with the yeast biosensor was also prepared for the International Space Station (ISS) (Cahill 2004, Knight 2004). The device could be manually triggered to mix a yeast suspension with a nutrient solution, and expose half of the yeast to space radiation keeping the second half as a shielded control. The yeast would then be analysed upon its return to Earth. The device was given the acronym FORRAY, for Fluorescence Orbital Radiation Risk Assessment using Yeast. Syringe type plungers allowed yeast to mix with nutrient and pass into an exposure chamber. The final unit was scheduled to fly with the Russian Soyuz rocket to the ISS in April 2004. A commercial system for general testing of genotoxicity is being developed by Gentronix in the UK (Knight 2004).

Other lines of basic radiobiology may also have applications to dosimetry. For example, NASA's Exploration Systems Mission Directorate have funded studies at UMD, Maryland which find that some long-lived bacteria, for example halobacterium have especially efficient DNA-repairing enzymes which work extremely well on radiation damage. Tracking the mechanism of these repairs can possibly assist radiation

tolerance in human crew but may also possibly give a simple measurement of dose received. [<http://science.nasa.gov/headlines/y2004/10sep_radmicrobe.htm?list724700>, <http://life.umd.edu> and Kotteman et al. 2004]

3.2.11 Unconventional MOS Detector of UV Variability

A novel idea which we are considering in the present project is the use of far UV (FUV) or Extreme UV (EUV) as the hazard detector. It is possible that, with development, a "solid-state UV detector" based on emission into a dielectric, in this case a metal-oxide-semiconductor (MOS) device. The method should be less cumbersome and lighter than most other detectors in the UV or soft-X-ray range. FUV covers the important hydrogen Lyman alpha line at 121.8 nm and EUV covers some other important helium and hydrogen lines (helium being at 32.4 nm).

3.2.11.1 Application to Flare Warnings of a Solid-State (MOS) Imager for UV and X-Rays

There has been considerable research during the past four decades to measure the variability of solar EUV irradiances and to model this wavelength region (Hinteregger et al 1981). The 8 years of observation by the SOHO mission has formed an excellent picture of local emissions and their relation to sun-spot regions. Because the short wavelength emissions are significantly greater than the solar blackbody spectrum, the heating of planetary atmospheres by EUV is important in space weather forecasting, especially in forecasting orbital drag and other atmospheric effects. The sources of the solar EUV emission lines and their variability are well-known. Short-term variations in EUV, lasting from minutes to hours, are firmly related to eruptive phenomena (Nusinov, 1984). Intermediate-term variations on the order of months are modulated by the 27-day rotation period of the Sun and are also correlated with disturbed regions of the Sun. (Lean 1987, 1991), Rottman (1987), and Tobiska (1993) have reviewed solar EUV variability and the SOHO mission has added further detailed information.

Since variations in EUV are firmly related to eruptive phenomena, then there is an argument for employing solar-pointing EUV detectors in the warning system - and indeed directly on the manned spacecraft in order to give data on eruptive behaviour to the crew at the speed of light. An EUV channel would be independent in many ways from the radio and X-ray information commonly used. Using a simple but specially-designed silicon device (preferably an imaging array), a measurement of local charge in the device, similar to that used in the RADFET (see Section 3.2.5) would give the required EUV picture rapidly. The measurement method is capable of yielding both dose-rate measurements vs time or an image of local integrated EUV intensities over the disk of the Sun. An ideal wavelength for the MOS charging effect is the hydrogen Lyman alpha line at 120 nm (10 eV).

Positive charge induced in the oxide layer of the MOS system by FUV, EUV and X rays is caused by the generation and trapping of mobile holes in the oxide. Work by Holmes-Siedle and Groombridge (1975) with a hydrogen-alpha lamp has shown that the response is efficient and is linear over many decades of detectable charge buildup. Such work has also established that, using a broad-band source of UV (UV lamp or the Sun) or

a simple change of a filter to 250 nm, we can also remove the trapped holes. In other words, the device is *erasable* by supplying a near-UV flood beam between exposures. The applicability of the method is broad, working for all photons from UV to hard X-rays. The MOS capacitor arrays used are much more rugged than CCDs, already widely used in solar research on rockets and satellites.

3.2.11.2 UV Filters

Data on the spectrum of solar UV can be obtained using UV filters or gratings. For a fixed waveband, filters may be evaporated direct on the wafer surface. The spectral responses for conventional silicon detectors and the MOS method are very different.

3.3 Measuring Radiation Outside the Vehicle

3.3.1. General

Detectors are likely to be needed on the outside of the vehicle, where the local radiation environment is in its "raw" state. Warnings of radiation hazards to the crew are partly based on the count rates of protons and other positive ions in the immediate vicinity of the spacecraft. The most precise method of detecting this would be to extend particle and possibly photon counters from the spacecraft on a boom. We can refer to this category of monitor as giving information from "outside the walls" of the vehicle. Given the normal, thick walls of a manned spacecraft, many particles bombarding the surface are stopped or grossly transformed on their way through the walls of the spacecraft. Thus the information available to a detector array *inside* the walls, while important for determining dose rate to the humans therein, may not contain some of the vital clues to future solar activity given by the raw environment *outside* the walls. Hence the title of this section

The counters outside will be a combination of one or more of the sensors mentioned above and a collimator - a mass of material or "absorber" of selected atomic weight and precisely machined shape, to collimate or align the radiation into a "beam". A typical collimator for electrons and protons will be an aluminium hemisphere in which is machined a conical aperture. This will then admit a beam of particles (usually omnidirectional in space) from that conical, solid angle. The aperture will be blocked at some point by a "window" often an Al or Ti membrane which stops electrons below a certain energy. By controlling these thickness values, the system designer can admit to the sensor a certain fraction of the known particle spectrum. The collimator does not discriminate between electrons and protons but the electronic analysis of the detector counts can do this by finding the dE/dx of the particle passing through. Alternatively, a magnetic field may be used to deflect protons and electrons in opposite directions. By making several detectors with various collimator designs and with calibration on ground-based accelerators, the counting and characterization of the particles, though a highly skilled art, can become very accurate. Such accuracy is required for the initial proving of a trajectory in space but may be relaxed somewhat once the path is well tried.

Making an extended series of collimators produces a detector with a very limited angle of view, which can be called a "telescope". However, electronic methods may remove the necessity for a cumbersome and heavy structure such as that. A pair of

detectors which sense the passage of a particle at instants apart "coincidence", also acts as a telescope.

3.3.2 Diode Point Sensor Outside

Medium-sized diodes are used in a very efficient range of personnel pocket dosimeters, nuclear trackers and counters and unmanned spacecraft monitors. A few spacecraft sensors contain semiconductors of higher atomic weight (e.g. GaAs, CdS, HgI). Enhanced forms of these existing spacecraft designs (commercially designed) may well be produced for external monitoring on deep-space manned vehicles, where, suitably collimated and shielded, they could operate well for (a) trapped radiation, (b) streaming particles from the Sun and (c) CGR heavy ions. In such situations the features of this device will be traded off against competing compact silicon arrays and luminescent sensors.

3.3.3 Solid-State Arrays and Telescopes Outside (ISS-CPDS)

Many forms of arrayed diode have been designed for high-energy physics, including the microstrip array and the CCD particle-tracker (see e.g. Holmes-Siedle and Adams 2002). These are designed to sense gigavolt protons, muons and other nuclear fragments. On the ISS spacecraft, a double plane of silicon diodes, the Charged Particle Directional Spectrometer (CPDS) is giving data including type, energy and direction of the megavolt and gigavolt particles likely to affect the blood-forming organs in crew. Clearly that principle could also be adapted for exterior monitoring.

3.3.4 TLDs Outside

Thermoluminescent Dosimeters (TLD), because they are minute in size, passive in action and are made of material which is roughly tissue-equivalent, are used very widely in radiobiology, medicine and radiation protection on Earth (Furetta 2002) and in space (see Section 6 below). TLD readers, designed for lightness, may fly on the manned Moon and Mars missions. Clearly this principle is NOT well - adapted for routine exterior monitoring but, in research flights, may be useful as a cross-check of data from electronic monitors.

3.3.5 Chambers Outside

3.3.5.1 The Geiger Counter Outside

This principle has often been used for exterior monitoring and its purpose would be a crude count rate of all ionizing particles above an energy capable of penetrating the tube walls. Size and power drain can be made quite small and the simplicity of the counting circuit is an advantage.

3.3.5.2 Proportional and Ionization Chambers Outside

Both types of chambers give a crude measure of external fluxes and outside measurement would help to correlate data from the Tissue-Equivalent Proportional chambers (TEPC) already designed for ISS. Since the TEPC gives a simulation of ionization in human cells then a chamber outside could be designed to simulate human doses during Exra-Vehicular Activity (EVA).

3.3.5.3 Other Chambers Outside

In high-energy physics, special chambers containing wet air, liquid hydrogen and spark gaps are used only as imaging particle trackers. They are probably too cumbersome for the present applications and no obvious purpose has been identified for such devices. However, a few unconventional approaches such as these should be examined in future work.

3.3.6 Scintillators Outside

Scintillators give very useful information on particle types and energies. This has proved very useful in space science. However the commonly-used photomultiplier tubes may well be deemed too fragile to fly outside on a manned deep-space mission. On the other hand, there are several other scintillator approaches mentioned in Section 3.2.10. These include the "scintillator fibre with photodiode" - a lightweight and rugged device - and the small "scintillator array" which acts as a visual, "real-time track detector".

Using a visual display similar to the Ruchti device, a human performing EVA might gain important information on ambient high-energy particle fluxes. Such awareness of the frequency, type and direction of the particle tracks in the scintillator may make it possible to move/alter work practices to minimize exposure during the EVA.

3.3.7 MOS Detector for EUV Outside

If the principle of EUV observation as a warning method, proposed in Section 3.2.11, is accepted as relevant to the Mars or Moon missions, spacecraft or ground station, then it would of course be mounted on the outside of the vehicle and pointed at the Sun. The design studies would decide whether or not the spacecraft would require filters or optics. The practical aspects are further discussed in Section 6.

3.3.8 Nuclear Track Detector

These detectors would give valuable track information after the event whether inside or outside the vehicle. However, the tracks would need development later, in tanks inside the vehicle.

3.5 Flight Detectors to Date

3.5.1 Mars Odyssey - MARIE

Mars Odyssey is an unmanned spacecraft but the objectives of its Martian Radiation Environment Experiment (MARIE) sensor system clearly include the characterization of the radiation harmful to a future crew. The data already emerging from this mission are correspondingly very useful to this project. The array of detectors is mainly made of silicon, so that tissue dose is not indicated unambiguously.

The 2001 Mars Odyssey spacecraft arrived in Mars orbit in October 2001, carrying MARIE, a stack of solid-state silicon detectors for high-energy particles designed to measure GCRs and SPEs in the 20 – 500 MeV/u energy range (minimum LET: ~0.5 keV/μm). MARIE records the ionization energy loss (*dE/dx*) of incident particles, which can be converted with some confidence into radiation dose in tissue. Protons are well-measured in the 30 – 100 MeV energy range (that matches the proton spectra in a typical SPE). Particles between ^{4}He and ^{20}Ne are accurately measured in the 70 – 500 MeV/u energy range. The higher range of energy and Z are identified, but without determining all parameters. For example, for reasons of range in silicon, ions heavier than Ne are recorded as hits, but with no useful *dE/dx* information. MARIE began acquiring data in orbit in March 2002 and operated until October 2003. It has observed several SPEs (ten, as of April 2003) as well as GCRs up to Z = 14 (LET ~60 keV/μm). For parts of this period, Mars and Earth were on nearly opposite sides of the Sun, so that important data was available on the radial and longitudinal distributions of particles produced in SPEs.

The largest dose rate observed by the instrument during 2002 (>10 mGy/d) occurred in July. It was confirmed that the combined effects of the angular separation between Earth and Mars, the location of the Coronal Mass Ejection (CME) on the Sun and the type of propagation event play a major role in the SPE magnitude seen at either the Earth and/or Mars [Atwe03b]. This confirms the complexities of developing an efficient crew warning system based on external observations of solar events and prediction of the radial propagation of solar protons for up to 1.5 A.U. Despite some "glitches" in the operation of MARIE, the results are positive in that there is agreement within 10 % between the transport code HZETRN and the dose rate observed by MARIE in Mars orbit (This is dealt with further in RxTec 2004). The measurements of MARIE suggested that radiation would expose astronauts in deep space to an effective dose 2.5 times greater than that received by humans in LEO aboard the ISS. Extrapolated to 3 years, they represent about 1 Sv, which are still manageable doses, indicating that radiation will not be a "show stopper" for human Mars missions but that shield weight is a crucial part of the budget and choice of GCR minima in the solar cycle, suggesting a strong preference for manned exploration and future colonization to be scheduled near solar maxima.

The radiation environment on the surface of Mars will probably be similar to that seen in orbit. Even though shielded by the thin planet's atmosphere and modified by the presence of "albedo" neutrons produced in the upper layers of the surface, it poses a similar risk. Proving missions will have to perform very detailed experiments to measure the absorbed dose in a tissue-equivalent material on Mars at a location representative of

the expected landing site as a function of shielding and body part. The experiment should, in particular distinguish the radiation dose contribution induced by charged particles from that induced by neutrons (NAS02, Zeit03). MARIE is clearly a pioneering effort and the data will assist the evolution of the future stages of exploration by unmanned probes in deep space.

3.5.2 CEASE Dosimeter

This is one of the few commercial "ready to-fly" spacecraft dosimeters made and advertised worldwide. It is a hybrid of a silicon particle-counter and an electronic dosimeter. Silicon diodes are mounted under aluminium hemispheres in the same way as for scientific counters. So far, they have been flown only in Earth orbit on unmanned spacecraft such as CRRES (Ray 1992). Only the dose(Si) vs. depth characteristics of megavolt protons and electrons are of interest in such missions. The currents produced in silicon diodes are converted to signals which are accurately proportional to the energy deposited in the silicon.

The manufacturer (Amptek, 2004) cites the system as "a multipurpose easily integrated, environmental hazard sensor package, the Compact Environmental Anomaly Sensor (CEASE), covering Environmental Threats, Total Radiation Dose, Radiation Dose Rate, Surface and Deep Dielectric Charging and Single-Event Upset in ICs. With such monitoring, operators can modify operations during hazardous conditions, predict performance loss and end of life, and launch replacement satellites if necessary."

It can be seen from this that the system is a dedicated design for unmanned, operational spacecraft. However, the performance parameters in Table 7 show the typical weight and power requirement of a dosimetric spaceborne detector.

CEASE I Properties	
Size	4.0 x 4.0 x 3.2 cm^3
Mass	1.0 kg
Power	1.5 Watts
Standard Interface	RS422 or MIL-STD-1553B
Telemetry (minimum)	10 bytes per 60 sec
SEE Detector Particle Telescope Shielded Dosimeters [light and heavy]	

Table 7. Properties of CEASE I. (Amptek 2004)

3.5.3 The SOHO Particle Counters

SOHO was launched in Dec-1995 at 08:08 UTC and works now at the Lagrange point L1, 1.5 million km from the Earth. The COSTEP-EPHIN detector designed by Kiel University, RAL Chilton and others is typical of scientific semiconductor particle-counter whose role, placed on the OUTSIDE of a space vehicle, is to fulfil a specific scientific

measurement of space particles and fields. Typically, the electronics box is placed in the electronics bay of an unmanned spacecraft. EPHIN is a novel telescope for the measurement of energy spectra of electrons from 250 keV to more than 8.7 MeV and of hydrogen and helium isotopes from 4 MeV/nucleon to more than 53 MeV/nucleon. Mounted on SOHO, it is pointed steadily at the Sun. Charged particles are registered in the sensor by ionization. The EPHIN sensor consists of a semiconductor stack with five layers. These are enclosed by a sixth semiconductor detector (F) and a scintillation detector (G), operated in anticoncidence. Note that this construction allows precise scientific measurements and also removes any possibility of using routine semiconductor production techniques in fabrication and assembly. It is a precision-engineered device. The SOHO/COSTEP instrument uses pulse height analysis (PHA) (i.e. the transient energy loss of particles is recorded). It is optimized for the observation of protons and Helium ions of SPE events above ~4 MeV. COSTEP EPHIN consists of a solid state detector stack within active anticoincidence. CELIAS HSTOF uses electrostatic deflection plates. Incoming particles are selected. Again, it is a precision-engineered device. Reitz and co-workers flew a silicon detector telescope on Shuttle flights STS 76, 81 and 84.

ERNE, the "Energetic and Relativistic Nuclei and Electron" counter by the University of Turku, Finland, (UTU 2004) also operates on the SOHO spacecraft. It carries two particle counters LED and HED. While the objectives are mainly fundamental research, the lessons learned about particle acceleration will assist the design of more precise space weather forecasting systems, especially helped by the position and imaging capability of SOHO. The scientific objectives of the ERNE experiment are:

1. energy spectra of ions and electrons above 1 MeV/nucleon
2. elemental and isotopic abundance H to Fe in SPE [first survey]
3. particle acceleration in the solar atmosphere and interplanetary shocks
4. particle propagation in the solar corona and in the interplanetary space
5. study both large and small scale properties of the IMF
6. short-period temporal variations of particle flux
7. flux anisotropy within the apparatus viewing cone
8. flux of protons penetrating the instrument (even decay solar neutrons)

3.5.4 RADFET Flights by ESA

A MOSFET first flew in space in 1978 (Adams and Holmes-Siedle, 1978), courtesy of the European Space Agency. FOTON has carried the devices (Demets 2000). A six-MOSFET experiment flew on METEOSAT-3. Commissioned by ESTEC Product Assurance as a proof of principle, it proved that several that commercially-produced, special MOSFET dosimeters or RADFETs would return consistent data on the geostationary trapped-radiation environment for several years (Holmes-Siedle, Ward et al 1990).

ESTEC supports one research centre on further development of RADFETs. ESA has found that greatly increased radiation sensitivity is obtained from "electrically-stacked pMOS dosimeters", so that the potential exists for a specialised MOSFET device set to be

developed for manned, deep-space use, the major selling point being the potential for the simplicity of the system and the extremely low weight, size and power drain. In "Tactical dosimetry" for military personnel (Brucker et al 1993), medicine (Gladstone et al 1991; Soubra et al 1993; Chuang et al 2001) and high-energy physics, these special properties have already created a terrestrial market (see e.g. Camanzi et al 2000). As a result, the technology has spread to other space agencies (Japan, Korea, Malaysia and the USA). This industrial presence will in general facilitate the procurement of technological development for Mars missions.

Typically, the RADFET electronics box is placed in the electronics bay of an unmanned spacecraft. Measurement of the dose rate due to the outside environment by the RADFET s is typically by means of a cut-out in the vehicle's thermal cover.

3.5.5 SREM; the ESA Standard Radiation Monitor

SREM is a particle detector, developed for space applications. It is the successor of the Radiation Environment Monitor (REM), the original ESA standard radiation monitor, adaptable to most ESA flight systems. It measures high-energy electrons and protons with a fair angular and spectral resolution and provides the host spacecraft with radiation information as well as passing scientific information to the ground, used by ESA in its environment models. SREMs have been flown on ESA spacecraft INCLUDING PROBA, INTEGRAL and ROSETTA since the year 2000, and additional international spacecraft such as Strv-1c. ROSETTA will traverse the Earth-Mars orbital distance and the SREM will be kept on the whole time with 2-minute temporal resolution.

The merit of recording particle counts in the same package as total doses in Gy(Si), demonstrated in SREM on unmanned spacecraft, is one which should be transferred and elaborated on manned deep-space missions. In our Geiger counter analogy of Section 6.6.6, the spacecraft dose management system records "clicks per second" but should also supply the individual with "clicks per day (today, yesterday etc)" and "your clicks in the mission so far". RX/TEC and REM have demonstrated a day-by-day warning system in a simulation programme, described in Section 6.7

SREM was developed and manufactured by CONTRAVES SPACE AG in cooperation with Paul Scherrer Institute. SREM counter diodes respond to an energy spectrum of protons up to 600 MeV aand electrons up to 5 MeV. The numerical simulations of the detector response are performed with the GEANT code. The SREM on Rosetta was launched on March 2 2004 and has recorded proton and electron counts and cumulative internal dose and will continue to do so at least until rendezvous with the target comet. PROBA, launched in October 2001 into low sun-synchronous Earth Orbit, is recording hourly the rapid changes in particle-count rate as it moves in and out of the trapped-radiation zones including the South Atlantic Anomaly and the polar regions [see <http://www.contraves-space.com> for a picture of SREM in an electronics bay of PROBA and <http://srem.web.PSI.ch> for calibration data and scientific reports]. Key features of SREM are shown in Table 8.

SREM Properties	
Mass	2.5 kg
Dimension	96 mm x 122 mm x 217 mm
Power	< 2W
Compatibility with most spacecraft standards Sensors: Three precision silicon particle counters and internal total doses using a RADFET array.	

Table 8. Properties of ESA SREM.

3.6 Cumulative Radiation Dose Inside the Vehicle

3.6.1 General

We have said that there are two very different sets of methods of radiation measurement in space. Radiation sensors on scientific satellites usually count photons or measure the energy flux in a defined range of photon energies with a minimum of shielding, i.e. with thin windows. These are count or dose *rates* and they are done *outside* the vehicle. On the other hand there is the measurement of the "human radiation environment". The parameter of interest here is the *cumulative or integrated dose,* not individual count rates. What matters in this case is mainly what happens "inside the wall" of the spacecraft and also inside the skin of the crew member [the eye, the gonad or the various blood-forming organs]. This different measurement is done by very different detectors, including those in Table 8, which describes planned instrumentation of the ISS spacecraft [Goli98]. Essentially, then, the sensors have "thick windows", measuring doses arising from the particles which penetrate the relatively thick wall of the pressure capsule and also the crew-members tissues. Many secondary emissions are generated by high-energy particles during the transit of the material include neutrons by spallation of nuclei, X-rays, and mesons by other atomic processes. To obtain the tissue dose, we must know the Linear Energy Transfer (LET) figure and the Quality Factor (Q) (Holmes-Siedle and Adams 2002). The spectrum or radiation being measured by the scientific probes *outside* can only give us an initial guide as to what spectrum is being experienced *inside*, in various locations. The rarer case of extra-vehicular activity (EVA) is, of course, a subset of the second case, where the "wall" is now a much thinner spacesuit.

The majority of the science instruments we list above have no relevance to the energy absorption process which occurs in human tissue [see especially the discussion of the TEPC, Section 3.6.6]. The latter type of instrument is known as a "dosimeter". Often, it, can measure either dose rate or cumulative dose as a matter of choice. Both modes have their place in assessing risks to the human environment constantly throughout the flight. Table 9 deals mainly with the dosimetry but includes some counters mounted inside the vehicle. For REMSIM purposes, we may decide that, while suitable for research, the weight and power drain of such counters will not fit the weight and power budget of a deep-space mission.

3.6.2 Advanced Internal Dose Mapping - Deduction of Human Hazard from On-Board Particle and Dose Signals

DOSMAP is a programme of DLR, Koln, Germany, for the ESA-NASA manned spaceflight programme (Reitz 2002). A package called Dosimetric Mapping (DOSMAP) was provided by the Deutsches Zentrum fur Luft und Raumfahrt (DLR), Cologne. In the ISS twelve thermoluminescence dosimeters (TLD) measure the cumulative absorbed dose in terms of dose [tissue or bone]. The dosimeters, placed in various locations throughout the space station, typically remain absorbing radiation during a three-month period. Some are gathered up every two weeks and taken to a device that records the radiation information and allows it to be saved on one of the station computers. Other dosimeters record all the radiation absorbed during a mission and are analyzed on Earth later. The data gathered by the various dosimeters provides scientists with a dose map which plots the distribution of tissue damage rates inside the station. The importance of dosimetric mapping in the deep-space mission will be high, because the protection given in LEO is lost. Sections 6.2.6 and 6.6.6 of this report stress that minimizing cosmic ray doses by adjusting work pattern is best done by a combination of mapping and real-time dose-rate data given to individuals.

1.	Bonner Ball Neutron Detector (March – December 2001)
2.	Charged Particle Directional Spectrometers – CPDS (2001 - present)
3.	Dosimetric Mapping – DOSMAP (array of TLDs within vehicle skin; 2001-present)
4.	Passive Dosimetry (1999 – present) ➢ nuclear emulsion [thick photographic films] ➢ nuclear activation foils [pure elements as pellets or foils] ➢ nuclear track detector emulsion [CR39 plastic]
5.	Phantom Torso (March – August 2001)
6.	Tissue Equivalent Proportional Counter – TEPC (2000 – present) [NASA02]
7.	EVA Radiation Monitor an active badge containing a MOSFET sensor, sponsored by the Canadian Space Agency (February 2002 – present).

Table 9. Radiation measurement instruments/experiments aboard the ISS.

3.6.3 Dose from Secondary Particles

The Japanese space agency NASDA contributed a radiation detector called the “Bonner ball” to the ISS project. The Bonner Ball Neutron Detector (BBND) is a piece of equipment developed by the National Aeronautics/Space Development Agency of Japan (NASDA) as part of a set of experiments to study the environmental and biological effects of space radiation.

In January of 1998, the Bonner Ball Neutron Detector (BBND) first flew aboard the Space Shuttle Endeavor to measure the neutron fluxes inside the vehicle during mission STS-89 to the Mir orbit. This was the first time that neutron energy deposition was ever measured with an “active” detector inside the Space Shuttle, previous neutron measurements having been made using emulsions and foils. The BBND was able to

differentiate between neutrons and protons. The Bonner Ball Neutron Detector also flies aboard the International Space Station to collect continuous data for many months. The BBND consists of two units - Control and Detector (CU and DU). The CU features a removable computer, time stamping, system calibration and adjustment. The DU is composed of several detector spheres that contain Helium (3He) at 6 at pressure, surrounded by about 25 mm of polyethylene. A central electrode is biased to +1000V. Neutrons are thermalized in the polymer ball, enter the gas, where the reaction

$$n + He\text{-}3 = p + H\text{-}3 + 0.764 \text{ MeV occurs.}$$

The proton ionizes the gas and produces one pulse per neutron entering the chamber (NSBR99; see also <http://www.nsbri.org>).

Whereas terrestrial models of the Bonner ball have a diameter of 200 mm, the compact space form is reduced to only about 30 mm. This may lead to the loss of some neutron counts because the neutrons are not fully thermalized and hence do not interact as above with the gas during their passage. The acceptable size for the deep space neutron environment might prove to be different from this model, designed for the Earth's magnetosphere but tests of several designs on early test missions would quickly establish an optimum for operational crew protection.

3.6.4 The ISS Photographic Emulsions and Neutron Foils

Passive techniques require a complex laboratory environment for successful reading, including a low radiation background not readily available in a deep-space mission, for example to the Moon or Mars. Thus, while they give an independent method for measuring some parts of the environment they are no substitute for active radiation sensors such as solid-state electronic dosimeters and the Bonner neutron detector.

3.6.5 The ISS Nuclear Track Detectors (NTD)

NTDs provide a detailed record of the particles which have traversed the package during its flight. Data on direction, energy and charge of the heavy ion component are obtained. These small packages are placed around ISS. Each package contains 3 strips of CR39 plastic, one for each of 3 perpendicular axes. The films are returned to Earth for laboratory analysis. The role of track detectors in deep-space missions must be further analyzed carefully because the combination of detailed data, ruggedness and compactness make their use, even if only in long-term research and development, very attractive

3.6.6 The ISS Tissue Equivalent Proportional Counter (TEPC)

The TEPC provides an efficient method of determining radiation dose and dose-equivalent in complex (mixed) radiation fields. It records the linear energy spectra for determining dose-equivalent exposures. Given the size, power and voltage requirements of TEPCs, it remains to be seen whether a lighter, smaller TE counter, possibly based on a solid-state detector, can be developed for deep-space missions.

3.6.7 The ISS Charged Particle Directional Spectrometer (CPDS)

This measures particle energy and direction in the same general environment as the TEPC. Since the interactions of heavy ions and their secondaries with tissue are not at all well understood, proton and heavy ion spectra both incident upon and inside the spacecraft will be measured. The DOSimetry TELescopes (DOSTEL) containing two thin silicon detectors will be used to measure the flux (and the LET distribution) of charged particles. Two of these are placed near each other in an empty rack space in the ISS U.S. Lab.. Several small mobile dosimetry units (MDU) can be used by crewmembers as a personal dosimeter or placed throughout the station and monitored by the same central unit. Given the size, power and voltage requirements of spectrometers, it remains to be seen whether the information from such an instrument can be justified in a deep-space missions.

3.6.8 The ISS Instrumented Phantoms Radiation Inside the Vehicle Skin [Human]

Radiation damage to humans in orbit is a process of transformation of the energy of charged particles in the vacuum to the local release of energy within the human cell. In energy terms, this is the degradation, through many steps of megavolts of kinetic energy to a few electron-volts of ionization energy in cell subelements. We have said that the low level of absorber "outside the S/C wall" means that particles bombarding the surface are grossly transformed on their way "through the S/C wall", a process handled by the GEANT transport programme. The environment "inside the vehicle skin" thus requires an entirely new range of detectors - tuned to different species and energy ranges and able to handle the attenuated radiation levels. A further modification occurs as the radiation passes *through the human body* as the different material in human tissues gives range to a new photon equilibrium and particle mixture. This part of the transformation has been studied in radiotherapy and the technology is being adapted by ESA in an unusual hybrid of the internal and external space-environment sensing. This is the Rando human phantom torso experiment. Layers of different atomic composition represent layers of the body (hence the name "Matroshka" after the Russian matrioshka dolls). The final stage in radiation damage to cells is handled by the science of microdosimetry, where the release of energy in the cell plasma or nucleus is simulated in sensors which resemble tissue in regard to their geometry and the media used.

Early experiments to plot an accurate model of dose[tissue] as a function of depth in a lump of material of a given shape were done by NASA on their manned vehicles, including the Apollo Moon missions (Benton 2001) and by ESA and the Russian Space Agency on MIR and FOTON (Demets 2000; Dura02). Experience with the deep-space environment was limited to Apollo until the MARIE experiment but NASA now has a major programme called Full Interplanetary Radiation Environment Simulation (FIRES) which should lend impetus to the acquisition of a highly accurate model of radiation damage in deep space, with adequate in-orbit verification.

The NASA Phantom Torso Experiment was flown in 1998 near solar minimum and the ISS Human Research Facility. The first experiments with Matrioshka concern dose within a human body when outside the capsule on an EVA. The phantom was

installed on an EVA from the ISS in 2004. Specialised detectors are within the body organs of interest. Results from the same phantom inside the vehicle will also give greater breadth to the experiment and useful points on the human dose vs depth curve in Earth orbit for comparison with previous and less exact dosimeter stack experiments [see e.g. Benton]. The results of Matroshka will be a useful comparison with the earlier, Phantom Torso Experiment, flown of 1998 near solar minimum and the ISS Human Research Facility experiments in progress since 2001, near solar maximum (Atwe03a) and the MIR-Biopan of ESA (Demets 2000; Dura02). We have the advantage of a period of solar minimum approaching, in which solar protons are reduced and cosmic rays are the dominant "invasive" or "penetrating" environment for humans and provide the major radiation background. Thus, measurements of the biological radiation environment in space and its simulation in accelerators is likely to be the theme of the new plan to for the Mars missions. See also FIRES, already moving and ESA Life Science programmes (Schi02, Schi03).

It is likely that development missions in deep space will carry similar phantoms, in order to plot dose maps for the human body in that environment.

3.6.9 The ISS NASA-JSC Phantom Torso

3.6.9.1 Role of a Phantom

Johnson Spacecraft Center (JSC) have also designed a "phantom torso". Organ level dose equivalent measurements are required in order to assess exact radiation risk in manned spaceflight Experimental and operational methods in the early 2000s were limited to the measurement of surface (skin) dose followed by the calculation, using *very conservative factors,* of the resulting organ-level doses. These often over-conservative factors are detrimental if they actually deny some of the more experienced astronauts some flight opportunities. The NASA Torso experiment will develop the capability to remove the undue conservatism described above. This is done by making actual measurements of organ-absorbed dose in a simulated human or "phantom". This experiment employs a fully instrumented phantom torso and head to provide the measurements of depth-dose, especially near blood-forming regions such as the sternum. Depth-dose-equivalent measurements are taken as a function of spacecraft altitude, attitude, location and time. These sensors are backed up by simultaneous measurements from the Tissue Equivalent Proportional Counter and the Charged Particle Direction Spectrometer in the same crew spaces. Similar equipment was flown on earlier shuttle missions.

3.6.9.2 Design of the "Phantom Torso"

The Phantom Torso itself is a tissue-muscle plastic equivalent anatomical model of a male head and torso comprised of 35 sliced "sections" housed in a Nomex suit. Each section is connected via a system of pins and holes. Voids within the phantom are used for active and passive radiation detectors. The five small active dosimeters are located at strategic radiobiological points of interest (head, neck, heart, stomach and colon) within the phantom and provide real time measurements. Data collection occurs without crew intervention. Every 7-10 days a crewmember downloads data from all three hardware

components to the HRF PC. These data are then downlinked to the Telescience Center at JSC in Houston. The Phantom Torso is deployed in the US lab of the ISS in a location that will not interfere with the daily activities of the crew.

3.6.10 MOSFET Dosimeters for Crew on EVA

As noted in Table 7, the Canadian Space Agency's dosimetric system employing MOSFETs measured doses during astronaut EVA while assembling and commissioning the ISS. The advantage of the MOSFET in this context is its size. Traditional personnel dosimeter technologies that monitor levels of radiation on people can be cumbersome and, unlike the MOSFET, cannot be sewn into undergarments. During ISS Flight UF-1 (STS-108), the Canadian Extravehicular Activity Radiation Monitors (EVARM) were tested during the EVAs of astronauts assembling the International Space Station. The prime objective of the experiment was to determine the radiation dose to astronauts during Extravehicular Activity (EVA) and to relate this to factors in the environment which can help reduce this dose, e.g., shielding, orbital position, radiation environment, etc. The experiment will result in recommendations for future mitigation of radiation during EVAs. Given the enhanced environment in deep space, analogous methods for mitigation of total doses received will be needed this environment.

For the EVA phase, crew members carried miniature MOSFET chip "badges" (a) close to the eyes, (b) in temporary pockets sewn into undergarments near BFO and (c) in a few skin locations. Leg and torso badges were located on the Liquid Cooling and Ventilation Garment (LCVG) worn inside the suit.

In current experiments other chips are placed in the astronaut's Communications Carrier Assembly (CCA) near the head. The badges are read periodically throughout EVA to measure background radiation. Pre- and post-EVA, the devices, which store the total dose signal for long times, are read by means of an external electronic reader. The dose data is downloaded from Earth orbit to the Portable Computer and batch downlinked to the ground. In a deep-spacecraft, fewer downloads of nonessential personal telemetry will be made because of the heavier demands on data relays in such a mission.

It can be seen that the small size of the MOSFET sensor chip, less than 1 x 1 mm, is a major advantage here. The disadvantage for alarm purposes is the low accuracy at the low end of its cumulative-dose range, say at 1E-2 Sv, when compared with a non-emergency dose rate in EVA of perhaps 1E-3 Sv/hr.

3.7 Dosimeter Tradeoff Studies

3.7.1 General

The AURORA PROJECT is a preparatory programme for deep-space exploration, proposed to all ESA members (for more information on Aurora see <http://www.esa.int/SPECIALS/Aurora/SEMZOS39ZAD_0.html>). Technology studies will occupy the first five years but decisions as to manned flights to Mars will be taken later in the present decade. As the Aurora project proceeds, weight, power and size budgets for radiation instruments will be decided upon. As the spacecraft construction is decided, the shielding - specially-designed or intrinsic built-in protection from GCRs and

solar protons - will be decided, leading to dose maps which the dosimetry experts can use. At that point in the programme, it will be appropriate to perform detailed tradeoff studies of the sensor technology, reading hardware and risk-management software appropriate to the space vehicle and its mission..

A very general tradeoff is shown in Table 9. Tables 9 and 10 compare dose sensitivity and size. We give examples below of the way in which REM has made tradeoffs of dosimetry for clients seeking advice on the choice of small rugged dosimeters in given situations, medical and industrial. These are not specific to space use but some criteria may apply. None of the technologies listed are for particle counting or characterization, only for measuring the cumulative deposition of energy [dosimeters].

3.7.2 A Comparison of Four Dosimeter Technologies

Before 1940, virtually all dosimeters employed the conductivity due to ionization in the air. The first ever absolute air dosimeter was used by Mme Curie, who used a gold-leaf electrometer which was discharged by conductivity in air. In the 1920-40 period, many basic types of "gas tubes" were designed. These placed a high voltage across a defined volume of air.

After 1945, new phosphor and silicon technology gave rise to the scintillator, the TLD and the p-n photodiode. In 1974, Holmes-Siedle published a radically-new principle - the Space-Charge (SC) Dosimeter. This arose from what was the “creative use of “failure”: the Metal-Oxide-Semiconductor transistor (MOSFET) was intended to be “hard” to radiation environments. Instead, because of trapped space charge in the dielectric its performance degraded rapidly under exposure. At RCA, where the MOSFET was invented, Poch and Holmes-Siedle (1969) decided that the trapping of SC in MOS structures was useful as a versatile dose measurement technique - a solid form of air ionization. Because it was “frozen” in the wide-band-gap oxide layer, the charge did not have to be collected. For an extended account, see Holmes-Siedle and Adams’ review of 1986. A perspective on the history of development of the RADFET and readers is given by the bibliography on RADFET dosimetry given in Holmes-Siedle and Adams (2002).

3.7.2.1 The Air Ionization Chamber

An early member of the class was called a “gas tubes”. Dozens of different gas tubes have been invented for the detection and measurement of radiation, the commonest being the Geiger counter. High voltage is needed in this case. The air ionization chamber works in a voltage region where the current generated is exactly linear with dose rate (see Section 3.2).

3.7.2.2 The Silicon Diode

This employs the same photovoltaic effect as the solar cell, invented by Bell Labs in the 1940s. Radiation is measured as a voltage or very small photocurrent which persists only as long as the radiation lasts. Some personal dosimeters convert the very small currents

into “counts”; others store them as charge on a capacitor [electrometers]. No high voltages are required.

3.7.2.3 The Thermoluminescent Crystal Dosimeter (TLD)

The TLD was developed in the 1950s. This method employs an effect similar to the TV screen phosphor - a pre-war discovery. The reader measures light output upon heating, using a photomultiplier, a current integrator and a high voltage. Other forms of luminescence are used in dosimetry and also in particle counting (“scintillators”).

3.7.2.4 The RADFET

The RADFET was invented in 1969. This method employs the field effect in silicon to read trapped space-charge in a dielectric. A field is generated by “Trapped Oxide Space-Charge, Qot” in the oxide layer above the silicon channel. No high voltages are required. An acronym for dosimetry system using the SC principle arises from the above subscript, “ot”. For the commercial system, REM has proposed the acronym “DOT”, short for “Dosimetry by Oxide Trapping”.

3.7.3 Tradeoffs in Dosimeters

In Table 10, we give a size comparison and tradeoff of a number of methods suitable for measuring ionization kerma in a manned vehicle is given. The small size of the RADFET by comparison of the sensitive region with that of other ionization sensors is obvious. The ionization-sensitive, thin layer of oxide (white), is attached to a chip of charge-sensitive silicon (grey). Two or more of such sensitive regions, of size less than 0.1mm, are arrayed in a single sensor chip. The sensitive volumes of dosimeter diodes is a simple slab of doped (a diffused junction) semiconductor silicon or a higher-Z semiconductor [InP, HgI]. The whole diode volume is about 5 x 5 x 0.3 mm. The active volume [depletion region] is a fraction of this. The Thermoluminescent dosimeter is a simple slab - a typical TLD crystal is about 3 x 3 x 1 mm, most of which is sensitive. There is a large jump to the volume of a gas ionization chamber. This is a cylinder of air at least 10mm long. In addition to the size of the sensor part, the user has to consider the size, weight and power of the electronics required to read the dose information. The larger types require the measurements of very low currents with any time variations measured with nanoampere accuracy. Furthermore, spurious electrical noise must be excluded rigorously. With the RADFET, only a DC voltage has to be read and can be sampled as many times as necessary for accuracy.

Advantages and disadvantages of four types are shown in Tables 10 and 11. Not surprisingly, the small size and simple readout technique for the RADFET have disadvantages in the matter of accuracy, as shown in Table 12. For the diode, the high density, possibility of scaling up the volume and manufacturability of the device make this a very acceptable candidate for measuring low dose rates. Essentially, one can increase the number of diodes or the volume of the depletion region until the problem of noise currents is defeated. Space dosimetry system designers with no commercial limitations can also use complex circuit designs for the monitoring of low signal currents.

For several sound reasons, in 2004, the RADFET method of trapped space-charge with readout by field-effect has by far the greatest potential for increases in accuracy, compactness and reduction of power drain.

In summary, because of the different characteristics of the four dosimeters described, there is, "niche" for the applications of each in a manned mission. The four principles shown in the table also compete in fields, such as in the quality control of radiation beams and in the monitoring of environmental radiation. The small volume of the RADFET is a disadvantage for the monitoring of INTERNAL dose rates in manned vehicles but makes it suitable for EXTERNAL monitoring [strictly, monitoring in deep space behind thin "walls" such as space suits. The MOSFET technology of 2004 is marginal for the sensitivity needed but there is time for radical advances during the time-scale of Aurora. The most appropriate broad applications of the 2004 RADFET system are high-dose requirements such as unmanned vehicles in GEO, radiotherapy, beam calibration and emergency radiation releases. However FUTURE development can produce orders of magnitude of improvement in all performance features and may change the above analysis. The strong present thrust of development of MOSFET dosimetry for medical and emergency dosimetry is likely to throw up such large improvements. Large improvements are less likely in the TLD and the air chamber although Optically Stimulated Luminescence Dosimetry may show the way to higher sensitivity in luminescence-based dosimetry.

3.7.4 Performance of Some Miniature Air Ionization Chambers

To illustrate the expected difficulty in the use of air ionization chambers in "tight corners" [situations in which there is small space available, severe weight and power restriction and noise], we will describe a number of designs of air chamber. Text books on radiological physics give details of the theory and large variety of chambers, large and small which are used in radiotherapy, radiation protection of personnel, quality assurance and on-line control of machines ranging from nuclear reactors to medical LINACs. In all of the practical designs, currents caused by ionization are measured. Air is split into electrons and ions and a small current is generated by sweeping these to a pair of electrodes with a voltage of the order of 300V. Measuring the current in ionized air gives an absolute and very reliable measure of the dose rate, typically in roentgens [R] per hour. Mme Curie's gold-leaf electrometer operated on the same principle; the rate of collapse of the gold leaf, discharged by conductivity in the air, gave the dose rate. For IMRT phantoms, some dosimeter companies, for example Exradin, have constructed very small cylindrical chambers filled with air and made of tissue-equivalent, conductive plastic. The problem here is the measurement of measuring the conduction in a very small volume of air. Text books say that, at 1 R/hr, 1 litre of air gives conduction of one picoampere. It is difficult to measure such a current along a cable. The current may be integrated as picocoulombs of charge on a capacitor but cable leakage and capacitive pickup are now factors in signal to noise ratio. Engineers will know that electrometers will do this but also that they are very sensitive to disturbances. RADOS of Finland has made a truly miniature air chamber of volume less than 0.01 cc, where the above noise problems have been reduced by a variant of Mme Curies method - discharge of a floating electrode, the voltage being measured by means of a MOSFET. This microminiature air

chamber is named the Direct Ion Storage (DIS) dosimeter and is being investigated for personnel protection. This method avoids the use of a cable for currents; only the DC output of a MOSFET is measured, as in the RADFET. The difference between the last-mentioned pair of devices is in the volume of the ionizable medium. In one case, air and the other, silica. Air chambers may often be excellent pieces of precision engineering but the figures below show that, by comparison with the RADFET, they suffer in size where fitting into "tight corners" is concerned. In addition, the charge generated from the air is mobile and volatile (not trapped in a solid as in the MOSFET). Table 10 illustrates these facts and extends the comparisons shown in Table 9. It shows the approximate dimensions and response figures for three commercial air chambers [recommended for IMRT dosimetry] and also for the DIS and the RADFET. Even though the calculated sensitive volumes are not exact, the figures illustrate magnitudes of size and also the engineering problems of measuring dose very accurately at therapeutic levels, within a small cavity. The electronic engineer will have little doubt which signal he would rather measure at a dose rate of say 10 Roentgen [0.08 Gy] per minute.

SENSOR	SIZE	READER COMPLEXITY	DATA instant ?	stored ?	SYSTEM COST
RADFET	0.1 mm	Simple	Yes	Yes	Low
DIODE	over 1 mm	Complex	Yes	No	Moderate
TLD	over 1 mm	Very Complex	No	Yes	High
IONIZATION CHAMBER	10 mm	Very Complex	No	Yes	High
Notes: RADFET = Radiation-Sensitive Field Effects Transistor; DIODE - short for p-i-n diode dosimeter; TLD = Thermoluminescent Dosimeter.					

Table 10. System comparison of four competing compact rugged dosimeters.

SENSOR TYPE	LOWEST DOSE MEASURED ROUTINELY		PERIOD REQUIRED FOR IMPROVEMENT
	(mrad)	(mGy)	(yrs)
RADFET	100	1	1-3
DIODE	1	0.01	1-3
TLD and OSLD	1	0.01	3-5
IONIZATION CHAMBER	0.1	0.001	None
OSLD = Optically Stimulated Luminescence Dosimetry			

Table 11. Dose comparison for four competing compact rugged dosimeters.

	dimensions (mm)	volume (mm^3)	response
air chambers*			
Exradin 18l	8 x 6 x 6	288	17 pC/R
Exradin 14	6 x 4 x 4	100	3 pC/R
Exradin 16	3.4 x 3.4 x 3.4	40	2 pC/R
Solid-state*			
Direct Ion Sensor**	2 x 2 x 1	4	1000 mV/rad [Si]
RADFET **	0.5 x 0.5 x .0.1	0.025	10 mV/rad [Si]
Notes: * current outputs ** voltage outputs volumes calculated for rectangles. actual volumes of air chambers are annuli [sources: EXRADIN website 2004; RADOS ; REM.]			

Table 12. Gas vs. solid dosimeters; size and acceptable signal.

3.7.5 Performance of some "Silicon Ionization Chambers" (Diodes)

The p-n junction diode can be thought of as a “silicon ionization chamber”, in which the junction depletion region relaces the air. In all of the practical designs, electrons and holes are generated by the radiation and a small current is generated by sweeping these to a pair of electrodes. Measuring the current in the junction gives an absolute and very reliable measure of the dose rate, typically in cGy[Si] per hour. For our application, those currents are in the picoampere range for a small chip of silicon. Thus, many of the engineering problems of noise and electrometer design resemble those of the air chamber.

3.7.6 The MOSFET Reader

Circuits for tracking the threshold voltage of the MOSFET have been developed by several groups. The European Space Agency produced threshold-voltage tracking circuits for laboratory use and then sponsored the development of several readers suitable for external and internal environment monitoring aboard unmanned spacecraft (e.g. the SREM, developed by PSI, Villigen). Thomson Neilson Associates of Canada produced a bench-top reader for clinical use, sterilization and beam checking. A student project at Harvard Medical School designed a PC-controlled reader for clinical use with the REM RADFET, for which Dr David Gladstone won the Young Investigator prize of the American Association of Physicists in Medicine of 1991 (Gladstone 1991). This was one of the first systems used in the clinical treatment of cancer.

REM and Satellites Internation Ltd produced bench-top readers for the US Army and Sandia laboratories produced similar devices for the US Army's testing of RADFETs before a production RADIAC, the AN/UDR-13, a miniature pocket reader, was produced for the armed forces by a manufacturer (AN/UDR 2004). Some other NATO countries also produced domestic versions of the AN/UDR-13.

The BaBar project at Stanford Linear Accelerator, California, has developed an automated RADFET Monitoring Board which worked well for the 5 years of the experiment.

The Centre for Medical Radiation Physics (CMRP) at University of Wollongong, Australia has developed a Clinical Semiconductor Dosimetry System (CSDS) which is available for commercial development.

3.8 Development of Radiation Sensor Technology for Deep Space

3.8.1 General Pointers for Development

The term "housekeeping" is used in US space projects for sensors and systems of which the main function is to keep the spacecraft running rather than to acquire scientific knowledge. The radiation monitors on the manned deep-space mission to Mars or the Moon will be "housekeeping", concerned with safety. If a space science instrument were to be chosen as a starting point that, in order to optimize it for such a "housekeeping" function, it would probably be radically simplified, i.e. have complex and costly parts removed. For example, a counter will yield crucial warning signals by counting pulses derived from a broad range of particles - then the "housekeeping" design would save weight and power by omitting some of the specialized counting circuits which finely analyze the composition of those particles for a scientific purpose. Other complex sensing principles might be rejected while other fairly crude ones might be found useful. Examples of the two types are scintillation and Geiger counting. The first requires avalanche detectors for counting, plus the analysis of low-amplitude pulse-heights; the second requires only a crude count-rate meter. Another example close to REM's interests is the RADFET principle - not yet accepted for space science but widely used already for "housekeeping" in the electronics bays of unmanned spacecraft and in terrestrial radiation applications such as robotics and medicine.

3.8.2 Examples of Simplification

One of the guiding principles which must be a foundation of further study of hardware for radiation protection on this mission will be the possibility of "simplification for housekeeping". If this requires unconventional thinking, then designers of unconventional sensors should be brought into the manning of the Aurora contract teams.

An example of the use of solid-state sensing to simplify cumbersome apparatus in commercial imaging was the replacement of the vacuum TV camera-tube sensors by silicon Charge Coupled Device (CCD) and silicon CMOS sensors. In the commercial world, this was a response to relentless design pressure to lower power drain and size.

The "webcam" can be thought of as a good "unconventional outcome" of the bulky TV broadcast camera of 1950. The sensors and the encoding of the signals have been simplified. Silicon imaging sensors from the same factory are used in industrial control and microsatellites and scientific CCDs which are produced at much larger cost to CERN, ESA and NASA for flybys of the planets, X-ray astronomy or particle tracking (Camanzi et al 2000; Holmes-Siedle et al 1995, 1997).

Ruchti's group has recently described a fine scintillator matrix, coupled to an intensified CCD**,** which will visualize the tracks of Galactic Cosmic-Ray muons at ground level (Bambaugh 2000). A portable demo-model is available to the project. Bubble chambers giving similar information weighed tons.

Many high-technology engineering materials other than MOSFETs react to radiation energy so that they can be used as dosimeters (examples are glass fibres**,** organics and wide-base diodes, see Holmes-Siedle and Watts 1997; Holmes-Siedle and Adams 2002). There have also been strong efforts to perform "housekeeping" monitoring for neutrons induced by cosmic rays in aircraft (Dyer 1999, 2000).

We have proposed earlier in this Chapter to use UV as a detector of hazards. This may be less cumbersome than detectors in the soft-X-ray range, such as those used at present by NOAA weather satellites to classify solar flares.

3.8.3 Simplification of Advanced Detectors for Housekeeping on Spacecraft

Examples of "simplification for housekeeping" is of course, what REM has done with MOSFET dosimeters in some fields [space, robotics] and webcam CCD designers for "housekeeping" and industrial control at ground level. Bambaugh and Ruchti (2000) have recently written about a glass scintillator array coupled to an intensified CCD for tracking Galactic Cosmic-Ray muons by eye. Patterns created in such an array may contain clues to forthcoming dose-rate changes during flares.

There have also been strong efforts to do monitoring for spallation neutrons in aircraft as a part of crew healthcare, using CCDs and diode arrays as well as the usual large neutron counters. A hypersensitive form of the p-i-n diode neutron dosimeter might assist in managing the severe spallation-neutron problem in deep space.

3.8.4 Summary on Development

In summary, there will be three equally important locations for REMWARN sensors: those which

1. bolt on the outside of a vehicle and sense photons or incident high-energy particles.
2. sit inside the bulkheads of the vehicle, which may be half-inch aluminium, and sense penetrating particles and showers including neutrons.
3. are attached to the individual crew members.

Size, weight and power budgets will demand some radical re-thinking of sensor system design, software and placing and ergonomics will be involved in their application.

3.9 Conclusions

We have given here an overview of radiation warning monitors. We have noted some further tasks that are required, especially the need for simplification of certain functions to meet the weight, power and size constraints of a spacecraft for a Deep-Space trajectory and a long mission. By moving from the old technology of the bulky Geiger counter to the much smaller solid-state technology, **we can achieve similar results in space with a huge factor less power, weight and size**. We have described some technical thinking on unusual detector types such as (a.) a MOS detector of UV variability (b.) a portable combination of a scintillator and an intensifier CCD that displays visible tracks of cosmic rays and may be obtained for demonstration. There may be avenues for research collaboration with existing ESA projects such as the radiation dosimetry activity aboard the ISS, including the use of phantoms in orbit. The discussion on system aspects of radiation monitors continues in Chapter 6. Specific detector development work is included in various proposals for future work, which are made in Section 6.8.

4. Feasibility to Use and Integrate Existing Systems

In order to assess the feasibility to use and integrate existing systems, we focus our attention on the case of a mission to Mars. Terrestrial space weather systems rely on early warning from the L1 point, where detection of SPEs provides a warning time of less than an hour. These existing systems could also be used for Moon missions by relaying the L1 alert to the onboard warning system. This approach however is not feasible for true interplanetary missions, at locations away from the Sun-Earth line. The scenario of a mission to Mars addresses interplanetary issues, which do not exist for a mission to the Moon. Moreover, in the solar system this scenario remains one that may come true in the next decades and carries with it many hopes and expectations for our future in space.

This chapter investigates whether a warning system using the existing monitoring and warning capabilities, based on Earth, in the geospace environment or at L1, as presented in Chapter 2, would be sufficient to provide accurate forecasts to the crew of an interplanetary mission to Mars or for preventing hardware deterioration. Four parameters describing the scenario are investigated:

1. the orbit of Mars
2. telecommunications (signal travel time)
3. location of Earth and Mars in relation to forecasting
4. radial extrapolations of SPEs

4.1 Mars Orbital Parameters

Mars's orbit is slightly elliptical, coming closest to the Sun at about 1.4 AU before moving out to about 1.6 AU. The motion of Mars, which is farther from the Sun than Earth, is slower. As Earth keeps racing ahead and Mars falls behind, there are instances when the two planets form a straight line, with the Sun interposed between them. The planets are said to be in conjunction (Figure 19). Mars disappears from Earth's view behind the disk of the Sun, and is as far away from Earth as it can be - about 400 million kilometers (see Figure 20).

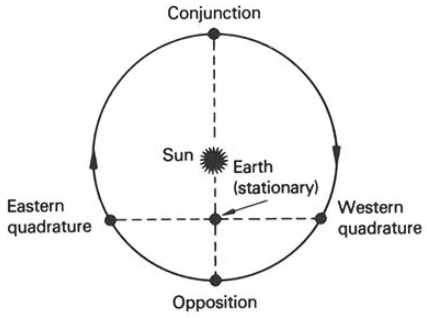

Figure 19. At conjunction of Mars and Earth, Mars becomes invisible in the Sun's rays. Best observation period is from quadrature to quadrature (Glasstone, 1968).

In Figure 21, a Mars-Sun-Earth angle value near +/-180° corresponds to conjunction; a value near zero corresponds to solar opposition (Sun, Earth and Mars form a straight line with Earth in the middle). When the Sun, Earth, and Mars describe a right angle, Mars is said to be in quadrature.

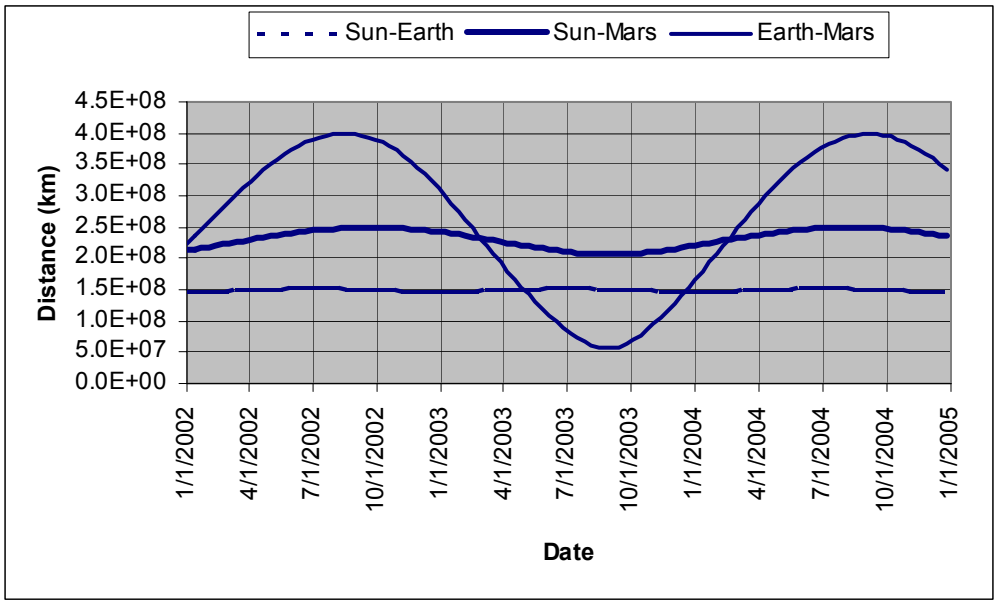

Figure 20. Distances (km) Sun-Earth, Sun-Mars and Earth-Mars. The graphs were generated with data obtained from the Planetary Data System Mars Ephemeris Generator 2.1, available at:<http://ringmaster.arc.nasa.gov/tools/ephem2_mar.html>.

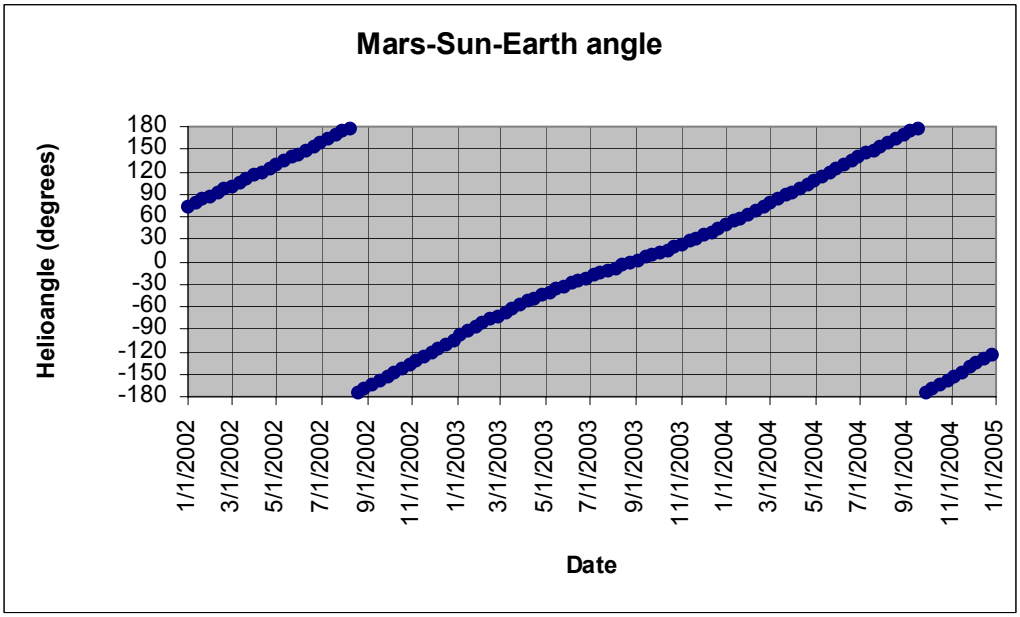

Figure 21. Heliocentric Mars-Earth angle. Same source as in Figure 20.

Consequently, Earth and Mars move in and out of favourable phasing for transfers to and from each other. It takes approximately 26 months (roughly two years) before the phasing is appropriate. This parameter gives roughly the minimum trip time required for a manned mission to Mars.

4.2 Telecommunications

The Earth-Mars distance is a parameter important for telecommunications from Earth. The distance varies from about 56 million km up to 400 million km, when the Earth is on the opposite side of the solar system from Mars (Figure 20). Thus the time required for radio communication from Earth to a spacecraft on Mars varies from 3.1 up to 22.2 minutes.

It is important to mention that when Mars is at conjunction, communication is not possible at all. For instance, during August 2002, at the time of conjunction, no MARIE data were received for approximately two weeks (Atwell et al., 2003).

4.3 Spatial Relations between Earth and Mars Environments

The Mars-Sun-Earth angle (Figure 21) is a parameter important for an Earth-based space weather system. Real-time monitoring from Earth is limited to the solar disk and limb activity and to CME observations on the plane of the sky.

This is sufficient to give warnings of near-Sun injection events for the period of time when Mars is near opposition or connected to the Western solar hemisphere as seen by an observer on Earth. When Mars is magnetically connected to the limb regions as seen from Earth, the predictions may be based on chromospheric and coronal activity observations. Existing alternative techniques based on far-side imaging services and corotation projections may provide additional information for the limb regions and some information on the backside, but risk estimates would be much less reliable when Mars is connected to these longitudes.

Most of the accelerated particles move along spiral interplanetary magnetic field (IMF) lines after escaping the flare site. The longitude of the field lines connecting the Sun and the Earth changes with the solar wind speed. The effect and importance of the solar wind speed for model predictions is illustrated in Figure 22 for an idealized, extremely localized impulsive SPE originating at a flare on the footpoint of the IMF, with no cross-field diffusion. A summary is given in Table 13.

This is a very, in fact often unrealistic, set of constraints in practice. The flare acceleration region may be large enough to encompass a range of footpoints. In addition, some accelerated particles diffuse across the IMF and then transport out along new field lines. Diffusion away from the flare site will slowly affect regions at heliolongitudes distant from the flare footpoint. So in Figure 22, accelerated particles could be seen in cases (a) and (c) at Mars, but in diminished numbers and at different times.

In IP shock dominated events, most of the accelerated particles move along spiral interplanetary magnetic field (IMF) lines after escaping the shock front. Some diffuse across the IMF and then transport out along new field lines. Combination of an extensive shock front and diffusion away from a shock front can quickly fill the heliosphere.

SPEs at Earth	Conditions for an observer on Earth	Mars lagging Earth by 90° as in Feb. 2002	Mars at conjunction as in Aug. 2002	Mars leading Earth by 90° as in Jan. 2003	Mars lagging Earth by 20° as in Nov. 2003
Near-Sun injection SPE (from the western solar hemisphere)	a) W67, V_{SW}=350 km/s	No SPE at Mars			No SPE at Mars
	b) W51, V_{SW}=450 km/s				SPE at Mars
	c) W42, V_{SW}=550 km/s				No SPE at Mars
IP shock dominated SPE	Western CME (rapid rise and decline)	No SPE at Mars	Poorly connected until shock passage-SPE at Mars	SPE at Mars (shock front)	SPE at Mars (rapid rise and decline)
	Halo front-sided CME (shock front at Earth)	SPE at Mars (rapid rise and decline)	No SPE at Mars	Poorly connected until shock passage-SPE at Mars	SPE at Mars (shock front)
	Eastern CME (poorly connected until shock passage)	SPE at Mars (shock front)	SPE at Mars (rapid rise and decline)	No SPE at Mars	Poorly connected until shock passage-SPE at Mars
	Halo back-sided (no SPE)	Poorly connected until shock passage-SPE at Mars	SPE at Mars (shock front)	SPE at Mars (rapid rise and decline)	No SPE at Mars

Table 13. Mars orbital dependent SPE predictions and qualitative estimate of the flux profile, based on solar wind speeds for near-Sun injection events and the CME direction for IP shock dominated events.

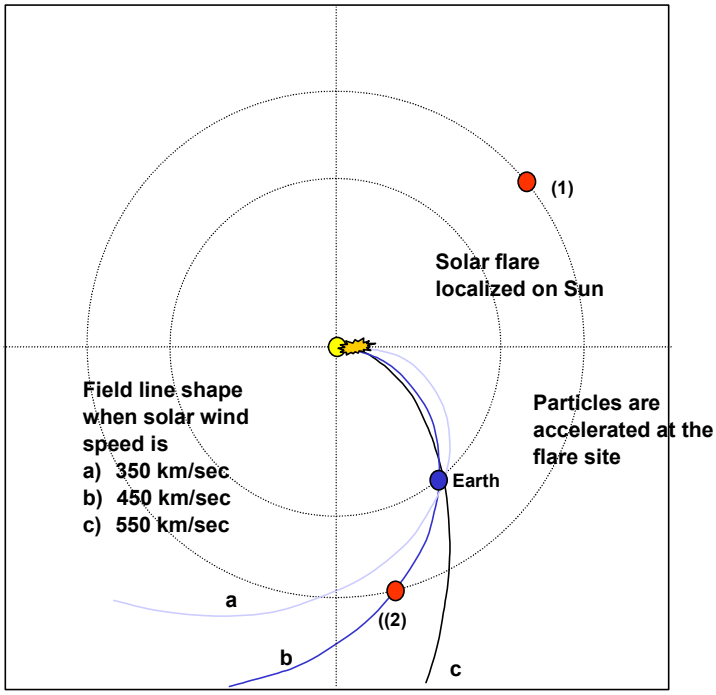

Figure 22. "Impulsive" solar particle events. (a) is connected to W67, V_{SW}=350 km/s; (b) is connected to W51, V_{SW}=450 km/s; (c) is connected to W42, V_{SW}=550 km/s. In case (2), Mars is lagging by 20° behind Earth as in November 2003. For the well-connected field line (b), the event is seen both at Earth and Mars. For conditions (a) and (c), the event is seen at Earth, but not at Mars. After Turner (2003), with a different perspective.

Knowledge of the Mars-Sun-Earth angle and an estimate of the CME direction as seen from Earth could provide an estimate of the expected flux profile. Figure 23 illustrates the different flux profiles according to the position of Mars for a halo front-sided CME as seen from Earth. The flux profile will be one of:

(a) "rapid rise and decline" when Mars is well-connected to the nose of the shock, and is lagging Earth by 90° as in February 2002, from where the CME is seen to propagate Westwards.

(b) "flat profile peaking at the shock passage" when Mars is lagging Earth by 20° as in November 2003, from where the CME is seen as a front-sided halo.

(c) "poorly connected profile until the shock passage" when Mars is leading Earth by 90° as in January 2003, from where the CME is seen to propagate Eastwards.

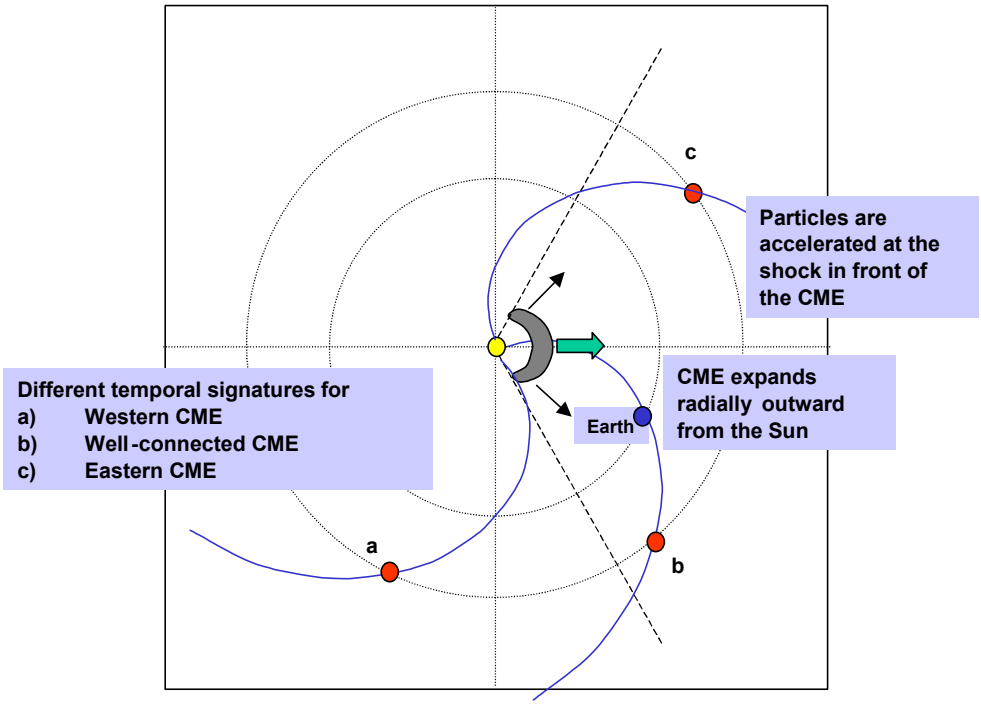

Figure 23. "Gradual" solar particle events. Different temporal signatures are observed depending on Mars orbital position, from where the IP shock accelerated particles are associated with (a) a western CME, (b) a halo CME or (c) an Eastern CME (Turner, 2003).

This behavior follows the results shown in Figure 22. The logic is applied to other simple geometry combinations in Table 13. This is however a simplified rule of thumb. For instance, it may happen that a SPE is observed at Earth following a full halo backsided CME.

Examples of energetic particles from the far side of the Sun obtained by the SOHO spacecraft are given at:
<http://solar.physics.montana.edu/nuggets/2001/010420/010420.html>

The flux profile and time arrival of the shock front are particularly difficult to predict for detected backsided CMEs. In this case, several large errors can be made when trying to:

- locate the solar origin of the CME on the backside of the Sun
- estimate the onset time without detection of an associated flare or X-ray flux onset
- estimate the shock velocity without a metric type-II report.

As a result, flux profile predictions for IP shock dominated events associated with backsided CMEs, when Mars is near conjunction, are highly compromised. Consequently, for more than half of the mission duration, when Mars is on the opposite side of the Sun than the Earth, the accuracy of predictions is compromised.

4.4 Radial Extrapolations

The Sun-Mars distance is a parameter important for radial extrapolations of solar wind speed, particle flux and fluence. Mars's orbit is slightly elliptical, at the helioradial distance of 1.4-1.6 AU. The usual method for estimating the energetic proton environment for a Mars mission is to take the solar proton observations at 1 AU and then extrapolate these observations to other radial distances.

4.4.1 Near-Sun Injection Events

Assuming that the proton flux is confined to a magnetic "flux tube" and that the volume of the tube behaves in a classical manner as the radial distance R from the Sun increases, then the peak flux extrapolations should behave as a function of R^{-3}, and the fluence extrapolations should behave as a function of R^{-2}. The limited experimental data of measuring the same event at different radial distances generally confirm the utility of this type of radial extrapolation, however with a modified form of the power laws. The working group consensus recommendations for radial extrapolation documented in a JPL report edited by Feynman and Gabriel (1988) are summarized in Table 14.

Extrapolations from 1 AU to		< 1 AU	> 1 AU
FLUX (cts/s)	Functional form	R^{-3}	$R^{-3.3}$
	Variation range	R^{-3} to R^{-2}	R^{-4} to R^{-3}
FLUENCE (cts)	Functional form	$R^{-2.5}$	
	Variation range	R^{-3} to R^{-2}	

Table 14. Radial extrapolations for solar flare proton flux and fluence (Feynman and Gabriel, 1988).

4.4.2 IP shock Dominated Events

The class of interplanetary shock dominated events does not seem to scale with radial distance as expected by the power law geometry (Reames et al. 1997a; Reames and Ng, 1998; Smart and Shea, 2003). Smart and Shea (2003) suggest that the radial extrapolations (commented in the previous section) only apply to specific types of well-connected solar flare associated events, and that they do not apply to the case of general shock accelerated events. The interplanetary shock dominated events generate a maximum flux as the shock passes the detection location, but the flux does not scale in the classical manner with radial distance. A radial gradient R^{-3} predicted by theory (Ng and Reames, 1994) is likely to apply to the shock peaks and the streaming plateau, but not to the invariant spectral region behind the shock where the radial gradients are small (Reames, 1999a, b).

4.5 Summary and Conclusions

Many researchers on SPEs seem to agree that intense and gradual SPE events are due to interplanetary shock waves driven by CMEs, and that particles accelerated in the flare (which are characterized by, for example, a high 3He/4He ratio) are observed only as a small and impulsive event (only when the flare is located at the well-connected longitude).

However, many fast CMEs (e.g., > 1500 km/s, as observed by LASCO) have nothing to do with SPE events, and more importantly we still cannot isolate the solar signatures of shock-associated CMEs. Actually, CME initiation in general is still an open issue. It is believed that a CME can be directly observed in X-ray/EUV images when there is enough temporal/spatial/temperature coverage, unless it is launched at very high altitudes. Despite the difficulty to forecast CMEs, estimates of SPE flux profiles can rely on the knowledge of three parameters: the solar origin, the onset time and the shock velocity. The parameter measurements demand solar observations, which, in the existing space weather systems, are limited to our terrestrial point of view.

With our terrestrial space weather system, the best case for reliable estimates of SPE flux profile predictions is therefore the case when Mars is near opposition. This is also the best case to allow timely telecommunications.

As shown in Table 15, consequences for forecasting strategies can be summarised to three main requirements: onboard warning and forecasting systems, a multi-viewpoint system and the development of interplanetary models to be tested against data.

Mars Orbital Parameters	Terrestrial Space Weather System		
	Telecommunications	**Observations**	**Models & predictions**
Earth-Mars distance	Radio travel time: 3.1 - 22.2 light minutes		
Mars-Sun-Earth angle	Mars at conjunction: ~ 2 weeks without contact	Limited to solar disk and limb activity	Accuracy of warnings for near-Sun injection events compromised for most of the mission duration
		Limited to limb-to-limb radio bursts & CME observations on the plane of the sky	Flux profile predictions for IP-shock dominated events most compromised for back-sided events with Mars near conjunction
Sun-Mars distance (1.4-1.6 AU)			Radial extrapolations: solar wind speed (effect on longitudes of IMF lines connected to the observer); no classical gradients for particle flux ($\sim R^{-3.3}$) and fluence ($\sim R^{-2.5}$)
Favorable Mars-Earth phasing			Mission start and duration: predictions with respect to solar cycle; input to proton fluence models.
Requirements	On-board warning and forecasting system	Multi-viewpoint-system	Test of comprehensive simulations of the interplanetary medium to fit readings from numerous unmanned missions.

Table 15. Mars orbital parameters versus Earth-based space weather system, and consequences for forecasting strategies.

5 Integration of Models and Data Systems

5.1 Space Weather Model Development

Space weather modelling aims to develop models that use information from places where instruments happen to be and to specify and forecast conditions at places where the information is wanted. Instruments are deployed in space and on the ground in arrangements intended to optimise their usefulness. Nonetheless, there are strategic gaps in instrument coverage that future planned missions will help fill. The following projects, which should eventually contribute to reducing radiation risk, merit attention.

5.1.1 The Underlying Solar Physics

Projects aimed at understanding the underlying physics of CMEs and solar flares are needed for developing an end-to-end capability for forecasting the hazards of radiation for humans in space.

Fry et al. (2003) recommend development of a 3-D, time-dependent, low coronal density model, in order to understand where shocks first develop, which is a key determinant of the particle acceleration process (Cane, 1997). Better observations of, and insight into, the sources of type II solar radio emissions would provide improved initial shock speed estimates, which would be valuable for initialising and testing models.

5.1.1.1 SHINE

Solar, Heliospheric and Interplanetary Environment (SHINE) is an affiliation of researchers within the solar, interplanetary, and heliospheric communities. Their work is dedicated to promoting an enhanced understanding of the processes by which energy in the form of magnetic fields and particles are produced by the Sun and/or accelerated in interplanetary space and on the mechanisms by which these fields and particles are transported to the Earth through the inner heliosphere.

Its research focuses upon the connection between events and phenomena on the Sun and their relation to solar wind structures in the inner heliosphere. The goal of SHINE activities is to enrich and strengthen both the physical understanding and the predictive capabilities for these phenomena.
<http://www.shinegroup.org/>

5.1.1.2 SOLAR-B

Solar-B is an international collaboration building on the highly successful Japan/US/UK *Yohkoh* (Solar-A) experience. The mission consists of a coordinated set of optical, EUV and X-ray instruments that will apply a systems approach to the interaction between the Sun's magnetic field and its high temperature, ionised atmosphere. The result will be an

improved understanding of the mechanisms, which give rise to solar magnetic variability and how this variability modulates the total solar output and creates the driving force behind space weather.

The Solar-B spacecraft is scheduled for launch in September 2006. It will be placed in a sun-synchronous orbit about the Earth. This will keep the instruments in nearly continuous sunlight, with no day/night cycling for nine months each year. The SOLAR-B web-site is located at: <http://science.nasa.gov/ssl/pad/solar/solar-b.stm>.

5.1.1.3 SDO

SDO is the first Space Weather Research Network mission in the Living With a Star (LWS) Program of the National Aeronautics and Space Administration (NASA). SDO is being designed to help us understand the Sun's influence on Earth and Near-Earth space by studying the solar atmosphere on small scales of space and time and in many wavelengths simultaneously. SDO has four main goals:

1. Understand the Solar Cycle.
2. Identify the role of the magnetic field in delivering energy to the solar atmosphere and its many layers.
3. Study how the outer regions of the Sun's atmosphere evolve over time - ranging from seconds to centuries - and space.
4. Monitor the radiation (ex: UV, EUV, etc.) levels of solar output.

The capabilities of the three SDO instruments are as follows:

- The Helioseismic and Magnetic Imager (HMI) will extend the capabilities of the SOHO/MDI instrument with continuous full-disk coverage at considerably higher spatial and temporal resolution line-of-sight magnetograms with the optional channel for full Stokes polarization measurements and hence vector magnetogram determination.

- The Atmospheric Imaging Assembly (AIA) will image the solar atmosphere in multiple wavelengths to link changes to surface and interior changes. PI: Alan Title, PI Institution: Lockheed Martin Missiles and Space Advanced Technology Center

- The Extreme Ultraviolet Variablity Experiment (EVE) will measure the solar Extreme-Ultraviolet (EUV) irradiance with unprecedented spectral resolution, temporal cadence, and precision.

For more information see:<http://sdo.gsfc.nasa.gov/>.

5.1.2 Development of Flare Prediction Models

Most of the impulsive SPEs reach Earth nearly as rapidly as any electromagnetic signatures (~8 to 80 minutes), leaving insufficient time to make appropriate changes in most EVAs. As a result, flare monitoring with present and upcoming spacecraft will

provide only short-term warning, at best, of oncoming energetic particles from such events. To lengthen the lead-time available for incorporating information on flare occurrence into EVA scheduling, "flare prediction models" should be given increased attention.

5.1.3 The Particle Acceleration Problem

Quantitative, theoretical attacks on the "particle acceleration" problem are sorely needed. Numerical simulations alone can illuminate the details of the acceleration process under realistic conditions, but such efforts have only just begun. Aspects of shock acceleration in SPEs still elude quantitative understanding. Among the less mature areas of understanding in the field of Sun-Earth connections, this area is particularly critical. Until we understand how particles are accelerated at shocks, there can be no first-principles numerical code for predicting SPE parameters from solar inputs.

Several theories exist for the process of acceleration of particles by CME shocks (Lee, 1997; Reames, 1997b; 1999b), quantitative modelling of which provides the only feasible way to connect the MHD characteristics of the CME-shock system with the flux and spectrum of SPEs at 1 AU and to spacecraft located in the interplanetary medium. This is a challenging task, as both large-scale MHD characteristics and small-scale particle properties must be considered. A related problem is our incomplete understanding of the flare-driven component of SPEs. Observations by SOHO, Wind, and other spacecraft are clarifying some of these complex phenomena.

The SEC event in Figure 13 was unique in that the interplanetary type II radio emissions were observed until the time of the shock arrival, suggesting that the Wind spacecraft was very close to the radio source region at that time. For this event, both the electron beam and intense plasma (Langmuir) waves were detected for several minutes just before the passage of the shock (Bale et al., 1999), directly confirming the generation of the type II radiation in the foreshock region upstream of a CME-driven shock. These observations suggest that the shock surface has small-scale (few 10s of RE) structure that provides local regions of quasi-perpendicular field connection. Two-point measurements with the STEREO mission of the type II source region, in concert with the IMPACT/STE suprathermal electron observations will resolve this structure with unprecedented time resolution and shed light on the physics of type II generation.

IMPACT will provide information on SPE behavior over a large angular swath of the heliosphere near 1 AU. With the insight into the relationship to solar signatures provided by the STEREO imaging investigations, we may be able to substantially improve the process for radiation warnings. The coupled analysis of data and models is expected to lead to new insights that translate to space weather applications. The information gained from the more physically rigorous STEREO IMPACT models, verified by IMPACT measurements, are the answer to improved Wang/Sheeley-type schemes and to the better identification of solar signatures that lead to disturbed interplanetary conditions.
STEREO/IMPACT: <http://sprg.ssl.berkeley.edu/impact/welcome.html>

5.1.4 Three-Dimensional MHD Simulations

In the ideal situation, all models are self-consistently coupled so that changes in the driving forces of the system are communicated through the different regions of space. It is time to move beyond existing one- and two-dimensional models to three-dimensional MHD simulations in order to correctly model the initiation of solar storms, the associated shocks, their propagation through the interplanetary medium, and their impact between 1-1.6 AU.

The physical models must not only be brought into existence, but they must be also transferred into operational codes that will allow accurate space weather forecasts and nowcasts. Observational inputs, preferably real-time, to initialise and drive MHD simulations are now feasible and can impart much-needed realism to the modelling results. Real-time monitoring of the ambient interplanetary medium properties to establish "background conditions" would improve the accuracy of CME and shock propagation models. The combination of heliospheric modelling with real-time solar data could be used to predict arrival times and magnetic-field characteristics of CMEs directed toward Earth with a 1- to 2-day lead time.

The relationship between CMEs, which are identified as solar phenomena, and magnetic clouds, which are observed as interplanetary structures, is an unresolved puzzle that merits increased attention by both observers and theorists.

Despite these caveats, the heliospheric phase of space weather development is reasonably well understood. Consequently, models of interplanetary propagation hold great promise for supporting efforts to keep astronauts from being exposed to harmful levels of radiation. One criterion bearing on the likely usefulness of a model is a model with low false alarm rates. On the modelling side, the situation can be described as encouraging. Forecasting the time of arrival at Earth of interplanetary shocks following solar metric type II activity is an important first step in the establishment of an operational space weather prediction system. In the most recent comparative study, Fry et al. (2003) use 173 solar events between February 1997 and October 2000 to set thresholds for the Hakamada-Akasofu-Fry version 2 (HAFv.2) model and then present the results of a comparison of the performance of this model to the STOA and ISPM solar wind models. The evaluation of input parameters to the models showed that the accuracy of the solar metric type II radio burst observations as a measure of the initial shock velocity was compromised for those events at greater than 20° solar longitude from central meridian. A variety of statistical comparisons among the three models show them to be practically equivalent in forecasting shock arrival time (SAT). The uncertainty of the SAT estimates as determined by RMS error is about 12 hours for each model. Although the HAF kinematic model performance compares favourably with ISPM and STOA, it appears to be no better at predicting SAT than ISPM or STOA. However, given in retrospect the average observed transit time of all shocks, a crude model based upon initial velocity-dependent and longitude-dependent thresholds would have performed as well as the three models. There are presently no plans to improve STOA and ISPM, whereas HAF continues to be upgraded.

HAFv.2 takes the inhomogeneous, ambient solar wind structure into account and thereby provides a means of sorting event-driven shock arrivals from corotating interaction region (CIR) passages. Once an eruption has begun, it is a relatively

straightforward matter to simulate its propagation as that of a pulse travelling through the heliosphere, as long as the plasma and magnetic-field conditions along the way are known. Unfortunately, this requirement becomes increasingly difficult to satisfy at and after solar maximum, when close sequences of CMEs or eruptive flares and a highly distorted heliospheric current sheet prevent the establishment of a predictable, quiescent interplanetary medium.

In its fully developed form, the ultimate space weather model will solve a set of multispecies, generalized, time- dependent MHD equations and will self-consistently describe the complicated interplay among the physical processes controlling the structure and dynamics of the heliosphere, including the solar wind outflow, the generation and propagation of transient interplanetary structures, such as CMEs or CIRs.

5.1.5 Exploration of the Interplanetary Space

A prototype of a "comprehensive interplanetary space weather simulation tool" could be developed. Several existing advanced, data-based space weather nowcast and forecast codes could be integrated to give the ability to forecast some radiation-risk parameters on the far side of the Sun. These predictions should be tested against the radiation data collected from (robotic) interplanetary missions.
As summarised in Table 16, there is a wealth of current and future missions designed to explore the solar system and the interplanetary space. The knowledge gained in these missions is vital to help the development of an interplanetary space weather simulation tool.

Ongoing and upcoming space weather missions of International Living With a Star member agencies together represent the largest fleet of spacecraft ever focused on a single scientific objective. Charting these planned missions on a single timetable (see Figure 24) is helping the ILWS steering committee coordinate new projects that could fill any potential gaps in its coverage of the Sun-Earth system. Assessment of Mission Size: Trade-offs for NASA's Earth and Space Science Missions (2000)
<http://www.nap.edu/html/ssb_html/Mission_Tradeoffs/missionmenu.shtml>

The Earth's magnetic field acts as an invisible force that reflects away some of the harmful components, such as cosmic rays, brought by the solar wind. On Mars, interactions with the solar wind also ionise particles, but they fly away because the planet lacks a magnetic field and a strong gravitational field. Over time, the release of particles continuously erodes the Martian atmosphere.

Earth's magnetic field is very dynamic, and constantly changing in response to activity of the Sun (including the solar wind, CMEs and solar flares). Mercury's magnetic field, which on average is a dipole field, like Earth's, was shown by Mariner 10 to experience similar dynamics. In contrast, the Moon and Mars lack a global dipole magnetic field, but they have local magnetic fields centred on different rock deposits. It is not certain how such local fields were formed, and it is also not clear how much of Mercury's field comes from smaller local fields, as on the Moon and Mars.

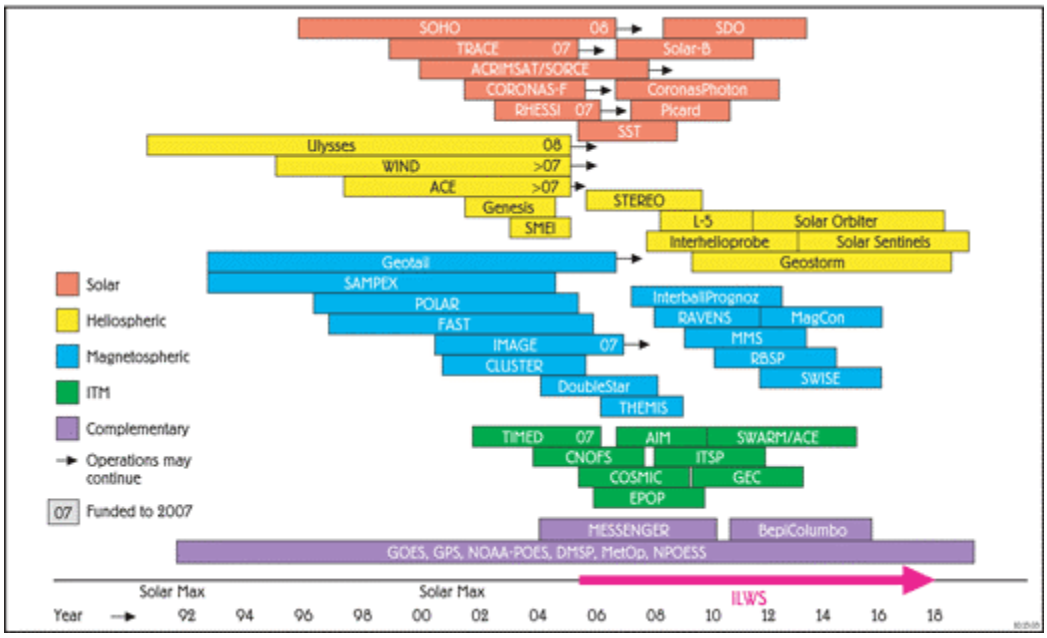

Figure 24. "International Living With a Star" missions.

In general Mars's magnetic environment bears striking resemblance to that of Venus. The solar wind ionises the uppermost portion of the planet's atmosphere to create an ionosphere, forming a bow shock. The bow shock could arise because of a weak intrinsic magnetic field, the ionosphere, or a combination of the two. Because of the uncertainty, the boundary between the shocked solar wind plasma and the planet's own ionospheric plasma has been given the purposefully vague name of "planetopause".

Some missions aim to study the "magnetospheric" physics near non-magnetized celestial bodies, such as planets (Mars, Venus), satellites (Titan, Moon), comets and small celestial bodies. Measurements of the solar wind, charged particles and plasmas may give the only indirect evidence of a weak intrinsic magnetic field. The knowledge gained in these missions is vital to help the development of an interplanetary space weather simulation tool. Other missions are helpful to provide in situ measurements or remote observations from a different viewpoint, adding input constraints to the interplanetary models. Considering one or both of the above purposes, past, current and future missions to interplanetary space, of interest for the interplanetary space weather development, are reviewed in the following sections.

In Section 5.2, we review missions that study the Martian radiation environment. In Section 5.3, we review missions that study other radiation environments in the solar system or that can be used as occasional monitors in interplanetary space. For instance, the Cassini mission will explore plasma environment near Titan and bring new interesting information about the solar wind interaction with atmospheres/ionospheres near non-magnetised objects. ESA's missions in development to the other terrestrial planets, Venus Express (launch 2005) and the BepiColombo mission to Mercury (launch 2011/2012), will carry experiments that look at solar wind interactions with their respective planets.

To ensure adequate warnings of potential large SPE fluxes, multi-spacecraft systems require a separation angle between the spacecrafts that allow stereoscopic reconstructions and reconstructions of spatial characteristics in the solar wind. The forecasting strategy is to provide continuous observations of solar regions generating solar disturbances, including the far side from Earth, and to provide a global picture of the interplanetary medium, where solar wind disturbances propagate. In Section 5.4, we study the particular example of the STEREO mission to introduce the concept of solar satellite networks necessary to the interplanetary space weather development. In Section 5.5, we review other planned interplanetary solar satellite networks, and in Section 5.6, we develop tradeoffs for multi-spacecraft systems.

Not all missions are reviewed here. Current NASA interplanetary missions include Galileo, NEAR, Mars Global Surveyor, Stardust, Voyager, and Ulysses missions. Future NASA interplanetary missions include Deep Impact, Messenger, Dawn, and New Horizons.

New Horizons: <http://pluto.jhuapl.edu/>

Note: access to homepages for NASA's science missions may be made through the menu item "Missions" on the Office of Space Science homepage at:
<http://spacescience.nasa.gov/>.

Mission	Celestial body	Launch Date	Orbit Insertion /Landing /Impact	Science Mission	Data Relay Mission	Status
Mars 2001 Odyssey	Mars	07-Apr-2001	24-Oct-2001	Jan 2002 – Jun 2004	Feb - May 2004	In orbit around Mars
Mars Express	Mars	02-Jun-2003	22-Nov-2003 - 24-Dec-2003	24-Dec-2003 - 30-Nov-2005	24-Dec-2003 - 30-Nov-2005	In orbit around Mars
Nozomi	Mars	04-Jul-1998	January 2004			Failed to enter Mars orbit
Mars Exploration Rovers	Mars	MER-A (Spirit): 10-Jun-2003 MER-B (Opportunity): 25-Jun-2003 to 15-Jul-2003	Landing (MER-A): 04-Jan-2004 Landing (MER-B): 25-Jan-2004	Jan. 2004 - April 2004	2004	In operation
MESSENGER	Mercury	11-May-2004	Mercury flybys 16-Oct-2007, 7-July-2008. In Orbit: July 2009		2004	Venus flybys 28-Aug-2005, 22-Oct-2006
Deep Impact	Comet 9P/Tempel 1	30-Dec-2004	04-Jul-2005		2005	
Cassini	Saturn / Titan	15-Oct-1997	01-Jul-2004		2005	Jupiter Swingby: 30-Dec-2000 En route to Saturn
Mars Reconnaissance Orbiter	Mars	Aug 2005	Mar 2006	Mar 2006 - Jul 2008	Jul 2008 - Feb 2010	Under Study
Mars Scouts	Mars	1: Dec 2006 2: Oct 2011	1: Feb 2009 2: Sep 2012	1: Feb - Aug 2009 2: Sep - Dec 2012		Under study
Dawn	Vesta, Ceres (Asteroid Belt)	27-May-2006	Vesta Arrival: 30-Jul-2010 Vesta Departure: 03-Jul-2011 Ceres Arrival: 20-Aug-2014 Ceres Departure: 26-Jul-2015		Feb. 2007 (Jupiter Swingby)	Planning stages
New Horizons	Pluto / Kuiper Belt	January 2006	Pluto Arrival Window: 17-Nov-2016 - 11-Jul-2017 Flyby of Kuiper Belt Objects: 2018 - 2022		2007	Preliminary design study
Rosetta	Comet 67 P/Churyumov - Gerasimenko	2 March 2004	2014			

Table 16. Current and future interplanetary missions.

5.2 The Martian Radiation Environment

5.2.1 Introduction

With opportunities every 26 months, the current Mars Exploration Program (MEP) consists of Mars Odyssey currently orbiting Mars; NASA Mars Exploration Rovers, ESA Mars Express; Mars Reconnaissance Orbiter (MRO) in 2005; ASI-NASA Telesat and French Premier-07 science orbiter, and French-led Netlanders in 2007; and NASA Science Mobile Laboratory, NASA Marsat, and ASI-NASA SAR science orbiter in 2009. In addition, NASA will have completed Scout missions in 2005 and 2007.

Space missions of interest for the data collected or to be collected about the plasma and radiation environment near Mars are listed in Table 17 and reviewed in the following.

Interplanetary mission	Specific instrument	Period coverage
Russian mission Phobos-2	Energetic Charged-Particle Spectrometer (SLED)	30 January–27 March 1989
NASA's 2001 Mars Odyssey Orbiter	Martian Radiation Environment Experiment (MARIE)	March 2002 – October 2003
ESA Mars Express Orbiter	Energetic Neutral Atoms Analyser (ASPERA-3)	December 2003 – ongoing.

Table 17. Interplanetary missions of interest for the data collected about the Martian radiation environment.

A catalogue of Mars atmosphere resources can be found here:
<http://sgodata.sgo.fi/pub/1999/JK/temp1/0-catalogue.html>

5.2.2 Phobos-2

The primary objective of the Russian mission, as with its sister probe Phobos-1, was to explore the larger of Mars' two moons, Phobos. Phobos-2 operated nominally throughout its cruise and Mars orbital insertion phases, gathering data on the Sun, interplanetary medium, Mars, and Phobos. The Phobos-2 spacecraft arrived at Mars on 30 January 1989, but was lost while manoeuvring in Martian orbit to encounter Phobos on 27 March 1989. The loss was traced to either a failure of the on-board computer or of the radio transmitter (which was already operating on the backup power system). Due to the loss of the spacecraft, much of the original science objectives were not met. However, the 57 days of data that were obtained did yield a number of important results. These are summarized in Goldman (1990).

For instance, observations of Mars' ionosphere from the Viking orbiters showed that this layer of ionised gas extends much farther out from Mars than expected. The Phobos-2 spacecraft discovered later that a large amount of ions were escaping Mars.

In addition, Phobos-2 returned observations made by the Energetic Charged-Particle Spectrometer (SLED). During this period of the early rising phase of Solar Cycle 22, particles reaching energies of several tens of MeV were recorded close to Mars under disturbed interplanetary circumstances (McKenna-Lawlor et al., 1998).

<http://nssdc.gsfc.nasa.gov/space/space_phys/phobos2.html>
<http://heasarc.gsfc.nasa.gov/docs/heasarc/missions/phobos2.html>

5.2.3 NASA Mars 2001 Odyssey: Results from MARIE

The Martian Radiation Environment Experiment (MARIE), a payload on the NASA's 2001 Mars Odyssey Orbiter, has collected data continuously from the start of the Odyssey mapping mission in March 2002 until late October 2003. MARIE was designed to characterize aspects of the radiation environment both on the way to Mars and in the Martian orbit, using an energetic particle spectrometer (SEP events are measured from 15 to 500 MeV/nucleon).

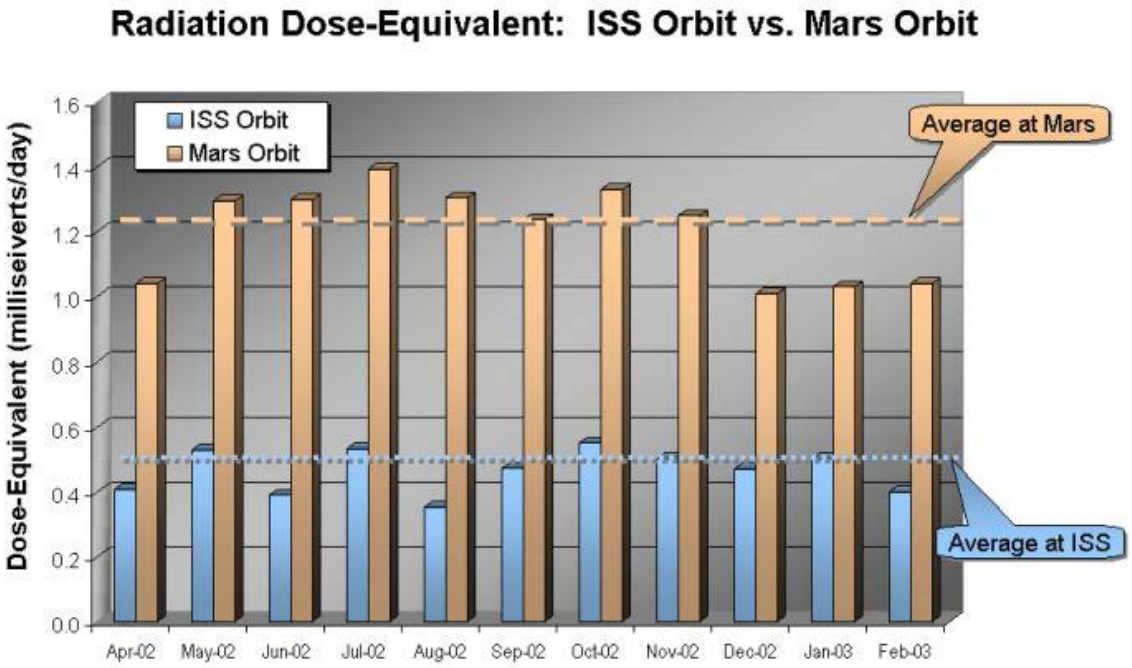

Figure 25 This graphic shows the radiation dose equivalent as measured by MARIE at Mars and by instruments aboard the International Space Station, for the 11-month period from April 2002 through February 2003. Image Credit: NASA/JPL/JSC.
Source: <http://photojournal.jpl.nasa.gov/targetFamily/Mars>.

Validation of radiation models is a crucial step in predicting radiation-related health risks for crews of future missions. As seen in Figure 25, the accumulated total radiation dose equivalent in Mars orbit is about two and a half times larger than that aboard the International Space Station. The dose equivalent from galactic cosmic rays agrees well with predictions based on modelling (Saganti et al. 2004; Cucinotta et al., 2002; Zeitlin et al., 2003). Averaged over the 11-month period from April 2002 through February 2003, about 10 percent of the dose equivalent at Mars is due to solar particles, although a 30 percent contribution from solar particles was seen in July 2002, when the Sun was particularly active. Starting on July 16 2003, the largest SPE was observed by MARIE with a dose rate > 1000 mrad/day (Atwell et al., 2003). This event can be associated to the fast CME, seen from Earth as a powerful backsided halo CME, and which left the Sun on July 16 2003, at a time when Mars was on the opposite side than the Earth. In this situation, no global interplanetary tool is available to reliably simulate the observations and measurements of SPEs at Mars.

On Oct. 28, 2003, during a period of intense solar activity (an X17.2 flare, associated to a CME, occurred), the instrument stopped working properly. Controllers' efforts to restore the instrument to normal operations have not been successful.

The original Principal Investigator of MARIE, Dr. Gautam Badhwar of NASA Johnson Space Center, tragically passed away in August 2001, and Dr. Cary Zeitlin of the Lawrence Berkeley National Laboratory has been appointed as the new PI.

<http://mars.jpl.nasa.gov/odyssey/technology/marie.html>

MARIE documents:
<http://marie.jsc.nasa.gov/Documents/MARIEScienceComments-Sep03.pdf>
<http://marie.jsc.nasa.gov/Documents/MARIEScienceComments-Oct03.pdf>
<http://www.magnet.oma.be/wrmiss/workshops/seventh/program.pdf> (p.15)

News article: <http://www.jpl.nasa.gov/releases/2003/156.cfm>

5.2.4 ESA Mars Express: ASPERA-3

Mars Express is the first European mission to Mars. It was launched on 2 June 2003 and was injected into an elliptical polar orbit around Mars at Christmas 2003. The orbiter Mars Express collects data on meteorology, the upper atmosphere, and carries out photogeology and mineralogical mapping.

Onboard is the ASPERA-3 (Analyser of Space Plasmas and Energetic Atoms) instrument, which studies how the solar wind affects the Martian upper atmosphere. ASPERA-3 comprises four sensors to measure electrons, ions, and energetic neutral atoms (ENA). The Neutral Particle Imager (NPI) provides measurements of the integral ENA flux over the energy range <0.1 – 60 keV. The Neutral Particle Detector (NPD) provides measurements of the ENA differential flux over the energy range 100eV – 10 keV (H) and 0.3 – <100 (O). The ELectron Spectrometer (ELS) provides electron measurements in the energy range 0.001 – 20 keV. And the Ion Mass Analyser (IMA) provides ion measurements in the energy range 0.001 – 40 keV/Q. These measurements are below the range to measure SPEs.

ESA Mars Express: <http://sci.esa.int/science-e/www/area/index.cfm?fareaid=9>

ASPERA-3:
<http://www.aspera-3.org/>
<http://www.irf.se/rpg/aspera3/>
<http://www.irf.se/press/MEX.html>

5.3 Other Radiation Environments and Occasional Monitors

In this Section, we review missions that will study other radiation environments in the solar system and/or that could be used as occasional monitors in interplanetary space.

5.3.1 Nozomi

Nozomi (Japanese for Hope and known before launch as Planet-B) was a Mars orbiting aeronomy mission designed to study the Martian upper atmosphere and its interaction with the solar wind and to develop technologies for uses in future planetary missions. The Planet-B/Nozomi spacecraft was launched to the planet Mars under direction of the Japanese Institute of Space and Astronautical Science (ISAS).

The High Energy Particle Instrument (EIS), together with Ion Mass Imager (IMI), worked as a long-term valuable monitor of SPEs. The Magnetic Flux Instrument (MGF) revealed how the magnetic field in the solar wind changes with the distance from the Sun and the Earth.

On 2003 December 9, ISAS ground controllers failed to repair a short circuit, caused by the 2002 April 21 solar storm in the spacecraft system. They corrected Nozomi's orbit to lower the impact probability. Nozomi is circling the Sun somewhere beyond the fourth planet. Engineers will continue trying to fix the circuit so that they can use the probe for alternative space observations, including monitoring solar activity, as it carves a wide path round the solar system. One lap is expected to take two years. Although the probe will continue on to circle the Sun outside the planet's orbit and scientists will continue to modify Nozomi to carry out alternative missions, such as monitoring solar activity, at this stage it remains to be seen whether or not the spacecraft can be stabilized.

News Articles:
<http://space.com/missionlaunches/nozomi_update_031121.html>
<http://news.bbc.co.uk/2/hi/science/nature/3304131.stm>
<http://edition.cnn.com/2003/TECH/space/12/09/japan.mars.ap/index.html>
<http://www.isas.ac.jp/e/snews/2003/1120.shtml>

<http://nssdc.gsfc.nasa.gov/database/MasterCatalog?sc=1998-041A>
<http://www.isas.ac.jp/e/enterp/missions/nozomi/cont.html>
<http://www.planet-b.isas.ac.jp/index-e.html>

5.3.2 Cassini Mission to the Saturn System

Cassini, a joint NASA/ESA mission to Saturn and its moon Titan, was successfully launched October 15, 1997. The Cassini mission will explore plasma environment near Titan and bring new interesting information about the solar wind interaction with atmospheres/ionospheres near non-magnetised objects.

One of the major scientific instruments aboard is RPWS (Radio and Plasma Wave Science), which is gathering data for the Radio and Plasma Wave Science investigation. Type-III Radio Bursts Produced by the Oct. 28 and Nov. 4, 2003, X17.2 and X28 Solar Flares were detected by the Cassini RPWS Instrument. This supports the idea that Cassini can also be used as an occasional monitor to help determining Parker spiral magnetic field lines from the triangulation of type-III radio bursts (Gurnett et al., 1978; Reiner et al., 1998).

Type-III bursts detected by Cassini RWPS: <http://www-pw.physics.uiowa.edu/space-audio/typeIII.html>

CASSINI RPWS: <http://www-pw.physics.uiowa.edu/plasma-wave/cassini/home.html>

5.3.3 MESSENGER Mission to Mercury

The NASA Mercury Surface, Space Environment, Geochemistry and Ranging (MESSENGER) mission begins during a launch window that opens May 11, 2004. The first of three Venus flybys is scheduled to occur about six months later, when the spacecraft approaches the planet from its night side on November 2, 2004. MESSENGER dashes past the dayside of Venus on August 28, 2005, then again on October 22, 2006. The Venus flybys provide important opportunities to calibrate MESSENGER's instruments on the way to Mercury and make new scientific observations of Earth's "sister planet". The team plans to image the upper cloud layers at visible and near-infrared wavelengths for comparison with earlier spacecraft observations. Magnetic field and charged particle observations will allow them to watch for solar wind pick-up ions and ultraviolet (UV)-visible spectrometry will allow them to check for changes in the composition of the upper atmosphere. MESSENGER will also search for lightning on the night side and for Venus' "signature" at X-ray wavelengths.

The Mercury flybys on October 16, 2007, and July 7, 2008 provide the first close-up looks at Mercury in more than 30 years. On both flybys the spacecraft approaches Mercury near the terminator (the day-night boundary) and departs with sunlit views of the planet, taking pictures of the half not seen by Mariner 10. MESSENGER will also map nearly the entire planet in colour and measure the composition of the surface, atmosphere and magnetosphere. This early science return will be invaluable in planning observation strategies for MESSENGER's historic yearlong orbit mission, which begins in July 2009.

MESSENGER's magnetometer will characterize Mercury's magnetic field in detail from orbit over four Mercurial years (each Mercurial year equals 88 Earth days), to determine its exact strength and how its strength varies with position and altitude. The effects of the Sun on magnetic field dynamics will be measured by the magnetometer and by an Energetic Particle and Plasma Spectrometer (EPPS), which measures the makeup and characteristics of charged particles within and around Mercury's magnetosphere.

The Energetic Particle and Plasma Spectrometer (EPPS) on MESSENGER is designed to measure ions (H, 3He, 4He, O, Ne, Na, K, S, Ar, and Fe) from about 10 keV to 5 MeV and electrons from about 20 to 700 keV. These measurements are below the range to measure SPEs. Scientific objectives of the instrument are to study the exosphere and magnetosphere of Mercury. The instrument consists of a FIPS (Fast Imaging Plasma Spectrometer) head for thermal plasmas and an EPS (Energetic Particle Spectrometer) head for energetic ions and electrons.

MESSENGER: <http://messenger.jhuapl.edu/>.

5.3.4 ESA/ISAS BepiColombo Project

After MESSENGER, the next mission planned to Mercury is the BepiColombo project of the European Space Agency and the Institute of Space and Astronautical Science in Japan. BepiColombo would involve the launch in September 2012 of two separate spacecraft that will orbit the planet. ESA is building one of the main spacecraft, the Mercury Planetary Orbiter (MPO), and the Japanese space agency ISAS/JAXA will contribute the other, the Mercury Magnetospheric Orbiter (MMO). The MPO will study the surface and internal composition of the planet, and the MMO will study Mercury's magnetosphere.

Instruments onboard the MMO include a magnetometer, ion spectrometer, ion/electron analyser, wave analyser, cold plasma detector and an energetic particle detector. Contrary to MESSENGER, the MMO mission could benefit to Mars missions by providing additional in situ measurements of particles and SPEs, at locations around the Sun, which vary with respect to the Sun-Mars line.

BepiColombo Project <http://sci.esa.int/science-e/www/area/index.cfm?fareaid=30>

5.3.5 ESA Venus Express

Venus Express's science objectives are to study the atmosphere, the plasma environment, and the surface of Venus in great detail. Venus Express is scheduled for launch in November 2005. Of particular interest for the study of the Venus radiation environment are the Analyser of Space Plasmas and Energetic Atoms (ASPERA-4) and a Magnetometer (MAG).

The ASPERA-4 design is a re-use of the ASPERA-3 design flown on Mars Express, adapted to suit the different thermal and radiation environments that will be encountered during the Venus Express mission.

MAG, the magnetometer instrument, is designed to make measurements of magnetic field strength and direction. This information will be used to identify boundaries between the various plasma regions, study the interaction of the solar wind with the atmosphere of Venus and provide support data for measurements made by other instruments.

Venus Express
<http://sci.esa.int/science-e/www/area/index.cfm?fareaid=64>

ASPERA-4
<http://sci.esa.int/science-e/www/object/index.cfm?fobjectid=33964&fbodylongid=1441>

MAG
<http://sci.esa.int/science-e/www/object/index.cfm?fobjectid=33964&fbodylongid=1443>

See also Venus Climate Orbiter (2008).

5.3.6 NASA Jupiter Icy Moons Orbiter (JIMO)

The Jupiter Icy Moons Orbiter is an ambitious proposed mission to orbit three planet-sized moons of Jupiter (Callisto, Ganymede and Europa), which may harbour vast oceans beneath their icy surfaces. One of the science goals is to determine the radiation environments around these moons and the rates at which the moons are weathered by material hitting their surfaces. The mission would launch in 2012 or later.

NASA would choose the final suite of instruments through a competitive process open to proposals from scientists worldwide. Probable ones include instruments to study charged particles, atoms and dust that the spacecraft encounters near each moon.

JIMO <http://www.jpl.nasa.gov/jimo/>.

5.3.7 ROSETTA

The International Rosetta Mission was approved in November 1993 by ESA's Science Programme Committee as the "Planetary Cornerstone Mission" in ESA's long-term space science programme and was launched on 2 March 2004. On its ten year journey to reach the Comet 67 P/Churyumov-Gerasimenko it will hopefully pass by atleast one asteroid <http://sci.esa.int/science-e/www/area/index.cfm?fareaid=13>. The mission has onboard the SREM instrument and provides energetic protons and electrons measurements.

5.4 STEREO: a Prototype Multi-Spacecraft-System

Reports dealing with the potential hazards (e.g., Turner, 1997) point out the need to monitor solar activity from many viewpoints to ensure adequate warnings of potential large SPE fluxes.

To ensure adequate warnings of potential large SPE fluxes, multi-spacecraft systems require a separation angle between the spacecrafts that allow stereoscopic reconstructions and reconstructions of spatial characteristics in the solar wind. The forecasting strategy is to provide continuous observations of solar regions generating solar disturbances, including the far side from Earth, and to provide a global picture of the interplanetary medium, where solar wind disturbances propagate.

5.4.1 Remote-Sensing Multi-Viewpoint Observations

5.4.1.1 Coronal and Heliospheric Imaging

The combination of coronagraphs and EUV imaging is essential to distinguish frontsided from backsided halo CMEs. Radiation protection operations for future human missions (both to the ISS and to Mars) should be provided with observations of CME's from several vantage points, such as would be provided by SOHO and the future STEREO mission.

The primary goal of the Sun Earth Connection Coronal and Heliospheric Investigation (SECCHI), a component of the STEREO mission, is to advance the understanding of the three-dimensional structure of the Sun's corona, especially regarding the origin of CMEs, their evolution in the interplanetary medium, and the dynamic coupling between CMEs and the Earth environment. SECCHI is a suite of remote sensing instruments consisting of two white light coronagraphs (COR1 and COR2) and an EUV imager (EUVI), collectively referred to as the Sun Centered Imaging Package (SCIP), and a Heliospheric Imager (HI). See Figure 26 for a summary of the scientific goals of SECCHI.

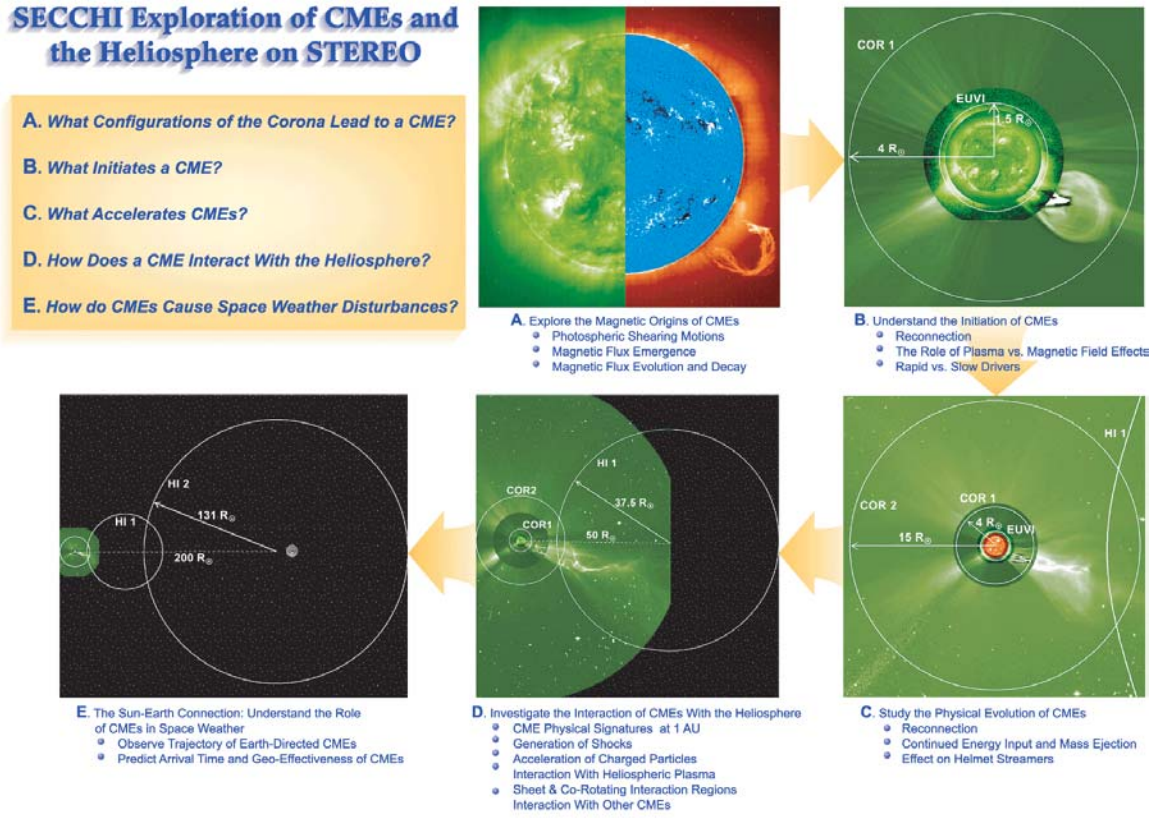

Figure 26. SECCHI scientific goals.

5.4.1.2 Improving Shock Speed and Intensity Estimates

Complementary to the plane-of-sky speed measured by a single optical imager, the interplanetary type II radio tracking provides one important means of accurately determining the radial speed of the CME-driven shock through the interplanetary medium from ~0.1 AU or less to 1 AU or more and thus accurately determining CME arrival times. Another fundamental problem of space weather research is estimating the strength of a shock. It has previously been shown that the intensity of the radio emissions varies approximately as the shock speed cubed (Lengyel-Frey and Stone, 1989). Thus the brighter and faster type II radio sources are more likely to have large shock strengths and generate accelerated particles.

In addition to tracking the radio source and estimating the shock strength, the stereoscopic technique allows intrinsic characteristics of the radio source to be derived. Beam and scattering patterns can be fed back into models to better understand radio generation mechanisms and propagation effects.

Data from the STEREO SWAVES radio burst tracker will enable us to estimate the speed of a radio-generating Earth-directed CME and estimate the intensity of the shock days in advance of its encounter with an observer near the Sun-Earth line. As more data becomes available, predictions will be continually refined and a space weather metric based on type II radio emissions will be developed (Wolf and Fuller-Rowell, 1999). In principle, Earth encounter times should be accurately predicted to within hours of the actual arrival times. This will be of benefit for space weather forecasting at Mars, which will be near opposition around the time the STEREO mission is launched at the end of 2005.

5.4.1.3 Type III Bursts Tracking by Triangulation

To avoid using a heliospheric density model, type III bursts must be tracked by triangulation. Gurnett et al. (1978) used three rotating spacecraft (Imp 8, Hawkeye 1, and Helios 2) to successfully track a type III radio burst through the IPM, and showed that the emission was harmonic. 3-D triangulation was done by Reiner et al. (1998) using Wind and Ulysses data (Figure 27). That analysis showed that the suprathermal electrons followed a spiral track to the south of the ecliptic plane. Triangulation allows the frequency drift rate, exciter speed, source size, and intensity to be determined unambiguously. These parameters are crucial for constraining theories of type III radio emission. Radio measurements from the two future STEREO spacecraft will make reliance on a density model and mode assumptions unnecessary because the radio source location is the intersection of two measured lines of sight.

SWAVES observations of type II and type III bursts will allow an unprecedented study of these effects together. This is crucial to understanding the relationship between CMEs and type II bursts, and finally, using type II parameters to remotely diagnose CME parameters.

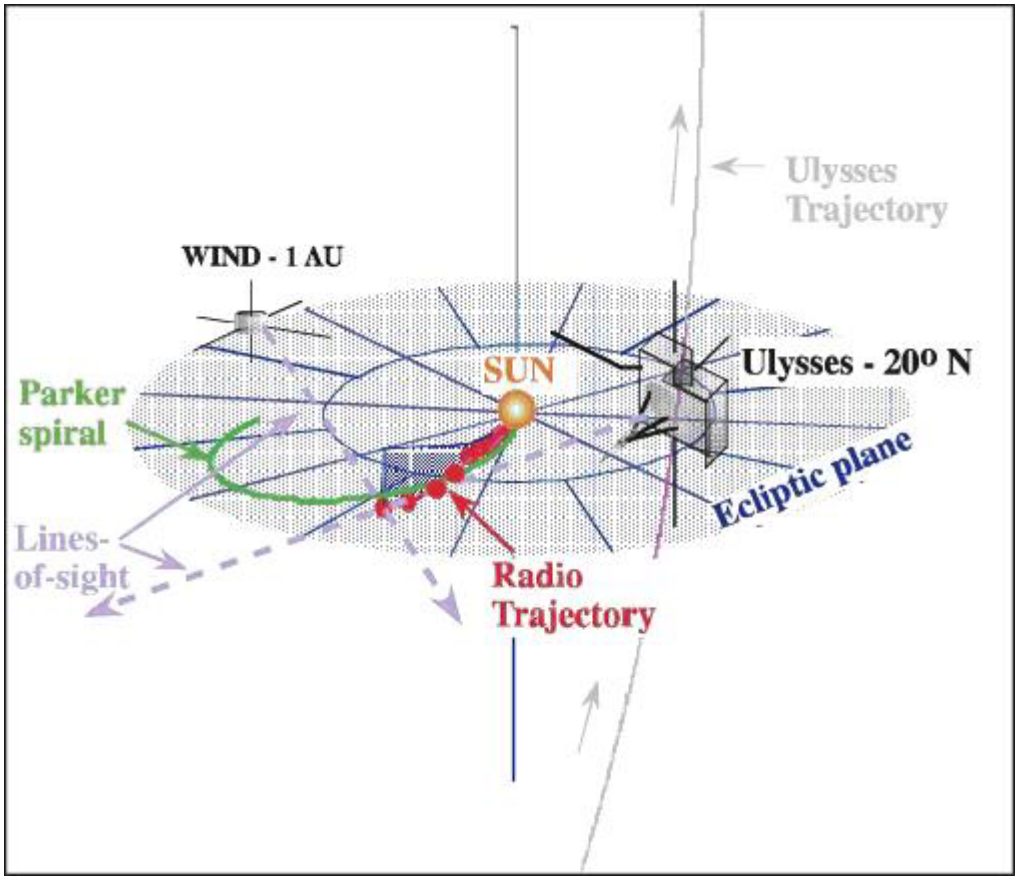

Figure 27. 3D view of triangulation of a type III burst observed by Ulysses and Wind. Type III source at each frequency is intersection of line of sight from each s/c. Type III source lies along Parker spiral south of ecliptic plane (Reiner et al., 1998).
Source: <http://www-lep.gsfc.nasa.gov/swaves/swavesf3.jpg>.

5.4.2 In-situ Multi-Spacecraft Measurements

5.4.2.1 Angular Extent of ICMEs and Corotating High-Speed Streams

When there are multiple spacecraft observations, inhomogeneities in spatial characteristics can be catalogued and related to specific solar wind source features. Two or more spatially separated spacecraft can be used. In some instances, only one spacecraft will pass through a structure, at other times there will be a combination of both spacecraft and/or near Earth measurements available.

By their recurrent nature, high-speed streams originating from solar coronal holes are more predictable than interplanetary CMEs (recurrent storms mainly occur in the declining phase of the solar cycle and are expected to peak in 2004-2005). However, CMEs launched while corotating streams are present have a tendency to be caught in the structure, thus affecting the CME propagation through space. Hence, knowledge of high-speed stream structures obtained by two or more spacecraft will be important for space weather forecasting.

The STEREO mission will provide a test of the ability of ***in situ*** experiments at solar longitudes different than that of the Earth. During the mission, there will be a drifting in longitude of the STEREO spacecraft with respect to Earth and to each other. An Earth-Sun-STEREO angle of 20^{o} corresponds to 36 hours of solar rotation. The STEREO mission will allow the compilation of a meaningful statistical database of the observed angular extent of interplanetary CMEs and high-speed streams, which can be directly correlated with the angular extent of the solar origins.

5.4.2.2 STEREO Beacon Data

In-situ Measurements of Particles and CME Transients (IMPACT) is a suite of seven instruments that will sample the 3-D distribution of solar wind plasma electrons, the characteristics of the solar energetic particle (SEP) ions and electrons, and the local vector magnetic field. IMPACT will be one of the STEREO mission's four measurement packages whose principal objective is to understand the origin and consequences of coronal mass ejections (CME's).

In-situ data from satellites along the Sun-Earth line at L1 are in a better position to issue warnings that an interplanetary CME is in a direct line with Earth. However, STEREO in-situ instruments will provide important contributions to this emerging forecast system with information about the dynamics of the longitudinal structure of the inner heliosphere. It will issue real-time flags for the spacecraft "BEACON" mode when certain conditions indicating the passage of a shock or interplanetary CME structure are observed. For example, high alpha to proton (a/p) density ratios (>10%) or higher than nominal ionisation states (e.g., O^{+7}/O^{+6} ratios) in the solar wind can be calculated (to first order) onboard by the PLasma And SupraThermal Ion Composition Investigation (PLASTIC). Unlike other in-situ indicators, these signatures are believed to be unique to interplanetary CMEs. Additional warning flags can be generated by PLASTIC and/or IMPACT based on kinetic temperatures and their anisotropies for solar wind ions and electrons, electron bi-directional heat flux, and large deltas in the magnitudes of the B, v, or n.

With the STEREO spacecraft slowly drifting apart from Earth one will be able to estimate the optimal spacecraft longitude for the forecast of recurrent high-speed streams. The two sets of STEREO in-situ measurements, combined with those at the Earth solar longitude, will allow for the first time a determination of the temporal evolution of these co-rotating structures. Any changes can then be directly compared with the solar observations of temporal changes in the corresponding solar wind source longitude.

IMPACT supplies low rate (~1 min) basic solar wind plasma electron, magnetic field, and SPE information processed on-board to conform to the designated telemetry allocation. These in situ beacon data are for direct dissemination to NOAA-SEC and other users. The beacon data include plasma density, magnetic field vector components, and SPE fluxes.

STEREO/PLASTIC: <http://stereo.sr.unh.edu/stereo.html>.
STEREO/IMPACT: <http://sprg.ssl.berkeley.edu/impact/>.
STEREO/SWAVES: <http://www-lep.gsfc.nasa.gov/swaves/>.

5.4.3 STEREO Put in Real Situation

An examination of the relative positions of Mars and the STEREO spacecraft over the course of the STEREO mission shows that STEREO will provide an occasional upstream solar wind and imaging monitor for any ongoing Mars mission. STEREO launch is planned for the end of 2005, at a time when Mars is closest to Earth (opposition will occur on the 30th of October 2005). In the ecliptic plane, the STEREO spacecrafts (Ahead and Behind) will move at the angular rate of 22 degrees per year with respect to a fixed Earth-Sun line (Figure 28).

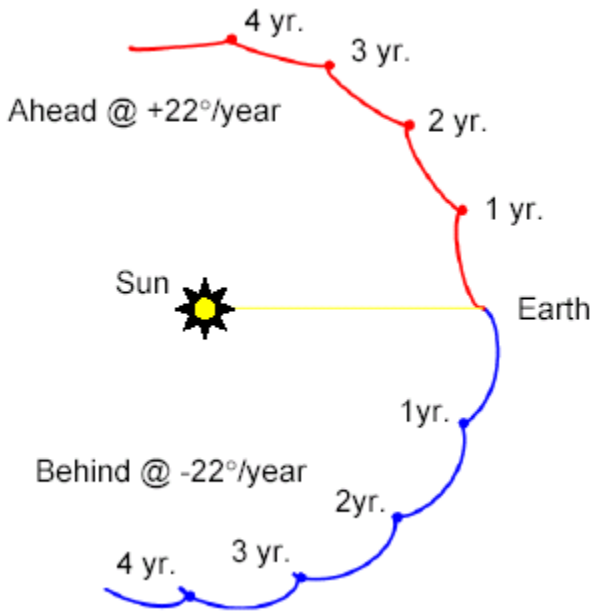

Figure 28. Geocentric Solar Ecliptic Coordinates - Fixed Earth-Sun Line (Ecliptic Plane Projection) Launch: Nov. 15 – Nov. 28, 2005 (UTC) - First lunar swingby (Behind escapes) S1: Jan. 9, 2006 – Second lunar swingby (Ahead escapes) S2: Feb. 15, 2006 - 2 year mission (Driesman et al., 2003).

One can then distinguish four chronological periods, according to the relative positions of Mars, the Earth and the STEREO spacecrafts with respect to the Sun, as illustrated in Figure 29:

A) when Mars is within 90° of heliolongitude behind the trailing STEREO spacecraft
B) when Mars is on the far sides of both STEREO spacecrafts.
C) when Mars is within 90° of heliolongitude ahead of the leading STEREO spacecraft.
D) when Mars is in the vantage point covered by Earth-L1 and the two STEREO spacecraft.

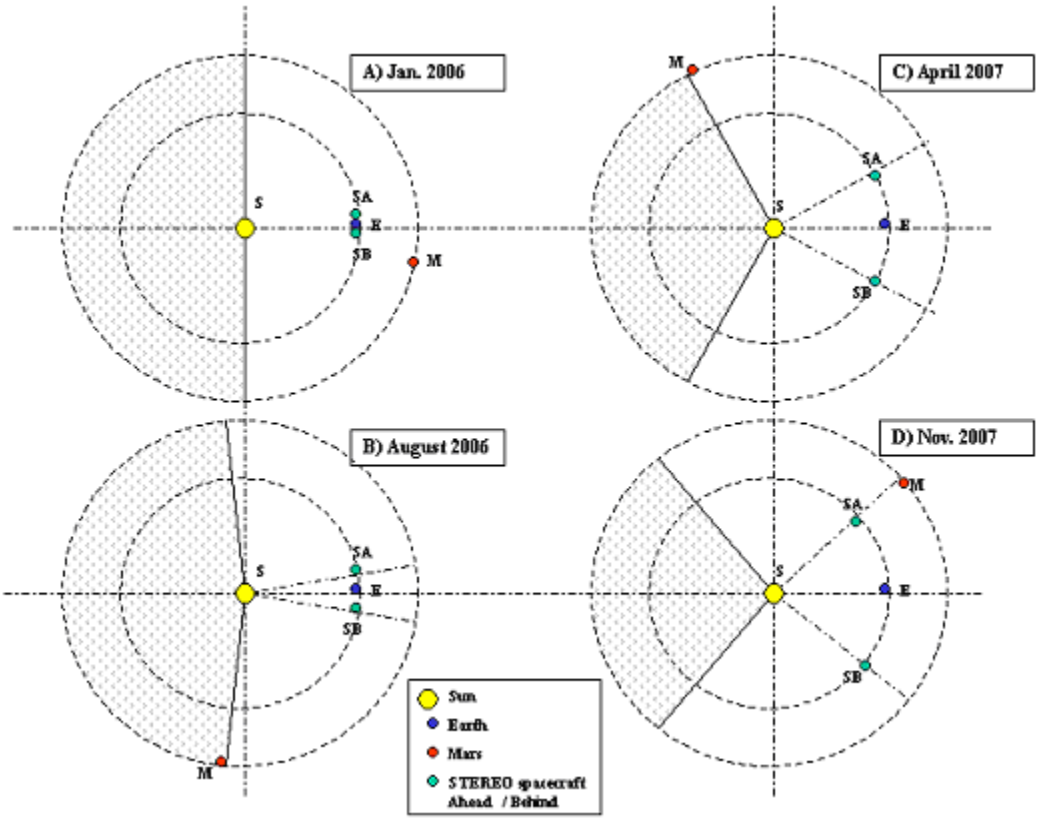

Figure 29. Ecliptic plane projection showing the relative positions of Mars and the STEREO-Earth L1 system for four different epochs: A) STEREO lunar escapes, Mars is within 90° of heliolongitude behind the trailing STEREO spacecraft; B) Mars enters the far side from the STEREO system for about 8 months; C) Mars is within 90° of heliolongitude ahead of the leading STEREO spacecraft; D) Mars enters the zone covered by the STEREO-Earth L1 system.

In period (D), a Mars mission will benefit from the full capacity of the forecasting allowed by the combination of STEREO and the Sun-Earth line information. The SPE beacon data allow forecasts of the arrival of an interplanetary shock and its ICME driver. In particular, if both leading and trailing spacecraft detect a gradual SPE event, the probability of the shock and ICME impacting Earth's magnetosphere is very high. If an event observed at the trailing spacecraft has a rapid rise-time, it is likely that the shock nose is between the two STEREO spacecraft. Any SPE information from upstream of Earth could be combined with this information to further diagnose the shock nose position with respect to the Sun-Earth line.

In period (A) and (C), the coronagraphs and EUV imaging from respectively the trailing and leading STEREO spacecraft will improve the solar activity monitoring of the limb regions, to anticipate the arrival at Mars of corotating structures and warn of potential SPE events. However the quality of forecasting is difficult to assess at this time.

Impulsive SPE events from flares are likely to be seen at only one STEREO location at a time. However, in the period (B), if an impulsive event is detected at the leading spacecraft, and the associated active region at the Sun as seen by the imagers seems long-lived, improved corotation projections can warn of potential impulsive events at Mars. STEREO information is found at: <http://stereo.jhuapl.edu/>.

5.5 Interplanetary Solar Satellite Networks

5.5.1 Solar Sentinels

Solar sentinels were imagined in the Living With a Star program. They could form a distributed network of spacecraft:

- to observe the entire solar surface, including the far side from Earth:
  - to obtain "missing" seismology data from the solar far side, providing measurements of the solar interior.
  - to provide continuous observations of solar regions generating solar disturbances.
- to observe globally and in stereo solar wind disturbances from the Sun into interplanetary space.

This LWS program element includes the Inner Heliospheric Sentinels (IHS) and the Far Side Sentinel (FSS) missions, each with its own distinct concept.

The Far Side Sentinel (FFS) could be launched in January or November 2009. It is planned to go and station on the far side of the Sun, after one year cruise following a trajectory on the Venus orbit. Contrary to STEREO, the FFS is planned to carry a doppler magnetograph to image the solar surface and provide measurements of the solar interior. In the early phase of the mission, the combination with other datasets (similar to MDI/SOHO) could allow observations of the magnetic shear buildup that is associated with CME initiation, and later in the mission it could provide "missing" seismology data from the solar far side. Recommended instruments onboard include an EUV imager, a doppler magnetograph, a magnetometer, a solar wind analyser, energetic particle detectors and a radio science experiment.

The Inner Heliospheric Sentinels (IHS) could be launched in December 2008. They form a network of 4 identical spacecrafts with elliptical heliocentric orbits (0.5-0.95 x 0.72 AU) in the ecliptic. With orbit periods between 5.9-7.9 months, the sentinels are more or less spread in longitude. There exist however periods of longitudinal spread between the sentinels (including IHS, FFS and one spacecraft at L1) greater than 120 degrees.

Preliminary studies (Szabo, 2003) recommend:

- 4 identical spinning spacecrafts with at least 5-year lifetime.
- 4 elliptical heliocentric orbits (0.5-0.95 x 0.72 AU) in the ecliptic.
- Instruments: magnetometer, solar wind analyzer, energetic particle detector, radio waves instrument.

5.5.2 RSA InterHelios

Interhelioprobe (or Interhelios) is an IZMIRAN-led project to investigate coronal heating and solar wind formation, the fine structure of the solar atmosphere, the origin of solar flares and CMEs, and solar energetic particles. It is planned to be launched in 2007-2008.

The solar corona and the near-Sun solar wind are the last regions of the solar system to remain unexplored by *in-situ* measurements. The "Sun Observer" or "InterHelios" (IH) is a mission specifically designed to close these gaps of knowledge by exploring the inner solar system with the objectives to understand the processes that heat the solar corona and accelerate the solar wind and to investigate the plasma itself.

Science Objectives:

- Fine structure of the solar atmosphere
- Stereo imaging of the Sun
- Inner heliosphere and solar wind
- Plasma turbulence and energetic particles near the Sun
- Mercury

Instruments:

- High-resolution solar disk imaging (White-light, EUV, X-ray)
- Imaging of corona and full Sun in white light
- Measurements of ions and electrons
- Plasma waves
- DC magnetic field
- Energetic particles
- Interplanetary dust particles
- Radio waves
- Solar neutrons and gamma-rays
- Planetary Instruments (camera, UV and IK spectrometers, radar)

For more information see <http://www.izmiran.rssi.ru/space/solar/ihelios.html>.

5.5.3 CRL (Japan) L5 mission

The Japanese L5 mission will offer a side view of CMEs propagating towards Earth, at solar maximum from 2008-2013. The solar wind plasma instrument to be carried by the L5 solar observation mission will directly measure solar wind parameters such as density and velocity at the Earth-Sun L5 point. The Earth-Sun L5 point is in the Earth's orbit, trailing the Earth at 60°. Because the Sun's rotational period is 27 days, the high-speed plasma reaches Earth four to five days after it has been observed at the L5 point, thus enabling early forecasting.

Recommended instruments include: Wide field coronal imager, high resolution coronal imager, solar wind plasma analyser, high energy particle instruments, magnetometer, plasma wave detector.

<http://ilws.gsfc.nasa.gov/crl_kickoff.pdf>
<http://ilws.gsfc.nasa.gov/ILWS_Nice_Minutes_final.pdf>

5.5.4 ESA Solar Orbiter

By approaching as close as 45 solar radii (or 0.21 AU), the Solar Orbiter will view the solar atmosphere with unprecedented spatial resolution (35 km pixel size, equivalent to 0.05 arcsec from Earth). Tuned to the solar rotation, the Solar Orbiter will examine the solar surface and the space above from a corotating vantage point. It will provide images of the Sun's polar regions from heliographic latitudes as high as 38° out of the ecliptic.

ESA Solar Orbiter mission (launch Jan-2011) addresses several Solar Sentinel objectives, i.e. topside view of polar regions and backside of the Sun.

All Solar Orbiter's science instruments are currently in the concept phase. They will however be divided into two packages:

1. Solar remote sensing instrumentation:
Visible-light Imager and Magnetograph, EUV Spectrometer, EUV Imager, Ultraviolet and Visible-light Coronagraph, Radiometer.

2. Heliospheric instrumentation:
Solar Wind Plasma Analyser, Radio and Plasma Waves Analyser, Magnetometer, Energetic Particle Detector, Neutral Particle Detector, Dust Detector, Neutron Detector, Coronal Radio Sounding.

Other potential solar instruments are:

- A heliospheric imager capable of imaging almost a full hemisphere of the sky to watch for the way disturbances in the solar wind come towards the Earth.
- An X-ray instrument dedicated to measuring the high-temperature portion of the solar atmosphere's emission.

ESA Solar Orbiter: <http://sci.esa.int/science-e/www/area/index.cfm?fareaid=45>

5.5.5 NASA Solar Probe

The closest approach ever made to the Sun, 0.31 AU (67 solar radii RS), by the Helios spacecraft in the 1970s, is more than twice the outer limit of any remote sensor. The smoothing of solar wind structures, caused by solar rotation and variations in propagation speeds, make detailed connections between the in situ and remote sensing measurements impossible. Solar Probe (launch in 2012) will make measurements in situ from the wind regime at 0.5 AU into the coronal volume sampled by remote sensing at 0.02 AU (4 RS),

for the first time providing the physical connections that will allow us to understand the solar processes that govern the solar corona and the solar wind.

Measurement Strategy:

- In-situ instruments: Solar wind electron & ion composition, magnetometer, energetic particle composition, plasma wave sensor, & fast solar wind ion detector
- Remote-sensing instruments: Provide context for in-situ observations
- Characterize the solar wind within a high-speed stream
- Characterize the plasma in a closed coronal structure and probe the sub-sonic solar wind
- Image the longitudinal structure of the white-light corona from the poles
- Characterize the changes in the solar wind during the cruise from Jupiter to the Sun during two different periods of solar activity
- Characterize plasma waves, turbulence, and/or shocks that cause coronal heating

Solar Probe: <http://solarprobe.gsfc.nasa.gov/>

5.6 Tradeoffs for Multi-Spacecraft Systems

5.6.1 Instrument Comparison

Multi-spacecraft systems and occasional monitors (such as listed in Table 18) may be of particular interest for the interplanetary space weather development. Multi-spacecraft systems include L1-Earth-based satellites, such as SOHO and future Solar-B (2006) and SDO (2007) missions, and interplanetary solar satellites.

The interplanetary multi-spacecraft systems planned for launch are STEREO (2005), the Solar Sentinels (2008-2009), ISAS L5 mission (2008-2013), RSA Interhelios (2007-2008), the ESA Solar Orbiter (2011) and NASA Solar Probe (2012). As if we consider the case of a hypothetic manned mission to Mars taking place during these missions' lifetimes, we assess the potential of these missions to insure sufficient interplanetary space data coverage and forecasts. Table 19 compares what types of instruments are taken onboard.

There exist periods of longitudinal spread between the sentinels (including IHS, FFS and one spacecraft at L1) greater than 120 degrees. With the concept of the sentinels, the probability that a manned mission could be present in the middle of that gap should be checked carefully during mission planning, or complementary solutions such as the monitoring platform at the Sun-Mars L1 point should be considered.

Interplanetary mission	Specific instrument	Interest and limitations
NASA/ESA Cassini mission to the Saturn system: ongoing.	Radio and Plasma Wave Science (RPWS)	To determine Parker spiral magnetic field lines: triangulation of Type-III radio bursts (Gurnett et al., 1978; Reiner et al., 1998).
ISAS mission Nozomi: failed to reach the Martian orbit.	Electron and Ion Spectrometer (EIS)	Hope for alternative space observations, including monitoring solar activity.
ESA/ISAS BepiColombo Mercury Magnetospheric Orbiter: launch in 2012.	Energetic particle detector	In situ measurements of particles and SPEs in the Inner Heliosphere.
ESA Rosetta Mission	Standard Radiation Environment Monitor (SREM)	Measures energetic protons and electrons.

Table 18. Interplanetary missions of interest for the occasional monitoring of the environment

Instruments		STEREO	FSS	IHS	L5	IH	Solar Orbiter	Solar Probe
Remote sensing	High-resolution white light imager					X		?
	High-resolution coronal imager (EUV/X-ray)				X	X		?
	Visible light imager					X	X	
	Coronal imager (EUV)	X	X		X	X	X	
	EUV spectrometer						X	
	X-ray instrument / gamma-rays					X	X	
	Doppler magnetograph		X				X	
	UV/whitle-light coronagraph	X					X	
	Heliospheric imager	X					X	
	Radio experiment (Coronal radio sounding/Radiometer/Radio Spectrometer)	X	X?				X	
In situ	Solar wind (plasma) analyser	X	X	X	X	X	X	X
	Magnetometer	X	X	X	X	X	X	X
	Energetic particle detector	X	X	X	X	X	X	X
	Neutral Particle Detector						X	
	Dust Detector, Neutron Detector					X	X	
	Radio / Plasma Waves Detector/Analyser		?	X	X		X	X

Table 19. Recommended and candidate instruments onboard future interplanetary solar satellite missions: STEREO, Solar Sentinels, L5 Mission, InterHelios (IH), Solar Orbiter and Solar Probe. Solar Sentinels include the Far Side Sentinel (FFS) and the Inner Heliospheric Sentinels (IHS).

5.6.2 Far Side of a STEREO System

The concept of the Far Side Sentinel (FSS) is similar to the one of MagSonas (Magnetic structures on and around the Sun), which was a low-cost SMEX mission, proposed in 1997 by Ruzmaikin et al., to be launched in 2001 and to go and station on the far side of the Sun, taking a drifting trajectory on the Venus orbit. Associated with the STEREO mission, a satellite such as the Far Side Sentinel or MagSonas could have provided a complementary sentinel on the far side of the STEREO system. Contrary to STEREO, the MagSonas spacecraft would have carried a Doppler magnetograph to image the solar surface throughout the mission and advanced radio communications to sound the inner corona from the other side of the Sun. In the early phase of the mission, the combination with other datasets such as MDI/SOHO would have allowed observations of the magnetic shear buildup that is associated with CME initiation. When the spacecraft is viewing from the Sun's back side with respect to Earth, radio sounding using polarized X and Ka band signals would have permitted the observation of magnetic fields within the corona off the limb of the Sun before and during CMEs.

5.6.3 A Monitoring Platform at the Sun-Mars L1 Point

As long as the manned spacecraft or station is in the vantage point covered by the system, the forecasting operations would be feasible, but multi-viewpoints are required beyond. Strizzi et al. (2001) reviewed the advantages to use satellites orbiting the Sun-Mars L1 and L2 points serving as Earth-Mars communication relays and in addition to use the satellite at L1 as a solar activity monitoring platform. This secondary mission for solar activity monitoring increases in importance when the Earth is on the opposite side of the solar system from Mars.

5.6.4 Combined Mission Scenario Options

Combined mission scenario options were suggested to accomplish International Living with a Star (ILWS) programme goals:

- Joint Solar Orbiter-Solar Sentinels WG
- BepiColombo – MMO in close collaboration with Japan L5 mission
- BepiColombo – MMO & Inner Heliospheric Sentinel
- Investigation of synergism/potential of Solar Orbiter, BepiColombo, and Solar Probe.

Monitoring platforms at the Sun-Earth L1 points such as SOHO are not only useful for terrestrial space weather and missions to the Moon, they are also necessary to develop our interplanetary space weather expertise. We need to make sure that future platforms provide all necessary instruments.

6. Recommendations for Warning Systems

6.1 Radiation Warnings in Manned Deep-Space Missions

6.1.1 Introduction

In Work Package 5000, one objective is to develop a system concept for giving warning to astronauts of space radiation hazards. Having discussed radiation instrument technology in Chapter 3, we discuss here many options for technical approaches at the systems level which fit into the long development time. In other parts of REMSIM, biological radiation effects and risks are being evaluated. BIRA, Brussels have responsibility for the wider topic of Space Weather "monitoring", especially the key topic of prediction of solar flares from a systematic network of detectors. REM Oxford Ltd is studying the topic of instrumentation and warning. REM has studied the existing instrumentation of space stations, shuttles and biosatellites, consisting of on-board radiation sensors inside and outside a pressure vessel, if any. At this stage, no hardware is to be designed so, in Chapter 3, we gave factual descriptions of the sensor technology available and how they are converted to space-radiation monitors by selection of structure and circuitry. In this Chapter, we move on to the Analysis of, and Recommendations for Warning Systems.

In designing radiation protection systems for a manned vehicle on a long deep-space mission, radiation detectors which give daily awareness of the background rate and incipient surges of radiation are an important subsystem which can save lives. In this section, we work towards a concept for such as system. The crew dose criteria were developed in WP1000, studies of the shielding were made in WP2000 and detector technology is dealt with elsewhere in WP5000. We discuss here options for technical approaches for radiation protection. REM has studied the applicability of radiation monitors used on Earth-orbiting space stations. Wider issues from medical physics, radiation testing and nuclear fallout protection are also considered (see e.g. Williams and Thwaites 1993; Holmes-Siedle and Adams 2002). The present study discusses how to optimize arrays of monitors for the conditions of deep space and landing on a planetary body, including modes in which they can interface with the main control system of the space vehicle [computing, fire-and-gas warning subsystems]. The other terrestrial and orbital instruments used for Space Weather monitoring are described elsewhere by BIRA. At this stage, no hardware is to be designed but system ideas are to be in keeping with hardware concepts and trial computer codes developed by the REMSIM team (Rx/Tec 2004, REM 2004).

6.1.2 Protection from the Environment

Radiation protection is a part of personnel protection and involves the intelligent avoidance of radiation exposure as well as the "brute-force" method of massive shielding. In spacecraft engineering, "shielding" is rarely in the form of an object dedicated solely to absorbing radiation. In a manned deep-space mission, the shielding will include both supplies and wastes, especially water, strategically distributed around the habitat. In the

design of spacecraft, the stringent weight budgets have always blurred the distinction between structure and shielding (Holmes-Siedle and Adams 2002). Because space radiation is omnidirectional, the simplest analysis of protection due to the available absorbers uses the concept of a spherical shell around the "dose point" in question, having the same thickness at all points. Actual situations are of course better represented by a spherical shell of different thicknesses at different points with radiation represented by "ray-drawing" procedures. In this context, we may refer to "a shell or wall of 1 gm cm^{-2}" as an abbreviated term for "a spherical shell which, at all points has a thickness of 1 gm cm^{-2}". In REMSIM, shielding analysis is more subtle, since Monte Carlo procedures follow radiation as it is scattered and register interconversions such as hadronic interactions. Included in the GEANT 4 model is a "water box" representing "the astronaut" and a blood-forming organ as a dose point within the box (INFN 2004).

Particle and photon counters "outside the walls" are bolted to the walls of the vehicle or out on booms. They are vitally necessary to quantify the fluxes of incident particles. Inside a crew compartment or a space suit on EVA, an array of tissue dosimeters is needed, plus particle counters at key points inside the vehicle so as to characterise penetrating or secondary species. The counters will be a combination of one or more of the sensors discussed in Chapter 3 "Radiation Monitors". The dosimeters will be adapted forms of those now used in personnel protection. Sometimes unconventional forms will be developed for Aurora. There is a technology period available for intensive development of sensors in the Mars programme.

6.2 Assumptions on the Environment

6.2.1 General

A review of the radiation sources to which manned missions to destinations such as the Moon and Mars are exposed was performed in WP1000 of REMSIM. The assumptions which we discuss below derive mainly from that study (RxTec 2004) updated by more detail supplied elsewhere in this chapter. Some other relevant statements from TN1, TN 2 and this report, are repeated for emphasis.

Radiation doses absorbed by astronauts in a mission to Mars will be almost entirely from two sources : 1.) galactic cosmic rays (GCR) and 2.) solar proton events (SPEs). GCRs propagate through the solar system from outside. Due to their very high energies [GeV] the light and heavy ions involved are only slightly attenuated even by the heaviest practical spacecraft shields [say 50 gm cm^{-2}]. The ideal stopping material is liquid hydrogen; next in merit is hydrocarbon as fuel or polymer, which can serve dual purposes before use. For a dedicated shield, sandwich materials containing much hydrocarbon or a stronger type of polymer are planned. SPEs have a lower range, for example, the range of a 100-MeV proton in aluminium is 9.20 gm cm^{-2} [34.1mm]. Thus, going by our previous comments it is difficult to shield against protons higher than 100 MeV but some attenuation of those of lower energy is a practical proposition.

6.2.2 The Crew Environment

6.2.2.1 Inside S/C - Deep Space

In space-radiation protection, the important fluxes of high-energy radiation bombarding the outside of a vehicle in deep space consist of electrons, protons and heavier GCR ions. Solar ions and photons may have diagnostic value but we do not need to take measures to protect against them. In the Aurora vehicle, the crew are in a "shirtsleeve environment" and protected by the equivalent of 1.5 to 30 mm Al or 0.5 to 10 gm cm^{-2} depending on their position and the stowing of heavy hardware. The simplest shielding analysis employs a spherical shell of the same thickness at all points. Actual situations are of course better represented by a spherical shell of different thicknesses in different sectors. That model has been summed up in a curve of the distribution of mass as a function of solid angle. In the following sections, when we refer to "a shell of 1 gm cm^{-2}", a useful nominal we mean "a spherical shell which, at all points has a thickness of 1 gm cm-2, for example 3.7 mm of Al".

The most hazardous conditions in the REMSIM group of missions are the long trajectories in deep space. The radiation hazard on Earth is reduced by the atmosphere, which provides 1030 gm cm^{-2} of shielding to us. The lack of atmosphere on the Moon [0 gm cm-2] and Mars [16 gm cm^{-2}] heightens the hazard but there is shadow protection from man-made structures and the land. This radiation hazard will on average be less on the surfaces of the Moon and Mars than in deep space. We begin with an intuitively useful model of the radiation environment of a deep-space crew and present ways in which the warning signals should be given.

Average Earth background from rocks etc is 2E-7 Gy/s. This is 100x less than the average "deep-space background", which is about 2E-5 Gy/s, as shown in Figure 30. This is no worse than the level permissible for radiation workers on Earth. But it is worth putting this dose-rate difference in terms of the "clicks" on a typical terrestrial Survey Geiger counter. The usual **"click per second",** which we are used to in most of Europe (an ergonomic indication that the environment is "OK") would be raised in the deep-space situation of location C in a spacecraft, at a quiet time, to **a "roar" of 100 counts per second**. Moreover, at this same location C, during a solar storm, the same instrument would be **"off-scale" say at 10,000 counts per second**. The reduction given by moving into a "shelter" on the spacecraft might barely be noticed by the human ear. Clearly, the astronaut is at risk from radiation as well as from other dangers of the mission and the ergonomics of the terrestrial Survey Geiger has to be changed for warning of hazard on a spacecraft. Suitably, the concept has been adopted as a "motto" in the final report (REMSIM 2004a).

A representative example of dose rates and corresponding total doses during a mission lasting about 1000 days [24,000 hours] is given in Figure 30. The figures are taken mainly from careful shielding calculations by Wilson (Wils97a and b) and NASA co-workers on solar flares and cosmic rays with other inputs from ESA's HUMEX study. The dose rates and accumulated doses are calculated for exposure to the "GCR background" in a mission to Mars during 1977 with a shielding of 1 g/cm^2 of Al. Likely readings on monitors of dose rates and total dose values are shown. The Galactic Cosmic-Ray (GCR) "background" is modulated by distance and planetary attenuation. Two

values of dose rate are given for the GCR level. In Section 6.7, we discuss the movement of crew members between extremes like these and simulate them with an algorithm.

The readings of total dose will show steps during solar-proton events as shown in Figure 30. There are dose-rate surges due to solar-proton events, shown as pulses or "spikes", that go "off-scale" but never stay off-scale for more than a few hours (see Section 6.7). The readings of total dose will show steps corresponding to those spikes. With good dose management, the likely mission total should lie somewhere between the two dotted lines, which are cumulative dose values for two rates, 2E-5 and 4 E-5 Sv/hr (2 and 4 mrem/hr). The mission total of about 0.6 Sv (60 rem) lies below the usual limit set for lifetime biological damage to crews - namely 1 Sv (100 rem). The dose rates during the flares can be as high as 0.1 Sv/hr behind thin shields. As the AURORA and REMSIM projects proceed, more detailed dose maps will be developed for the reference Mars spacecraft. This will allow more precise versions of Figure 30 to be developed for specific locations on the S/C.

The average rise time for maximum particle rate (at energies >10 MeV) for the 6 larger events in the 1976-1986 cycle, for instance, was 40 hours with a minimum time of 10.5 hours [NCRP89]. During the SPE of August 1972 the dose equivalent rate to the BFO with 1 g/cm^2 Al shielding grew from ≈0.1 mSv/h to ≈1 mSv/h in the first hour, yielding a total dose of ≈0.5 mSv in the first hour [Wils97c]. During the SPE of October 2003 the counts per minute measured by MARIE grew from ≈500 to ≈50000 in the first 11 hours. SPE's probability is higher around solar maximum. [www.SpaceWeather.com ; from <http://marie.jsc.nasa.gov>].

6.2.4 Outside vehicle - Deep Space EVA and Flares

During EVA, the crew are in a spacesuit environment and protected by the equivalent of less than 1.5 mm Al or 0.5 gm cm-2 unless bulky body-shields are worn. The exposure to GCRs is not greatly raised from that described above but flare protons during EVA could deliver a lethal dose. 10 MeV protons penetrate a space suit and this is one reason why "10 MeV fluxes" are routinely reported by forecasters at the Space Environment Center (SEC). The characteristics of solar events are found in Chapter 1.

6.2.5 The Surfaces of the Moon and Mars

A review of the radiation sources and hazards on the Moon and Mars was performed on WP1000.

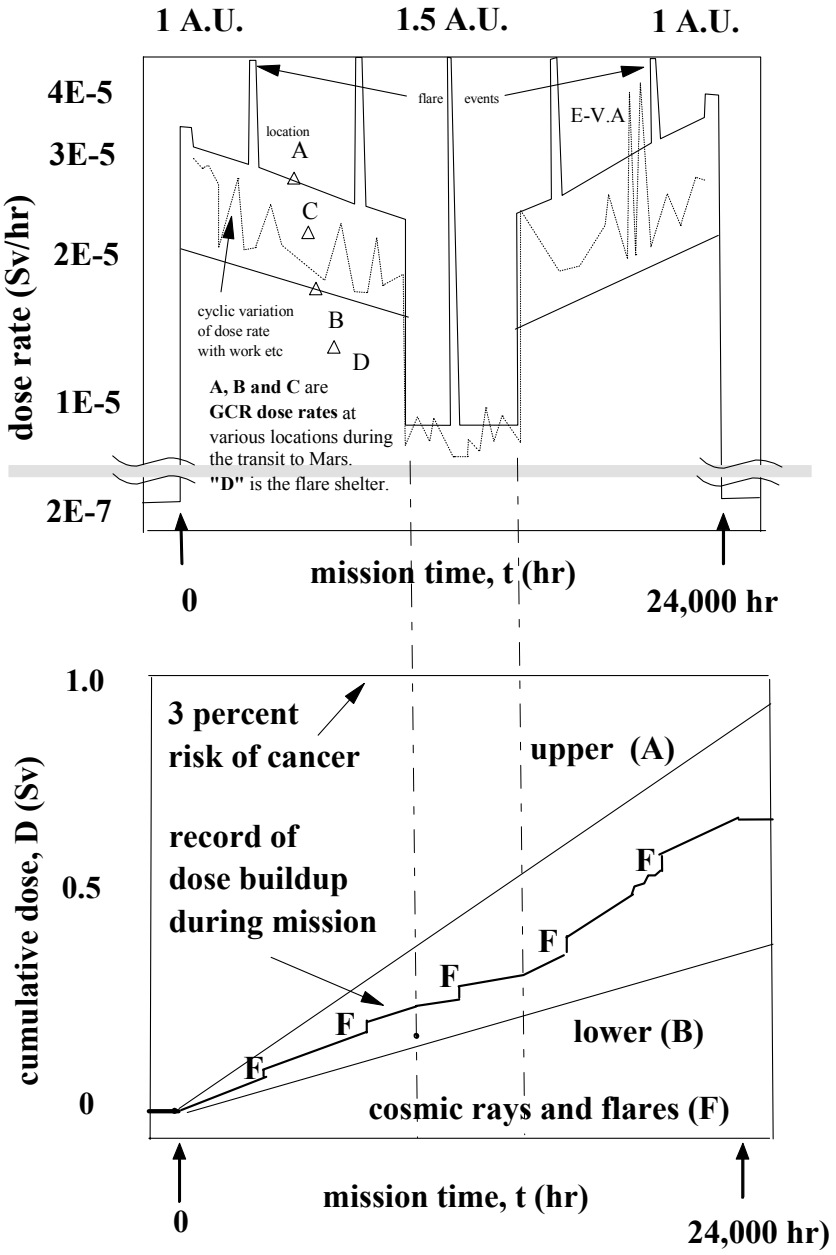

Figure 30. Manned mission to Mars. Likely readings on monitors of (a) dose rates and (b) total dose values ("dosimeters") as a function of mission position and time in hours. Features shown are the Galactic Cosmic-Ray (GCR) "background", modulated by distance and planetary attenuation; dose-rate surges due to solar-proton events [symbol F]; minor peaks due to transit of the Earth's trapped radiation regions. Two values of dose rate are given for the GCR level. These are nominal values representing a well-shielded location (B) and one which is less well shielded (A). Future studies will have to consider the movement of crew between extremes like these.

6.2.6 Environmental Issues of GCR - "Dose-Rate Lowering"

The selection of a model for GCR particle fluxes and for the conversion to mission doses is important because such doses may well dominate over doses from solar protons in the dose budget for the crew; GCR flux varies only slowly with time and there is very little ability to effect a major change in crew GCR dose for the mission by discretionary action once the shielding weight budget is decided upon. The crucial weight decision is made years before launch leaving only small discretion by changing geometry and average atomic weight. Note that GCR assumptions should include a 15% error bar to account for the uncertainty in the GCR background.

The usefulness of feedback information from on-board dosimeters through a slower and more subtle process is recommended here, by which crew learn to lower their average dose rates as they go about their work in situations of "no radiation alert". An example might be the spending of discretionary time near to existing built-in masses such as food and water supplies. Dosimeter displays should give individuals the correct information to optimize this "GCR dose-rate lowering" process for the individual.

6.2.7 Literature Statements on Manned Spacecraft Protection Values

Technical Note 1 [TN1] of this project deals with a: "a spacecraft with a mean shielding of 1 g.cm-2 Al" - for which tentative mission dose equivalents are given, subject to later phases of the project. In space engineering terms, this is a "very thin wall" compared with previous manned space vehicles. For example, Benton and Benton (2001) deal with Earth-orbiting vehicles with much thicker shielding, namely 10 g cm^{-2} Al , for which mission dose equivalents are given. In another place TN1 states "The minimum of shielding for ... deep-space mission can be taken as that provided by the pressure envelopes of the ISS or the NASA-STS orbiter. These provide a shield of 30 g/cm²." It is likely that the actual design will be much less than this. In another place TN1 states "A modern light space suit provides only 3g/cm2 [Apel99]." The earlier ESA HUMEX project's simulated mission radiation models were for three (spherical?) shielding levels of 1, 5 and 10 gm cm^{-2}.

The comprehensive human-shielding calculations by Wilson et al. [Wils97a, 97c] set us a standard for completeness and method. These workers selected shield levels: I.) 0.4 g/cm², II.) 1 g/cm² and III.) 5 g/cm², and assumed that the spherical shields of Al represent I.) the Space suit II.) the Pressure vessel III.) the Equipment rooms.

Wilson et al. plot continuous curves for the variation of time-integrated doses vs. shield thickness, for a GCR background and an SPE, in logarithmic intervals all the way from 0.3 to 50 gm cm^{-2}. They make the shielding calculations specific for various parts of the body by adding an additional internal layer of absorber to represent the situation of the skin, the eye and the BFO compartments in the body. Differences in inner-layer values appear to be as much as 5 gm cm^{-2} and the skin and BFO doses from solar protons differ by a factor of 5 to10 over the main part of the depth range. These curves will be a useful benchmark for our studies.

6.2.8 Status of the Total-Dose Figures

Our preliminary proposals for dose limits (RxTec 2004) are set only for total doses within a (spherical) shield of 1 gm cm^{-2}. Working in a well-protected area may give protective shielding of 5 times that effective depth. See for example the statement in RxTec 2004 that STS provides 30 gm cm^{-2}. Therefore, the present table of limits, being set at 1 gm cm^{-2}, does not give all of the figures needed for the calculation of alarm dose rates in well-protected locations as they are envisaged at present. The plan to have an inflatable pressure vessel (REMSIM 2004a) adds additional complexity connected with tasks occurring near the outer foam structures or windows, where the shielding is much lower than in the core region of the vehicle. Where that window or pressure bulkhead is not clad with further material, the radiation hazard may be very high.

The calculations above are a useful starting point not sufficient for the long-term nature and more complex trajectory of the Mars mission. These points will be clearly identified when the GEANT programme has been provided with a detailed model of the spacecraft and can draw isodose contours for all points in crew compartments. The distribution and use of the mission weight budget will have a crucial effect (1) on the GCR mission dose, where it will affect daily work practices (2) on the probabilities of an additional large dose from an exceptionally large SPE. Thus **the successors of the REMSIM study must place strong emphasis on a "Radiation Isodose Map" and its impact on crew practices and the design philosophy for on-board warning devices**. The next section gives examples of actual measurements in manned missions in Earth orbit

6.3 Data on the Crew Environment

6.3.1 General

Studies by NASA Space Radiation Analysis Group at Houston have accumulated many thousand of hours of dosimetry data from the Shuttle and the ISS [Mart95, NCRP89, Cuci03b]. This is our baseline of actual experience, especially the dose a given astronaut receives as he moves about during a working day, from rest, to exposed places near the vehicle walls.

The highest recorded radiation exposure to a U.S. astronaut is 115 mSv, on the 84 day Skylab-4 mission. In other words, the "alarm level/1 year" of 0.5 Sv and "alarm level/947 days" of 1 Sv for the Mars mission, as recommended in Table 22 in Section 6.6.1, is a considerably worse total exposure than this "highest yet" in the NASA programme. In the orbital environments of the Space Shuttle, the authors of TN1 extrapolate this orbital dose to a dose equivalent of 790 mSv/y. The difference is thus not in space dose rate but the enforced length of the Mars mission. The small population size of astronauts makes it extremely difficult to show any attribution of increased cancer risk to radiation: for example a 3% excess fatal cancer risk on a cumulative 21% basis corresponds to an excess relative risk (ERR) of 1.14.

For the ISS, the dose to the BFO is ≈1E-3 Gy/d [4.1E-5 Gy/hr], of which ≈90% is from trapped protons. In free space, however, HZE ions from the GCR contribute about

3E-4 Gy/d [1.4E-5 Gy/hr]. The amount of shielding does not alter the GCR dose greatly. Shielding has a greater effect on solar protons. In 1999 the NSBRI (NSBR99) affirmed that so far no American astronaut has received doses anywhere near NASA's radiation limits for humans in LEO, as set by NCRP-93. SPEs were routinely detected inside the MIR station. Dose equivalents for MIR ranged from 0.6 to 1.0 mSv/d [Reit00].

Characteristics of radiation environment onboard the Russian segment of the ISS were measured by the monitoring system. The mean dose rate measured during the first year of operation by the 4 shielded detectors is respectively 1.7% lower or 2.6%, 5.2%, 20% higher than that measured by the 4 unshielded ones. Dose values range from 0.132 to 0.235 mGy/d (48.2 – 85.7 mGy/y).

In October 1989 a large and fast increase of the radiation level inside the Mir space station was observed, the dose rate was increased by a factor 30 to 60 times [Dachev, 1999]. On an interplanetary mission, the dose due to the solar flare would have been more than 102 times greater than those that were encountered in MIR orbit. During the August 1972 event, the dose equivalent to the blood forming organs was estimated by calculation to be 0.2 Sv with a shielding of 1 $g.cm^{-2}$ Al. However, a shielding of 10 $g.cm^{-2}$ would lead to a reduction in dose by a factor 10 [Wils99]. These numbers emphasize the importance of the shielding or the shelter of the spacecraft, or of Martian bases but they will be optimized for solar protons rather than GCRs.

If we attribute an effective shielding depth to each detector, we can consider the dose dependence on effective depth. It can be seen, that for GCRs (outside the SAA) no reasonable dependence is observed. The dependence is quite marked in other cases, especially for SPEs (Petr02).

6.3.2 The Mars Reference Mission

Hoffman and Kaplan (1997) specify a reference mission taking 2.5 years [913 days]. The two deep-space sections occupy 2 years [730 days] and the surface stay is 6 months [183 days]. The two calculations of accumulated dose are for spherical-shell shield thickness values a decade apart:

- 1 gm cm^{-2} Al ... 0.54 - 1.54 Sv
- 10 gm cm^{-2} Al .. 0.44 - 1.14 Sv.

The HZETRAN programme [Wils00] estimates annual doses in deep space to be:

- 1 gm cm^{-2} Al ... 0.40 - 1.40 Sv
- 10 gm cm^{-2} Al .. 0.30 - 1.00 Sv.

These levels are very close to the maximum stochastic risk levels which planners wish to place on an astronaut's life. Therefore, assuming average dose rates lying in the middle of the above ranges [say 0.75 Sv / 900 days = 3.5E-5 Sv/hr], the engineering effort must attempt to lower those predicted dose rates by ingenious co-operative use of shielding, radiation monitors and work pattern. This should cover both emergency actions in SPE periods AND daily routines in the GCR background.rate [about 2.5E-5Sv/hr]. Some monitors, by their design, should be "tuned" to the GCR [spallation products, low-LET

primaries] conditions and others to the incipient SPEs, signified by rapid excursions from the steady background and new species of spallation products.

6.3.3 First Stop - the Moon

Routine human missions to the Moon will no doubt be the predecessor for any human mission to Mars. Only several days away the Moon offers us new opoortunities for studying the space environment, as well as being host for our first solar system space colony. Regular trips to the Moon will mean traversing the Earth's radiation belts on a regular basis as well as being submitted to continuous GCR radiation and unpredictable SPEs. Spacecraft shielding requirements, including storm shelters, both on the spacecraft and on the Moon, need to be taken into consideration as a function of the length of time any person will be performing these trips and the solar cycle. It is recommended that the Moon implement an on-site forecasting capability that later can complement on-board forecasting requiremnts on spacecraft going to Mars.

Indeed the recent "Sixth International Lunar Conference on the Exploration and Utilization of the Moon", held 22-26 November 2004 in Udaipur, India, hosted by PRL and ISRO, and cosponsored by the International Lunar Exploration Working Group (ILEWG) and ESA, investigated many aspects of this above-scenario. The President of India, Dr. Abdul Kalam, addressed the group encouraging space agencies to coordinate and integrate their plans in a robust international Moon-Mars roadmap in coordination with the ILEWG roadmap, where the partners can identify their contribution for an effective implementation using their skills
<http://sci.esa.int/science-e/www/object/index.cfm?fobjectid=36182>.

6.3.4 Near-Earth Flight Experience and Wilson's Predictions for Deep Space

Some reassurance that man can survive radiation accumulated in long space missions is given by the measurements collected by Benton and Benton from dosimetry on manned missions in the 1975-2000 period and summarised here. Some worst known cases of human exposure have been selected by the present authors and presented in Table 19. High background rates compared to Earth and sharp peaks are likely in both LEO and Mars missions, although particle sources and spectra are different in the two missions. The conditions are difficult to reproduce in the laboratory because such possible simulators as therapy sources and High Energy Particle (HEP) accelerators are not designed to give the correct spectra and rates. Thus space experiments, such as a "Skylab in deep space" are essential to establishing manned exploration capability.

The Benton paper (2001) is a comprehensive review of dosimetry on major US and Russian flights prior to the ISS. Dozens of flights in the range of 100 - 150 days since 1975 showed that man can fly without serious effects appearing over the following 20 years while absorbing total doses in the region of 7E-2 Gy [TLD] at average dose rates of 2E-5 Gy/hr, with much higher peak dose rates due to passages through Earth's trapped radiation belts.

Table 20 lists the highest doses and dose rates observed in LEO and lunar flights. The conditions marked "Mir outside" will not be experience by men for more than a few hours of EVA. The line marked "Bart" shows data on the dose rate of neutrons collected inside the ISS. Hanslmeier (2003) comments that Apollo 14, flown in late January 1971, is a fair model for GCR conditions during a Mars mission. None of the Apollo flights encountered a major flare event, although sunspot activity was near the maximum of Cycle 20 (Hanslmeier 2002).

The dose rates expected in deep space are of the same order as those observed in the ISS although, as Table 21 shows, the crew compartments of an Aurora vehicle may not provide as much built-in shielding and the hazard is harder to predict because of the larger fluxes and the probabilistic nature of solar flare proton exposures. Furthermore, the much longer duration of the flights and the distance from home base greatly increase the risks. These factors suggest a different radiation-monitoring philosophy, presented in this report, with more active devices and hour-to-hour awareness of radiation fluxes in given positions in the compartments.

Mission	**Orbit**	**Duration (days)**	**Average (Gy/d)**	**Dose Rate** (Gy/h)**	**Total Dose (Gy)**
Salyut 6	LEO	140	2.4E-4	1.0E-5	3.5E-2
Voshkod	LEO	50?	6.5E-4	2.7E-5	3.2E-2
Mir inside	LEO	130	4.5E-4	1.8E-5	6.0E-2
Skylab-4	LEO	90	8.6E-4	3.6E-5	7.7E-2
Apollo-14	Lunar	90	1.3E-3	5.4E-5	1.1E-2 ???
Shuttle	LEO transfer	--**	4.8E-3	2.0E-4	--- **
Mir outside (Fig 32, 1991 solar max.)					
2.0 gm cm^{-2}	LEO	130	1.0E-1	4.2E-3	1.3E+1
0.2 gm cm^{-2}	LEO	130	1.0E+1	4.2E-1	1.3E+3
Neutron doses [Bart02]					
ISS	LEO	--	2E-4	8E-6	---

NOTES

* mainly in LEO, except for Apollo; in LEO, doses derive mainly from low-energy trapped particles not abundant in deep space

** the protection values inside the vehicle were typically 26gm cm^{-2} [nearly 10 mm Al equivalent] see for example ref. Schon98.

Table 20. Worst-known doses and dose rates from US and Russian dosimetry projects 1975-99, selected from [Bent01] *

The figure shows that, in the August 1972 SPE, whose calculated average dose equivalent rate to the BFO behind a 1 gm/cm^2 Al equivalent compartment wall grew exponentially from background level [say 2E-5 Gy/h] to 0.1 mSv/h to 1E0 Gy/h in the first hour (see Fig. 4.4.2-1) and persisted near that level for 10 hours. For the REMSIM case, we lower the rate by a factor of 2 to represent the dose rate behind a thicker compartment wall (as is done for total doses in Wils97c Table 6).

Figure 32 is the basis for the flare figures discussed in Table 20 of this report. The dose contained in the peak region is approximately the product of 5E-2 Gy/hr for about 10 hours, giving about 0.5 Gy. The dose due to galactic cosmic rays (shown as "GCR background") is the product of about 2E-5 Gy/hr and over 20,000 hours, giving about 0.4 Gy. We note on the figure that thinner compartment walls (this includes space suits used in EVA) admit a much larger flux of protons, raising the dose rate to the BFO by a factor of two or more (Wils97c). The figure also shows that the change in the dose rate in the rising edges of the radiation pulse, to which crew-compartment sensor technology must be sensitive, is the double differential of the total dose versus time and is of the order of 5E-2 Gy/hr/hr. A triggering of warnings at a dose rate of about 1E-3 Gy/hr appears to be a reasonable ab initio choice. However, engineering studies may show that this is not the optimum point. To support Table 21, we reproduce Fig 4.4.2.1 (RxTec 2204), showing the characteristic rise times observed (see Figure 31).

6.3.5 Proton Energy Deposition in the 10-100 MeV Energy Range

Many issues in REMSIM, such as the degree of protection in the crew compartment and the design of radiation monitors are strongly bound up with the figures for the energy deposition rates and ranges of protons. Therefore, this specialised piece of solid-state radiation physics is introduced here to illustrate the point that future technical studies should pay special attention to certain particle and photon energy ranges and the special technical limitations of dosimeters when exposed to low-energy photons, charged particles and neutrons.

In Table 22, we compile a list of ranges and energy deposition values for a critical range of protons, 10-100 MeV. Simply dividing energy by range in Al, we can see that the average rate of energy deposition drops from 16.5 to 2.9 MeV/mm Al in that range. Because of this, the proton sensitivity of some solid-state dosimeters is different at the upper and lower end of this energy span. This energy span is also critical because a large number of incident solar-flare protons lies within it and a one-inch [2.5 mm] structural element only excludes a part of the energy range. Detectors which monitor these particles on spacecraft employ absorbers of three thickness values, designed to "cut off" the detector response near 10, 30 and 100 MeV. Data is given in the table for these three energies and some other significant values lying close to them such as the proton energies where the CSDA range is an integral number of millimetres of Al. Since the Linear Energy Transfer (LET) is the controlling factor in the solid-state response per particle, we can extrapolate cautiously to alpha particles and heavier ions (Ma89, Oldh00). Information from INFN 2004 has also been added, giving cutoff energies for protons, alphas, C and Fe ions. Estimates of these energy values can be made from the graphical outputs on the REMSIM web and the TN2 draft issued in May 2004. Values for the LET are given where significant for calculating the proton sensitivity of some solid-state

dosimeters. In these devices, some electron-hole pairs escape trapping by a process called columnar recombination, leading to "deficits" in the dose reading (Ma89, Oldh00). The proton energy range 4 to 100 MeV embraces the transition from columnar to geminate recombination and figures for track density are given. Allowance must be made for this process when converting measured dose to biological response. The mass density selected in REMSIM as a nominal value for the compartment wall is noted in the table. The material selected for the wall is not, however, aluminium but a multilayer including polymeric fibre-reinforced resin.

PARTICLES	**Duration (hours)**	**RATE (Gy/h)**	**DOSE (Gy)**	**NOTES**	**DOSE (Gy)**
GCR at Solar Min	2E4	4E-5	8E-1	Steady flux of GCR	0.8 Gy
GCR at Solar Max.	2E4	2E-5	4E-1	Steady flux of GCR	0.4 Gy
Protons at Solar Max. during anomalously large flare **	1E1	5E-2	5E-1	Short period Probabilistic	0.5 Gy
TOTAL SOLAR MAX DOSE					0.9 Gy
NOTES * BFO = blood-forming organs ; Mars exploration mission of 2E4 hours in flight * * August 4 1972 flare [Wilson 1998]; the shielding includes compartment walls (5 gm/cm2) and the tissue surrounding the BFOs; use of shelter reduces dose further; 10 hours at peak dose rate					

Table 21. Estimates of deep-space dose rate and dose to BFO within vehicles near 1AU *

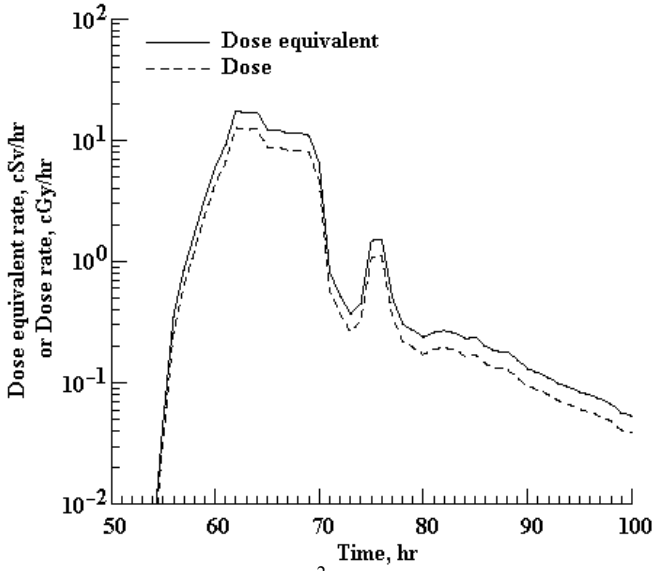

Figure 31. Dose rates to the BFO with 1 g/cm^2 Al shielding during the SPE of August 1972 [Wils97c].

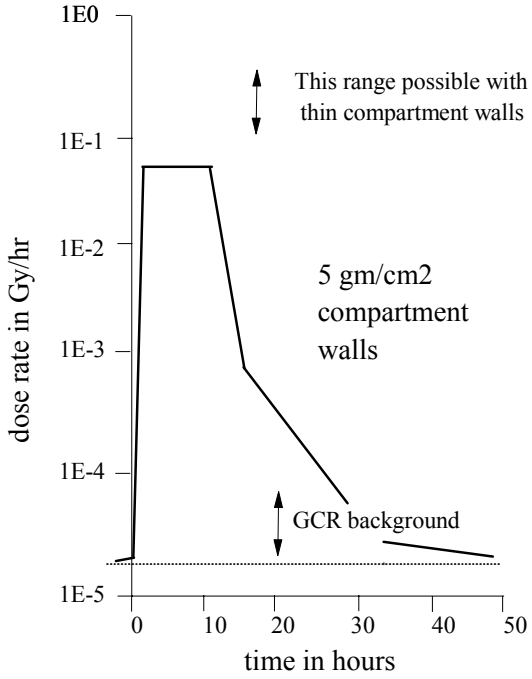

Figure 32. Simplified time-profile of a solar flare, based on Figure 31, modified to represent the dose rate to a crew member's blood-forming organs (BFO) given as a 5 gm/cm² Al compartment wall, a situation similar to that used in the REMSIM modelling of vehicle structure and radiation warning systems.

Energy	CSDA Ranges **		Notes
(MeV)	(mm Al)	(gm/cm2)	
4	0.126	0.034	LET ~ 90 MeV cm^2/gm
			tracks in SiO_2 ~ 1.1E-7 ehp/cm [columnar recombination] [b]
10	**0.604**	**0.16**	**detectors for "Ep > 10 MeV" [c]**
			LET ~ 45 MeV cm^2/gm
			tracks in SiO_2 ~ 5.7E-6 ehp/cm
13	1	0.27	equivalent of 0.040" cover glass for solar cell
25	3	0.81	lowest energy of interest in sensors within unmanned S/C.
			LET ~ 20 MeV cm^2/gm.
			tracks in SiO_2 ~ 2.5E-6 ehp/cm
30	**~ 4**	**1.1**	**detectors for "Ep > 30 MeV" [c]**
			LET ~ 15 MeV cm^2/gm.
			tracks in SiO_2 ~ 1.9E-6 ehp/cm
			REMSIM basic multilayer element
48	10	2.7	AURORA compartments will not see protons lower than this [d]
			1cm Al largely cuts off protons below 40 MeV *
			1cm Al largely cuts off alphas below 160 MeV *
			1cm Al largely cuts off C ions below 1GeV *
			1cm Al largely cuts off Fe ions below 10GeV *
			LET ~ 13 MeV cm^2/gm.
			tracks in SiO_2 ~ 1.6E-6 ehp/cm
74	20	5.4	LET ~ 10 MeV cm^2/gm.
			tracks in SiO_2 ~ 1.3E-6 ehp/cm
100	**34.1**	**9.2**	**detectors for "Ep > 100 MeV" [c]**
			35 cm Al largely cuts off protons below 90 MeV *
			35 cm Al largely cuts off alphas below 350 MeV *
			35 cm Al largely cuts off C ions below 2.5GeV *
			35 cm Al largely cuts off Fe ions below 20GeV *
			LET ~ 8 MeV cm^2/gm.
			tracks in SiO_2 ~ 1E-6 ehp/cm [all geminate recombination] [b]

Notes

[a] values suitable for calculating the sensitivity of detector instruments [not relevant to tissue]

[b] ehp = electron-hole pairs; LET in MeV cm^2/gm from tables is converted to track density in SiO_2 in electron-hole pairs per cm using a factor of 0.126. A track density below 1E6 ehp/cm gives rise to pure geminate recombination; a track density above 1E7 ehp/cm gives rise to columnar recombination [Ma89, Oldh00].

[c] these are absorber thickness values suitable for building absorbers for solar proton detectors set for : Ep > 10, 30 and 100 MeV.

[d] this is the mass density of the REMSIM multilayer compartment wall.

* preliminary results from GEANT 4 / REMSIM studies (INFN 2004).

** ranges calculated using the continuous slowing down approximation (CSDA).

Table 22. Proton energy deposition in the 10-100 MeV energy range - selected values for Al [a]

6.4 The Choice of Radiation Dose Limits for the Crew

6.4.1 General

The comments on dose limits, protection and crew health presented here are given with the purpose of setting the parameters for monitoring and warning systems and acknowledging earlier work packages of REMSIM, especially WP1000. An objective proposed in these earlier parts for the present studies is to limit the health effects in the crew to 3 percent increases in stochastic effects such as lifetime cancer risk. This is already NCRP's assumption for LEO operations in 2004 but of course does not remove the obligation of the ALARA principle - to undershoot these levels if "reasonably achievable" - a term which could trigger much debate in the design phase. The choice of units for measurements is dose equivalents in human blood-forming tissue.

Alarm and warning thresholds are recommended in TN1. Those studies, in turn, acknowledge a debt to NASA, for example Cucinotta and colleagues [Cuci96 , Cuci00a, Cuci00b, Cuci01a, Cuci01b, Cuci01c, Cuci02., Cuci03a Cuci03b] Benton and Benton (2001), have assembled much of the basic evidence for doses to crew in LEO and have extrapolated it to doses in deep space behind spherical shells varying from 1 to 50 cm of polymer. Due to weight constraints, it is likely that the protection from the structure of the Mars vehicle will lie in the lower part of that thickness range. Plans for strategic arrangements of water tanks to supplement the structural shielding are already being studied. For a shell of 1 $g.cm^{-2}$ (3.07 mm Al), the total dose equivalent for a model deep-space mission ranges between 0.54 and 1.54 Sv. For a mean shielding of 10 $g.cm^{-2}$ Al, the mission dose equivalent ranges from 0.44 to 1.14 Sv [Benton, 2001]. Dose limits for Mars missions based on crew health are under study by NASA. Decisions await more study of the acceptable levels of risk for such missions [Cuci03b].

The NCRP Report No.132 recommends Gray-equivalent limits in LEO for deterministic and stochastic effects on BFOs to be 0.5 Gy-Eq (1 year) and 0.25 Gy-Eq (1 month) [NCRP00] These values are not applicable to deep space [NASA98] and more must be known before estimates of the health effects of exposures in deep space can be made[Fry00]. However, so that engineering of Mars spacecraft could proceed, the authors of TN1 began the preliminary study of a set of rational dose limits which could then be applied tentatively to the design of a radiation warning and alarm system and scaled later as different stochastic limits are set. Reasons were given in TN1 for setting, for an age-selected crew, a warning threshold of 0.80 Sv and alarm threshold of 1.00 Sv for the whole mission. These values were chosen as being 80% and 100 % of the ten year astronaut career limits based on an excess lifetime risk of fatal cancer of three percent [NCRP 132].

It was also desirable to have a threshold for 1 year and 1 month. For these, the following limits were set - 0.20 Sv for 1 month and 0.40 Sv for 1 year and the alarm threshold at 0.25 Sv for 1 month and 0.50 Sv for 1 year. These values are 80% and 100 % of the limits for bone marrow deterministic "sickness" effect on all ages. The choice relative to the mission dose was made on the following reasoning. The limits are set on the most restrictive BFO values. This makes an easier management of dosimetric data with respect to alarm and warning signals while maintaining a good margin, well below the onset of acute [deterministic] effects during the mission.

6.5 Methods for Reducing Dose in the Mission Using Sensors

6.5.1 General

Sensors which give a prompt signal proportional to dose rate -such as a photocurrent- will provide the first sign of an SPE transient. The signal which rises above the typical CGR background signal of 2.5E-5 Sv/hr. TN1 illustrates this principle with Wilson's dose-rate profile [Fig. 31] of the August 1972 solar flare, anomalously large and well characterized as to fluxes. The choice by Wilson of a thickness of 1 gm/cm2 is arbitrary - most cases in REMSIM will be for shielding several times thicker than this. TN1 proposes a dose rate trigger at hour 54 on the abscissa of Figure 32, the point at which the internal BFO dose rate rises through the value 1E-3 Sv/hr [1E-1 rem/hr] behind 3 mm Al, a rate well above background rate. This particular flare went on to peak at a dose rate 100 times higher, namely 1E-1 Sv/hr [1E1 rem/hr] eight hours later, at hour 62. The flat-topped profile stayed at a similar dose rate for 10 hours, giving a central square pulse of exposure of 1 Sv [100 rem] to the BFO behind 1 gm cm-2. A large attenuation during 10 hours could be obtained with a shelter of 5 to 10 gm cm-2, so, in the presence of that flare, whether near Earth or Mars, that attenuation would greatly reduce health risks, possibly even save one's life. This is the principle of "emergency sheltering" – to be made available as soon as one of those rare, large flares is sensed. We will, however, note in several places that sensors which generate "advice to take emergency shelter" are only one element in the overall radiation monitoring scheme. Equal attention is due to the sensors dedicated to "GCR avoidance".

6.5.2 Alerts Produced from Dose-Rate Measurement

As noted in RxTec 2004, the dose-rate threshold for detecting these early signs of solar activity can lie well above the GCR level. Serious detriment is not caused in the early stages of a pulse. RxTec 2004 notes that the proposed warning trigger level is only microsieverts per minute. Future research will show whether the probability of later serious total dose changes rapidly with dose rate or whether there is a characteristic change of dose-rate with time that indicates a "bad flare" is on the way. It has been noted that the rising edge of the SPE dose rate pulse, both inside and outside the vehicle, does NOT inform us of its ultimate peak flux - meaning that we do not know the true hazard of the flare just detected until the peak has already passed. There are still high chances of false alarms which could prove a serious distraction. This fact will motivate research on the rising edge of solar-flare fluxes.

6.5.3 Alerts Produced from Total-Dose Measurement

Sensors which give a signal proportional to cumulative dose will not be the first to sense a flare but the growth of total dose vs. time will possibly, at later times, provide a characteristic profile of dose vs. time that indicates a "bad flare" on the way and, in this predictive mode, back up the dose-rate signals generated by the rate meters. It is of course obvious that a similar signal is obtained by integrating the signal of the rate-meter. Several independent measurements are more valuable than one alone. TN1 notes that a

suitable “warning” trigger level based on ALARA and cancer risk is about 1 E-6 Sv per minute. Detecting a 1-minute dose signal of 1 microsievert with only small errors requires quite a sensitive integrating dosimeter system and it may be that, to avoid false alarms, the one-minute range should not be used for alarms. This sensitivity range should be avoided and left to a dose-rate sensor. Given the steep slope of the dose rate shown, higher doses are very soon reached in bad flares, so that the decision-making power of the cumulative sensors can be switched at a chosen time. Such decisions are part of the trade-off of weight, power and cost which have to be made.

SREM is a particle detector, developed for space applications. It is described in Section 3.5.5. It measures high-energy electrons and protons. SREMs have been flown on ESA spacecraft including PROBA, INTEGRAL and ROSETTA since the year 2000, and additional international spacecraft such as Strv-1c.

The merit of recording particle counts in the same package as total doses in Gy(Si), demonstrated in SREM on unmanned spacecraft, is one which should be transferred and elaborated on manned deep-space missions. In our Geiger counter analogy (Section 6.2.2.1), the spacecraft dose management system records “clicks per second” but should also supply the individual with “clicks per day (today, yesterday etc)” and “your clicks in the mission so far” as described in Section 6.7

6.5.4 Conclusions on Dose and Rate Limits

In planning radiation protection for human missions to Mars, we have the advantage of a framework built up in Columbus, the USA and Russia, for the management of crew radiation exposures in LEO. We now have to modify and extrapolate to a condition for which there is much scientific evidence but no experience. Humans have not flown in deep space except rapidly to and from the Moon and the measurements on those trips and the well-appreciated hazards of cosmic rays alone will make the attempts cautious. We have the advantage of a period of solar minimum approaching, in which cosmic rays are the dominant “invasive” or “penetrating” environment for humans providing the major disturbance to the radiation background. This should be used for the development and trial of active radiation-sensing methods in deep space and this recommendation is taken further in Section 6.8.

For crew protection, warnings and alarms have to be derived from signals from on-board hardware, balanced with extensive intelligence from outside - an array of sensors and forecasts from base control centre or more local but remote detectors. The on-board hardware has to be backed up with reliable software. The study will include total doses and dose rate measurements and their relative weights as triggers of alarms and will consider how dose rates and total doses shift slightly in importance as one moves from solar maximum to solar minimum conditions.

On the hardware level, there are two aspects to warning and ALARA. There is the “emergency condition” which has to be dealt with by urgent crew action; this being entirely a matter of detecting and reacting to solar flares, their propagation towards the vehicle - either missing or impacting it. The rising edge of the SPE dose rate pulse, both inside and outside the vehicle, does NOT inform us of its ultimate peak flux and hence of the true hazard of the flare just detected. Despite the great array of sensors available, there are still high chances of false alarms yielding unnecessary disruptions of work or

the delay of planned manoeuvres which could prove disastrous. Thus, the rising dose-rate signals from on-board counters and dosimeters should **possibly be subjected to the best possible gaming techniques, betting on the likelihood of a "bad go" versus a "mild go"** of protons. Possibly, some crew will have to take turns at staying out of the shelter, taking a chance of a "bad go" while the rest of the crew reduces its risks.

The second aspect of hardware was discussed in Section 6.2.6 "Environmental Issues of GCRs – "Dose-Rate Lowering"". Information must be fed back from other, individual dosimeters. From this steady information flow, crew learn to lower their average dose rates as they go about their work. Dosimeter displays must give individuals the correct information to optimize this "GCR dose-rate lowering" process.

6.6 REMSIM Model of Total Dose to a Crew Member

6.6.1 Mission Limits

TN1 proposed a set of "warning and alarm_thresholds" for dose accumulated over the following set periods:

- 1 minute
- 1 hour
- 1 day
- 1 month
- 1year
- The Mars Mission [expected to be 947 days].

Although, for solar flares, the emergency is perceived by virtue of a changing "dose rate", it is not generally possible to set health standards by means of instantaneous dose rates. Total dose is the parameter which affects the human. Even approximate criteria for a dose rate consistent with good health limits cannot be set without a precise case of daily tasks. Therefore the authors of RxTec 2004 logically chose to make a set of TOTAL DOSE [TD] criteria, based on the accepted long-term risk of cancer associated with given TD values. A new aspect of the TN1 study was to make targets for TD values in times as short as a minute. Hardware and software take signals from dose-rate meters, integrate them and inform the crew of their cumulative totals. Table 23 reproduces Table 4.4.3.1 from RxTec 2004.

	1 minute	1 hour	1 day	1 month	1 year	mission
Warning	**3 µSv**	**0.8 mSv**	**10 mSv**	**0.20 Sv**	**0.40 Sv**	**0.80 Sv**
Alarm	**3 warnings**	**1.0 mSv**	**12 mSv**	**0.25 Sv**	**0.50 Sv**	**1.00 Sv**

Table 23. Proposed equivalent dose limits for a mission to Mars (RxTec 2004).

An Alarm Dose Threshold value of 1.00 Sv for the whole mission is to be used to precipitate firm action - countermeasures by the crew to avoid breaching the planned mission dose, including use of the thickest shielded compartment. The Warning Level of TD is about 20 percent below the alarm level and prepares the crew for emergency action. The dose value is approximately double the analytically predicted mission dose from GCRs as calculated for "a shell of 1 gm cm-2". This choice allows men above 35 years of age and women above 45 years of age to fulfil the requirement of 3% E.R.Risk which is the result of the maximum dose set for the whole mission (1 Sv).

The "Warning Dose Threshold" value of 0.80 Sv for the whole mission is to be used to start precautionary procedures used to initiate countermeasures by the crew (e.g. reduced or no EVA). As with most of the other sets, the value is exactly 20% below the Alarm Dose Threshold value.

6.6.2 Short-Period Limits

Setting annual, monthly, daily and hourly limits allow a better control of the exposure during the mission. The values, when converted to DOSE RATES allow judgements on the likelihood of the various immediate ["deterministic"] radiation effects [broadly "radiation sickness"]. They will also be set WELL BELOW the mission limits on TOTAL DOSE for long-term ["stochastic"] radiation effects like cancer. These short-period limits add the new question of short term deterministic effect considerations

For one year and one month, RxTec 2004 proposes the organ dose limits suggested by NCRP-132 for protection against deterministic effects of astronauts in LEO missions (Table 4.3.8-1), and in particular those referred to as the most radiosensitive tissues, namely the BFO: alarm threshold at 0.50 Sv for one year and 0.25 Sv for one month. With the purpose of monitoring the equivalent dose during astronaut activities during the mission (e.g. EVA), shorter time scale alarm and warning thresholds are set. Such levels should be high enough to avoid setting off false alarms due to random fluctuations in the GCR flux and, at the same time, low enough to allow detecting risky total exposure. The alarm threshold is set at 12 mSv and a warning threshold at 10 mSv, such values being higher than the average doses due to GCR exposures.

For one hour, the alarm threshold is set at 1.0 mSv and a warning threshold at 0.8 mSv, such values being MUCH HIGHER than the average doses due to GCR exposures calculated in the HUMEX study. The one-minute dose is set to match the rise times typical of a severe solar event behind thin shielding (1 gm/cm2, when its contribution to the dose is not yet dangerous but has become significantly larger than radiation exposure to the GCR flux inside a spacecraft. For a thin shield, the average dose equivalent rate to the BFO grows exponentially from 0.1 mSv/h to 1 mSv/h in an hour. Thus, for a shield of 1 gm/cm2, one can estimate that the integrated dose after one minute to the BFO of a phantom is 0.1 mSv/h × 1/60 h = 1.7 μSv. It is pointless to set a warning threshold that would trigger only seconds before the alarm signal, so the warning threshold is set at 3 μSv. A new feature here is that, in order to get rid of false alarms, software would ensure that the alarm would only be triggered after a number [say 3] of repeated triggers i.e. for a cumulative dose higher than 9 μSv in three minutes.

These limits are much higher than the existing ones for radiation-exposed workers on Earth, but this is unavoidable for a manned, deep space operation like a Mars mission,

where a 3% long-term sickness risk for astronauts due to ionising radiation can be considered acceptable compared with other mission risks. Our Tables 24, 25 give the limit values for total doses over various periods, given inTN1. It then gives a simple calculation of the dose rates for short and long time exposure, as suggested by Table 24 and 25.

6.6.3 Organizing Radiation Health for a Deep-Space Mission

As AURORA develops an infrastructure, several of the radiation protection procedures used by NASA may be adapted. For example, in the ISS, a Space Radiation Analysis Group **[**SRAG**]** provides crew with preflight mission-exposure projections by examining available space weather data, reports, and forecasts. The group then give real-time support by monitoring of space weather conditions and, during flight, immediate notification of evidence of SPEs. EVA exposure is controlled by the flight surgeon in the management team, alerting flight management of any change to space weather conditions. Radiation dose monitoring activity meets medical and legal requirements by reporting crew exposure status and space weather conditions to flight management. Task schedules are managed to avoid long durations in high-radiation regions.

Typical Rates			**Comment**	**Integrated Dose for 1,000 days**
(μGy/day)	**(Gy/day)**	**(μGy/hr)**		**Gy**
2,400	2.4E-3	1E-4		2.4
1,000	1E-3	4.17E-5		1*
480	4.8E-4	2E-5	This rate observed on lunar missions	0.48
240	2.4E-4	1E-5	A few LEO flights were above this rate	0.24
100	1E-4	4.17E-5	Many LEO flights were below this rate	0.1
* This total perhaps within REMSIM guidelines				

Table 24. Summary of actual doses, dose rates and times in manned spaceflight to date.

Time (T)	1 min	1 hr	1 day	1 mo	1 yr	Mars
T (sec)	6E1	3.6E3	8.766E3	2.63E6	3.156E7	8.18E7
T(hr)	1.7E-2	1	2.4E1	7.305E2	8.766E3	2.27E4
T(days)	6.7E-4	4.2E-2	1	3.044E1	3.6525E2	9.47E2
Dose limit D (Sv) *	**9 E-6 ****	**1E-3**	**1.2E-2**	**2.5E-1**	**5.0E-1**	**1.0E0**
dose rate H' (Sv/sec)	1.50E-7	2.78E-7	1.39E-8	9.72E-8	1.58E-8	1.22E-8
H' (Sv/hr)	5.4E-4	1.0E-3	5.0E-4	3.4E-4	5.7E-5	4.4E-5
H' (Sv/day)	1.3E-2	2.4E-2	1.2E-2	8.2E-3	1.4E-3	1.1E-3

* RxTec2004
** the trigger level is arbitrarily set at 3 times the threshold dose value of Table 22 for ergonomic reasons, see text.

Table 25. Relations of some doses, dose rates and times in the REMSIM dose-threshold scheme for a Mars mission, shown in Table 23.

6.6.4 On-board Tasks and Rest Periods

Given that a crew's working life will be the alternation of work and rest, we can represent the total mission dose of an individual as:

Dose[wk1] + Dose [rst1] + Dose[wk2] + Dose [rst 2]....+ Dose[wk i] + Dose [rst i] ....

The task of day-to-day total-dose monitoring is to determine the actual cumulative total dose as accurately as possible. Active dosimeters provide estimates from hour to hour. These can be allowed a large error [say 10 percent] so long as more accurate monthly records are being kept by other personal monitors [say 3 percent accuracy]. In the AURORA missions, the object of good task management is to bring the crew back with a minimum risk of cancer.

6.6.5 Personal Monitors and the Registering of GCR Background

Individual cumulative doses to radiation workers are usually monitored using active "pocket dosimeters" such as miniature Geiger counters, the Siemens electronic [diode] dosimeter or in the case of NATO troops, the MOSFET pocket RADIAC (AN/UDR 2004; Kronenberg 1968). In addition to equipment ALREADY available on the terrestrial safety market, a new generation of radiation instrumentation has been developed to assist in interpreting the in-flight results for man in Earth orbit [SRHP93]. NASA-JSC's tissue equivalent counter (TEPC) gives a simulation of tissue response although there is no way to measure scientifically the difference between entrance dose and organ dose.

Organ dose could be measured, but after some delay, by the use of taking a blood sample on which "biological dosimetry" is carried out on chromosomes and blood

proteins. In addition, experimental animals [insects, canaries?], cultures of human cells and particle-trackers can possibly be developed to give additional pointers to the factors needed to predict early and late biological radiation effects. It has been explained why - more so than in the ISS - the most important sensors will be of the active type which registers dose rate and not dose since that parameter will provide *the first autonomous sign* of internal disturbances, large and small, in the dose rate. It is expected that audible monitoring - a tone or a click rate, will be acceptable ergonomically but other signals - perhaps visual, should also be examined.

6.6.6 Click Rates from Survey Geigers - an Example of Human Monitoring

The natural background dose rate in a building in the UK is 2e-7 Sv/hr, composed mainly of gamma-rays from the minerals and a few penetrating cosmic ray products [Earth's atmosphere is 1000 gm cm-2 thick]. The circuit settings evolved for survey Geigers used by safety workers on Earth give a noticeable count rate of 1 click per second at the natural background level. This is an ergonomically based signal that the personal environment is "OK". However, workers are in fact allowed to work at well above this rate. Even the public dose-rate limit for limited times is 0.75E-5 Sv/hr. At this dose rate, a survey Geiger is giving quite a "strident" warning of more than 30 cps. We propose that a similar low audible rate of "clicks" [say one click per second] be set for the GCR rate in a well-protected part of the Deep Space vehicle - such as location B on Figure 30. This means that moving into a less protected location such as A will give an easily noticeable rise, possibly a threefold rise. For the guidance of the crew, the count rate/dose rate factor of their personal detectors should be set accordingly by the appropriate combination of deep-space requirement, detector and software type and ergonomic design. **The exact rate and type of "clicks" can be developed on ergonomic principles to meet the desired day-to-day claims on crew attention and allow the individual to practice good personal dose-management as a part of overall health-management.** The figures will form part of the Human-Factors plan. As crew move between light and heavy shielding, they must be given the opportunity to learn the avoidance of GCR Hot spots. In order to have a sense of confidence and control over radiation, humans in elevated environments require some sensors or signals which are under personal surveillance and power so that they are in control to do something to modify the radiation fluxes affecting their bodies. It is fortunate that, at least, the psychological situation of astronauts will be improved over salt miners and uranium miners, whose "radiation safety at work" could not be improved in any practical way.

6.6.7 Warning and Alarm Threshold Values

6.6.7.1 The Shielding Conditions

The REMSIM project has assessed the radiation protective properties of the nominal mission vehicle compartments. The construction is planned to be of inflatable type, presumably for the major weight saving possible. Weight-saving on dead-weight structure is good BUT lower total mass means lower total built-in protection and more

need for dedicated shield structures. The outer wall of the inflatable vehicle may be as little as one-quarter of the thickness provided by Mir [Bent01]. The dedicated shields may be designed as water tanks. While shielding strategies are being worked out, the present study assumes some guidelines on the approximate equivalent thickness of spacecraft protection which the crew on a deep-space mission is likely to obtain during normal work. The output from TN 4 may change these assumptions. The important protection levels assumed for "operational conditions" for a human are:

(a) working well-protected in the middle of the manned spacecraft [**10 gm cm-2** from all solid angles except small fractions of 4pi]

(b) working "near the skin" i.e. poorly protected within the manned spacecraft, for example working close to the wall of the pressure-vessel; shielding is, say, **2 to 5 gm cm-2** over half the solid angle and 10 gm cm-2 from the rest]

(c) working "outside the skin" i.e on EVA [suit protection **well below 1 gm cm-2** in all directions].

Later, a "region D" - a "flare shelter" in the spacecraft will be designed. This will be thicker than region A, above. We do not at present assign a value to this parameter on the spacecraft but REMSIM 2004 has stated that the Moon and Mars shelters are partially buried under regolith material. These definitions of operational levels A to C make it possible in future to perform calculations of quiet-time and flare-time dose rates in these regions. It is important to decide approximate dose rates especially in regions B and C and develop work patterns which make the best use of region A.

6.6.7.2 Alerts

RxTec 2004 recommends that crew should be alerted in less than1 hour to the arrival of a severe SPE. The crew must have time to move to a well-protected region. Doses should therefore be monitored and registered at very short intervals. Hence the inclusion of a "1-minute" dose threshold in the specification.

6.6.8 Remote Warning

X ray detection or other means could be used for prompt reaction to a SPE (several consecutive readings of >10 cm^{-2} s^{-1} imply a SPE is detected (RxTec 2004). In such cases, the short time warning and alarm values should be reconsidered and, eventually, expressed in other units.

It should be noted that the 1- YEAR CUMULATIVE dose limits proposed are much higher than the existing ones for radiation exposed workers on Earth but cancer risk for astronaut crews is held to be at an acceptable level.

6.6.9 An Algorithm for Radiation Warning and Alarm

Forecasting flares seems as difficult as forecasting the weather on Earth. The probability of the intensity of SPE radiation follows a log distribution; based on this, the probability of an SPE large enough to exceed the recommended 30-day dose limit during one year in space is a few percent. The long duration of the Mars trip makes protection from SPEs an absolute necessity.

Flares can only be detected a couple of hours in advance, and it is even more difficult to predict SPEs [flares which carry protons to the neighbouring region of space]. Detection of light and X-rays allows for some prediction of the dangerous radiation. The proton flux increases 2-3 orders of magnitude within about an hour. WHILE A PROTON COUNTER IS USEFUL, THE X-RAY OBSERVATION GIVES AN EARLIER WARNING OF THE order of energy contained in the event. Because of the rapidity of the X-ray signal, we recommend study of this technology in the "Development" section. Depending on the time profile of the proton fluxes and how far from the Sun they are, this warning time may be lengthened to between 20 minutes and 3 hours to reach the most shielded area inside the spacecraft. The on-board method is so much more favourable that it has been strongly recommended [SICS89].

Flare-detection instruments placed only at or near the Earth are not effective because they do not view the back-side side of the Sun, which may be the source for the deep-space vehicle. One set on board the spacecraft and one at the Mars base will then give three views of the solar disk. This scheme will suffice if and only if the crew can accommodate a warning time of 10 minutes to reach safety in the storm shelter. A better warning system would also have instruments on satellites at other points in solar orbit.

6.6.10 Type of Warning

TN1 proposes the following species of data for warning. Sections of TN5 describe these environments in detail.

- X-Ray flare
- SPE ≥ 10 pfu (proton fluence unit = protons / cm^2 s srad) @ ≥ 10 MeV
- Energetic SPE ≥ 1 pfu @ ≥ 100 MeV
- Major Geomagnetic Storm: $A_B \geq 50 – K_B = 6$

Biological dosimetry (Knight 2004) is a special technique which may assist dose management but it clearly cannot be monitored frequently enough to confirm flare alerts.

6.7 Issues of Space Weather and Protecting Radiation Health

6.7.1 General

This section deals with monitoring techniques for two modes of radiation avoidance:

(1) Emergency Mode, avoiding occasional radiation from solar activity

(2) Background Mode, avoiding steady background radiation from GCR

A flare monitor succeeds if the crew can react quickly and reach safety in a "storm shield". Dose rate, D' rises sharply in minutes. By contrast, the important lowering of GCR dose comes gradually as crew members move into or out of significant shield mass. In this case, monitoring is in the long term and could be relative, for example could be done by the measurement of dose D or rate D' in a phantom. We have seen that the prediction of SPEs requires an elaborate network of detectors, probably including a wide electromagnetic sensing array as well as proton and ion counters and more elaborate stacks of dosimeters. For GCR avoidance, the important features concern ergonomics and training of crew.

The warning systems evolved for the STS and the ISS in LEO and practiced by NASA's SRAG for NASA or aircraft crew managers (Truscott et al 1998; Dyer et al 1993-2004) can probably be adapted in some managerial aspects but the existence in deep space of much higher spikes of proton dose, with different energy spectra will make the requirements sharper. Understanding and minimizing exposures from space weather events is an important implementation of the ALARA principle for manned, deep-space missions [Euro 1997] and in this case, there will be a larger number of sensors estimating in real time BFO doses either in individual crew or in a "model crew phantom" which is being tested in an ISS mission. Given the longer message-delay time between Earth and a Mars vehicle, the management of alerts must have greater autonomy than the LEO situation.

6.7.2 The Algorithm - Present Version

6.7.2.1 General

The core system requirement for monitoring is that the detectors should reduce human exposure i.e. by means of active on-board warning devices. In order to enforce the ALARA system on space crews, a warning and alarm system must embrace a wide network of space weather detectors which set the general level of alertness, in other words, the known risks. There must be master sensors accurately estimating in real time the personal BFO doses accumulated by crew members. Messages coming from the master sensors must be processed by an algorithm assessing the rate and the total dose and the relation of these to the targets for limits to these parameters for hours, months, years etc. Clearly the overriding targets are to avoid short-term radiation sickness and also preserve the dose limits set for stochastic effects [long-term risk], especially for BFOs below the given limit. A development programme for the radiation-safety software in AURORA is discussed in this section.

6.7.2.2 Emergency Mode [Solar Activity]

ALERT messages should give the crew the signal that an SPE event is starting, in order to prepare themselves to move into the sheltered area. This would trigger at a certain point the rising dose-rate signal.

6.7.2.3 Background (GCR)-Avoidance Mode

The cumulative total equivalent dose should be computed at every point in the mission, personally, for each member of the crew and converted to an average background dose rate for chosen periods. The object is to inform the crew member of the relation between his activities and the average dose rate. From this information, plus rate monitoring in the relevant rest and work areas, it should be possible to create a larger picture of where the "good" and "bad" areas to work in might be.

The Norwegian Institute for Energy Technology (IFE 2004), Virtual Reality Centre is performing for ESTEC a study for mapping radiation fields in manned spacecraft compartments. The Dose Estimation by Simulation of the International space station Radiation Environment (DESIRE) project aims at accurate predictions of radiation fluxes inside the ESA Columbus module (ESA2004a) of the International Space Station is taking advantage of work already done on industrial nuclear power through the OECD Halden Reactor Project. DESIRE RadVis (RadVis 2004) is a Java 3D programme adapted to display total-dose predictions, made by radiation transport programmes including the Geant4-based DESIRE system. The objective is faster, more intuitive assessment of radiation flux and dose levels in manned spacecraft so that designers can maximise the use of spacecraft mass budget for crew protection. In the future, virtual reality can enhance the radiation awareness of astronauts during a deep-space flight. The techniques can clearly be applied to the development of a Radiation Management System.for the Human Mars Mission.

6.7.2.4 Monitor Logic

In the logic description below, we take the dosimetric signal to be, for convenience, a voltage but clearly any digital quantity would serve. ΔH_i is the signal from the *i*-th dosimeter, converted to dose by use of the calibration factor of the dosimeter and the quality factor or the particle in question. To accord with the set limits, the H values would be calculated for the BFO compartments of the body.

TN1 recommends this sequence. ...

1. initialize the time counter at the beginning of the mission ($t = t_0$);
2. initialize the dosimeter counter ($i = 0$) and the temporary dose equivalent ($\Delta H = 0$);
3. increment the dosimeter counter by one time interval ?;
4. read from the *i*-th dosimeter the "instantaneous" value V_i of the dosimetric signal voltage;
5. compute the absorbed dose $\Delta D_i = f(V_i)$ on the *i*-th dosimeter during the time interval Δt between two readings;
6. compute the dose equivalent ΔH_i, multiplying ΔD_i by the proper quality factor Q_i;
7. add the contribution ΔH_i from the *i*-th dosimeter to the temporary dose equivalent ΔH;
8. if the total number *n* of dosimeters has not yet been reached, then go to step 3;

9. add the contribution ΔH received during the time Δt to the previous integrated value of dose, i.e. $H_{tot}(t) = H_{tot}(t-\Delta t) + \Delta H$; in this way $H_{tot}(t)$ is the integral of the dose equivalent from the instant t_0 to the instant t;
10. if H_{tot} is larger than the pre-defined alarm threshold, then display a message and go to step 12;
11. if H_{tot} is larger than the pre-defined warning threshold, then display a message; wait for a time Δt , increment t by Δt and then go to step 2.
12. Activate alarm "advice to seek emergency shelter".

This algorithm was implemented by RX/TEC in a demo programme (see TN1). Other versions in which the measured quantity is dose rate $\Delta D_i / \Delta t$ can be simply evolved from the above.

In several earlier sections, we noted that prompts from a Radiation Management System are needed to help crew in the avoidance of radiation, especially GCR. Rx/Tec has developed a demonstration programme "ALWARN". It simulates the situation of crews in deep space, logging their doses as a function of time and designed to give prompts when an individual dose rate is too high. The inputs in the programme are (1) a GCR dose rate figure, fluctuating with time; (2) a massive "dose-rate spike" of solar protons constituting a major 14-hour perturbation on the GCR background. The demonstration pulls together several of the disciplines exercised on the REMSIM study. Absolute dose rate is varied according to the shielding thickness, selected by means of a button on the dialogue box. The accumulated dose to date is indicated and also the dose received in the latest hour, day and month. When safety limits are not approached, a "warning" panel indicates "OK". When safety limits are approached, a beep is sounded and the panel indicates one of several available warnings, based on Table 22. The symbol indicates, for example, that the allowed one-hour dose limit [1 mSv] was received in the last hour.

Tables 26 to 28 show a listing of some input values used in this programme, derived from Technical Note 1 of the REMSIM study. Figure 33 shows some outputs of dose vs. time for a specimen 48-hour period which includes a large flare (Rx/Tec 2004), for several locations, A to E are plotted. A is a lightly-shielded location (3 gm/cm²); B is a well-shielded location (20 gm/cm²); C is an average location (10 gm/cm²); D is a deeply sheltered location (50 gm/cm² on a vehicle but deeper on a ground location); E short for Extra-Vehicular Activity (1 gm/cm² implies a spacesuit only).

In Fig. 33, we see curves E and A go off-scale, while locations B and D stay safe. Crew would use the warning signals to tell them to move from an average location such as C to a location deeper in the vehicle (not necessarily a shelter) until the warnings cease. Readings for which a warning will appear are shown on curve C and Table 27. Note that the solar proton even at location C produces only about 5 percent of the likely mission dose. The larger part will probably come from GCR since the rates found at position C are about 0.6 mSv/day or 0.6 mSv per 1000 days. This is a tenable mission-dose target, since 1 mSv is taken at present as the organ dose inducing a 3 percent increase in cancer risk.

The time scale in Figure 35 represents a very small part of the scale in Fig. 30(b) which showed the likely accumulation of organ dose (essentially the accumulation of cancer risk) for the whole Mars mission. In future radiation management studies, this is a

tool we can use to break up a mission into short time periods and compile the mission doses in a spreadsheet for better ergonomic analysis. To obtain a final balance of the absolute and relative risks of of cancers from solar protons and GCR with respect to their relative contribution to cancer risk, much more developmental data is required in other fields, includingh fundamental work in biological damage, a motion study of the crew, a variety of mission plans and an accurate sector analysis of the spacecraft. The present demonstration tool thus however, inaugurates a method worthy of recommendation to the future radiation management activity. The first stage of this activity within ESA might be initiated by the team which performed the Human Mars Mission study (HMM 2004).

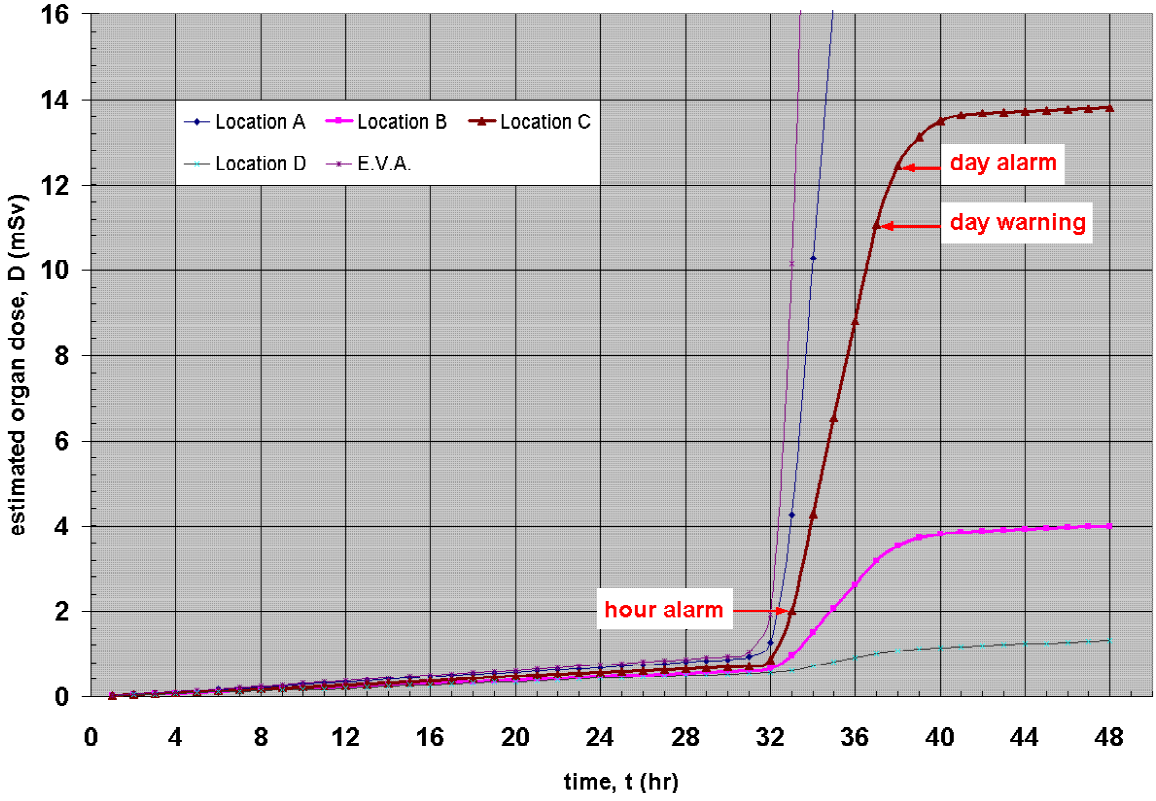

Fig 33. Simulated traces of dosimeters at selected points A to E on a Human Mars Mission spacecraft. Symbols are explained in the text.

SHIELD THICKNESS (gm/cm^2)	TRANSMISSION (percent)
0	100.0
1	96.2
3	88.8
10	72.1
20	60.3
50	54.0

Table 26 Attenuation of GCR by water *
* Estimates by NASA-JSC for solar maximum, deep space, 1AU

Al SHIELD THICKNESS (gm/cm²)	TRANSMISSION (percent)
0	100.0
1	82.0
3	29.9
10	11.2
20	2.7
50	0.4

Table 27. Attenuation of solar protons *
* Wilson 1997 TN3682 Table 6, estimates of dose to blood-forming organs for the August 4 1972 A.L. flare, converted to percent transmission.

hour, warning = 0.8
hour, alarm = 1
day, warning = 10
day, alarm = 12
month, warning = 200
month, alarm = 250
year, warning = 400
year, alarm = 500
mission, warning = 800
mission, alarm = 1000

Table 28. Warning and alarm thresholds in ALWARN (mSv) [terms inserted in the AL:WARN programme * to compare the latest cumulative dose with the limits decided]
* Rx/Tec 2004, REM 2004

6.7.2.5 The Organization of the Monitoring System

Local monitors including some carried by crew members and a fixed array of sensors of several types. They should interface with the main control system of the space habitat (computing and fire-and-gas warning subsystems). Dedicated software recognizes hazards and attunes crew behaviour to fit the hazard both in quiet times and during high solar activity.

6.8 Development

6.8.1 General

Our part of REMSIM is a study of space-borne equipment for the generation of warning signals, indicating radiation hazards to the crew of spacecraft. The case under study here is a long-duration exploratory mission in deep space. Past missions actually flown do not compare closely with the expected conditions. We have stated that the variation with respect to time should be monitored differently and, furthermore, the cumulative total equivalent dose should be computed at every point in the mission, personally, for each member of the crewChief among the differences from past missions is the long-term, full strength of the Galactic Cosmic-Ray flux. Several missions will, however, provide some engineering information on the environment inside a massive capsule (a) the US Moon missions; (b) the recent start of the International Space Station (ISS). Future unmanned deep-space missions between now and 2030 must build up our knowledge of deep-space monitoring

As AURORA develops an infrastructure, the radiation protection procedures discussed here can be developed further. Building on the existing terrestrial radiation safety industry and radiotherapy instrumentation, a new or adapted generation of radiation safety instrumentation can be developed to meet the special conditions of spaceflight and the major risks to crew health represented by solar protons and galactic cosmic rays.

Some advanced thinking is needed - about how to accomplish a radiation warning function on the REMSIM mission. For example, a hazard detector may not need all the "bells and whistles" expected of a space-science instrument. Some sensor types unsuitable for space science may be suitable for hazard warning. Section 3 considers some "unconventional solutions" for detector devices and some of these could be the subject of "try-outs" (speculative development).

Co-operation is desirable. NASA experimental research on similar problems is already in motion. For example the "Full Interplanetary Radiation Environment Simulation" (FIRES) programme (Schi01 and 02). Co-operation with a programme like this could help the ESA study. It is also possible that some of the NASA and ESA research threads could later mesh in collaborative experiments.

6.8.2 The Algorithm - Development

The core system requirement for monitoring is that the detectors should reduce human exposure i.e. by means of active on-board warning devices. With regard to solar-flare events, a warning and alarm system must embrace a wide network of space weather detectors which set the general level of alertness, in other words, the known risks. There must be local sensors accurately estimating in real time the BFO dose rates accumulated by crew members. Messages coming from the local sensors must be processed by an algorithm assessing the dose rate and the total dose and the relation of these quantities to a predetermined set of "danger levels" - targets for limits to these parameters for hours, months, years etc. Clearly the overriding targets are (1) to avoid short-term radiation sickness and (2) to preserve the total-dose limits set for stochastic effects [long-term

risk] below the given limit. Out of this body of information, rapidly assembled during a flare alert, comes the "alarm" or "advice to take emergency shelter" during the rare large solar flare event.

However, as well as covering those emergencies and generating alerts the system must include round-the - clock information on individual doses from cosmic rays and also indicate how to modify wprl practice to reduce dose buildup.

A typical engineering development problem is stated in our discussion of the flare dose rate, which rises rapidly at the start of a solar event. Figure 31 shows that the change in the dose rate in the rising edges of the radiation pulse, to which crew-compartment sensor technology must be sensitive, is high. A triggering of warnings at a dose rate of about 1E-3 Gy/hr appears to be a reasonable ab initio choice but detailed engineering studies are needed to show that this is the optimum point. The conflicting demands of "earliest possible warning" and "limiting false alarms" make this a complex engineering tradeoff.

Recent plans for a Mars mission will stimulate research into measurement of the biological radiation environment in space and its simulation in accelerators (Schi02 and 03), in-flight results from man in Earth orbit (SRHP93). In addition, there is the opportunity to take blood samples from crew after their return, on which the monitoring of "biological dosimeters" such as chromosomes and blood protein levels can be carried out. In addition, experimental animals, cultures of animal cells and of plants and particle-trackers of the most sophisticated kind can provide additional background to biological radiation effects.

6.8.3 Beam Tests and Flight Experiments

Many years of radiation-beam tests and many further unmanned, often robotic flight tests of dosimeters and detectors will precede a manned mission. Proving missions will have to perform very detailed experiments to measure the absorbed dose in a tissue-equivalent material behind very thick shields in deep space and on Mars at a location representative of the expected landing site as a function of shielding and body part. The experiments should, in particular distinguish the radiation dose contribution induced by charged particles from that induced by neutrons (NAS02, Zeit03) and the risks attached to the high background of GCR. Some tests of this type are starting under NASA's Deep Space Test Bed programme. These are a combination of high-energy beam tests, for example the ICCHIBAN tests in Japan and the USA (Uchihori 2004), polar high-altitude balloon flights (NASA 2004a) and tests of new shielding material (Benton, personal communication).

We have said that terrestrial accelerators do not simulate deep space completely. Thus space experiments, such as a "Skylab in deep space" are essential to establishing manned exploration capability. A Skylab or other habitat at the Lagrangian point or other lunar orbit would escape the distorting effects of the Earth's magnetic field but highly elliptical high Earth orbits might be more economical in launch energy. Such a laboratory is not explicit on ESA's plan for the AURORA concept. Polar balloon experiments, now run by the NSF, inevitably run at a very low dose rate and accumulation of total dose value but are nevertheless being utilised where possible by some cosmic-ray investigators (NASA 2004a).

For both beam tests and flight experiments, there is an opening for silicon detectors to increase the accuracy and breadth of the testing. For manned missions, advances in radiation sensor technology can increase the following features of the experiments:

- Compactness by miniaturization
- Smartness by silicon integration and micromechanical device methods
- The proper measurement of biological damage in beams - for example by the incorporation of protein, DNA etc.

Fig. 34 shows a sketch of a silicon Radiation-Sensitive metal-oxide-semiconductor field effects transistor (RADFET dosimeter) on a chip carrier. This miniature dosimeter technology was described in detail in Section 3 of this report. In the case shown **an array of silicon devices has a different amount of radiation absorbing material between each sensor and the bombarding radiation beam. Note the small dimensions**. Miniature arrays like the one shown have been flown for some years on spacecraft, internally or externally, logging the accumulation of radiation dose at a number of locations automatically over many years. In addition, such an array can enter the development process early in radiation-beam experiments; the array technique gives high-resolution dose profiles of test beams from soft X-rays to GeV ions. The advantage of this dosimetric technology for deep-space missions is that it matches the need for "smartness" and the extreme restrictions on weight, size and power imposed by the mission.

6.8.4 Unconventional Approaches to Warning Systems

6.8.4.1 Unconventional Alerts

The influencing of work habits in deep space to minimize GCR dose as well as the short emergencies associated with solar proton events is a part of radiation monitoring which, while not yet "conventional" or used in large numbers like radiation badges, should be recognized. Unlike "radiation alarms", the aim would be an awareness of the dose picked up in a chosen interval [e.g. 5 minutes, 1 hour or one work shift]. No bells would ring and no rush for shelter take place. Because GCRs are so penetrating, constant and cannot all be shielded out (see e.g. INFN 2004; RxTec 2004; Wilson 97, 98), a subtler technique of "GCR dose lowering" is needed based on such high round-the-clock awareness of the particles involved, their directions and any shadows afforded by large masses in the spacecraft. **Ergonomists and psychologists should collaborate with software designers on this aspect of radiation health.**

Another future approach not yet in the "conventional" class is the use of badges containing a biological material which registers more accurately the cell damage done in a given period. The method is based on yeast cells which change colour when mutagenesis takes place (Walmsley (1998); Knight 2004; Billinton et al 1998). A controlled experiment on the principle is being tested on ISS [Knight, personal communication]. The principle is discussed in sub-section 3.2.10.3 of this report. Other

cellular changes [chromosomes, lymphocytes etc) have long been studied as methods of "biological dosimetry" (Madhvanath (1976).

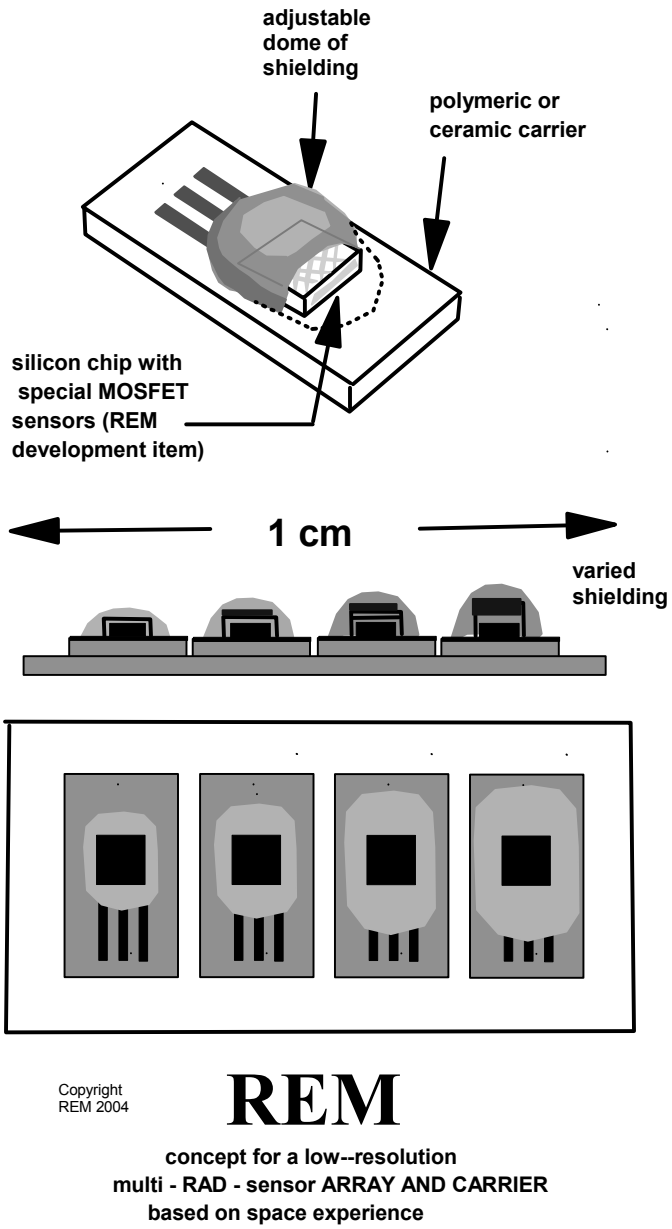

Figure 34. Sketch of a silicon Radiation-Sensitive metal-oxide-semiconductor field effect transistor (RADFET dosimeter) on a chip carrier. The sensitive region is a small region on the surface of the silicon chip (see Section 3). This is always covered by a protective encapsulant. In this case, there is an array of silicon devices and each has a different amount of radiation absorbing material between the sensor and the bombarding radiation beam. The silicon sensor chip is bonded and wired to a carrier substrate, which can be rigid or flexible and acts as as a connector to the "dosimeter reader". Miniature arrays like the one shown have been flown for some years on spacecraft, internally or externally, logging local dose values automatically over many years. For laboratory radiation-beam experiments, the array technique can give high-resolution dose profiles of test beams [note the small dimensions of the array shown].

6.8.5 An Unconventional Monitor of Solar UV Variability

6.8.5.1 General

In sub-section 3.2.11 we mentioned an unconventional approach, to the measurement of UV radiation using a MOS device. Variations in UV may possibly be used as a warning of SPE. The proposed "MOS detector of UV Variability" is likely to be more compact than the scientific EUV detectors shown in Fig. 35 for the IMAGE spacecraft. It is also likely to be more compact than "solar weather" detectors of soft X-rays used on weather satellites to classify solar flares. In other words, new detector technology could augment the spectral range and lower the weight budget for the long deep-space missions. Accordingly, design studies under the Aurora mission should be considered.

Fig. 36 shows NASA's IMAGE spacecraft, designed for scientific observation in the magnetosphere. Since the trajectory of IMAGE is an elliptical Earth orbit and the vehicle is spin-stabilised, the design of the instrument is different from any that would be placed on an interplanetary craft. However, by the nature of its operation an MOS point sensor is likely to be lighter and smaller in all cases.

Other examples of major findings using EUV and FUV are the SOHO and TRACE spacecraft. NASA's TRACE satellite has been observing the Sun in EUV and FUV wavelelngths, using a coated silicon Charge-Coupled Device (CCD). The whole small spacecraft is a solar-pointing UV telescope on a sun-synchronous 600x650 km Earth orbit. The spectrum of interest in the region 10 to 200 nm includes the following spectral lines 17.1nm FelX, 19.5nm FeXII, 28.4nm FeXV, 121.6 Hydrogen I 155.0nm C IV, 160nm continuum (NASA 2004b).

6.8.5.2 Advantages of the MOS Detector for UV

This is a new proposal for the design of an array useful in any solar-astronomy study but particularly appropriate to a warning system of minimised weight and power, such as that needed on missions related to the Aurora programme. It is best applied to the EUV and soft X-rays. Its advantages are light weight, low power and small size, convenience as a qualitative measurement, easily interpreted, erasability, broad application in EUV science and scalability from a point sensor to megapixel arrays. Some comparisons as to weight and power compared to other EUV instruments are made in Sections 3.2.11 and 3.3.7.

6.8.5.3 Development of EUV Observation for Aurora

If the principle of EUV observation as a warning method is accepted as relevant to the Mars or Moon missions, spacecraft or ground station, then designs and a development programme could be proposed, based on arrays of metal-oxide-semiconductor capacitors with or without UV optics. Engineering plans to perform such a design are already on file with one of the authors (Holmes-Siedle, personal communication).

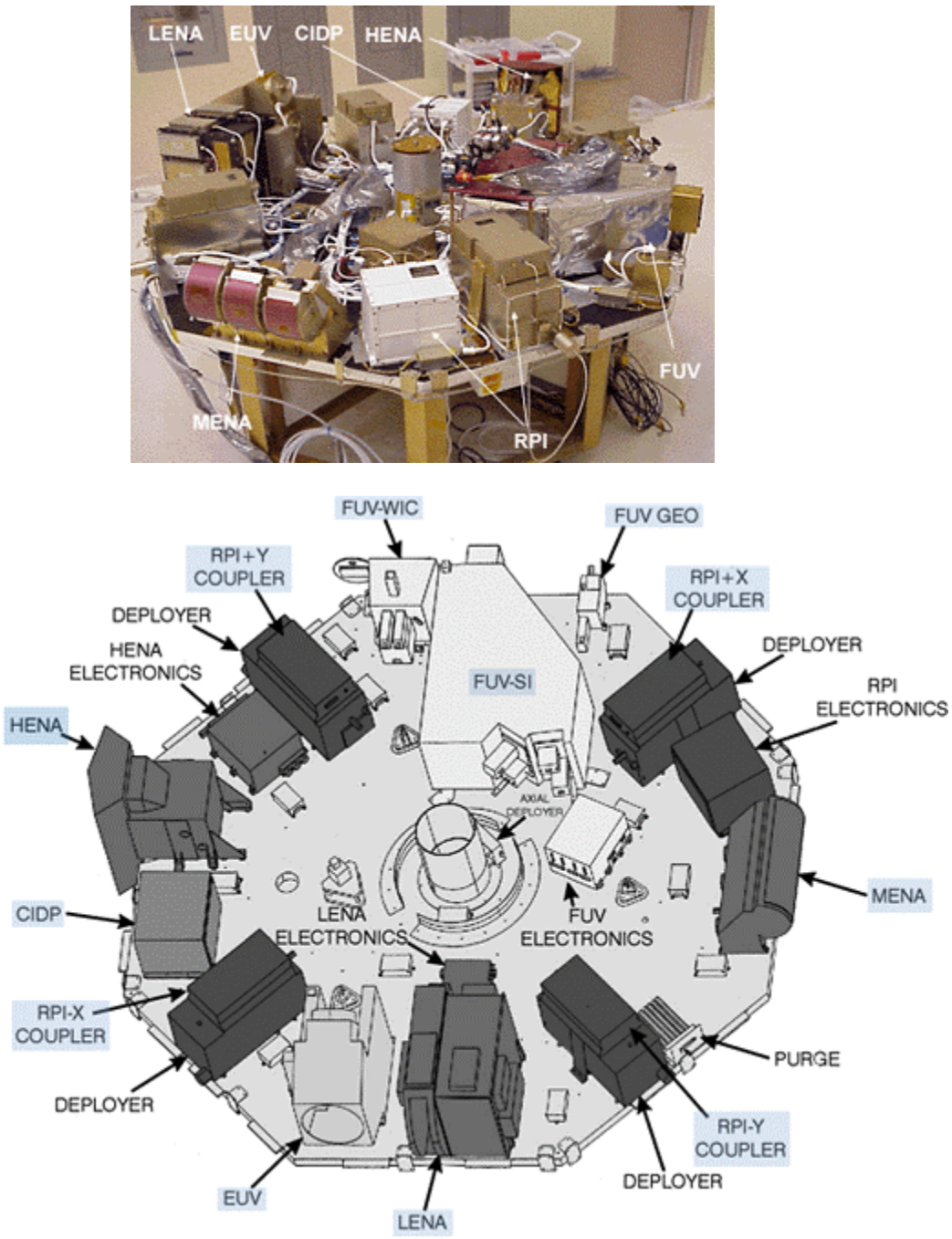

Figure 35. The instrument platform of the NASA IMAGE space probe, showing instruments including four UV detectors with different roles. The instrument set is designed for scientific observations in the Earth's magnetosphere. (upper panel) photograph; (lower panel) sketch

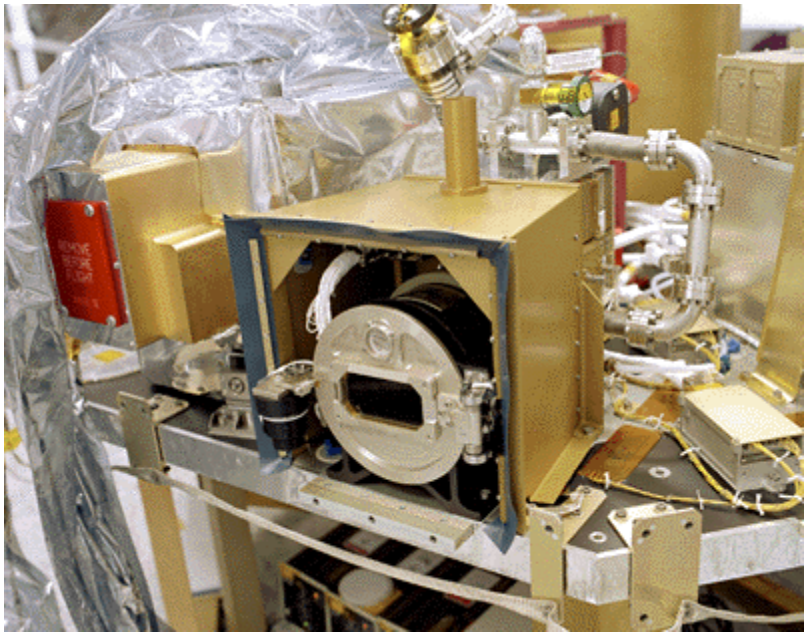

Figure 36. Close-up of the wide-angle FarUV on the instrument deck of the NASA IMAGE space probe, showing the medium-sized FUV-WIC. The instrument set is designed for hourly imaging of hydrogen-line emissions from the upper atmosphere and the Earth's magnetosphere.

6.8.6 Unconventional Shielding Approach

It is perhaps not obvious that the radiation monitoring strategy depends on a good materials policy as regards the design of shielding. It is perhaps obvious that the deep-space exploration programme of ESA should develop radiation-tolerant organic materials optimized for the dual roles of radiation shield and spacecraft structures [high in hydrogen, strong, tough and machinable]. It may be less obvious that the nature of the radiation monitor design is "tuned" to the internal radiation dose rates from GCRs - the "background" (see Section 6.2.2 and Figure 30). Shield vs. weight tradeoffs are interdisciplinary areas for research, especially in the inflatable structural approach. Shields are not just water tanks - they can be load-bearing structures high in hydrogen. Polyethylene is widely fancied as a shield but that is not a high-strength polymer. We recommend the use of "all-polymer composites", that is polymer fibres in a polymer resin matrix as dual shield and structure. The shield designer should have the necessary choice of dual-purpose materials such as all-polymer composites. KEVLAR-reinforced epoxy is already used in place of aluminium in parts of ESA's Columbus [Alenia04]. We recommend that, in programmes following REMSIM/AURORA, advanced materials properties research should be performed on engineering materials such as KEVLAR [PPTA] and NOMEX [MPDI], to enhance the choice of polymeric composites available for construction and shielding. Work is already in progress on the examination of mechanical defects in NOMEX fibres on the nanometre scale. [see e.g. Martin 2003]. This should be extended to include radiation-induced defects in polymers, including those caused by neutrons and heavy ions and their effect on structural strength and on ageing in long-term use on planetary surfaces and deep-space trajectories.

6.8.7 Built-in Safety Technology

6.8.7.1 General

With regard to warning needs, protection systems against space radiation in deep space have some similarity to other protective systems needed for hazards such as the release of toxic gases or infectious organisms within transport systems [tunnels, ships, aircraft], the ever-present hazard of fire and the specialized hazards of nuclear release. Safety technology and warning methods in these very different spheres has received and will continue to receive a strong acceleration of interest due to novel terrorist threats. As they develop over the next five years, the design teams should take note of them.

6.8.7.2 Building in Radiation Safety

As described in Section 6.7.2.3 a Norwegian Virtual Reality Centre is performing for ESTEC a study for mapping radiation fields in manned spacecraft compartments (RadVis 2004). The Dose Estimation by simulation of the International Space Station Radiation Environment (DESIRE) project aims at accurate predictions of radiation fluxes inside the ESA. Because of the extra weight budget demands of deep space missions, this concept of "built-in shielding and safety" - using structure and stores as shields is vitally important to crew radiation management.

This work is mainly a software development as yet but later, mockups of crew compartments will be built and mapped for dose. In orbiting space-stations, real **dose contours or isodose maps** will then be checked with installed dosimeters, preferable active ones which speed the information to the management system.

We thus recommend that, as a part of co-ordinated design and deep-space spacecraft development systems: In isodose mapping of crew compartment models, radiation-transport software to be linked with a dosimeter network.

6.8.7.3 Conventional Safety Technology

In aircraft and other civil vehicles, conventional technologies for enhancing safety and warning methods received a strong acceleration of interest due to novel terrorist threats. As they develop over the next five years, the design teams should take note of that growing body of safety technology. In ESTEC, human safety already has high priority in spacecstation design and inputs from this activity meet the REMSIM type of study in the Co-Ordinated Design Facility (HMM 2004).

6.8.8 NASA Development Plans

6.8.8.1 NASA Approach to Sensor Selection in Deep-Space Manned Flight

NASA JSC is planning the hardware requirements, including development, for deep-space manned flight. Choice of sensor type and the operational and scientific content of a

development scheme have been outlined (Golightly, personal communication). ESA already obtains benefit from such studies by technical and managerial liaison.

The JSC Space Radiation group sees the need for the following co-ordinated sets of sensor. By "co-ordinated" we mean designed as a group, with the objective of minimizing weight and power and optimizing overlap in function.

External sensor:

- proton-helium ion spectrometer

Internal sensors:

- dose rate monitors distributed throughout the vehicle,
- internal charged particle monitor/spectrometer hybrid
- small (active) personnel dosimeter,
- a directional neutron spectrometer radiation environment monitoring management system.

A generally similar set would be required for the lunar and Mars surface. Following the mission, post-mission biodosimetry would provide an important cross check and calibration for later missions.

As regards software, JSC has developed an automated SPE analysis tool, Solar Particle Event--Real-Time, used for computing - in real time during the event - the exposure of crew from the protons detected by sensors array. In addition the software provides a "look-ahead" for the next 24 hours. The transport code portion of this tool uses a simple straight-ahead continuous energy loss algorithm but upgrades will also contain the Langley Research Center's BRYTRN code, which includes dose contributions from nuclear interactions.

6.8.8.2 NASA Approach to CAD of Shielding

Development in the above field must include system analysis and software development. NASA has adopted the IDEAS CAD package in several fields, including design and manufacture. One development includes a "point-and-click" facility for the tracing of "rays" of radiation – straight-line paths through a structure as followed by energetic particles. The result returns not only the thickness but the composition (material property) of the material logged on that path, allowing a rapid one-dimensional "layered-slab" assessment of effective shielding at any point in a spacecraft which exists as a CAD model. When designs are put into CAD by other engineering groups at JSC, then "shield model with incredible resolution and fidelity (in some cases down to the washer level)" have already been achieved (Golightly, personal communication). This software serves the purpose of a "quick look" at the shielding qualities of a concept during system engineering. Later, a more refined state-of-the-art space radiation analysis tool--some of the codes being evaluated/modified/linked as part of FLUKA and HETC transport code developments. The use of CAD is part of NASA's philosophy of "seamless integration of the original design intent into the manufacturing environment". NASA-GSFC pursues this aim using CAD systems including IDEAS, IGES, STEP and DXF (NASA 2004c).

6.9 Discussion

6.9.1 Philosophy of protection

The case under study here is a long-duration exploratory mission in deep space. It is arguable that **the variation with respect to time should be monitored differently from past cases.**

How should the philosophy of protection be different for this case? The following points of philosophy can be made now.

1. Warnings and alarms have to be derived from signals from **on-board hardware but balanced with extensive intelligence from outside**. The on-board hardware has to be backed up with extremely reliable software. Measurements of particle fluxes *outside* the vehicle have to be balanced with actual total-dose and dose-rate measurements *inside* the vehicle as close as possible to the human blood-forming organs. It is not only during solar activity that dose rates should be measured. Dose-rate measurements *inside* the vehicle must be designed to minimise crew dose from the background as well from GCRs (we need a dose map with many points). The various measurements shift in relative value to maintaining health as one moves from solar max to min conditions.

2. There are two aspects to warning and ALARA standing for dose values "As Low As Reasonably Achievable". There is (a) the "emergency condition [SPE]", requiring rapid reaction; and there is the (b) "chronic or background condition [GCR]" just as serious in the long run but requiring daily routines which value daily dose management as highly as daily diet and health management. In the case of GCRs, because transient dose-rate increases from this source are unheard-of, there is no requirement for an "alarm" system on their account, in contrast to transient increases from proton events, where a rapid-reaction system is essential. However, **ergonomically based instruments which guide crew in avoidance of GCR hot spots in the internal isodose map** are essential. Some of the applications of the ALARA principle to the REMSIM project and the resultant limiting dose figures have been given in report TN1.

3. As regards hardware and warning methods, the on-board detectors which trigger crew actions will be different in cases 2a and 2b. Case 2a (SPE) will be backed by a sophisticated, spread network of space-weather detectors. Case 2b (GCR) is a case of monitors for individuals and an exercise in patience - time and motion management to achieve the goal of "GCR dose avoidance". While the rapid forecasts and early alerts are the more impressive results, it may be that the regular if monotonous management of GCR dose may, by the end of a mission, have had the greater impact. The previous management by the crew of their own burdens of larger "backgrounds" of GCR dose COULD affect the **total-dose margin which individuals have left themselves** for the survival of an anomalous proton event, while GCRs may also have the strongest impact on risks of cancer later in life.

4. As regards hardware, we expect a **greater use of active dosimetry than in LEO**. This means **electronic dosimetry** which recognizes the nature of particles and photons received, as far as is required to determine their long-term biological effects. The characterization needed may be less than that employed in space research being conducted at present. **Economy in size, weight and power will naturally be enforced** by the weight budget of a deep-space manned mission including Mars. Thus, the choice of dosimetric instruments involved in generating warnings will be biassed towards types which mimic tissue [see e.g. the tissue-equivalent proportional chamber [TEPC] and semiconductor devices suitably modified to mimic the depth distribution of body organ and which have been adapted to the stringent weight and reliability considerations].

5. Humex has already studied the minimization of health effects in the long term by reducing uncertainties in exposure estimates, by advanced radiation risk analysis, optimizing the system design phase for radiation health factors (this involves using very good radiation transport codes in the design of structure and has already led to the employment of the GEANT code in system analysis). On-board techniques will include the provision of a radiation shelter and "biological dosimetry" such as blood tests. Humex divides the radiation environment in a manned operation into "Acute" and "Chronic" environments, implying respectively that solar proton events (SPE) give the "Acute" hazard of short-lived intense pulses of dose, varying in severity from "mild" to "killer"; while Galactic Cosmic Rays (GCR) give the "Chronic" or steady, very-slowly-varying environment, mainly due to galactic GeV protons. Because of the impossibility of seriously attenuating the latter, the "ChronicGCR" environment merits the additional title of "background radiation of deep space". The handling of this element has many similarities to the well-known "gamma-photon background" received by humans from rocks, food and air on Earth and possibly also from Moon and Mars rocks. Methods are developing (RadVis 2004) to **visualise such backgrounds; this encourages avoidance**.

6. The handling of the "Acute" environment will be a challenging problem of generating **valid warnings without false alarms**. Solar-proton events are probabilistic in nature, so that on-board detectors are only one element in a broad detector network which comes to a decision as whether the solar-induced variations sensed will culminate in the crew quarters as an insignificant change in "background" or a severe addition to the crew's total dose.

7. The effect of the solar cycle on impinging GCR rates is a factor of 5 to 7 times, lowest at solar maximum. This factor will **influence launch dates and have a major effect on radiation-induced risk.**

8. The nature of space radiation as a hazard has some similarities with other protective systems in terrestrial life, such as the release of radioactivity, toxic gases or infectious organisms within buildings or vehicles [tunnels, ships, aircraft or nuclear plants] and the ever-present hazard of fire. The team has taken note of the lessons of safety technology and warning methods in these very different spheres.

9. If GCR doses dominate over doses from solar protons in the dose budget for the crew and there is very little ability to change the minimum crew GCR dose for the mission by practical actions once the shielding weight budget is decided. The **weight assignments made years before launch** may determine the minimum crew GCR dose. There is still uncertainty in the GCR composition for the deep-space trajectories and the effect of GCRs on the average human blood-forming cell.

10. The final design of radiation detectors and dosimeters for low Earth orbit (LEO) and deep space trajectories will be altered by the mission constraints. For example, the size of a polymer ball for the neutron sensor or silicon diodes for particle spectrometers may be different from the model used on the ISS, where trapped protons produce much of the hazard. Only one pointing axis [x, y or z], rather than three, may be addressed. However, tests of **several specialised designs of dosimeter on unmanned proving flights** should quickly establish an **optimum dosimetric set** for operational crew protection.

6.10 Conclusions

Compared with any manned mission carried out so far, the internal radiation dose rates for the Mars mission are likely to be higher, the mass of shielding available is likely to be lower and hospital treatment facilities will be further away. Thus, some new thinking on hardware and software to warn crew and help them to avoid dangerous doses is needed.
In planning human missions to Mars, we have the advantage of a framework built up in the ESA Crew Medical Support Office, DEFINE, the NASA Space Radiation Group at Johnson SFC USA and Russian centres [Bent01], for the management of crew radiation exposures in LEO. We now have to modify and extrapolate to the deep-space condition, for which there is much scientific evidence but no experience.

As AURORA develops an infrastructure, the radiation protection procedures discussed here must be developed further, building on the existing space and terrestrial radiation safety infrastructure and increasingly sophisticated instrumentation for radiotherapy. The hazards of cosmic rays alone will be enough to make radiation health a key mission parameter. The solar-flare emergencies, if any, add to that background requirement.

Optimizing protection for the crew will be crucial in design. We note in several sections above places that sensors which generate “advice to take emergency shelter” are important but not the only part of the overall radiation monitoring scheme recommended. The conflicting demands of “earliest possible warning” and “limiting false alarms” make the engineering of radiation alarms a complex tradeoff. The distribution and use of the mission weight budget will have a crucial effect (1) on the GCR mission dose, where it will affect daily work practices (2) on the probabilities of an additional large dose from an exceptionally large solar flare. Thus the REMSIM study must place strong emphasis on a “Radiation Isodose Map” and its impact on crew practices and the design philosophy for on-board warning devices.

The dose rates expected in deep space are of the same order as those observed in the ISS although the crew compartments of an Aurora vehicle may not provide as much built-in shielding and the hazard is harder to predict because of the larger fluxes and the

probabilistic nature of solar flare proton exposures. The much longer duration of the flights and the distance from home base greatly increase the risks. These factors suggest a different radiation-monitoring philosophy, presented in this report, with more active devices and hour-to-hour awareness of radiation fluxes in given positions in the compartments.

With respect to launch date, there will be pressure to choose GCR minima in the solar cycle - meaning launch date pressure for these periods. This dependence on solar activity will apply both to present exploration AND future colonization. GCR minimum occurs at solar maximum. Instrument payload design may change depending on the phase of solar activity. Mission models suggest that a 3-year mission to Mars would exceed the LEO levels considered safe by NASA (NCRP-132, Asso03, Atwe03b, Brit03].

This section of WP5000 focussed on the objectives of protecting the crew, where signals from on-board dosimetric hardware and recommend crew actions and solar activity may trigger "advice to take emergency shelter". The internal measurements must be balanced by extensive intelligence from an array of remote sensors and forecasts. The on-board hardware systems have to be backed by extremely reliable and friendly software. We have studied total doses and dose rates and their relative weights as triggers of alarms. We consider how dose rates and total doses shift in importance as one moves from solar max to min conditions.

On the hardware system level there are two different dose-rate conditions to monitor. There is the "emergency condition" induced by a flare event which has to be dealt with by urgent crew action; and the "chronic condition" the health risks from low, steady cosmic ray dose rates in deep space. The emergency condition has been thoroughly dealt with in other publications cited in this report. Possibly, some crew will have to take turns at staying out of the shelter, taking a chance of a "bad go" while the rest of the crew reduces its risks. As regards the "chronic condition" in Sections 6.2.2.1 and 6.6.6, we made a homely comparison of various hazards of the Mars mission:

"one click per second on Earth" "a hundred clicks per second in Deep Space", except in a large flare, when the click rate would be "off-scale".

This has been adopted as the motto of the project in the REMSIM summary report by Alenia (REMSIM 2004a).

This illustrates that the health risks from cosmic rays in deep space are much more severe than on Earth; that they are steady, predictable and that some element of the risk can be avoided by good monitoring. This is recognised in the choice of this phrase as the motto for the project in the summary report (REMSIM 2004). There is time to develop novel methods during the technology phase of AURORA of giving the crew the information by which they can reduce their cosmic ray dose. ESA and NASA will back this up by research on radiobiology and chemical or biological protection methods.

We expect that, as well as installing monitors on the outside and inside of the spacecraft shells, individual crew doses will be monitored using passive dosimeters and possibly some active "pocket dosimeters" such as the conventional "electronic personnel dosimeter" plus the unconventional "EVA MOSFET" flown by the Canadian Space Agency.

In addition to equipment easily available on the terrestrial safety market, a new generation of radiation safety instrumentation should be developed to meet the major risks to crew health represented by radiation. Special individual monitors to promote "GCR dose lowering" are also needed. Sensors on the crew member must, inform him or her of particular rates and recommended actions, all the time and not only when on EVA is being performed. While the most hazardous conditions are in deep space, the lack of atmosphere on the Moon [0 $gmcm^{-2}$] and Mars [16 $gmcm^{-2}$] heighten the radiation hazard compared with that on Earth, where the air provides 1030 gm cm^{-2} of shielding.

The motivation for engineering development of radiation monitors on the AURORA programme is the ALARA requirement - a matter of policy in all agencies - to minimize long-term cancer risk for the crew. We have mentioned the conflicting requirements of "earliest possible warning" and "limiting false alarms".

Engineering development of dosimeters will make the radiation monitors economical of space, weight and power in the craft's engineering budget. The Aurora programme has initiated a Dossier of Enabling Technologies for the Mars programme and this includes radiation detection. A period of further development of sensors offers itself in the form of the ten-year AURORA technology development period, including many unmanned sample-return and manned spacecraft technology proving flights in which radiation counters and dosimeters can be included. We have noted that the flight test-beds should include a "Skylab in deep space", a heavy, shield testing spacecraft in very high Earth orbit. The development of radiobiological and physical models to deal with the effects of the deep-space, interplanetary radiation environment is also underway at academic and Agency level.

In this section and an earlier one called "Radiation Monitors", we have pointed to some of the technology and systems engineering needs. The sensors should interface with the main control system of the space habitat [computing and fire-and-gas warning subsystems]. Dedicated software recognizes hazards and attunes crew behaviour to fit the hazard both in quiet times and during high solar activity. Exterior observation platforms which assist this task have been described by BIRA. At this stage, no hardware is being built but block diagrams and sketches of hardware should make possible the formulation of a development programme fitted into Aurora. In consultation with the present investigators, specimen computer codes have been compiled for trial on the hardware in question [see TN1].

We have mentioned some "unconventional" approaches to radiation sensing and protection such as the adaptation of fire-alarm software and an existing "spinoff" from high-energy physics - an intensifier CCD that gives a display of visible tracks of cosmic rays. There may be several appropriate avenues for research in sensor technology and hardware development growing out of existing ESA projects such as the radiation dosimetry activity aboard the ISS and ESTEC space safety projects.

The Aurora programme is likely to provide a useful framework having adequate time in which to make important advances in sensor technology, suitable for the serious nature of the radiation hazards on a Mars mission.

Proposals for ergonomic "cosmic ray avoidance" methods to deal with the continuous "hundred clicks per second " from the steady background dose rate of cosmic rays are an

original contribution of this report. Parallel developments by ESA to make virtual-reality images of radiation fluxes (RadVis 2004) will find application in dealing with this problem.

This report advocates TWO WARNING MODES and hence two different modes of radiation avoidance

(1.) Emergency Mode, avoiding occasional high surges of radiation from solar activity, widely advocated

(2.) Background Mode, avoiding or "cutting down on" steady background radiation from GCR.

Avoidance of type 1 is done by **disruption** of routine - taking shelter during the emergency behind a very thick proton shield. The avoidance of type 2 is done by the ergonomic **adjustment** of routine - by moving routinely to locations where the AVERAGE shielding between oneself and outer space is more massive. An essential part of this radiation management is instrument-based. Prompts from the spacecraft system help the individual to "cut down" on his personal average dose rate (see our approach to an algorithm for this in Section 6.7). RX/TEC and REM have demonstrated **a day-by-day warning system,** using a simulation programme which is described in Section 6.7.

Radiation avoidance modes of types 1 and 2 are complementary. The first mode is like escaping from a lethal, smoke-filled room and the second is like "cutting down one's smoking" in daily life. The daily success of "cutting down" on GCR, mode 2, is easy to measure with dosimetric instruments. In our Geiger counter analogy, the spacecraft dose management system can be said to count not only the "clicks per second" as in a Geiger but also process and control the "clicks per day, month or year" for the long-term health benefit of every crew member.

Table 29 summarises the overall recommendations of the Monitoring and Warning section of this projects, which will combine to protect the health of the crew in a large number of different ways.

Monitoring - Recommendations in general	
1. Space Weather Monitoring for Lunar and Mars Missions (objective - solar monitoring network based on Earth-based infrastucture) *** "Sentinel" spacecraft e.g SOHO, Near-Side and Far-Side Sentinels, Mars orbiters** *** Earth and lunar-based weather monitors** (imaging, radio etc) *** Engineering model for solar protons and cosmic rays in deep space from Earth to Mars and Moon**	**2. Crew Habitat Monitoring** (objectives keep cancer risk below 3 percent/ avoid short-term radiation sickness) *** simplification of protection devices** (full scientific counter setup may not be necessary; use ISS as test bed) *** computer-based dose mapping** (GEANT and RadVis maximise computer power) *** warnings to take deep shelter** (tradeoffs in timeliness vs. false alarms) ***new concept - prompts for cosmic-ray avoidance** (ergonomics combined with instruments - demo available) *** research** **miniature silicon detector technology available** **biosensor technology available**

Monitoring - Recommendations in brief

Space Weather Monitoring
*** "Sentinel" spacecraft e.g SOHO, Near-Side and Far-Side Sentinels, Mars orbiters**
*** Earth and lunar-based monitors [imaging, radio etc]**
*** Engineering model for solar proton events**
*** Engineering model for cosmic rays**

Crew Habitat Monitoring
*** simplification of protection devices [ISS as test bed]**
*** computer-based dose mapping [GEANT and RadVis]**
*** warnings to take deep shelter**
*** ergonomic prompts for cosmic-ray avoidance [demo available]**

Table 29. Summary of recommendations for follow-on projects [post REMSIM].

REFERENCES

Adams L., Harboe-Sorensen R., Holmes - Siedle A.G., Ward A.K. and Bull R., [1991], "Measurement of SEU and total dose in geostationary orbit under normal and solar flare conditions", IEEE Transactions on Nuclear Science, NS-38 (6), 1686-92, Dec 1991.

Adams L. and Holmes-Siedle A.G., [1978], "The development of an MOS dosimetry unit for space", IEEE Transactions on Nuclear Science, NS-25, 1607-1611.

Adams L., Demets R., Harboe-S¢rensen R, Nickson R., Gmür K. and Heinrich W., [1996], "Radiation dosimetry for recoverable payloads", Proceedings of the Sixth European Symposium on Life Science Research in Space, Special Publication 390, 165-169 (European Space Agency – ESTEC, The Netherlands 1996).

Alenia, [2004], Lobascio et al, "REMSIM Final Report", No. ALS-RSM-0001 (2004).

Ambastha A., Hagyard M.J., West E.A., [1993], "Evolutionary and Flare-Associated Magnetic Shear Variations Observed in a Complex Flare-Productive Active Region", Solar Physics, 148, p. 277.

Amptek, [2004], "Compact Environmental Anomaly Sensor; Space Radiation Alarm", <http://www.amptek.com/cease.html>

AN/UDR-13, [2004], "Military Pocket Radiac designed for reliability and performance". <http://www.canberra.com/pdf/Products/RPI_pdf/anudr13.pdf >

Antiochos U.S., [1998], "The magnetic topology of solar eruptions," Astrophysical Journal, L181, p.502.

Apel99, U. Apel, "Human factors and Health in Space Tourism", 2nd International Symposium on Space Tourism, Bremen, April 1999.

Aran A., Sanahuja B., Lario D., Domingo V., [2001], "An Operational Code for Solar Energetic Proton Flux Prediction. First Approach", in "Space Weather Workshop: Looking Towards a Future European Space Weather Programme", 17-19 December 2001 ESTEC, Noordwijk, The Netherlands, ESA WPP-194, p.215. Available at: <http://www.estec.esa.nl/wmwww/wma/spweather/workshops/SPW_W3/PROCEEDINGS_W3/proc_aaran.pdf>.

Atwell W., Zeitlin C., Cucinotta F.A., Cleghorn T., Saganti P., Lee K., Andersen V., Pinsky L., Turner R., [2003], "Solar Proton Event Observations at Mars with MARIE", (SAE 2003-01-2329), 33rd International Conference on Environmental Systems (ICES), Vancouver, British Columbia, Canada, 7-10 July 2003. Warrendale, Pennsylvania, USA: Society of Automotive Engineers.

Bale S. D., Reiner M. J., Bougeret J.-L., Kaiser M.L., Krucker S., Larson D.E., Lin R.P., [1999], "The source region of an interplanetary type II radio burst", Geophysical Research Letters, 26, p.1573.

Bartlett D., Hager L., Tanner R., [2002], "Determination of the neutron component of the cosmic radiation field in spacecraft using a PADC neutron personal dosimeter", Proc. 7th WRMISS, Paris, September 2002.

Baumbaugh B., Bishop J., Castle L., Karmgard D., Kozminski J., Marchant J., Mooney P., Ruchti R. and Wiand D., [2000], (University of Notre Dame). "A portable cosmic ray detector and display", IEEE Transactions on Nuclear Science, NS-47 41 - xx.

Benton E.R., E.V. Benton, [2001], "Space radiation dosimetry in low-Earth orbit and beyond", Nucl Instrum Methods Phys Res B., 184 (1-2), 255-294.

Boeder C.P.W., Adams L. and Nickson R., [1993], "Scintillator fibre detector system for spacecraft component dosimetry", Proc. RADECS'93 Conference, St. Malo, September 1993, IEEE Catalogue no. 93 TH 0616-3, pp 262-5.

Bothmer V., Schwenn R., [1994], "Eruptive prominences as sources of magnetic clouds in the solar wind", Space Science Reviews, 70, p. 215.

Brucker G. J., Kronenberg S. and Jordan T., [1993], "Tactical army dosimeter based on p-MOS single and dual gate insulators", Proceedings of RADECS'93, St Malo, September 1993, France, IEEE Catalogue No. 93-TH-0616, pp. 56-62.

Burlaga L., Sittler E., Mariani F., Schwenn R., [1981], "Magnetic loop behind an interplanetary shock - Voyager, Helios, and IMP 8 observations", Journal of Geophysical Research, 86, p. 6673.

Cahill P.A., A.W. Knight, N. Billinton, M.G. Barker, L. Walsh, P.O. Keenan, C.V.Williams, D.J.Tweats and R.M. Walmsley (2004). Mutagenesis, 19 105-19 (2004).

Camanzi B., Holmes-Siedle A.G. and McKemey A., [2000], "The dose mapping system for the electromagnetic calorimeter of the BaBar experiment at SLAC", Nuclear Instruments and Methods in Physics Research A, to be published 2000 (first use in GeV particle physics).

Camanzi B., Holmes-Siedle A.G. and McKemey A.K., [2001], "The dose mapping system for the electromagnetic calorimeter of the BaBar experiment at SLAC", Nuclear Instruments and Methods in Physics Research Section A, 457, (3), 476-86 (21 January 2001).

Cane H.V., Stone R.G., Fainberg J., Steinberg J.L., Hoang S., Stewart R.T., [1981], "Radio evidence for shock acceleration of electrons in the solar corona", Geophysical Research Letters, 8, p.1285.

Cane H.V., [1984], "The relationship between coronal transients, Type II bursts and interplanetary shocks", Astronomy and Astrophysics, 140, p. 205.

Cane H.V., McGuire R.E., von Rosenvinge T.T., [1986], "Two classes of solar energetic particle events associated with impulsive and long-duration soft X-ray flares", Astrophysical Journal, 301, p. 448.

Cane H.V., Sheeley N.R., Howard R.A., [1987], "Energetic interplanetary shocks, radio emission, and coronal mass ejections", Journal of Geophysical Research, 92, p. 9869.

Cane H.V., Reames D.V., von Rosenvinge T.T., [1988], "The role of interplanetary shocks in the longitude distribution of solar energetic particles", Journal of Geophysical Research, 93, p. 9555.

Cane H.V., [1997], "The current status of our understanding of energetic particles, mass ejections, and flares" in Coronal Mass Ejections, Geophysical Monograph 99, AGU Washington D.C., Crooker, Joselyn, and Feynman, eds., p.205.

Canfield R.C., Hudson H.S., McKenzie D.E., [1999], "Sigmoidal morphology and eruptive solar activity", Geophysical Research Letters, 26, p.627.

Chen J., [1996], "Theory of prominence eruption and propagation: Interplanetary consequences", Journal of Geophysical Research, 101, p. 27499.

Chen P.F., Shibata K., [2000], "An Emerging Flux Trigger Mechanism for Coronal Mass Ejections", Astrophysical Journal, 545, p.524.

Chuang C., Verhey L., Xia P., [2002], UC San Francisco & Comprehensive Cancer Center, San Francisco, CA., "Investigation of the Use of MOSFET for Clinical IMRT Dosimetric Verification", Medical Physics, June, 2002.

Cliver E.W., Webb D.F., Howard R.A., [1999], "On the origin of solar metric type II bursts", Solar Physics, 187, p. 89.

Crooker N.U., Joselyn J.A., Feynman J., eds., [1997], "Coronal Mass Ejections", Geophysical Monograph 99, AGU Washington D.C.

CSA (Canadian Space Agency), [2004], "CSA – EVARM; Space Life Sciences. Extra Vehicular Activity Radiation Monitor.; Space Life Science Experiment".
<http://www.space.gc.ca/asc/eng/csa_sectors/ space_science/life_sciences/evarm.asp>

Cucinotta F.A., Saganti P.B., Wilson J.W. and Simonsen L.C., [2002], "Model Predictions and Visualization of the Particle Flux on the Surface of Mars", J Radiat Res (Tokyo), 43 Suppl., p. S35.

Cuci95 F.A. Cucinotta, J.W. Wilson, M.R. Shavers, R. Katz, "Effects of track structure and cell inactivation on the calculation of mutation rates in mammalian cells", Int. J. Radiat. Biol. 1995: 69(5); 593-600.

Cuci96 F.A. Cucinotta, J.W. Wilson, R. Katz, W.Atwell, G.D. Badhwar, "Track structure and radiation transport models for space radiobiology studies", Adv. Space Res. 1996: 18(2); 183-194.

Cuci00a F.A. Cucinotta, "Once we know all the radiobiology we need to know, how can we use it to predict space radiation risks and achieve fame and fortune?", 11th Annual NASA Space Radiation Health Investigators' Workshop, Arona, May 2000, Physica Medica - Vol. XVII, Suppl. 1, 2001.

Cuci00b F.A. Cucinotta, K. George, H. Wu, "Biodosimetry and Space Radiation Risks", 48th International Congress of Aviation and Space Medicine, Rio de Janeiro, September 2000.

Cuci01a, F.A. Cucinotta, W. Schimmerling, J.W. Wilson, L.E. Peterson, G.D. Badhwar, P.B. Saganti, J.F. Dicello, "Space Radiation Cancer Risk Projections for Exploration Missions: Uncertainty Reduction and Mitigation", NASA, JSC-29295, January 2001.

Cuci01b, F.A. Cucinotta, W. Schimmerling, J.W. Wilson, L.E. Peterson, G.D. Badhwar, P.B. Saganti, J.F. Dicello, "Space Radiation Cancer Risks and Uncertainties for Mars Missions", Radiation Research Vol. 156 No. 5, November 2001.

Cuci01c, F.A. Cucinotta, F.K. Manuel, J. Jones, G. Iszard, J. Murray, B. Djojonegoro, M. Wear, "Space Radiation and Cataracts in Astronauts", Radiat. Res. 156, 460-466, November 2001.

Cuci02 F.A. Cucinotta, L.E. Peterson, J.A. Jones, F.K. Manuel, "Dose Response for Cataract Incidence among Astronauts", 2nd International Workshop on Space Radiation Research, Nara, Japan, March 2002.

Cuci03a, F.A. Cucinotta, P.B. Saganti, X. Hu, M.Y. Kim, T.F. Cleghorn, J.W. Wilson, R.K. Tripathi, C.J. Zeitlin, "Physics of the Isotopic Dependence of Galactic Cosmic Ray Fluence Behind Shielding", NASA/TP-2003-210792, February 2003.

Cuci03b, F.A. Cucinotta, H. Wu, M.R. Shavers, K. George, "Radiation Dosimetry and Biophysical Models of Space Radiation Effects", Gravitational and Space Biology Bulletin 16 (2), June 2003.

Curt02, S. Curtis, "Fluence-Based and Microdosimetric Event-Based Methods for Radiation Protection in Space", 2nd International Workshop on Space Radiation Research, Nara, Japan, March 2002.

Daglis I.A. ed., [2001], Proceedings of the NATO Advance Study Institute on "Space Storms and Space Weather Hazards", Kluwer Academic Publishers.

De Angelis G., Wilson J.W., Clowdsley M.S., Nealy J.E., Humes D.H., Clem J.M., [2002], "Lunar Lava Tube Radiation Safety Analysis", J Radiat Res (Tokyo) 43 Suppl., p. S41.

Delaney C.F.G. and Finch E.C., [1992], "Radiation Detectors. Physical Principles and Applications", (Oxford Science Publications, Clarendon Press, Oxford. 1992).

Demets, R. (2000). ESA life science experiments on BION and FOTON; Part 1: radiation dosimetry. Proceedings of the First International Conference on Scientific and Technological experiments on Foton and Bion, Samara, Russia, June 2000.

Desai M.I., Mason G.M., Dwyer J.R., Mazur J.E., Smith C.W., Skoug R.M., [2001], "Acceleration of ^{3}He Nuclei at Interplanetary Shocks", Astrophysical Journal, 553, p. L89.

Domingo V., Sanahuja B., Heras A.M., [1989], "Energetic particles, interplanetary shocks and solar activity", Advances in Space Research, 9, p.191.

Dura01a, M. Durante, G. Gialanella, G.F. Grossi, M. Pugliese, P. Scampoli, "Radiosensibilità Cellulare per Irraggiamento con Adroni", xxxxx, ≥ 2001.

Dura01b, M. Durante, G. Gialanella, G.F. Grossi, M. Pugliese, P. Scampoli, "Dosimetria Biologica in Radioterapia e della Radiazione nello Spazio", xxxxxxxxx, ≥ 2001.

Dura02, M. Durante, F.A. Cucinotta, G. Obe, "Workshop Report: Biodosimetry and Space Radiation Risk, Capri, July 2002", Microgravity and Space Station Utilization, 3, 2002.

Dyer C.S., Truscott P.R., Peerless C.L., Watson C.J., Evans H.E., Knight P., Cosby M., Underwood C., Cousins T., Noulty R., Maag C., [1999], "Implications for Space Radiation Environment Models from CREAM & CREDO Measurements over Half a Solar Cycle", Radiation Measurements, 30, 5, pp 569-578, Oct 1999.

Dyer C.S., Truscott P.R., Sanderson C., Watson C., Peerless C.L., Knight P., Mugford R., Cousins T., Noulty R., [2000], "Radiation Environment Measurements from CREAM & CREDO During the Approach to Solar Maximum", IEEE Trans. Nuc. Sci, Vol. 47, No 6, pp 2208-2217, Dec 2000.

Dryer M., [1982], "Coronal transient phenomena", Space Science Reviews, 33, p. 233.

Dryer M., Smart D.F., [1984], "Dynamical models of coronal transients and interplanetary disturbances", Advances in Space Research, 4, p. 291.

Dryer M., [1994], “Interplanetary Studies: Propagation of Disturbances Between the Sun and the Magnetosphere”, Space Science Reviews, 67, p.363.

Duldig M.L. et al., [1993], “The Ground Level Enhancements of 1989SEP29 and 1989OCT22”, Proceedings of the Astronomical Society of Australia, 10, p. 211.

Encyclopedia of Astronomy and Astrophysics (Inst of Physics Publishing, Bristol UK 2004 and <lib.harvard.edu/e-resources/details/e/enastast.html >.

ESA WPP-155, [1999], “Workshop on Space Weather”, 11-13 November 1998, ESTEC, Noordwijk, The Netherlands. Available at: <http://www.estec.esa.nl/wmwww/wma/spweather/workshops/proceedingsw1/proceedings_w1.html>.

ESA WPP-194, [2001], "Space Weather Workshop: Looking Towards a Future European Space Weather Programme”, 17-19 December 2001, ESTEC, Noordwijk, The Netherlands. <http://www.estec.esa.nl/wmwww/wma/spweather/workshops/SPW_W3/PROCEEDINGS_W3/>.

ESA, [2002], “Space Weather Workshop: Space Weather Applications Pilot Project”, 16-18 December 2002, ESTEC, Noordwijk, The Netherlands <http://www.estec.esa.nl/wmwww/wma/spweather/workshops/spw_w4/proceedings.html >

ESA 2004a. <http://www.esa.int/export/esaHS/ESAAYI0VMOC_iss_0.html>

Exradin Co, [2004], www.Exradin.com see also <http://www.standardimaging.com/products/diagnostic/A17_model.html>

Falconer D.A., [2001], “A prospective method for predicting coronal mass ejections from vector magnetograms”, Journal of Geophysical Research, 106, p. 25185.

Feynman J., Spitale G., Wang J., Gabriel S., [1993], “Interplanetary proton fluence model - JPL 1991”, Journal of Geophysical Research, 98, p. 13281.

Feynman J., Martin S.F., [1995], “The initiation of coronal mass ejections by newly emerging magnetic flux”, Journal of Geophysical Research, 100, p. 3355.

Feynman, J., Gabriel, S. B., [2000], “On space weather consequences and predictions”, Journal of Geophysical Research, 105, p.10543.

Feynman J., Gabriel S. eds, [1988], “Interplanetary Particle Environment”, Proceedings of a Conference held in Pasadena, CA, 16-17 Mar. 1987, JPL Publication 88-28, Jet Propulsion Lab., California Inst. of Tech., Pasadena, CA.

Filippov B.P., [1996], “Coronal mass ejections caused by filament eruptions”, Astronomy and Astrophysics, 313, p. 277.

Fry00, R.J.M. Fry, “Radiation Protection: Exposures in Low-Earth Orbit”, Neuroscience & Radiation Biology Working Group, Houston, December 2000.

Fry C.D., Dryer M., Smith Z., Sun W., Deehr C.S., Akasofu S.-I., [2003], “Forecasting solar wind structures and shock arrival times using an ensemble of models”, Journal of Geophysical Research (Space Physics), 108, A2, p.1070.

Furetta C., [2002], “Handbook of Thermoluminescenece”, (World Scientific, Singapore 2002).

Garcia H.A., Greer S. and Viereck R., [1999], “Predicting Solar Energetic Proton Events from Flare Temperatures”, ESA-SP-448, Ninth European Meeting on Solar Physics: Magnetic Fields and Solar Processes, ed. A.Wilson, p. 983.

Gladstone D.J., Chin L.M. and Holmes-Siedle A.G., [1991], “MOSFET Radiation Detectors used as Patient Radiation Dose Monitors during Radiotherapy”, 33rd Ann. Mtg. Amer. Assoc. of Physicists in Medicine, San Francisco, July 21-25 1991, Paper S3,

Glover A., Ranns N.D.R., Harra L.K., Culhane J.L., [2000], “The Onset and Association of CMEs with Sigmoidal Active Regions”, Geophysical Research Letters, 27, p. 2161.

Goldman S.J., [1990], “The legacy of PHOBOS 2”, Sky and Telescope, 79, p. 156.

Golightly M.J. and Weyland M.D., [2002], “SRAG in Wonderland´--Operational Space Weather Support Needs for Manned Spaceflight” ESA Space Weather Workshop: Space Weather Applications Pilot Project, 16-18 December 2002, ESTEC, Noordwijk, The Netherlands.
<http://www.estec.esa.nl/wmwww/wma/spweather/workshops/spw_w4/proceedings/SRAG_in_wonderland.pdf>.

Goli98 M.J. Golightly, “Radiation Protection for ISS Astronauts: Managing Exposures from Space Weather Events”, ESA Workshop on Space Weather, ESTEC, Noordwijk, November 1998.

Gopalswamy N., Kundu M.R., Szabo A., [1987], “Propagation of electrons emitting weak type III bursts in coronal streamers”, Solar Physics, 108, p. 333.

Gopalswamy N., Kundu M.R., [1989], “Radioheliograph and white-light coronagraph studies of a coronal mass ejection event”, Solar Physics, 122, p. 145.

Gopalswamy N. et al., [1998], “On the relationship between coronal mass ejections and magnetic clouds”, Geophysical Research Letters, 25, p. 2485.

Gopalswamy N., Nitta N., Manoharan P.K., Raoult A., Pick M., [1999b], "X-ray and radio manifestations of a solar eruptive event", Astronomy and Astrophysics, 347, p. 684.

Gopalswamy N. et al., [2000], "Radio-rich Solar Eruptive Events", Geophysical Research Letters, 27, p. 1427.

Gopalswamy N., Kaiser M.L., [2002], "Solar eruptions and long wavelength radio bursts: The 1997 May 12 event", Advances in Space Research, 29, p. 307.

Gopalswamy N., [2003], "Coronal mass ejections: Initiation and detection", Advances in Space Research, 31, p. 869.

Gosling J.T., [1990], "Coronal mass ejections and magnetic flux ropes in interplanetary space", Washington DC American Geophysical Union Geophysical Monograph Series, 58, p.343.

Gosling J.T., [1993], "The solar flare myth", Journal of Geophysical Research, 98, p. 18937.

Gosling J.T., [1997], "Coronal Mass Ejections: An Overview" in Coronal Mass Ejections, Geophysical Monograph 99, AGU Washington D.C., Crooker, Joselyn, and Feynman, eds., p.9.

Gurnett D.A., Baumback M.M., Rosenbauer H., [1978], "Stereoscopic direction finding analysis of a type III solar radio burst - Evidence for emission at $2f_p$", Journal of Geophysical Research, 83, p. 616.

Hajdas W., P. Bühler, C. Eggel, P. Favre, A. Mchedlishvili, A. Zehnder, [2003], "Radiation environment along the INTEGRAL orbit measured with the IREM monitor", Astron. Astrophys. 411, L43-L47

Hakamada K., Akasofu S.-I., [1982], "Simulation of Three-Dimensional Solar Wind Disturbances and Resulting Geomagnetic Storms", Space Science Reviews, 31, p. 3.

Hanslmeier A., [2002] , "The Sun and Space Weather", Kluwer, Dordrecht.

Hanslmeier A., [2003], "Space weather effects on manned missions", Hvar. Obs. Bull. 1, 159-70.

Heinrich W., Becker E., Leugner D., Sommer O., Roecher H., Streibel T., Huentrup G., and Reitz G., [1997] "Analysis of CR-39 detectors flown in the EUROMIR 95 mission, the MIR97 mission and different STS missions",
<http://www.puk.ac.za/fskdocs/icrc97/srdw.html>

Heras A.M., Sanahuja B., Domingo V., Joselyn J.A., [1988], "Low-energy particle events generated by solar disappearing filaments", Astronomy and Astrophysics, 197, p. 297.

Heras A.M., Sanahuja B., Lario D., Smith Z.K., Detman T., Dryer M., [1995], "Three low-energy particle events: Modeling the influence of the parent interplanetary shock", Astrophysical Journal, 445, p. 497.

Hinteregger H.E., Fukui K., Gilson B.R., [1981], "Observational, reference and model data on solar EUV, from measurement on AE-E", Geophys. Res. Lett., 8, No. 11, 1147-1150.

HMM2004, "CDF study report - Human Missions to Mars (HMM)", ESTEC CDF20(A), March 2004.

Hoffman S.J. and Kaplan D.L., [1997], "Mars Reference Mission", NASA Special Publication TN 6107 (JSC, TX 1997), [cited in Bent01 ref. 58].

Holmes-Siedle A.G., [1974], "The Space Charge Dosimeter - General Principles of a New Method of Radiation Dosimetry", Nuclear Instruments and Methods, 121, 169-172.

Holmes-Siedle A.G. and Adams L., [1986], "RADFETs: A review of the use of metal-oxide-silicon devices as integrating dosimeters", International Journal of Radiation Physics and Chemistry, 28, (2), 235-244.

Holmes-Siedle A.G., Ward A.K., Bull R., Blower N. and Adams L., [1990], "The METEOSAT - 3 dosimeter experiment: observation of radiation surges during solar flares in geostationary orbit", Proc. ESA Workshop on Space Environment Analysis, October 9-12, 1990, Noordwijk, Paper S4, ESA Report No. WPP-23.

Holmes-Siedle A.G., [1994], "From space to therapy, the radiation sensitive silicon FET (RADFET)", Workshop Proceedings of Technology Transfer, held at ESA/ESTEC, Noordwijk, The Netherlands 25-27 May (1994), ESA SP-364, August 1994.

Holmes-Siedle A.G. and Groombridge I., [1975], "Hole Traps in Silicon Dioxide: A Comparison of Population by X-Rays and Band-Gap Light", Thins Solid Films 27 165 – 170.

Holmes-Siedle A.G. and Watts S.J., [1997], "Radiation effects in space, nuclear power and accelerators: impact on optics and light sensors", Invited paper, SPIE Conference, San Diego, CA, 27 July - 1 August 1997, San Diego, CA. Published in: Critical Reviews of Optical Science and Technology, CR 66-02, pp 37-57.

Holmes-Siedle A.G , Watts S.J. and Holland A. [1995], "Radiation evaluation of X-ray sensitive charge coupled devices (CCDs) for the XMM telescope", Final Report, ESA Contract 8815/90/NL, Brunel Report No. BRUCRD-ESACCD-95-1R (Brunel University, Uxbridge, England 20 October 1995) see also "The impact of space protons on X-ray sensing with CCDs". IEEE T-NS-43 (6) 2998-3004 (Dec 1996). ISBN 1-872-166-14-8.

Holmes-Siedle A. and Adams L., [2002], "Handbook of Radiation Effects" (2nd Edition, Oxford \University Press, 2002). Note that Appendix D is a bibliography of dosimeter research and Appendix G, Websites, gives space radiation effects links.

Hudson H.S., Webb D.H., [1997], "Soft X-Ray Signatures of Coronal Ejections" in Coronal Mass Ejections, Geophysical Monograph 99, AGU Washington D.C., Crooker, Joselyn, and Feynman, eds., p. 27.

Hudson H.S., Lemen J.R., St. Cyr O.C., Sterling A.C., Webb D.F., [1998], "X ray coronal changes during halo CMEs", Geophysical Research Letters, 25, p. 2481.

HUME99, "HUMEX – Study on the Survivability and Adaptation of Humans to Long-Duration Interplanetary and Planetary Environments", TN-2, ESTEC/Contract No. 14056/99/NL/PA, Noordwijk, 1992.

Hundhausen A., [1999], "Coronal Mass Ejections", The many faces of the sun: a summary of the results from NASA's Solar Maximum Mission. Edited by K. T. Strong, J. L. R. Saba, B. M. Haisch, and J. T. Schmelz, New York: Springer, p.143.

IFE, [2004], <http://www.ife.no/english/>

INFN, [2004], M.G. Pia and S. Guatelli, Technical Note 2 of REMSIM project. INFN Internal Report and "Title", to be published in proceedings of IEEE-NSS, Roma 2004.

ISU-International Space University, Summer Session Program, [1998], "Hazards to Spaceflight".

Jackson B.V., Sheridan K.V., Dulk G.A., McLean D.J., [1978], "A possible association of solar type III bursts and white light transients", Proceedings of the Astronomical Society of Australia, 3, p. 241.

Jokipii J.R., [1966], "Cosmic-Ray Propagation. I. Charged Particles in a Random Magnetic Field", Astrophysical Journal, 146, p.480.

Kahler S.W., [1994], "Injection profiles of solar energetic particles as functions of coronal mass ejection heights", Astrophysical Journal, 428, p. 837.

Kahler S.W., [2001], "Origin and properties of solar energetic particles in space", in "Space Weather", Song et al. ed., AGU Monograph 125, p. 109.

Kahler S.W., Sheeley N.R., Howard R.A., Michels D.J., Koomen M.J., McGuire R.E., von Rosenvinge T.T., Reames D.V., [1984], "Associations between coronal mass ejections and solar energetic proton events", Journal of Geophysical Research, 89, p. 9683.

Kahler S.W., Cliver E.W., Cane H.V., McGuire R.E., Reames D.V., Sheeley N.R., Howard R.A., [1987], "Solar energetic proton events and coronal mass ejections near solar minimum", 20th Int. Cosmic Ray Conf. 3, p. 121.

Kahler S.W., Burkepile J.T., Reames D.V., [1999], "Coronal/Interplanetary factors contributing to the intensities of E>20 MeV gradual SEP events", 26th Int. Cosmic Ray Conf., 6, p. 248.

King, J. H., [1974], "Solar Proton Fluences for 1977-1983 Space Missions", Journal of Spacecraft and Rockets, 11, p. 401.

Knight A.W., [2004], personal communication, see also
<http://www.gentronix.co.uk/keypapers.html>

Knoll G.F., [1989], "Radiation Detection and Measurement", 2nd ed Wiley, NY

Kotteman M., Kish A., Iloanusi C. and DiRuggiero J., [2004], Desiccation and gamma irradiation repair in the halophilic archaeon Halobacterium NRC1, in preparation as of Aug 2004, <http://life.umd.edu/cbmg/faculty/diruggiero/lab/pubs/>

Kronenberg S., [1968], "Tactical radiation dosimetry in the U.S. Army", Health Phys 14:41-44, 1968.

Kunches J.M., Heckman G.R., Hildner E., Suess S.T., [1991], "Solar Radiation Forecasting and Research to Support the Space Exploration Initiative", Space Environment Laboratory Special Report, 26 pp.

Lario D., Sanahuja B., Heras A.M., [1998], "Energetic Particle Events: Efficiency of Interplanetary Shocks as 50 keV < E < 100 MeV Proton Accelerators", Astrophysical Journal, 509, p. 415.

Lario D., Vandas M., Sanahuja B., [1999], "Energetic Particle Propagation in the Downstream Region of Transient Interplanetary Shocks", in "Solar Wind Nine", Habbal, S. R., et al. eds., American Institute of Physics Conference Series, 471, p. 741.

Lean J., [1987], "Solar ultraviolet irradiance variations: A review", J. Geophys. Res., 92, 839-868.

Lean J., [1991], Variations in the Sun's radiative output, Rev. Geophys., 29, 505-535.

Lee M.A., [1997], "Particle Acceleration and Transport at CME-Driven Shocks" in Coronal Mass Ejections, Geophysical Monograph 99, AGU Washington D.C., Crooker, Joselyn, and Feynman, eds., p. 227.

Lengyel-Frey D., Stone R.G., [1989], "Characteristics of interplanetary type II radio emission and the relationship to shock and plasma properties", Journal of Geophysical Research, 94, p. 159.

Lepping R.P., Chao J.K., [1976], "A shock surface geometry - The February 15-16, 1967, event", Journal of Geophysical Research, 81, p. 60.

Lindsey C., Braun D.C., [2000], "Basic Principles of Solar Acoustic Holography - (Invited Review)", Solar Physics, 192, p. 261.

Low B.C., Smith D.F., [1993], "The free energies of partially open coronal magnetic fields", Astrophysical Journal, 410, p. 412.

Low B.C., Hundhausen J.R., [1995], "Magnetostatic structures of the solar corona. 2: The magnetic topology of quiescent prominences", Astrophysical Journal, 443, p. 818.

Luhmann J.G., Gosling J.T., Hoeksema J.T., Zhao X., [1998], "The relationship between large-scale solar magnetic field evolution and coronal mass ejections", Journal of Geophysical Research, 103, p. 6585.

Ma T-P. and Dressendorfer P.V. (eds) [1989], "Ionizing Radiation Effects in MOS Devices and Circuits", John Wiley and Sons, New York.

MacKay G.F., Thomson I., Ng A. and Sultan N., [1997], "Applications of MOSFET Dosimeters on MIR and BION Satellite", IEEE Transactions on Nuclear Science, NS-44, 2048 - 51.

Madhvanath U., [1976], "Lymphocyte as a biological dosimeter: a different approach", Health Phys, 1976 Mar, 30(3):296-9.

Maia D., Pick M., Vourlidas A., Howard R., [2000], "Development of Coronal Mass Ejections: Radio Shock Signatures", Astrophysical Journal, 528, p. L49.

Mann G., Jansen F., MacDowall R.J., Kaiser M.L., Stone R.G., [1999], "A heliospheric density model and type III radio bursts", Astronomy and Astrophysics, 348, p. 614.

McAllister A.H., Dryer M., McIntosh P., Singer H., Weiss L., [1996], "A large polar crown coronal mass ejection and a "problem" geomagnetic storm: April 14-23, 1994", Journal of Geophysical Research, 101, p. 13497.

McAllister A.H., Martin S.F., Crooker N.U., Lepping R.P., Fitzenreiter R.J., [2001], "A test of real-time prediction of magnetic cloud topology and geomagnetic storm occurrence from solar signatures", Journal of Geophysical Research, 106, p. 29185.

McIntosh P.S., [1990], "The classification of sunspot groups", Solar Physics, 125, p. 251.

McKeever S.W.S., Moscovitch M. and Townsend P.D., [1995], "Thermoluminescence Dosimetry Materials: Properties and Uses" (Nuclear Technology Publishing, Ashford England 1995)

McKenna-Lawlor S., Afonin V.V., Kirsch E., Schwingenschuh K., Slavin J.A., Trotignon J.G., [1998], "An overview of energetic particles (from 55keV to > 30 MeV) recorded in the close Martian environment, and their energization in local and external processes", Planetary and Space Science, 46, p. 83.

Müller-Mellin R. et al., [1995], "COSTEP - Comprehensive Suprathermal and Energetic Particle Analyzer", Solar Physics 162, 483-504, 1995.

National Research Council, Space Studies Board, [2000], "Radiation and the International Space Station: Recommendations to Reduce Risk", Washington, DC: National Academy Press.
<http://www.nap.edu/catalog/9725.html>.

NAS00, "Space Science in the Twenty-First Century: Human Biology and Space Medicine" National Academy of Sciences, SSB, October 2000.

NAS02, "Safe on Mars: Precursor Measurements Necessary to Support Human Operations on the Martian Suface" National Academy of Sciences, SSB, 2002.

NASA98, "Strategic Program Plan For Space Radiation Health Research", NASA Publication, October 1998.

NASA02, "Understanding Space Radiation", NASA FS-2002-10-080-JSC, October 2002.

NASA03, "Bioastronautics Critical Path Roadmap – Baseline Document", NASA, July 2003.

NASA 2004a, "Deep Space Test Bed",
<http://sd.msfc.nasa.gov/cosmicray/DSTB/DSTB.htm>

NASA 2004b, "NASA's TRACE satellite ", <http://sunland.gsfc.nasa.gov/smex/trace/>

HASA 2004c., "Computer-Aided Design - IDEA method",
<http://web547.gsfc.nasa.gov/amb>

NCRP89, "Guidance on Radiation Received in Space Activities", NCRP Report No. 98, July 1989.

NCRP90, "The Relative Biological Effectiveness of Radiations of Different Quality", NCRP Report No. 104, 1990.

NCRP93, “Limitation of Exposure to Ionizing Radiation”, NCRP Report No. 116, 1993.

NCRP97, “Uncertainties in Fatal Cancer Risk Estimates Used in Radiation Protection”, NCRP Report No. 126, 1997.

NCRP00, “Radiation Protection Guidance for Activities in Low-Earth Orbit”, NCRP Report No. 132, 2000.

NCRP01a, “Evaluation of the Linear-Nonthreshold Dose-Response Model for Ionizing Radiation”, NCRP Report No. 136, 2001.

NCRP01b, “Fluence-Based and Microdosimetric Event-Based Methods for Radiation Protection in Space”, NCRP Report No. 137, August 2001.

NCRP02, “Operational Radiation Safety Program for Astronauts in Low-Earth Orbit: A Basic Framework”, NCRP Report No. 142, November 2002.

Ng C.K., Reames D.V., [1994], “Focused interplanetary transport of approximately 1 MeV solar energetic protons through self-generated Alfven waves”, Astrophysical Journal, 424, p. 1032.

Odstrcil D., Pizzo V.J., [1999a], “Three-dimensional propagation of CMEs in a structured solar wind flow: 1. CME launched within the streamer belt”, Journal of Geophysical Research, 104, p. 483.

Odstrcil D., Pizzo V.J., [1999b], “Three-dimensional propagation of coronal mass ejections in a structured solar wind flow 2. CME launched adjacent to the streamer belt”, Journal of Geophysical Research, 104, p.493.

Oldham T.R., [2000], “Ionizing radiation effects in MOS oxides”, World Scientific Publishing Co., USA, 2000, ISBN 9 810 23326.

Petr02, V.M. Petrov, V.V. Benghin, V.A. Shurshakov, I.V. Chernykh, A.V. Markov, V.I. Lyagushin, A.N. Volkov, A.P. Aleksandrin, Y.L. Germantsev, M.I. Panasyuk, G.Y. Kolesov, M.V. Tel'tsov, Y.V. Kutuzov, O.V. Morozov, “Characteristics of radiation environment onboard the Russian segment of the ISS measured by the radiation monitoring system”, August 2002.

Pick M., Lathuillere C., Lilensten J., Obs. Paris-Meudon, LPG, Alcatel-LPCE Consortium, [2001], “Ground Based Measurements”, Report for ESA Space Weather Programme Feasibility Studies, available at <http://www.estec.esa.nl/wmwww/WMA/spweather/esa_initiatives/spweatherstudies/ALC/WP3120GroundSegmentNov01.pdf>.

Poch W.J. and Holmes-Siedle A.G., [1969], "Long-term effects of radiation in complementary MOS logic networks". IEEE Transactions on Nuclear Science NS-17, 33-40.

RADVIS, [2004] <http://www.external.hrp.no/vr/products/radvis/info/index.html>

Ray K.P., Mullen E.G., Stapor W.J. and Circle R.R., [1992], "CRRES dosimetry results and comparisons using the space radiation dosimeter and p-channel MOS dosimeters", IEEE Transactions on Nuclear Science. 39 (6) 1846-50.

Reames D.V., [1997a], "Energetic particles and the structure of coronal mass ejections" in Coronal Mass Ejections, Geophysical Monograph 99, AGU Washington D.C., Crooker, Joselyn, and Feynman, eds., p. 217.

Reames D.V., [1997b], "Solar Energetic Particles: Is There Time to Hide?" Workshop on the Impact of Solar Energetic Particle Events for Design of Human Missions, Houston TX, Sept. 9-11, 1997.

Reames D.V., Kahler S.W., Ng C.K., [1997], "Spatial and Temporal Invariance in the Spectra of Energetic Particles in Gradual Solar Events", Astrophysical Journal, 491, p. 414.

Reames D.V., Ng C.K., [1998], "Streaming-limited Intensities of Solar Energetic Particles", Astrophysical Journal, 504, p. 1002.

Reames D.V., [1999a], "Solar Energetic Particles: Is There Time to Hide?", Radiation Measurements 30/3, p. 297.

Reames D.V., [1999b], "Particle acceleration at the Sun and in the heliosphere", Space Science Reviews, 90, p. 413.

Reiner M.J., Fainberg J., Kaiser M.L., Stone R.G., [1998], "Type III radio source located by Ulysses/Wind triangulation", Journal of Geophysical Research, 103, p. 1923.

Reiner M.J., Kaiser M.L., [1999], "High-frequency type II radio emissions associated with shocks driven by coronal mass ejections", Journal of Geophysical Research, 104, p. 16979.

Reiner M.J., Kaiser M.L., Bougeret J.-L., [2001], "Radio signatures of the origin and propagation of coronal mass ejections through the solar corona and interplanetary medium", Journal of Geophysical Research, 106, p. 29989.

Reiner M.J., [2003], "Radio signatures of solar energetic particle acceleration", Solar variability as an input to the Earth's environment International Solar Cycle Studies (ISCS) Symposium, Ed.: A. Wilson. ESA SP-535, Noordwijk: ESA Publications Division, p. 841.

Reit98, G. Reitz, "Biological effects of space radiation", ESA Workshop on Space Weather, ESTEC, Noordwijk, WPP-155, November 1998.

Reit00, G. Reitz, "European Dosimetry Activities for the ISS", 11th Annual NASA Space Radiation Health Investigators' Workshop, Arona, May 2000, Physica Medica - Vol. XVII, Suppl. 1, 2001.

Reitz G., Beaujean R., Benton E., Burmeister S., Dachev T.S., Deme S., Luszik-Bhadra M. and Olko P., [2002], "Space radiatuion measurement onboard ISS – the DOSMAP experiment" Insstituto Tecnologico e Nuclear, Portugal. <http://www.itn.mces.pt/ICRS-RPS/oralpdf/> Thursday13/ Session15_1/reitz02.pdf see also <http://www.dlr.de>.

REM 2004a, [2004], REMSIM technical contributions (REM Oxford, England 2004).

REM 1994, [1994], "From space to therapy, the radiation sensitive silicon FET (RADFET)", Workshop Proceedings of Technology Transfer, held at ESA/ESTEC, Noordwijk, The Netherlands 25-27 May (1994), ESA SP-364, August 1994.

REMSIM 2004a, [2004], C. Lobascio for the REMSIM collaboration. "REMSIM Final Report", Report No. ALS-RMS-VRP-0002. (Alenia, Torino, Italy, December 2004)

REMSIM 2004b, S. Eckersley for the REMSIM collaboration "The ESA REMSIM Study; Radiation Exposure and Mission Strategies for Interplanetary Manned Missions to the Moon and Mars", Team : Cesare Lobascio(1), Vincenzo Guarnieri(1), Paola Parodi(1) Maria Antonietta Perino(1), Steven Eckersley(2), Stephen Kemble(2), Claude Cougnet(3), Gianni Parisi(4) Vittorio Tamburini(4), Maria Grazia-Pia(5), Susanna Guatelli(5), Piero Spillantini(6), Claire Foullon(7), Norma Bock Crosby(7), Daniel Heynderickx(7), Andrew Holmes-Siedle(8), Petteri Nieminen(9). - POSTER, Royal Astronomical Society, London, Dec 10th 2004. "The Scientific Case for Human Space Exploration" to be published in Earth, Sky and Telescope.

Robbins M.S., Roy T., Hedges S.J., Holmes-Siedle A.G., McKemey A.K.and Watts S.J., [1993], "Quality control and monitoring of radiation damage in charge-coupled devices at the Stanford linear collider", IEEE Trans. Nucl. Sci., NS-40 (6), 1561-8.

Roelof E.C., [1969], "Propagation of solar cosmic rays in the interplanetary magnetic field", in "Lectures in High Energy Astrophysics", Ögelman, H., Wayland, J. R., eds., NASA Spec. Publ., SP-199, p. 111.

Rottman G.J., [1987], "Results from space measurements of solar UV and EUV flux, in Proceedings of a workshop on Solar Radiative Output Variation", ed. P. Foukal, p. 71-86, Cambridge Research and Instrumentation, Inc..

Ruffolo D., [1995], “Effect of adiabatic deceleration on the focused transport of solar cosmic rays”, Astrophysical Journal, 442, p. 861.

Rust D.M., Kumar A., [1996], “Evidence for Helically Kinked Magnetic Flux Ropes in Solar Eruptions”, Astrophysical Journal, 464, p. L199.

Rx/Tec, [2004], G. Parisi and V. Tamburini, “REMSIM Technical Report No. TN-1”, (Rx/Tec, Genova, Italy, December 2004).

Saganti P.B., Cucinotta F.A., Wilson J.W., Simonsen L.C., Zeitlin C. , [2004], “Radiation climate map for analyzing risks to astronauts on the mars surface from galactic cosmic rays”.
Available at: <http://marie.jsc.nasa.gov/Documents/RadiationClimateMap.pdf>.

Schi02, W. Schimmerling, F.A. Cucinotta, “Lighting FIRES – Full Interplanetary Radiation Environment Simulation”, Workshop on Radiation Monitoring on the ISS, September 2002, Paris, France.

Schi03, W. Schimmerling, “Overview of NASA’s Space Radiation Research Program”, Gravitational and Space Biology Bulletin 16 (2), June 2003.

Shea M.A. et al., [1988], “Toward a descriptive model of solar particles in the heliosphere”, Interplanetary Particle Environment, JPL Publication 88-28, p. 3.

Shea M.A., Smart D.F., [2002], “Solar proton event patterns: the rising portion of five solar cycles”, Advances in Space Research, 29, p. 325.

Sheeley N.R., Howard R.A., Michels D.J., Koomen M.J., Schwenn R., Muehlhaeuser K.H., Rosenbauer H., [1985], “Coronal mass ejections and interplanetary shocks”, Journal of Geophysical Research, 90, p. 163.

Saganti P.B., Cucinotta F.A., Wilson J.W., [2004], Simonsen L.C.; Zeitlin C., “Radiation climate map for analyzing risks to astronauts on the mars surface from galactic cosmic rays”, Space Science Reviews, vol. 110, no. 1-2, pp. 143-156(14) Kluwer Academic Publishers.

Schoner W. et al, WRMISS, [1998], see <http://www.magnet.oma.be>

SICS89, “Space Radiation Health Hazards: Assessing and Mitigating the Risks”, SICSA Outreach Vol. 2, No. 3, Houston, September 1989.

Smart D.F., [1988], “Predicting the arrival times of solar particles”, Interplanetary Particle Environment, JPL Publication 88-28, p. 101.

Smart D.F., Shea M.A., [2003], “Comment on estimating the solar proton environment that may affect Mars missions”, Advances in Space Research, 31, p. 45.

Smith Z., Dryer M., [1990], "MHD study of temporal and spatial evolution of simulated interplanetary shocks in the ecliptic plane within 1 AU", Solar Physics, 129, p. 387.

Smith Z.K., Dryer M., Armstrong M., [1994], "Can Soft X-Rays Be Used as a Proxy for Total Energy Injected by a Flare into the Interplanetary Medium?", IAU Colloq. 144: Solar Coronal Structures (V. Rusin, P. Heinsel, and J.-C. Vial, Eds), Kluwer Acad. Publ., Dordrecht, p. 267.

Smith Z.K., Dryer M., [1995], "The Interplanetary Shock Propagation Model: A model for predicting solar-flare-caused geomagnetic sudden impulses based on the 2-1/2D MHD numerical simulation results from the Interplanetary Global Model (2D IGM)", NOAA Technical Memorandum, ERL/SEL - 89.

Smith Z., Murtagh W., Detman T., Dryer M., Fry C.D., Wu C.-C., [2003], "Study of solar-based inputs into space weather models that predict interplanetary shock-arrivals at Earth", Solar variability as an input to the Earth's environment International Solar Cycle Studies (ISCS) Symposium, Ed.: A. Wilson. ESA SP-535, Noordwijk: ESA Publications Division, p. 547.

Soubra M., Cygler J., Mackay G., Thomson I. and Ribes A., [1994], "Evaluation of a dual bias dual metal oxide silicon semiconductor field effect transistor detector as radiation dosimeter", Med. Phys., 21, 567-72 (a competitor).

SREM, [2004], "ESA Standard Radiation Environment Monitor", <http://srem.web.psi.ch/html/srem_home.shtml>

SRHP93, "Radiation Protection Administration: Legal Requirements", SRHP, ≥1993.
SREM, [2004], <http://srem.web.psi.ch/html/srem_home.shtml>

Stassinopoulos E.G., [1975], "SOLPRO: A computer code to calculate probabilistic energetic solar proton fluences", NASA STI/Recon Technical Report 75-11, Greenbelt, Maryland, p. 23451.

Stewart R.T., [1985], "Moving Type IV bursts", in Radio Physics of the Sun, Ed. D. J. McLean and N. R. Labrum, Cambridge University Press, p. 361.

Strizzi J.D., Kutrieb J.M., Damphousse P.E., Carrico J.P., [2001], "Sun-Mars libration points and Mars mission simulations", Space Flight Mechanics, D'Amario L.A., et al. eds., Advances in the Astronautical Sciences 108, p. 807.

Sturrock P.A., [1989], "The role of eruption in solar flares", Solar Physics, 121, p. 387.

Sun W., Akasofu S.-I., Smith Z.K., Dryer M., [1985], "Calibration of the kinematic method of studying solar wind disturbances on the basis of a one-dimensional MHD

solution and a simulation study of the heliosphere disturbances between 22 November and 6 December 1977", Planetary and Space Science, 33, p. 933.

Szabo A., [2003], "Living with a Star Sentinels" LWS Management Operations Working Group (MOWG), June 2003. Available at:
<http://lws.gsfc.nasa.gov/docs/MOWG06_03/Sentinels.pdf>.

Thompson B. J. et al., [1999], "SOHO/EIT Observations of the 1997 April 7 Coronal Transient: Possible Evidence of Coronal Moreton Waves", Astrophysical Journal, 517, p. L151.

Tobiska W.K, [2000], "Status of the SOLAR2000 solar irradiance model", Phys. Chem. Earth, 25, No. 5-6, 383-386.

Tylka A.J., [2001], "New insights on solar energetic particles from Wind and ACE", Journal of Geophysical Research, 106, p. 25333.

Uchihori, [2004], Y. Uchihori, K. Fujikata, N. Yasuda and E.R. Benton (2004), "Comparison of r4esults from the ICCHIBAN-3 experiment and current status of the ICCHIBAN-5 experiment", (on behlalf of the ICCHIBAN Working Group). (WRMISS, Vienna, Sept 8-10 2004).

UTU 2004. <http://www.srl.utu.fi/projects/erne/led_english.html>

Vilmer N., [1999], "Solar activity: flares; CMEs; SEPs; solar wind", in "Workshop on Space Weather", 11-13 November 1998 ESTEC, Noordwijk, The Netherlands, ESA WPP-155, p. 73. Available at:
<http://www.estec.esa.nl/wmwww/wma/spweather/workshops/proceedings_w1/SESSION2/vilmer_solar.pdf>.

Wang Y.-M., Sheeley N.R., [1990], "Solar wind speed and coronal flux-tube expansion", Astrophysical Journal, 355, p. 726.

Wils93, J.W. Wilson, F.A. Cucinotta, J.L.Shinn, "Cell kinetics and track structure. Biological Effects and Physics of Solar and Galactic Cosmic Radiation", C.E. Swenberg, G. Horneck and E.G. Stassinopoulos Eds. Part A. New York. Plenum Press 1993; 295-338.

Wils97a, J.W. Wilson, J.L. Shinn, L.C. Simonsen, F.A. Cucinotta, R.R. Dubey, W.R. Jordan, T.D. Jones, C.K. Chang, M.Y. King, "Exposures to Solar Particle Events in Deep Space Missions", NASA Technical Paper 3668, October 1997.

Wils97b, J.W. Wilson, J. Miller, A. Konradi, F. A. Cucinotta, "Shielding Strategies for Human Space Exploration", NASA Conference Publication 3360, December 1997.

Wils97c, J.W. Wilson, F.A. Cucinotta, H. Tai, L.C. Simonsen, J.L. Shinn, S.A. Thibeault, M.Y. Kim, "Galactic and Solar Cosmic Ray Shielding in Deep Space", NASA Technical Paper 3682, December 1997.

Wils00, J.W. Wilson, F.A. Cucinotta, M.Y. Kim, W. Schimmerling, "Optimized Shielding for Space Radiation Protection", 11th Annual NASA Space Radiation Health Investigators' Workshop, Arona, May 2000, Physica Medica - Vol. XVII, Suppl. 1, 2001.

Wu S.T., Dryer M., Han S.M., [1983], "Non-planar MHD model for solar flare-generated disturbances in the heliospheric equatorial plane", Solar Physics, 84, p. 395.

Wu S.T., Guo W.P., Plunkett S.P., Schmieder B., Simnett G.M., [2000], "Coronal mass ejections (CMEs) initiation: models and observations", Journal of Atmospheric and Terrestrial Physics, 62, p. 1489.

Zeitlin C. et al., [2003], "Results from MARIE", Eighth WRMISS Workshop, available at <http://www.magnet.oma.be/wrmiss/workshops/eighth/zeitlin.pdf>.

Xapsos M.A., Summers G.P., Barth J.L., Stassinopoulos E.G., Burke E.A., [1999], "Probabillity Model for Worst Case Solar Proton Event Fluences", IEEE Trans. Nucl. Sci., 46, p. 1481.

Xapsos M.A., Summers G.P., Barth J.L., Stassinopoulos E.G., Burke E.A., [2000], "Probabillity Model for Cumulative Solar Proton Event Fluences", IEEE Trans. Nucl. Sci., 47, p. 486.

Williams J.R. and Thwaites D.I., [1993], Radiotherapy Physics (1st Edition. Oxford University Press, New York).

Wolf, R. A., Fuller-Rowell, T. J. [1999] "Study of metrics for the National Space Weather Program".

Workshops on Radiation Monitoring for the International Space Station (WRMISS), available at:
<http://www.magnet.oma.be/wrmiss/workshops/workshops.html>.

Zeit03, C. Zeitlin, T. Cleghorn, F. Cucinotta, P. Saganti, V. Andersen, K. Lee, L. Pinsky, W. Atwell, R. Turner, "One Year of Results from the Martian Radiation Environment Experiment", 14th Annual Space Radiation Health Investigators' Workshop, League City, Texas, April 2003.

LIST OF ACRONYMS

ACE	Advanced Composition Explorer
BBND	Bonner Ball Neutron Detector
BBSO	Big Bear Solar Observatory
BFO	Blood Forming Organ
CCD	Charged Coupled Device
CEASE	Compact Environmental Anomaly Sensor
CELIAS	Charge, Element, Isotope Analysis System
CIR	Co-Rotating Interacting Region
CISM	Center for Integrated Space Weather Modeling
CCMC	Community Coordinated Modeling Center
CME	Coronal Mass Ejection
CPDS	Charged Particle Directional Spectrometer
DOSMAP	Dosimetric Mapping
ESA	European Space Agency
ESF	European Science Foundation
ESP	Emission of Solar Protons total fluence
EVA	Extra Vehicular Activity
GNSS	Global Navigation Satellites Systems
GPS	Global Positioning System
GTO	Geostationary Transfer Orbit
ISES	International Space Environment Service
IGC	International Geophysical Calendar
ISS	International Space Station
LASCO	Large Angle and Spectrometric Coronagraph
LEO	Low Earth Orbit
LET	Linear Energy Transfer
MARIE	Martian Radiation Environment Experiment
MCA	Multi-Channel Analyzer
MCC	Mission Control Centre
MDI	Michelson-Doppler Imager
MEO	Medium Earth Orbit
MHD	MagnetoHydroDynamic
MOS	Metal-Oxide-Semiconductor
MTOF	Mass Time-of-Flight spectrometer
NOAA	National Oceanic and Atmospheric Administration
NSF	National Science Foundation
NTD	Nuclear Track Detectors
RADFET	Radiation-Sensitive Field-Effect Transistor
RHESSI	Reuven Ramaty High Energy Solar Spectroscopic Imager
RWC	Regional Warning Centre
SEC	Space Environment Centre
SI	Sudden Impulse
SIDC	Solar Influences Data analysis Center
SPE	Solar Proton Event
SOHO	Solar and Heliospheric Observatory
SRAG	Space and Radiation Analysis Group
SSC	Sudden Storm Commencement

SSO	Sun Synchronous Orbit
STC	Science and Technology Center
SWAN	Solar Wind Anisotropies
SWO	Space Weather Operations
SXT	Soft X-ray Telescope
TEPC	Tissue Equivalent Proportional Counter
TLD	Thermo-Luminescent Dosimeter

LIST OF FIGURES

CHAPTER 1

CHAPTER 2

15. Chart of additional skin exposure (mrad/mrem). Courtesy of Golightly and Weyland (2002).
16. The total X-ray flux time profiles provided by the GOES spacecraft.
17. Wind/WAVES radio spectrogram of the CME/magnetic cloud event of 6-10 January 1997. After it was launched from the Sun in the direction of Earth, the CME of January 6 was quickly lost from view because it became too diffuse to be seen by the LASCO telescope. Thus for its long journey of 1AU to Earth, the CME would have been completely out of sight except for the remote sensing capability of the WAVES instrument on the WIND spacecraft. The cartoons above the spectrogram illustrate the derived location of the shock at three times during its traverse from the Sun to Earth. From <http://www-istp.gsfc.nasa.gov/istp/cloud_jan97/waves_cme.html> , courtesy of M. Kaiser.
18. Solar proton episodes (at different energies) as a function of sunspot number. Image courtesy of Ron Turner of ANSER and Robert C. Reedy of Los Alamos National Laboratory.

CHAPTER 4

19. At conjunction of Mars and Earth, Mars becomes invisible in the Sun's rays. Best observation period is from quadrature to quadrature (Glasstone, 1968).
20. Distances (km) Sun-Earth, Sun-Mars and Earth-Mars. The graphs were generated with data obtained from the Planetary Data System Mars Ephemeris Generator 2.1, available at:<http://ringmaster.arc.nasa.gov/tools/ephem2_mar.html>.
21. Heliocentric Mars-Earth angle. Same source as in Figure 20.
22. "Impulsive" solar particle events. (a) is connected to W67, V_{SW}=350 km/s; (b) is connected to W51, V_{SW}=450 km/s; (c) is connected to W42, V_{SW}=550 km/s. In case (2), Mars is lagging by 20° behind Earth as in November 2003. For the well-connected field line (b), the event is seen both at Earth and Mars. For conditions (a) and (c), the event is seen at Earth, but not at Mars. After Turner (2003), with a different perspective.
23. "Gradual" solar particle events. Different temporal signatures are observed depending on Mars orbital position, from where the IP shock accelerated particles are associated with (a) a western CME, (b) a halo CME or (c) an Eastern CME (Turner, 2003).

CHAPTER 5

24. "International Living With a Star" missions.
25. This graphic shows the radiation dose equivalent as measured by MARIE at Mars and by instruments aboard the International Space Station, for the 11-month period from April 2002 through February 2003. Image Credit: NASA/JPL/JSC.
    Source: <http://photojournal.jpl.nasa.gov/targetFamily/Mars>.
26. SECCHI scientific goals.
27. 3D view of triangulation of a type III burst observed by Ulysses and Wind. Type III source at each frequency is intersection of line of sight from each s/c. Type III source lies along Parker spiral south of ecliptic plane (Reiner et al., 1998).
    Source: <http://www-lep.gsfc.nasa.gov/swaves/swavesf3.jpg>.
28. Geocentric Solar Ecliptic Coordinates - Fixed Earth-Sun Line (Ecliptic Plane Projection) Launch: Nov. 15 – Nov. 28, 2005 (UTC) - First lunar swingby (Behind escapes) S1: Jan.

9, 2006 – Second lunar swingby (Ahead escapes) S2: Feb. 15, 2006 - 2 year mission (Driesman et al., 2003).

29. Ecliptic plane projection showing the relative positions of Mars and the STEREO-Earth L1 system for four different epochs: A) STEREO lunar escapes, Mars is within 90° of heliolongitude behind the trailing STEREO spacecraft; B) Mars enters the far side from the STEREO system for about 8 months; C) Mars is within 90° of heliolongitude ahead of the leading STEREO spacecraft; D) Mars enters the zone covered by the STEREO-Earth L1 system.

CHAPTER 6

30. Manned mission to Mars. Likely readings on monitors of (a) dose rates and (b) total dose values ("dosimeters") as a function of mission position and time in hours. Features shown are the Galactic Cosmic-Ray (GCR) "background", modulated by distance and planetary attenuation; dose-rate surges due to solar-proton events [symbol *]; minor peaks due to transit of the Earth's trapped radiation regions. Two values of dose rate are given for the GCR level. These are nominal values representing a well-shielded location (B) and one which is less well shielded (A). Future studies will have to consider the movement of crew between extremes like these.
31. Dose rates to the BFO with 1 g/cm^2 Al shielding during the SPE of August 1972 [Wils97c].
32. Simplified time-profile of a solar flare, based on Figure xx, modified to represent the dose rate to a crew member's blood-forming organs (BFO) given as a 5 gm/cm² Al compartment wall, a situation similar to that used in the REMSIM modelling of vehicle structure and radiation warning systems.
33. Simulated traces of dosimeters at selected points A to E on a Human Mars Mission spacecraft. Symbols are explained in the text.
34. Sketch of a silicon Radiation-Sensitive metal-oxide-semiconductor field effects transistor (RADFET dosimeter) on a chip carrier. The sensitive region is a small region on the surface of the silicon chip. This is always covered by a protective encapsulant. In this case, there is an array of silicon devices and each has a different amount of radiation absorbing material between the sensor and the bombarding radiation beam. The silicon sensor chip is bonded and wired to a carrier substrate, which can be rigid or flexible and acts as as a connector to the "dosimeter reader". Miniature arrays like the one shown have been flown for some years on spacecraft, internally or externally, logging local dose values automatically over many years. For laboratory radiation-beam experiments, the array technique can give high-resolution dose profiles of test beams [note the small dimensions of the array shown].
35. The instrument platform of the NASA IMAGE space probe, showing instruments including four UV detectors with different roles. The instrument set is designed for scientific observations in the Earth's magnetosphere. (upper panel) photograph; (lower panel) sketch
36. Close-up of the wide-angle FarUV on the instrument deck of the NASA IMAGE space probe, showing the medium-sized FUV-WIC. The instrument set is designed for hourly imaging of hydrogen-line emissions from the upper atmosphere and the Earth's magnetosphere.

LIST OF TABLES

21. Estimates of deep-space dose rate and dose to BFO within vehicles near 1AU.
22. Proton energy deposition in the 10-100 MeV energy range - selected values for Al.
23. Proposed equivalent dose limits for a mission to Mars (RxTec 2004).
24. Summary of actual doses, dose rates and times in manned spaceflight to date.
25. Relations of some doses, dose rates and times in the REMSIM dose-threshold scheme for a Mars mission, shown in Table 23.
26. Attenuation of GCR by water * * Estimates by NASA-JSC for solar maximum, deep space, 1AU
27. Attenuation of solar protons * * Wilson 1997 TN3682 Table 6, estimates of dose to blood-forming organs for the August 4 1972 A.L. flare, converted to percent transmission
28. Warning and alarm thresholds in ALWARN (mSv) [terms inserted in the AL:WARN programme * to compare the latest cumulative dose with the limits decided]* Rx/Tec, 2004
29. Summary of recommendations for follow-on projects [post REMSIM]